SEISMIC RESPONSE AND ANALYSIS OF MULTIPLE FRAME BRIDGES USING SUPERELASTIC SHAPE MEMORY ALLOYS

A Thesis
Presented to
The Academic Faculty

by

Bassem Andrawes

In Partial Fulfillment
Of the Requirements for the Degree
Doctor of Philosophy in the
School of Civil and Environmental Engineering

Georgia Institute of Technology

May 2005

SEISMIC RESPONSE AND ANALYSIS OF MULTIPLE FRAME BRIDGES USING SUPERELASTIC SHAPE MEMORY ALLOYS

Approved by:

Dr. Reginald DesRoches, Advisor
School of Civil and Environmental Engineering
Georgia Institute of Technology

Dr. Rami Haj-Ali
School of Civil and Environmental Engineering
Georgia Institute of Technology

Dr. Barry Goodno
School of Civil and Environmental Engineering
Georgia Institute of Technology

Dr. James Craig
School of Aerospace Engineering
Georgia Institute of Technology

Dr. Laurence Jacobs
School of Civil and Environmental Engineering
Georgia Institute of Technology

Date Approved: April 12, 2005

AKNOWLEDGEMENTS

First of all I would like to thank my advisor, Dr. Reginald DesRoches for providing me the opportunity to work with him. I still remember the first conversation we had together about this relatively new material known as shape memory alloys. Since that day I knew that I am going to work with a talented ambitious professor. I really appreciate all the valuable advices he gave me throughout this research. I also benefited a lot from the discussions we had regarding my future career. I would like also to thank Dr. Barry Goodno, Dr. Rami Haj-Ali, Dr. Laurence Jacobs, and Dr. James Craig for serving in my thesis committee.

My beloved wife Marguerite; I guess I wont find the words that would express my gratitude and love to her. She accepted faithfully and gladly the challenges and uncertainties associated with the life of a doctoral student. She was a wonderful and supportive partner in every step I made during the analysis and writing of this thesis. I cannot even remember how many times she comforted me when I was stressed during the writing process. This work would have never been as it is now if she was not there.

The most important of all, I would like to thank my Lord for the support and guidance He granted me throughout my life. Every step I move forward in my life ensures that I am His child and He is my father.

TABLE OF CONTENTS

LIST OF TABLES

LIST OF FIGURES

NOMENCLATURE

SYMBOLS

A_f	Austenite finish temperature
A_s	Austenite start temperature
c_d	Damping coefficient
D	Young's Modulus
D_i	Initial hinge opening
D_r	Allowable hinge opening
D_y	Yield displacement
E	Global strain
E_e	Initial modulus of elastic material with gap in OpenSees
E_r	Initial modulus of steel restrainers
E_r	Initial modulus of steel material in OpenSees
F_f	Phase transformation finishing force
f_r	Structural restoring force
f_{res}	Residual force
F_s	Phase transformation start force
f_{SMA}	Shape memory alloy restoring force
F_u	Unloading force
G'	Shear storage modulus
G''	Shear loss modulus
k	Initial stiffness
K_A	Austenite elastic stiffness
k_d	Elastic stiffness
k_{eff}	Effective stiffness
K_M	Martensite elastic stiffness
K_m	Frames modified stiffness
K_u	Unloading stiffness
m	Mass
M_f	Martensite finish temperature
M_s	Martensite start temperature
Ms	Surface magnitude
Mw	Moment magnitude
N	Number of cycles
P_i	Modal participation factor
S_a	Spectral acceleration
S_M	Strain hardening ratio during martensitic transformation
SF	Ground motion scaling factor
T	Temperature
T_{eff}	Effective period
T_g	Predominate period
x	Displacement
$\dot{x}$	Velocity
$\ddot{x}$	Acceleration

$\ddot{x}_g$	Ground Acceleration

α	Strain hardening ratio during phase transformation
β	Hysteretic height parameter
γ	Strain hardening ratio after phase transformation
ε	Strain
ε_{ir}	Residual strain
ζ	Damping ratio
ζ_{eff}	Effective damping ratio
η	Loss factor
Θ	Thermoelastic coefficient
μ	Frames ductility ratio
ξ	Martensitic volume fraction
ξ_{A0}	Volume fraction of residual austenite
ξ_{M0}	Volume fraction of residual martensite
ρ	Frames period ratio
$\sum$	Global stress
σ	Stress
σ_{ir}	Residual stress
τ	Shear stress
Ω	Crystallographic material constant
ω	Circular frequency

ABREVIATIONS

A	Austenite phase
Au-Cd	Gold-Cadmium
BCC	Body Centered Cubic
Caltrans	California Department of Transportation
CQC	Complete Quadratic Combination
Ni-Ti	Nickel-Titanium
M+	First martensite variant
M-	Second martensite variant
MDOF	Multiple Degree of Freedom
MDR	Maximum drift ratio
MHDR	Maximum hinge displacement ratio
PGA	Peak Ground Acceleration
SDOF	Single Degree of Freedom
SE	Superelasticity Effect
SMA	Shape Memory Alloy
SME	Shape Memory Effect
TWSME	Two Way Shape Memory Effect
VE	Viscoelastic

SUMMARY

Past earthquakes have illustrated the inadequacy of the currently used steel restrainers in limiting relative hinge displacements in bridges. Upon yielding, steel restrainers lose a significant portion of their effectiveness due to the accumulation of plastic deformations. Shape memory alloy restrainers are an innovative alternative to traditional restrainers due to their large elastic strain range and unique hysteretic behavior.

The feasibility of using superelastic shape memory alloys in the retrofit of multiple frame bridges is investigated. First, three shape memory alloy constitutive models with various levels of complexity are compared in order to determine the significance of including subloops and cyclic loading effects on the structural response. The results show that the structural response is more sensitive to the shape memory alloys strength degradation and residual deformation than the sublooping behavior. Next, two parametric studies are conducted to explore the sensitivity of hinge opening to the mechanical behavior of the superelastic shape memory alloys. The first study is focused on the hysteretic properties of the alloy that could vary depending on the chemical composition or the manufacturing process of the alloy, while the second study targets the changes in the mechanical behavior of shape memory alloys resulting from the variability in the ambient temperature. The results show that the hysteretic behavior of shape memory alloys has only a slight effect on the bridge hinge opening as long as the recentering property is maintained. A detailed study on the effect of temperature shows that a reduction in the ambient temperature tends to negatively affect the hinge opening while an increase in temperature results in a slight improvement. Next, a parametric

study is conducted to examine the effectiveness of shape memory alloy retrofit devices in limiting hinge openings in bridges with various properties. In addition, a comparison is made with other devices such as conventional steel restrainers, metallic dampers, and viscoelastic solid dampers. The results illustrate that superelastic shape memory alloys are superior in their effectiveness compared to other devices in the case of bridges with moderate period ratios and high level of ductility, especially when subjected to strong earthquakes.

CHAPTER 1

INTRODUCTION

1.1 Problem Description

A major cause of bridge failure during earthquakes is the excessive movement of the bridge superstructure in the longitudinal direction. Excessive movement can result in damage to the bridge diaphragms and supports or unseating and subsequent collapse of the bridge deck. A significant number of bridges damaged during the 1989 Loma Prieta earthquake and the 1994 Northridge earthquake were due to excessive movement at the hinges. To limit the relative hinge displacement, restraining devices are commonly used. The restraining technology that is typically used in the moderate to high seismic regions of the United States is steel restrainers in the form of rods or bundled wires. Figure 1.1 shows a layout of simply supported and multiple frame bridges with restrainers installed at the intermediate hinges.

Steel restrainers have shown several deficiencies and have sustained damage in recent earthquakes (Schiff, 1995). Since those steel restrainers are only engaged under tension, and due to their high plasticity, once the steel restrainer yields it loses a significant portion of its effectiveness due to the accumulation of residual strain after each yielding cycle. This inelastic behavior leads to large hinge opening in bridges and subsequent unseating. In order to overcome such problems, the currently used restrainers are designed to remain elastic during earthquakes. This leads to another problem where large forces are transferred to the elements connected by the restrainers, which in some cases causes more damage to the bridge.

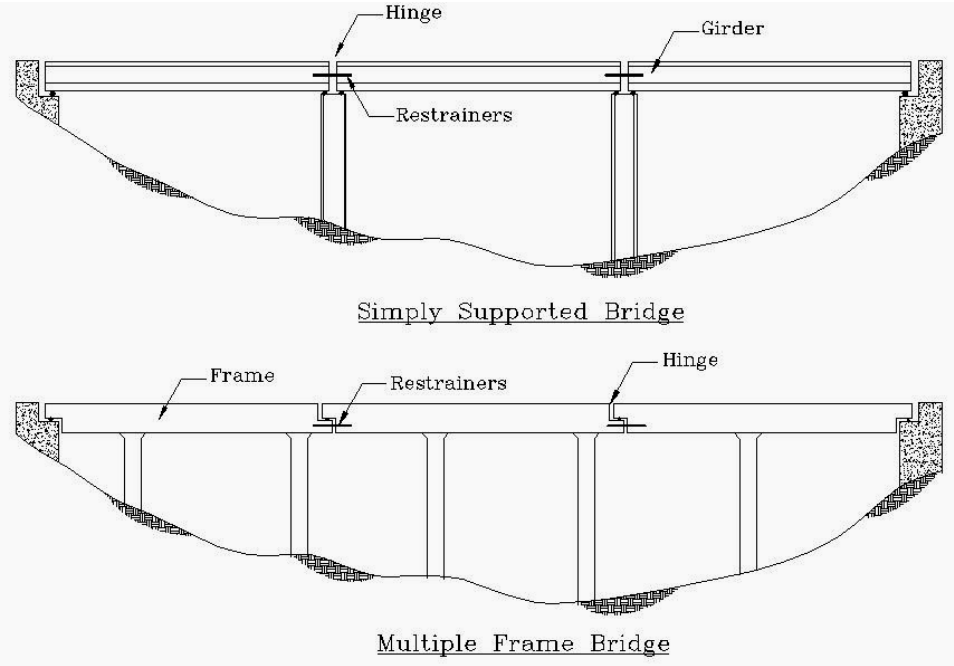

Figure 1.1 Schematic showing the layout of simply supported and multiple frame bridges with restrainers installed.

Other passive control technologies have been proposed for limiting hinge displacement including metallic dampers (Chen, 2001), viscoelastic solid dampers (Feng et al., 2000), and fluid viscous dampers. However, some of the proposed devices lack the recentering capability that is necessary for reducing the possible permanent damage and displacement, while the others are highly dependent on the frequency content of the ground motion and hence are not consistent in their effectiveness. Based on the current technologies a single retrofit technology that would effectively limit hinge displacements and reduce permanent damage in bridges is not yet available.

1.2 Scope of Research

Shape memory alloys (SMAs) are a class of metallic alloys that possess unique mechanical properties such as shape memory effect and superelasticity effect. This study focuses on evaluating the feasibility of using SMAs in developing seismic retrofit devices for multiple frame bridges. Figure 1.2 shows a schematic of the mechanical (stress-strain) behavior of superelastic SMAs. As illustrated from the figure, the superelasticity phenomenon (i.e. recovery of the original shape upon unloading) provides SMAs with high recentering capability, which is demonstrated by the large elastic strain range (typically 6-8%). Superelastic SMAs are also characterized by a nonlinear stress-strain hysteresis which provides constraints on the forces transmitted to the connected members. However, at large deformations (larger than 6%-strain) the alloy strain hardens. The strain hardening of superelastic SMAs at large strains would act as a second line of defense against unseating in the case of strong ground shaking. The large

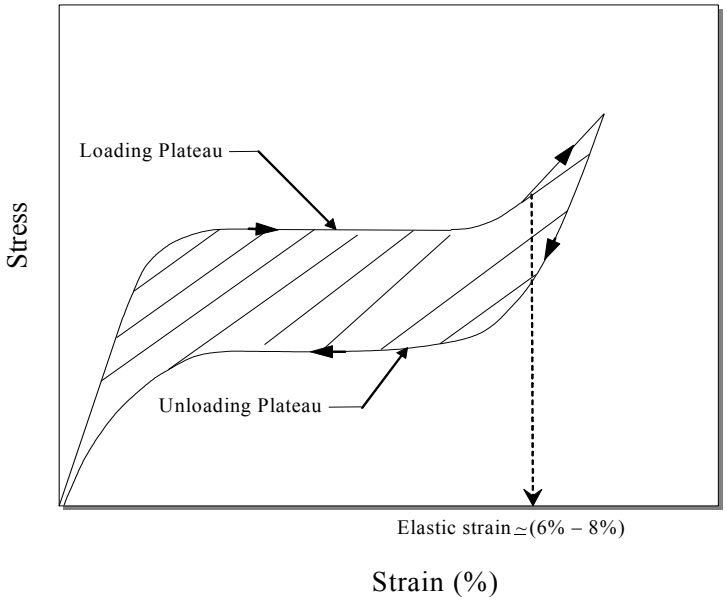

Figure 1.2 Typical mechanical behavior of superelastic shape memory alloys.

force associated with the linear behavior would play an important role in preventing bridge unseating.

Although all of the above characteristics allow SMAs to be one of the most promising candidates for the bridge retrofit as restraining devices, many questions still need to be addressed regarding the behavior of the SMAs in structures such as (1) How would the SMAs behave under cyclic loading such as the earthquake loading, (2) Is the performance of SMAs as bridge restraint devices sensitive to their hysteretic properties (shape), (3) How would the SMA devices that are designed for a specific ambient temperature behave at other temperatures, and (4) How would the SMA devices compare to other bridge retrofit devices which have higher damping capability or devices which are velocity-dependent.

Presented in this dissertation is a comprehensive study that addresses part of the concerns and questions that have been presented earlier with regards to the usage of superelastic SMAs in bridges. The study focuses on the multiple frame type of bridges which is the most commonly used type of bridges in California and part of the west coast.

1.3 Dissertation Outline

This dissertation is divided into the following chapters:

- **Chapter 2:** Presents an overview of the unseating problem in bridges during past earthquakes. An overview of a number of bridge retrofit technologies is also presented.
- **Chapter 3:** Presents an introduction to shape memory alloys and their mechanical properties.

- **Chapter 4:** A discussion is presented regarding different types of SMA constitutive models. A study is also presented which compares the behavior of SMAs in structures using different types of models.
- **Chapter 5:** Two parametric studies are presented to investigate the effect of variability in the SMAs mechanical properties on their performance in bridges. The first study focuses on the variability in the SMAs hysteretic shape, while the second study focuses on the ambient temperature variability.
- **Chapter 6:** A parametric study is presented using OpenSees to compare the effectiveness of SMA devices with other retrofit devices in limiting hinge opening in multiple frame bridges.
- **Chapter 7:** Three case studies are presented using OpenSees to address the conclusions and observations that were obtained in Chapters 5 and 6.
- **Chapter 8:** Conclusions and recommendations.

CHAPTER 2

OVERVIEW OF BRIDGE UNSEATING PROBLEM

This chapter starts with a discussion on the bridge damage resulting from the bridge superstructure during earthquakes. Some of the earthquakes events discussed occurred within the United States while the others were in various parts of the world. The discussion is focused more on the most recent earthquakes. The chapter then highlights three of the current and potential devices that are often used in the field of bridge retrofit. The three devices are the conventional steel restrainer cables, the metallic dampers, and the viscoelastic solid dampers. Those devices were selected since they will be the focus of comparisons in Chapters 6 and 7 of this dissertation.

2.1 Performance of Bridges in Previous Earthquakes

One of the earliest bridge unseating incidents that occurred in the early 20th century resulted from the 1923 Great Tokyo (Kanto) earthquake in Japan. On September 1st, 1923, one minute before noon a major earthquake of a surface magnitude M_s=8.19 devastated the southeastern part of Japan including the city of Tokyo. The life losses due to this earthquake exceeded 140,000 lives, while the property damage exceeded one billion 1923 U.S. dollars (James, 2002). The Tamagawa Bridge was a double track railroad bridge which experienced unseating of a number of its steel girders. Figure 2.1 shows part of the damage that occurred to the bridge. Almost 41 years later in June 16, 1964 the 7.5-magnitude Niigata, Japan earthquake triggered a tsunami which caused

Figure 2.1 Unseating of several steel girders of the Tamagawa rail road bridge in Japan due to the 1923 Great Tokyo earthquake. (EQllS and K. Steinbrugge Database)

severe damage to the structures in Niigata. Twenty eight people were reported dead (http://www.ce.washington.edu/~liquefaction). The excessive lateral movements of the Showa bridge foundation caused the simply supported girders of the bridge to unseat and collapse. A picture of the unseated bridge is presented in Figure 2.2.

In the United States before 1971, California bridges were designed for a minimal seismic force (Yashinsky, 1998). When the San Fernando earthquake struck the San Fernando Valley in Los Angeles, California in February 9, 1971, it damaged more than 60 bridges on the Golden State Freeway. This earthquake cost the state of California approximately $100 million in bridge repair (Cooper et al., 1994). One of the most seriously damaged bridges during this earthquake was the Route 210/5 Interchange, which suffered several incidences of span unseating due to excessive movements in the

Figure 2.2 Simply supported unseated spans of the Showa Bridge due to the 1964 Niigita, Japan earthquake. (EQllS and K. Steinbrugge Database)

Figure 2.3 Part of the damage of the 210/5 Interchange due to the 1971 San Fernando earthquake. (EQllS and K. Steinbrugge Database)

longitudinal direction during the earthquake. Figure 2.3 shows part of the damage in the Route 210/5 Interchange. After the 1971 San Fernando earthquake, the California State Department of Transportation (Caltrans) realized that many of the bridges were vulnerable to severe damage because of poor column details and short hinge seats. As a result, Caltrans initiated a statewide seismic retrofit program for bridges to systematically reinforce the older, non-ductile bridges. Phase-I of the Caltrans Bridge Seismic Retrofit program involved installation of hinge and joint restrainers to prevent deck joints from being separated. The unseating of the deck was the major cause of bridge collapse during the San Fernando earthquake (Roberts, 1994). Phase-I was completed in 1989 after retrofitting 1,260 bridges at a cost of approximately $55 million.

2.1.1 1989 Loma Prieta Earthquake

When the Loma Prieta earthquake struck the San Francisco Bay Area in October 17, 1989 with a magnitude of M_w=6.9, it caused damage to more than 80 bridges and resulted in more than 40 deaths in bridge-related collapses alone (Cooper et al., 1994). The cost to repair and replace highways damaged by this earthquake was $2 billion. With the exception of the Route 980 Southbound Connector OC and Route 92/101 Interchange, all of the state bridges with over $100,000 in damage as a result of the Loma Prieta earthquake were older bridges, without post-San Fernando seismic details. There were also state-owned bridges that suffered over $100,000 in damage during the earthquake.

Approximately one half of the cost of repairing and replacing the highway bridges damaged by the earthquake was to replace the Oakland Bay Bridge that had a devastating

collapse, which resulted in 42 deaths and 108 injuries (Yashinsky, 1998). The most significant damage occurred to this bridge was at Pier E9 where the top and bottom decks were pulled off their seats, causing them to fall. The bearing seat at Pier E9 was too short to handle the subsequent movement of 10 inches longitudinally and 5 inches transversely during the earthquake. Figure 2.4 shows a picture of the damage occurred to the Bridge

Another clear example for hinge failure was the damage induced in the Route 92/101 Separation. The most significant damage to this structure was at the hinge of the Northwest connector center frame shown in Figure 2.5. This hinge suffered serious damage due to relative movement between the three frames during. Apparently the grease and neoprene pads harden over time and the pads can fail in shear since they were not designed for earthquakes. The damage resulting from Loma Prieta earthquake provided the political pressure to undertake the large cost of Caltrans`s Phase-II seismic retrofit program. The main goal of this phase was to provide shear strength and ductility to existing bridge columns.

Figure 2.4 Fallen Decks at Pier E9 of the East Bay Crossing in the 1989 Loma Prieta Earthquake. (EQllS and K. Steinbrugge Database)

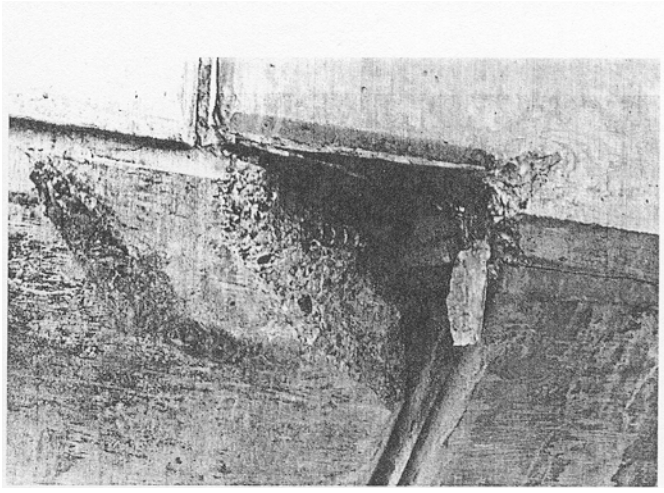

Figure 2.5 Spall at Northwest Connector of Route 92/101 Interchange due to the 1989 Loma Prieta Earthquake (Yashinsky, 1998)

2.1.2 1994 Northridge Earthquake

While the Phase-II retrofit program was underway, the Northridge earthquake (M_w= 6.9) shook the Northridge section of the San Fernando Valley for approximately 20 seconds in January 17, 1994. Most of the bridges that were retrofitted after the Loma Prieta earthquake performed extremely well during the earthquake. However, seven bridges experienced major damage during the earthquake. Some of those bridges had been retrofitted after the San Fernando earthquake (Phase-I). None of the bridges with Phase-II retrofit experienced significant damage (Yashinsky, 1998).

The Gavin Canyon Undercrossing, which composed of three frames, was retrofitted in 1974 with restrainer cable units at the 8 inches hinges connecting the three frames together. This bridge suffered major damage during the earthquake due to excessive hinge opening and a failure of the cable restrainers to limit superstructure movement. As a result, the cantilever spans moved off the hinge seats, breaking off the acute corner of

the cantilever spans (Schiff, 1995). Part of the Gavin Canyon unseated spans is shown Figure 2.6.

The 14/5 Interchange also experienced serious damage during the Northridge earthquake. This bridge was designed in 1968, modified after the San Fernando earthquake and constructed in 1975. During the earthquake, the first two spans along with pier no. 2 fell (Schiff, 1995). As a result, the abutment of the North connecter unseated and collapsed. Two of the restrainers were still connected to the abutment while the third restrainer was missing. Figure 2.7 shows a picture of the unseated abutment, while Figure 2.8 shows a picture of the second collapsed span. The relative displacement at the collapsed hinge shown in the figure was estimated as 10 in.

Figure 2.6 Damage occurred to The Gavin Canyon UC Bridge during the 1994 Northridge Earthquake. (EQllS and K. Steinbrugge Database)

Figure 2.7 Damage at abutment of the 14/5 Interchange North Connector due to the 1994 Northridge Earthquake. (EQllS and K. Steinbrugge Database)

Figure 2.8 Unseated span of the 14/5 Interchange during the 1994 Northridge Earthquake. (EQllS and K. Steinbrugge Database)

2.1.3 1995 Kobe Earthquake

A comparable earthquake to the earthquakes occurred in Loma Prieta and Northridge was the Hyogoken-Nanbu (Kobe) earthquake (M_w=6.9). This earthquake struck Kobe, Japan, and its surrounding area on January 17, 1995. During this earthquake there was a remarkable amount of damage to highways east of the epicenter. About 60% of the highway structures in the Hanshin area suffered some damage, and sixteen people lost their lives due to highway damage. One of the major consequences of this earthquake was the significant amount of damage experienced by the Kobe Route 3. This route measures about 39.6 km from Nishimoto in Osaka to Tsukimisan in Kobe. The superstructure consisted mostly of simple spans, steel girders with a concrete deck. One of the most common severe damage was girders falling off their bearings (Schiff, 1998). An example for such damage was the damage experienced by Nishinomiya at Hamawaki bridge, especially from Piers number 35 to 48. This bridge had a sever damage due to the falling of two spans off their supports onto National Highway 43 below. The unseated spans are shown in Figures 2.9 and 2.10. The unseating occurred as a result of the breaking of the steel restrainers connected to the four spans on either sides of the collapse.

2.1.4 1999 Chi-Chi (Taiwan) Earthquake

The Chi-Chi earthquake (M_w=7.6) that took place on September 21, 1999, and shook the village of Chi-Chi in central Taiwan, severely damaged several highways and bridges. The actual number of bridges that collapsed in this earthquake is unknown, however at least 12 bridges were identified as being collapsed after this earthquake (EERI Taiwan

Figure 2.9 Superstructure collapse at Pier 41 of Kobe Route 3 due to the 1995 Kobe, Japan Earthquake. (EQllS and K. Steinbrugge Database)

Figure 2.10 Collapse due to unseating at pier 40 of Kobe Rout 3 due to the 1995 Kobe Japan Earthquake. (EQllS and K. Steinbrugge Database)

CD-ROM, 2003). It was clear that the main cause for bridge failure was the large permanent ground deformation beneath the bridge or bridge abutment. The Wu-Shi bridge located across the Chelungpu fault line on Provincial Route 3, was one of the bridges that experienced collapse during the earthquake. One of the main reasons for the damage occurring to this structure was the unseating of the first two spans of the east bridge near the north abutment. This unseating was a direct result of a severe longitudinal movement of about 2.25 m (Hsu and Fu, 2004). A picture of the unseated spans is presented in Figure 2.11. Another clear example of the damage resulting from the unseating of bridge decks was the damage experienced by Ming-Ju bridge located south of the city of Ming-Jian. Three northbound spans and four southbound spans experienced collapse. The surface faulting appears to have moved the piers to the north, which would result in unseating of the decks. Figure 2.12 shows part of the unseated decks.

Figure 2.11 Unseating and shear key damage to east bridge portion of Wu-Shi Bridge after the 1999 Chi-Chi Earthquake. (EQllS and K. Steinbrugge Database)

Figure 2.12 Collapsed Ming-Ju Bridge spans at south abutment due to the 1999 Chi-Chi earthquake. (EQllS and K. Steinbrugge Database)

2.1.5 1999 Kocaeli (Turkey) Earthquake

On August 17, 1999 the most destructive earthquake (M_w = 7.4) ever experienced by Turkey shook more than 10,000 km^2 of land area, stretching from Duzce to Istanbul. An estimated 60,000 to 115,000 buildings collapsed or were damaged beyond repair. Although, the Kocaeli earthquake had a significant effect on residential buildings, the damage to the highway infrastructure was minor. The earthquake caused collapse to three highway bridges (EERI Turkey CD-ROM, 2003). The most dramatic and significant damage occurred to the highway system occurred at Arifiye Road over crossing of the TEM. All four simply supported spans forming the superstructure of the bridge collapsed, killing 10 people. The unseating of the bridge decks was clearly due to fault offset. The fault passed mid-way between the northeast abutment and the nearest

Figure 2.13 Collapsed bridge at TEM Arifiye Road overcrossing due to the 1999 Kocaeli Earthquake (EQllS and K. Steinbrugge Database)

Adjacent bent in 45 degree angle relative to the bridge centerline. The longitudinal component of the fault offset was sufficient to unseat the bridge girders (EERI Turkey CD-ROM, 2003). Part of the collapsed bridge is shown in Figure 2.13.

2.2 Bridge Retrofit Technologies

In the past three decades a relatively large number of devices have been either used or proposed for usage in the retrofit of bridges. Those devices vary on their methodologies in controlling the structural response during earthquakes. Hence, they all exert different impact on the performance of the retrofitted bridge. Despite the large number of current retrofit technologies, this section presents a discussion on the three technologies which are going to be addressed in some of the preceding chapters. Those three retrofit technologies are the steel cable restrainers, the metallic dampers, and the viscoelastic solid dampers. The steel restrainer is the main device currently used in bridges to prevent unseating, while the other two devices are energy dissipating devices.

2.2.1 Steel Cable Restrainers

Restrainers are elements that tie together the superstructure of the bridge with its substructure or used to tie adjacent structural segments in order to prevent them from large relative movements. Hinge restrainers are probably the least expensive retrofit strategy and they can be effective in preventing the largest consequences. They are therefore the most common form of bridge retrofit. Hinge restrainers could be used as either cables or rods depending on their configuration. Figure 2.14 shows a schematic of bridge restrainers with different configurations.

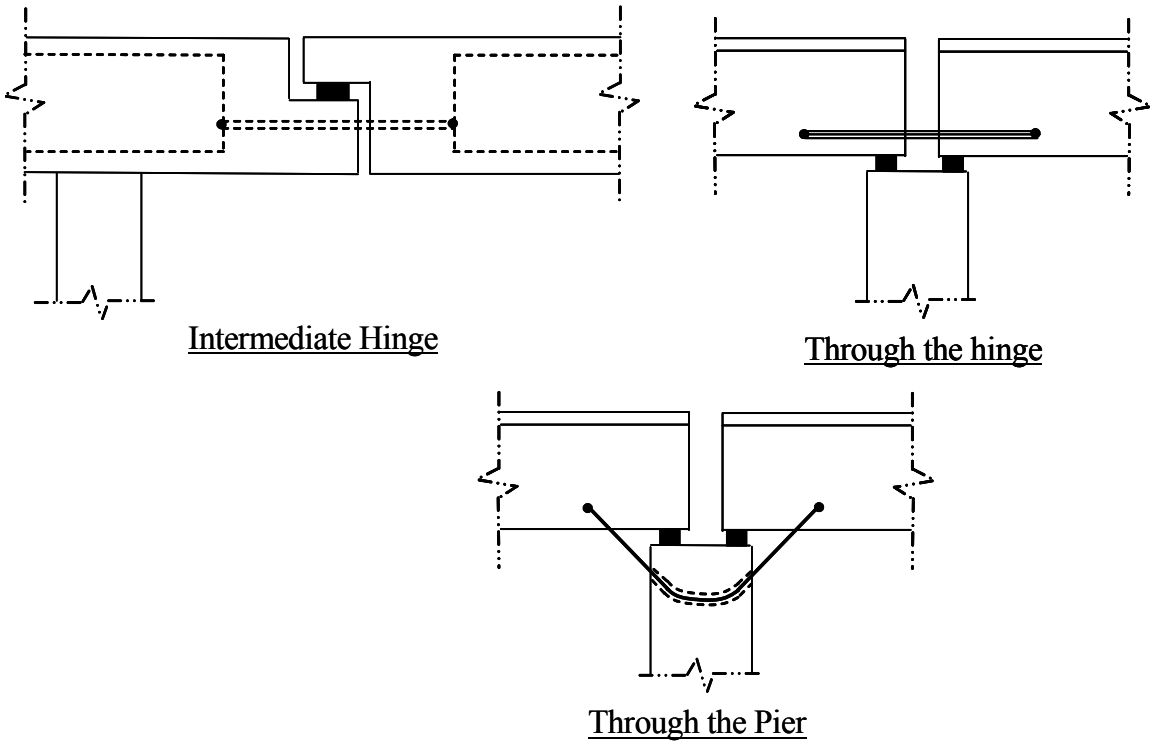

Figure 2.14 Different configurations for steel restrainers used in multiple-frame and simply supported bridges.

Since the 1971 San Fernando earthquake, Caltrans has been a leader in retrofitting bridges against spans unseating using restrainers. The most common type of restrainers used by Caltrans in retrofitting multiple-frame (MF) bridges is the high-strength steel cable restrainers. Each restraining unit consists of 5-3/4 in diameter 7 strand twisted cables. The Young's modulus of the restrainer cables is equal to 69,000 MPa (10,000 ksi), while the yield stress is 1210 MPa (176 ksi). A schematic of the typical restrainer cable configuration is presented in Figure 2.15. As shown in the figure, the restrainer cables connect the two adjacent frames together through their end diaphragms. Several restrainer units are usually used at each intermediate hinge. In order to install each unit, two holes are drilled in each of the two frames end diaphragms.

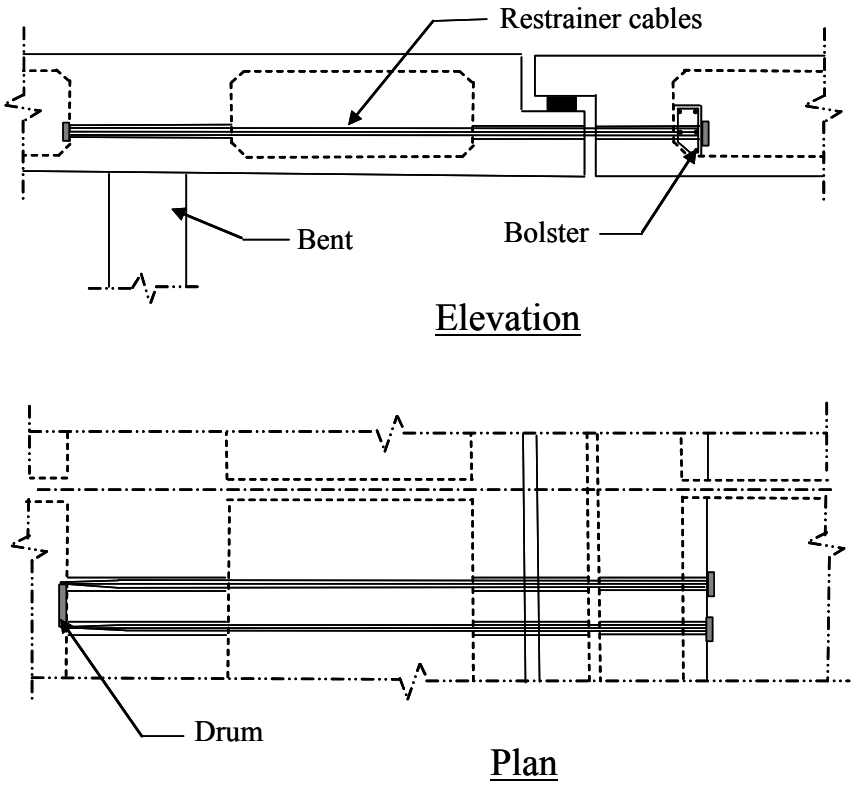

Figure 2.15 Common used configuration for steel restrainer cables in multiple frame bridges.

The cables pass through the four drilled holes back and forth. A reinforced concrete bolster is often used at the end diaphragm with smaller thickness to provide better grip for the anchored cables. On the non-anchored side, a drum unit is provided to create a rounded smooth transition for the cables.

The 1989 Loma Prieta and the 1994 Northridge earthquakes provided the researchers and the engineers with valuable information about the performance of steel restrainers during earthquakes. The Caltrans maintenance division identified 23 bridges that were retrofitted with restrainers and that were damaged by the Loma Prieta earthquake (Saiidi and Maragakis, 1995). During the Loma Prieta earthquake, it appeared that restrainers were activated in many instances, but they failed only in two cases. The 1994 Northridge earthquake led to larger hinge movements and unseating of several bridge spans such as in the case of the Gavin Canyon Undercrossing and the 14/5 Interchange that were discussed earlier in section 2.1.2. The failure of the hinge restrainers is not surprising, since restrainers are designed to behave elastically during earthquakes. This behavior will cause either the cables to break or the diaphragm walls at the two ends of the cable to suffer a punch-through action during a severe earthquake (Feng, 1994).

2.2.2 Damping Devices

Dampers are effective devices that are often used to reduce the response of bridges in earthquakes. The core technology for developing dampers involves the provision of an appropriate energy dissipation mechanism for the materials being used for energy dissipation. Various materials including steel, lead and oil have been used effectively (Kawashima and Unjoh, 1994). Energy dissipating (damping) devices is divided into two

main categories: displacement-dependant and velocity-dependent dampers. The following two subsections will discuss one type of dampers from each category.

2.2.2.1 Metallic Dampers

Metallic dampers are considered to be one of the most effective energy dissipating devices. Metallic dampers are displacement-dependent energy dissipating devices which dissipate energy through the yielding of metallic material. This type of damper is also known as hysteretic damper since its dissipated energy mainly depends on the relative displacement between the two ends of the damper. Several commercial metallic dampers are currently produced and utilized in retrofitting mostly buildings. A number of buildings in the United States, Japan, and Italy were retrofitted using metallic dampers (Soong and Dargush, 1997). Metallic dampers could be used in different configurations. The most common configurations for metallic dampers used in buildings are the X-shape and the triangular-shape dampers shown in Figure 2.16. The typical force-deformation

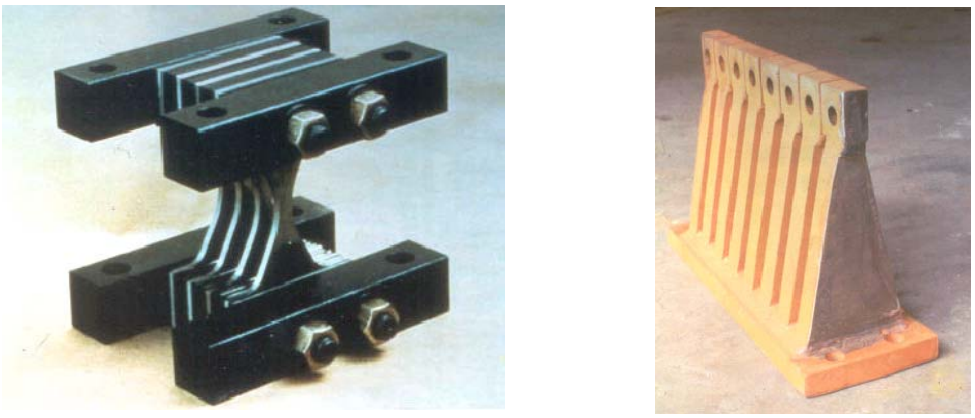

a. X-shape b. Triangle-shape

Figure 2.16 Different configurations for metallic dampers used in buildings.

relationship of metallic dampers is presented in Figure 2.17. The mechanical behavior of the metallic dampers is often modeled using either elasto-plastic or bilinear models (Hanson and Soong, 2001).

Chen and others (Chen et al., 2001) studied the feasibility of using metallic dampers made of circular steel rods as seismic retrofit devices for steel girder bridges. They used the dampers to connect the superstructure with the substructure so that the dampers would yield prior to the column yielding. The outcome of this research illustrated the effectiveness of the metallic dampers in reducing the strains in the bridge columns and the acceleration of the bridge girders.

2.2.2.2 Viscoelastic Solid Dampers

Viscoelastic (VE) dampers belong to the family of the velocity-dependent energy dissipating devices. The VE dampers that are typically used for structural applications are made of copolymers or elastomeric substance that dissipates energy when subjected

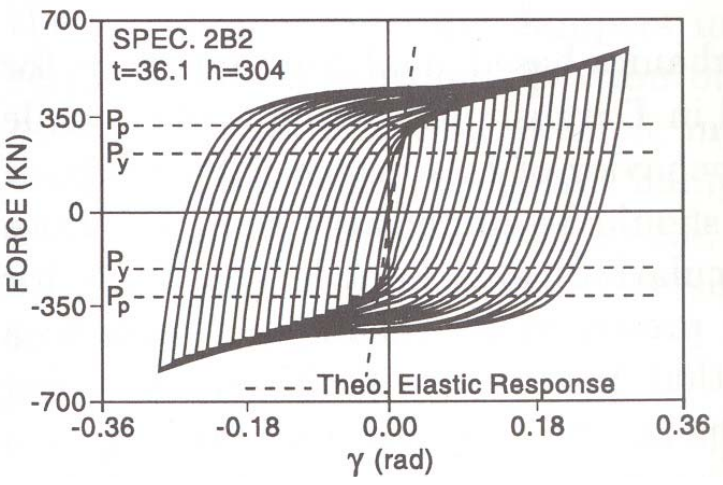

Figure 2.17 Typical force-deformation relationship for metallic dampers (Tsai et al., 1993)

to shear deformation. The simplest configuration of VE dampers consists of several layers of the VE material separated by steel layers such as the damper shown in Figure 2.18. The mechanical behavior of the VE dampers depends highly on the relative velocity (frequency) between its two ends. The thermal changes associated with the dissipated energy also affect the mechanical behavior of the VE dampers. Figure 2.19 presents a schematic of the stress-strain relationship characterizing the behavior of VE dampers. As shown in the figure, the hysteresis of the VE dampers consists basically of an ellipse with non-zero slope. The slope of the ellipse is controlled by the shear stiffness of the VE material while the area of the ellipse is controlled by the shearing rate. Hence the shear stress in the VE material is governed by the following equation:

$$\tau(t) = G'\gamma(t) \pm G''\dot{\gamma}(t)/\omega \tag{2.1}$$

where $\tau(t)$ is the shear stress as a function of time, $G'(t)$ is the shear storage modulus which provides the elastic shear stiffness, $G''(t)$ is the shear loss modulus which

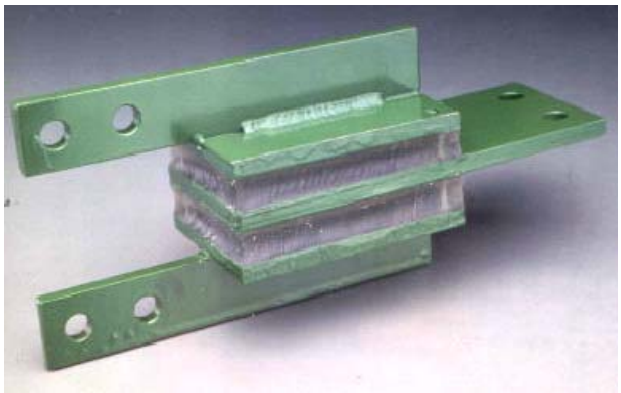

Figure 2.18 Viscoelastic damper consisting of viscoelastic layers separated by steel plates.

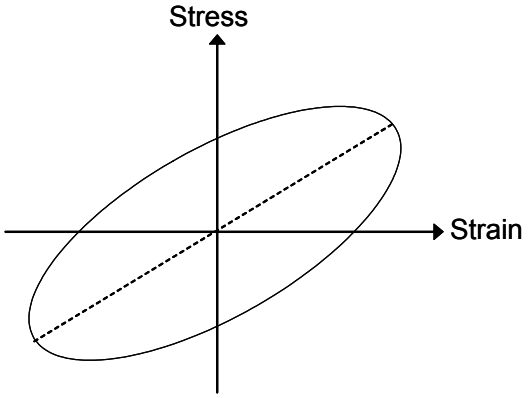

Figure 2.19 Typical stress-strain relationship for viscoelastic dampers.

represents the viscous stiffness of the material, $\gamma(t)$ is the shear strain as a function of time, $\dot{\gamma}(t)$ is the shear strain rate as a function of time, and ω is the circular frequency in radians per second (Hanson and Soong, 2001). From equation 2.1 we can relate the elastic stiffness with the viscous damping through the following equation:

$$c_d = k_d \eta / \omega \tag{2.2}$$

where c_d is the damping coefficient, k_d is the elastic stiffness, and $\eta = G''(\omega)/G'(\omega)$ which is known as the loss factor. Research (Soong and Dargush, 1997) has found that although $G'(\omega)$ and $G''(\omega)$ are functions of frequency their ratio η is almost constant at various frequency values.

Feng and others (Feng et al., 2000) studied the effect of using VE dampers at the expansion joints of highway bridges to prevent the unseating of superstructures off their seats and pounding of decks during earthquakes. The researchers performed a finite element analysis using the Kelvin and Maxwell models for the VE dampers. The

outcome of this research illustrated that using VE dampers reduces hinge openings in bridges without introducing a significant increase in the ductility demand.

CHAPTER 3

SHAPE MEMORY ALLOYS

This chapter presents an introduction to shape memory alloys (SMAs). First a brief description of the microstructure of SMAs is presented, followed by a discussion of the two main thermomechanical phenomena characterizing their behavior. A description of the SMA mechanical properties is also introduced in this chapter.

3.1 Introduction to Shape Memory Alloys

Shape memory alloys (SMAs) are a class of metallic alloys that exhibit unique characteristics such as shape memory effects (SME) and superelasticity effects (SE). These behaviors were first observed in an Au-Cd alloy in 1932, and were further publicized by their discovery in a Ni-Ti alloy in 1963 (Otsuka and Wayman, 1998). SMAs are found in two main phases: the high temperature phase, which is called austenite, and the low temperature phase, which is called martensite. In the case of Ni-Ti SMA, the austenite is characterized by a Body-Centered-Cubic structure (BCC), where there is a nickel atom at the center of the crystallographic cube and a titanium atom at each of the cube's eight corners. Since the austenitic phase is microstructurally symmetric it is considered to be the parent phase. The martensite phase of Ni-Ti is less symmetric where its lattice structure consists of a rhombus alignment with an atom at each of the rhombus corners. Figure 3.1 shows two adjacent Ni-Ti crystals in the austenite and martensite phases.

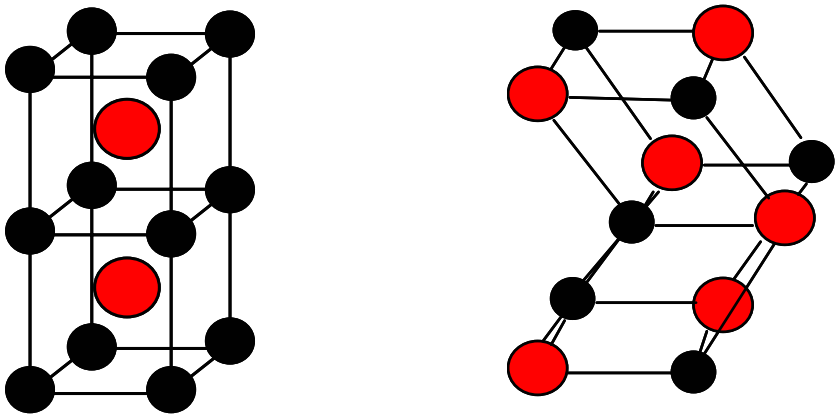

a. Austenite b. Martensite

Figure 3.1 Austenite and martensite lattice structure.

Figure 3.2 shows the SMA in austenitic and martensitic forms in a two-dimensional view. As shown in the figure, the austenite is symmetric and thus has one layout for the atoms, while the martensite could be found in two different alignments based on the level of stress applied to the alloy. The twinned marteniste exists when the alloy is free from any applied stress; however the detwinned martensite results when the twinned martensite is subjected to external stress. Based on the stress direction, the martensite could be detwinned either to the left or to the right direction. Thus from a two-dimensional point of view there are two possible variants for martensite.

3.2 Phase Transformation

The transformation from one phase to another in SMAs could be attained easily through the correct thermoelastic treatment of the alloy. The transformation from austenite to martensite is known as forward transformation or martensitic transformation,

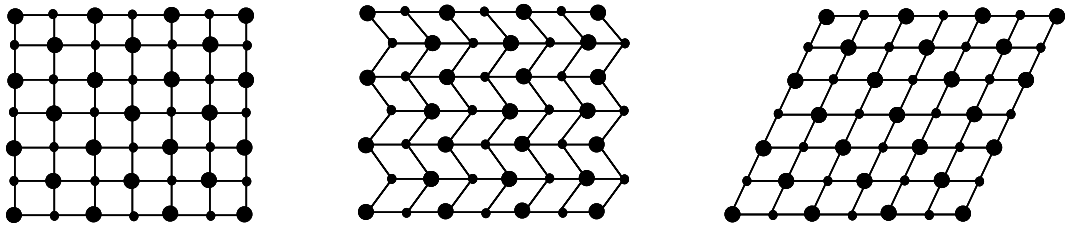

a. Austenite b. Twinned martensite c. Detwinned martensite

Figure 3.2 Austenite and martensite microstructural view in a two-dimensional plan.

while the transformation from martensite to austenite is known as reverse transformation. These transformations are diffussionless solid-to-solid transformations, which result from a rearrangement of the atoms while they are still close to each other. The SMA could be transformed from austenite to martensite either by reducing the temperature or applying a mechanical stress. On the other hand the martensite transforms into austenite through either increasing the alloy's temperature or removing the applied stress. This shows that mechanical loading and thermal loading have opposite effects on SMAs.

The temperature/stress which the phase transformation process initiates or ends varies from one alloy to another, based on the phase transformation temperatures that characterize each alloy. There are mainly four transformation temperatures for each alloy. These transformation temperatures are: a) the austenite start temperature (A_s), where the austenite starts to develop in the alloy; b) the austenite finish temperature (A_f), where the development of austenite in the alloy is 100% complete; c) the martensite start temperature (M_s), where the development of martensite starts; and d) the martensite finish temperature (M_f), where the development of martensite is 100% complete. Figure 3.3 shows the relationship between the phase transformation temperatures and the applied stress. From the figure, it is observed that increasing the applied stress would increase

the four phase transformation temperatures. This is due to the fact that stress and temperature have counter effect on the SMAs. The forward and reverse transformations between the austenite and martensite phases produce two interesting phenomena in SMAs: the Shape Memory Effect (SME) and the Superelasticity (pseudoelasticity) Effect (SE). These two phenomena will be discussed in the following two sections.

3.2.1 Shape Memory Effect

SMAs are found in their twinned martensite phase if the temperature of the alloy is below M_f. When the SMA is subjected to an external stress, the alloy deforms through the detwinning of the martensite, resulting in the formation of detwinned martensite. When the load is removed the SMA remains in its deformed detwinned martensitic phase.

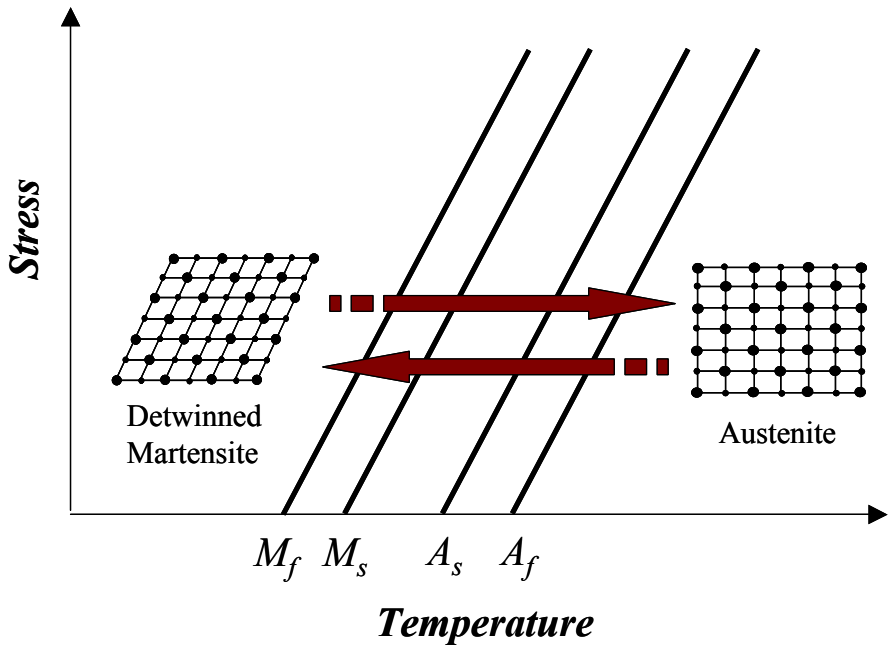

Figure 3.3 Relationship between phase transformation temperatures and applied stress.

The original shape of the alloy could be recovered through heating the SMA to a temperature greater than A_f. Increasing the temperature of the SMA above this temperature transforms the detwinned martensite into austenite, which has the same macroscopic shape as the twinned martensite, which is the original phase of the alloy. Figure 3.4 is a schematic that describes the SME phenomenon in SMAs. As shown in the figure, the austenite and martensite are separated by four horizontal lines that represent the four transformation temperatures. It is also noticed from the figure that both the austenite and twinned martensite have the same shape from a macroscopic point of view.

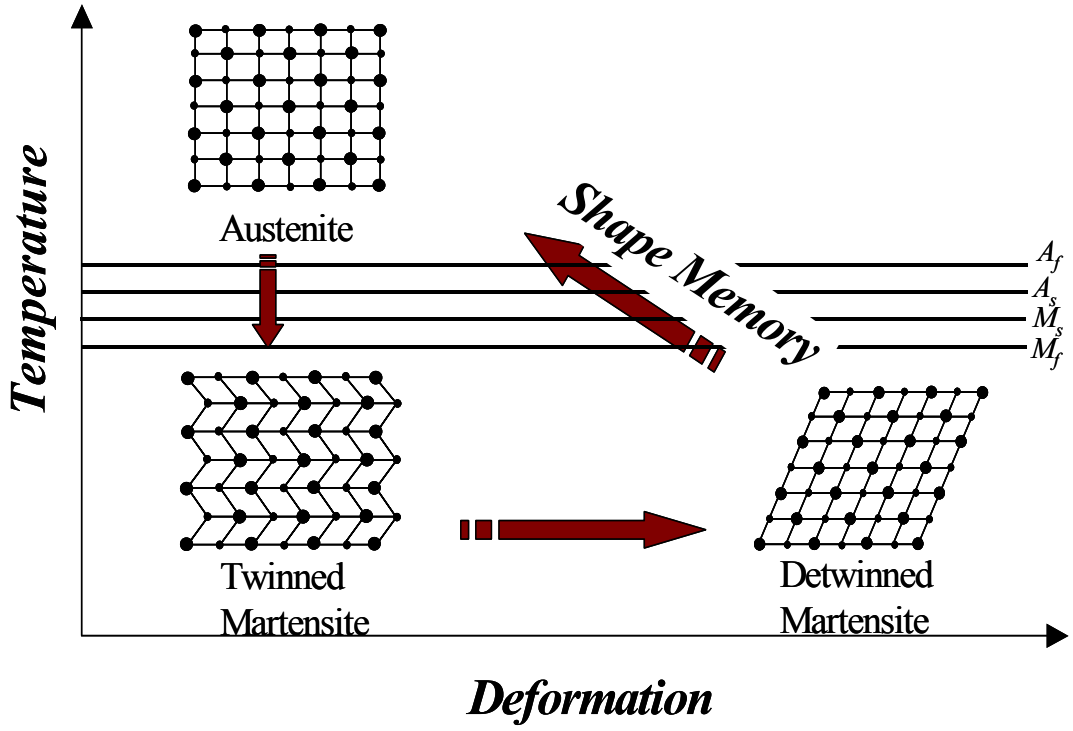

Figure 3.4 Shape memory effect phenomenon in shape memory alloys.

3.2.2 Superelasticity Effect

At a temperature above A_f the SMA is austenite. If the alloy is externally stressed, it deforms transforming into a detwinned martensite, which is unstable at high temperatures, thus when the load is removed the SMA transforms back into austenite and the original shape of the alloy is fully recovered. The loading and unloading paths during this loading cycle do not coincide, with the unloading path being a lower stress plateau compared to the loading plateau. As a result, there is an area enclosed under the stress-strain diagram which represents the energy dissipated. The microstructural superelasticity phenomenon is illustrated graphically in Figure 3.5. As shown in the figure, the stress-induced detwinned martensite converts back to austenite once the load is removed.

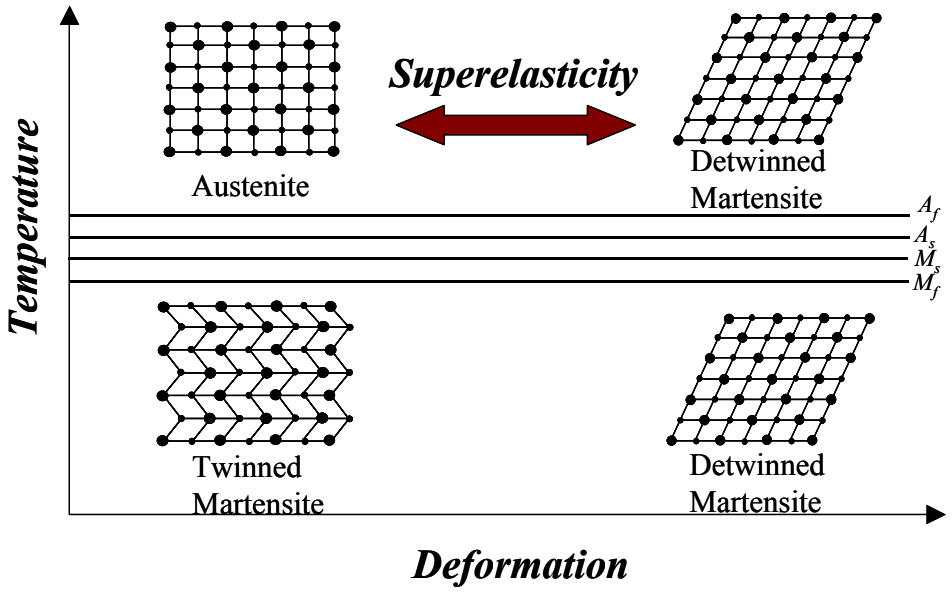

Figure 3.5 Superelasticity effect in shape memory alloys.

Figure 3.6 illustrates the mechanical behavior of SMAs during the austenite and martensite phases as a function of temperature. In order to relate the mechanical behavior of the SMAs which occurs on the macro level with the phase transformations that occur on the micro level, the microstructure of the alloy is shown in the figure at the various strain/temperature levels. At low temperatures, the SMA is 100% twinned martensite. The stress plateau at low temperatures is developed due to the detwinning of the martensite. It is noticed that the SMA unloads with a residual strain that could be eliminated by heating the alloy. At high temperatures, the stress-strain relation exhibits a flag shape. The figure demonstrates that the stress plateau at high temperatures is developed due to the conversion of austenite to detwinned martensite and vice versa.

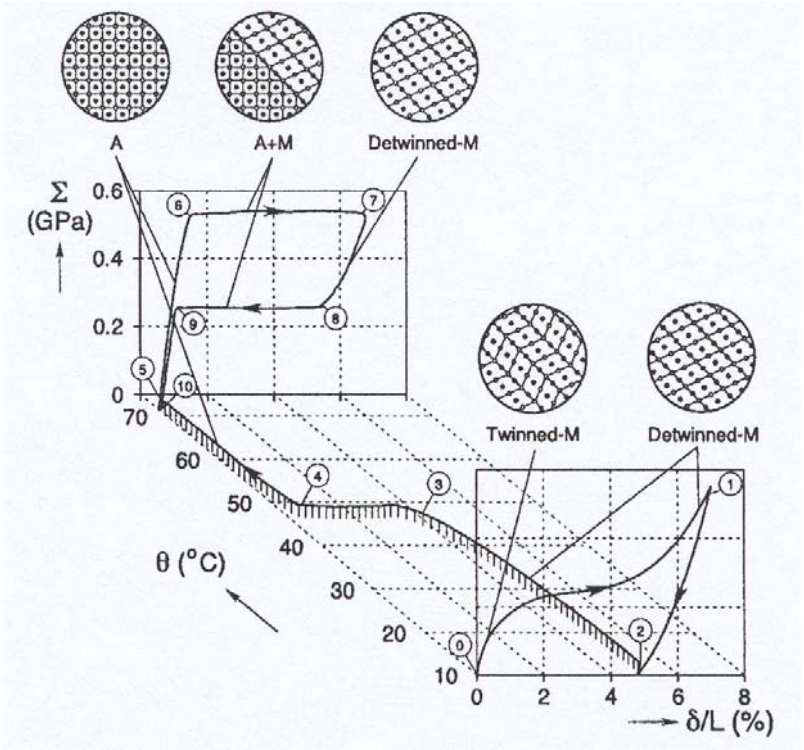

Figure 3.6 Stress-strain-temperature relationship in shape memory alloys (Shaw, 2002).

3.3 Mechanical Properties of Shape Memory Alloys

Since the discovery of SMAs in 1932 and more specifically the Ni-Ti in 1963 (Otsuka and Wayman, 1998) a relatively large number of researchers have been interested in exploring the mechanical characteristics of SMAs in its two phases. Researchers are interested in studying and specifying the mechanical properties of SMAs under various types of thermomechanical loadings. Several experimental studies have been conducted to specify the mechanical properties of SMAs (Dolce et al. 2000; Dolce and Cardone 2001; DesRoches and Delemont 2002; Piedboeuf et al. 1998; and Wu et al. 1996). The outcomes of experimental research in the past two decades assisted in developing a range for the mechanical parameters that would be expected from SMAs in its austenite and martensite phases. Table 3.1 presents a summary of the mechanical properties for Ni-Ti, which is considered the most commonly used type of SMAs. The table illustrates considerably large differences in the mechanical properties based on the SMA phase as well as with the phase. Research has shown that the variation in the SMA mechanical properties could be due to several factors such as alloys composition,

Table 3.1 Summary of Ni-Ti mechanical properties

	Austenite	**Martensite**
Modulus of Elasticity	30-83 GPa	21-41 GPa
Yield Strength	195-690 MPa	70-140 MPa
Ultimate Tensile Strength	895-1900 MPa	895-1900 MPa
Elongation at Failure	Aprox. 25%	Aprox. 25%
Recoverable Strain	Up to 8%	Up to 8%
Poisson Ratio	0.33	0.33

manufacturing process, strain rate, and cyclic loading.

3.3.1 Alloy composition

A main factor that controls the mechanical properties of SMAs is its chemical composition (Birman, 1997 and Serneels, 1999). The chemical composition of the alloy affects directly the phase transformation temperatures, which plays an important role in defining the alloys mechanical properties. Table 3.2 presents a comparison between the transformation temperatures in the case of two Ni-Ti alloys. The two alloys were processed identically, however the Titanium percent in one of the alloys was 50% while in the other alloy was 51%. Although the difference in the alloy composition is relatively small, the table shows a large difference in the austenite and martensite transformation temperatures. These large differences would result in significant changes in the mechanical properties of the two alloys.

Research has shown that Ni-rich alloys are more vulnerable to changes in the transformation temperatures due to alloy composition (Serneels, 1999). The difference between the austenite and martensite finish temperatures A_f and M_f is often referred to as the hysteresis width and is used to describe the mechanical behavior of SMAs. For

Table 3.2 Effect of alloy composition on transformation temperatures in Ni-Ti alloy

Alloy	**Austenite**		**Martensite**	
	A_s (^{0}C)	A_f (^{0}C)	M_s (^{0}C)	M_f (^{0}C)
Ni-50%wt Ti	80	110	69	37
Ni-51%wt Ti	-89	-40	-114	-153

typical Ni-Ti alloys the hysteresis width varies between 30 ^{o}C and 40 ^{o}C. This hysteresis width could be reduced significantly by increasing the percentage of Nickel in the alloy. This phenomenon is supported by the results presented in Table 3.2, where the hysteresis width in the case of the Ni-50%wt Ti alloy is 73 ^{o}C, while in the case of the Ni-51%wt Ti, which are less in Nickel the hysteresis width increased to 113 ^{o}C.

Another example that illustrates the sensitivity of SMAs mechanical properties to the alloy composition is the one shown in Figure 3.7. Figure 3.7 shows a comparison between the mechanical behaviors of two Ni-Ti alloys with slight different composition. The figure illustrates that the alloy with larger percentage of nickel has higher yield strength and less hysteresis area. This behavior agrees with the argument presented in the previous paragraph.

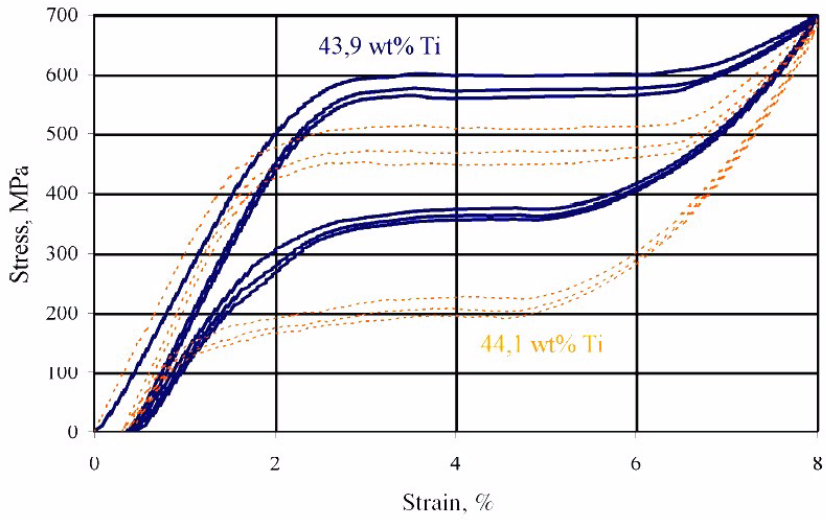

Figure 3.7 A comparison between the behavior of a 43,9 wt% Ti and a 44,1 wt% Ti Ni-Ti alloys (Serneel, 1999).

3.3.2 Manufacturing process

Research has shown that one of the main factors that influence the mechanical behavior of SMAs is the method used to process the alloy (Otsuka and Wayman, 1998). Figure 3.8 shows the stain-temperature curves of two alloys that were treated differently. One of the alloys was fully annealed while the other alloy was partially annealed. The two alloys were subjected to a thermal cyclic loading under a constant stress equal to 100 MPa. The partially annealed alloy was able to recover its original shape when the cycle is over, while the fully annealed alloy had a 1.5% residual strain. This shows that the level of annealing affects the shape memory effect capability.

The level of cold-working is another factor that could affect the mechanical behavior of SMAs. Figure 3.9 shows the effect of the cold work percentage that the alloy receives

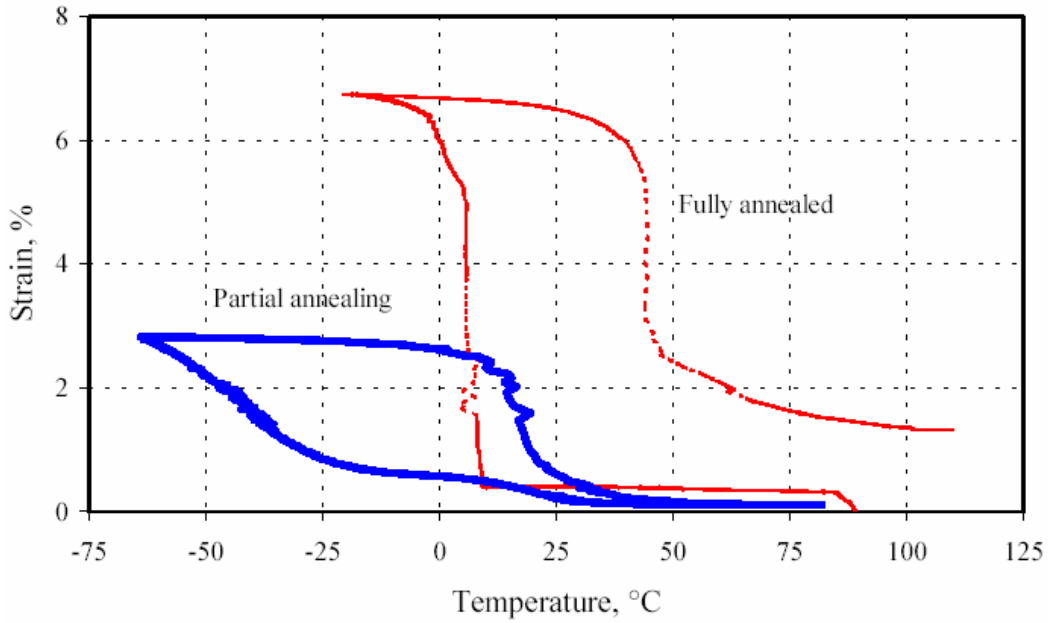

Figure 3.8 Comparison of the behavior of two alloys with different levels of annealing (Serneel, 1999).

on its austenite start temperature. It is noticed from the figure that more cold work tends to decrease the austenite start temperature by a value that depends on the treatment temperature. The effect of cold work on the austenite start temperature tends to minimize at higher levels of heat treatment temperature. Another example that illustrates the effect of cold work on the mechanical behavior of SMAs is shown in Figure 3.10. The figure shows a difference in the loading plateau associated with different levels of cold work. In this case, one of the alloys was treated with 46% of cold work while the other was treated with 36%. The figure shows that increasing the cold work by 10% resulted in elevating the plateau by approximately 9% and reducing the hysteresis area.

3.3.3 Strain rate

In order to better understand the capability of SMAs to withstand different types of dynamic loadings, many researchers (Dolce and Cardone 2001; Delemont 2002; and

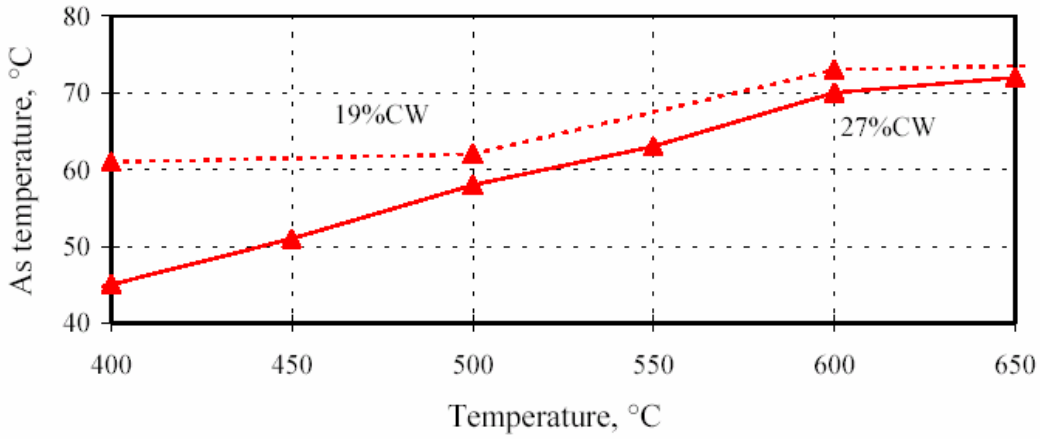

Figure 3.9 Effect of cold work on the phase transformation temperatures (Serneel, 1999).

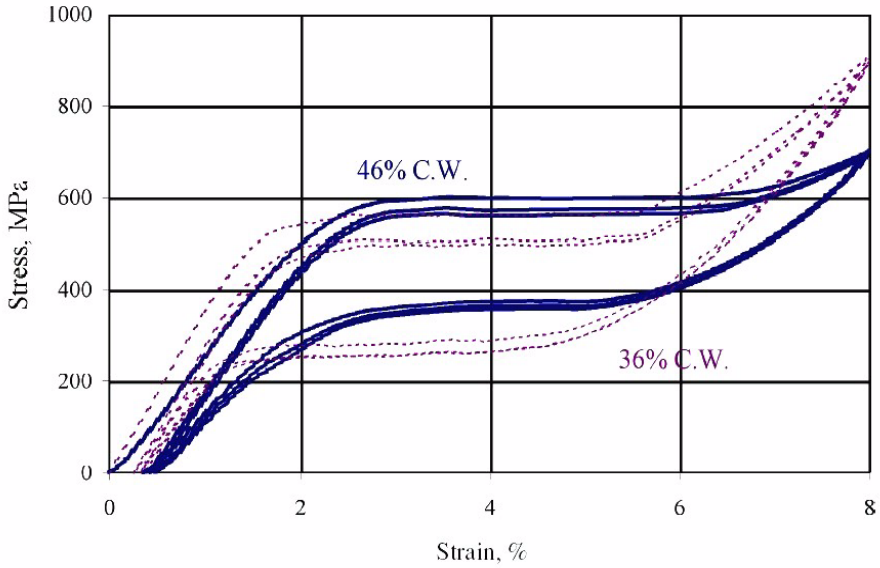

Figure 3.10 Effect of cold work on the loading plateau of an austenitic shape memory alloy (Serneel, 1999)

Tobushi et al. 1998) have focused their interest on studying the behavior of SMAs when subjected to dynamic loading with various strain rates. Most of the researchers agree that loading rate affects the mechanical behavior of the alloy (Graesser and Cozzarelli, 1991 and Dolce and Cardone, 2001). However, results varied from one reference to another (Delemont, 2002) on the extent of the effect, based on the range of strain rate that was used and type of alloy used.

In 2001 Dolce and Cardone conducted a series of experimental tests using Ni-Ti wires. The wires were tested under tensile loads with a strain rate that varied between 0.01 and 4 Hz. This range of frequency is considered sufficient to cover most of the dynamic applications in the area of civil engineering including structures subjected to earthquakes. Figure 3.11 shows part of the results of the study conducted by the two researchers. The figure shows the stress-strain curves in the case of testing the austenitic wires using 0.02 Hz, 0.2 Hz, and 2 Hz as strain rates for the cyclic load. As the rate of

loading is increased the loading and unloading plateau are shifted upwards. This shift is associated with a reduction in the hysteresis area. The authors found that the change in behavior tends to stabilize after a strain rate equal to 0.2 Hz, and no more significant changes in the stress-strain curve were noticed. On the other hand, Tobushi and his colleagues in 1998 conducted a series of experimental tests using strain rates that were smaller compared to Dolce and Cardone. Tobushi et al. found that at very small rates of loading, the stress-strain curves of the alloys are stable while at higher strain rates the

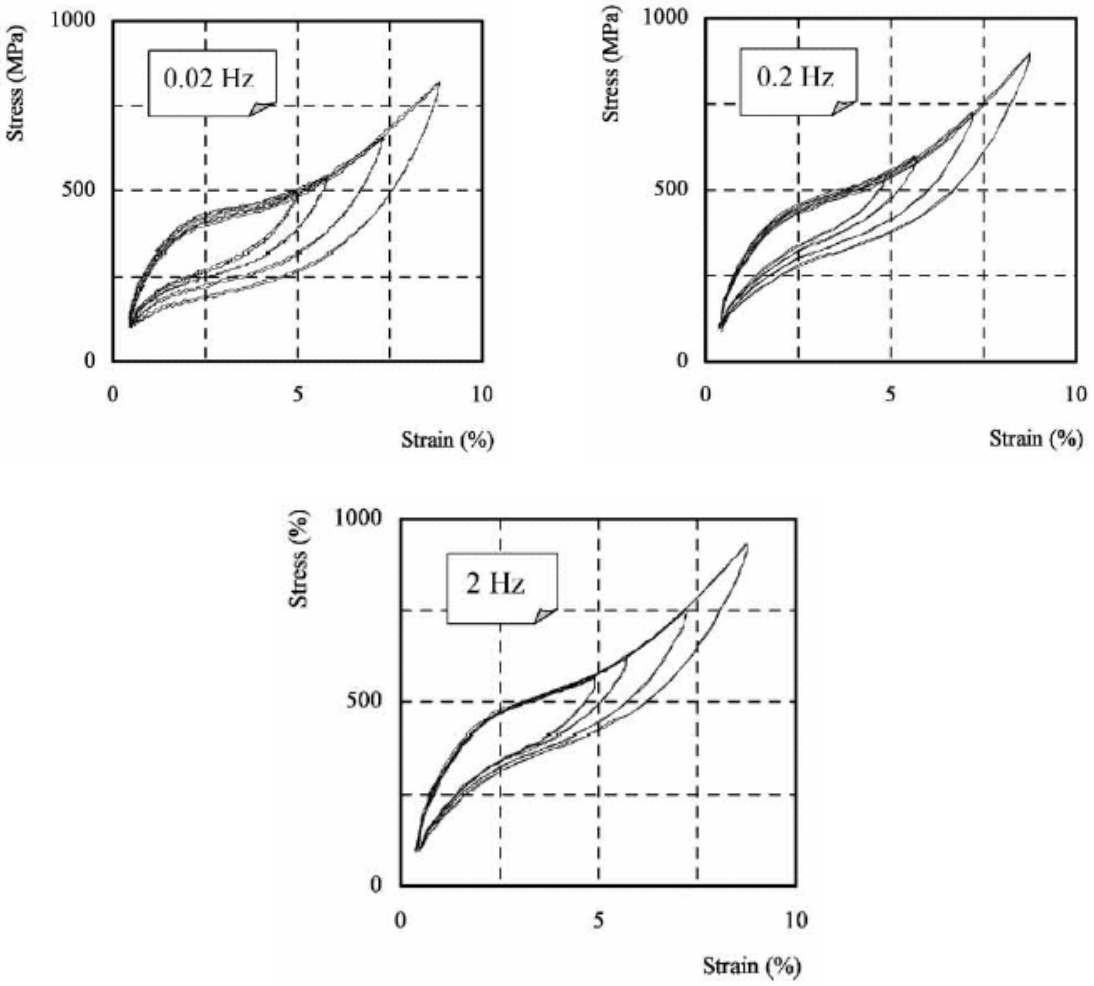

Figure 3.11 Stress-ctrain curves for austenite Ni-Ti alloy at 0.02 Hz, 0.2 Hz, and 2.0 Hz strain rates (Dolce and Cardone, 2001).

martensitic phase transformation is increased.

Most of the researchers agreed that the reason for such change in the material mechanical behavior at higher strain rates is the fact the material releases heat during the martensitic transformation and absorbs heart in the reverse transformation. If the strain rate is high, there will not be enough time for the material to transfer or absorb heat from the surrounding environment and this might lead to self-heating of the material, which results in changing the mechanical characteristics of the alloy (Wu, 1996 and Dolce and Cardone, 2001).

3.3.4 Cyclic loading

The subject of cyclic loading effect on SMAs mechanical behavior has been studied by a large number of researchers and most of them agreed that the changes in the mechanical properties that are associated with the cyclic loading in SMAs are mainly referred to the formulation of residual martensite, which accumulates with each cycle. This residual martensite is permanent martensite and thus never participates in proceeding phase transformation cycles (Tanaka et al., 1995).

Experiments have shown that SMAs experience change in their mechanical properties when subjected to cyclic loading. The repeated phase transformation that the SMA experience under cyclic loading results in a reduction in the stress required for forward transformation, a reduction in the area of hysteresis loops, and an increase in the residual strain (Tobushi et al., 1996; Friend and Morgan, 1999; Gall and Sehitoglu, 1999). Figure 3.12 shows the effect of cyclic loading with increasing the number of cycles (N) for a Ti-50.2at% Ni specimen. The alloy presented in the figure was lightly

annealed at 400 ^{o}C for 20 minutes. As shown in the figure, an increase in the number of cycles, results in the loading plateau shifting downwards more than the unloading plateau. This behavior leads to a reduction in the hysteresis area, and thus a reduction in the damping capability. Friend and Morgan believe that the sensitivity of the SMA to the cyclic loading is influenced by the treatment that the alloy receives during processing. They support their argument by an example presented in Figure 3.13. The figure shows the effect of cyclic loading on a Ti-50.5at% Ni alloy that was tested at different environmental temperatures. It is clear from the figure that the alloy's mechanical behavior is dramatically affected by the cyclic loading and the behavior requires additional cycles in order to stabilize compared to the alloy shown in Figure 3.12.

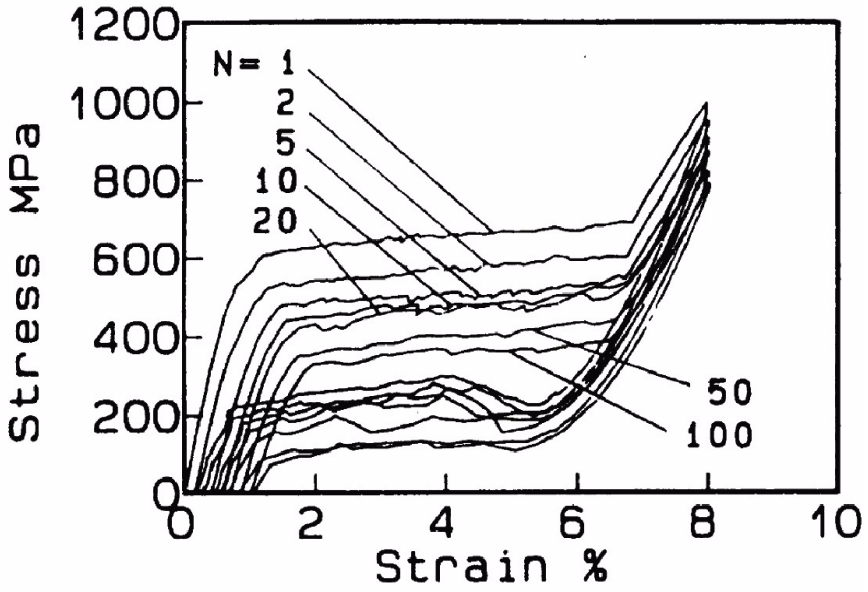

Figure 3.12 Cyclic loading effect on the stress-strain behavior of Ti-50.2at% Ni alloy annealed at 400 ^{o}C for 20 minutes (Friend and Morgan, 1999).

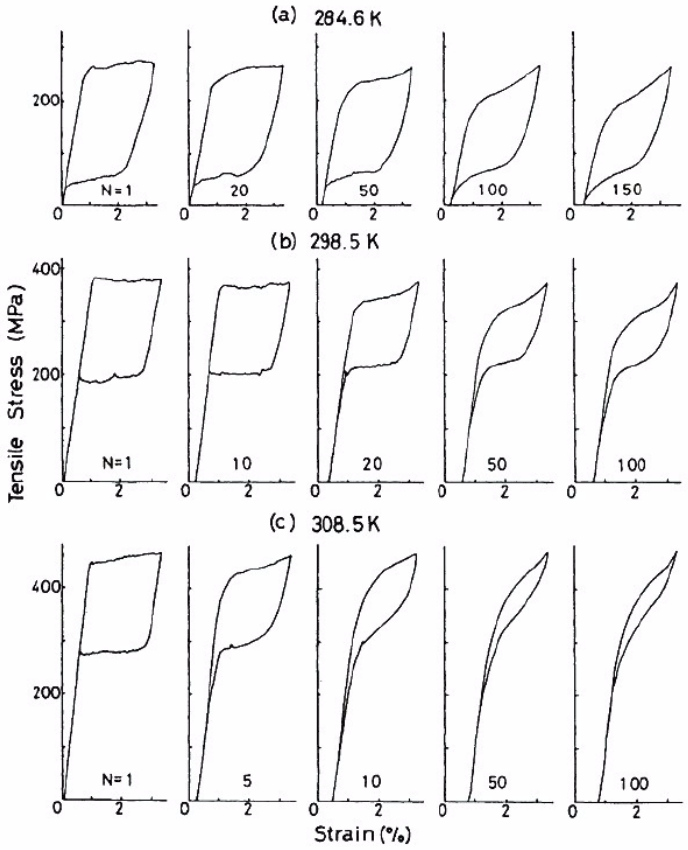

Figure 3.13 Cyclic loading effect on the stress-strain behavior of Ti-50.5at% Ni alloy annealed at 1000 ^{o}C for 1 hour (Friend and Morgan, 1999).

CHAPTER 4

MODELING OF SHAPE MEMORY ALLOYS

4.1 Introduction

Engineers and researchers use modeling as a quantitative tool that could be used in estimating the response of complex materials implemented in various systems. It is important to develop analytical models for SMAs to be able assess their effect on the response of different structures. The past two decades have witnessed the development of several models that have been used for describing the constitutive (stress-strain) behavior of SMAs. Those models could be divided into two main groups: phenomenological models and micromechanical models. The phenomenological constitutive models are based on the macroscale extensions of transformation thermodynamics (Lim, 1999). The function of such models is to reproduce a specific phenomenon with out describing the microstrcutural behavior behind such phenomenon. This makes the phenomenological modeling the simplest type of modeling. On the other hand, micromechanical models are a more complicated type of constitutive models. In such models, the crystallographic data and the micromechanics is used to estimate the behavior of the material. Figure 4.1 illustrates the macroscale and the microscale levels that are considered in developing SMA models. The following sections of this chapter introduce an overview of the research that has been conducted in the past two decades in developing phenomenological and micromechanical models for SMAs.

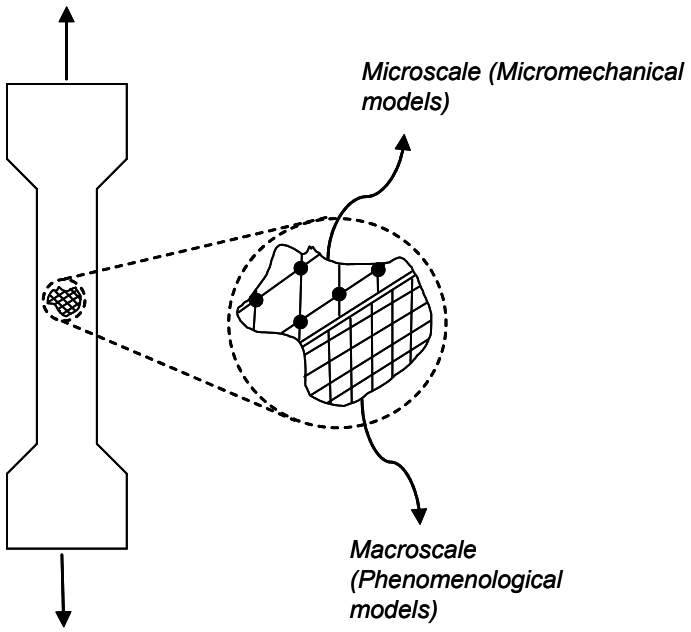

Figure 4.1 Different levels of scaling that are used to develop SMA models.

4.2 Overview of Phenomenological Models

4.2.1 Experimental-Based Models

The simplest type of phenomenological models is the experimental-based model. This type of phenomenological model is based on predicting the mechanical properties of the SMAs such as the Young's modulus and the phase transformation stress from experimental data. This type of model does not depend on the thermomechanical or microstructural behavior of the SMAs. Figure 4.2 shows an attempt at predicting the SMA hysteresis through the curve fitting of experimental data. As shown on the figure, the loading and unloading paths are predefined based on the experimental results. An example for this type of modeling is the model developed by DesRoches and Delemont (2002). This model was developed through combining a group of link and truss elements

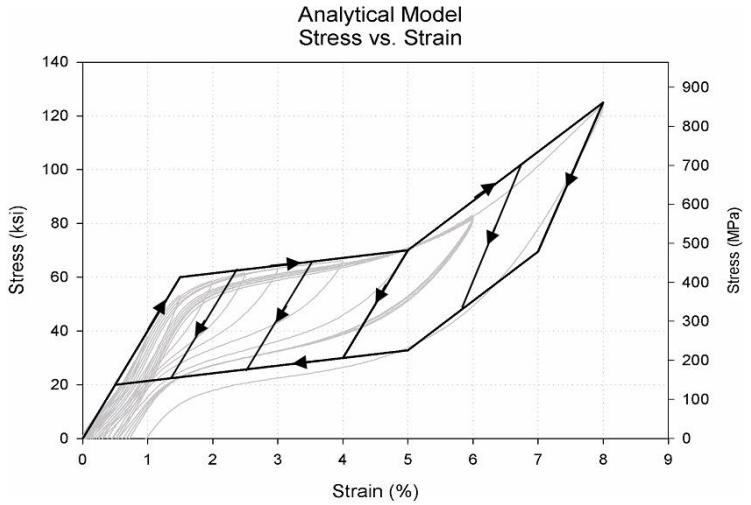

Figure 4.2 Predicting the mechanical properties of SMAs through curve fitting experimental data.

on parallel using the nonlinear finite element program Drain-2DX.

4.2.2 Thermomechanical-Based Models

In this type of model, the constitutive behavior of SMAs is described through the thermomechanical behavior of the material. This makes that type of phenomenological model more complicated than the experimental-based models discussed in the previous section. This is due to the fact that in order for the model to describe the behavior of the SMAs accurately, a number of material constants have to be defined first. These material constants are obtained from experimental tests, and vary in number based on the complexity of the model.

The thermomechanical-based phenomenological model are often referred to as the internal state variable models, where a specific variable is used to describe the phase transformation in the SMAs from austenite to martensite and vise versa. In most of the

models that have been developed recently, this internal state variable is defined as the martensitic fraction, which describes the percentage of martensite in the alloy. The martensitic fraction is usually affected by either thermal or mechanical type of loading, thus it has the capability of describing the formulation of martensite in the alloy due to temperature variation or stress variation.

Starting from early 1980's until now, a large number of research studies had been conducted to develop thermomechanical-based constitutive models for SMAs that are capable of describing their constitutive behavior under various loading conditions. One of the first models developed to describe the process of solid-solid phase transition was the model developed by Tanaka and Nagaki (1982). In this model, Tanaka and Nagaki used a continuum mechanics approach to describe such transition. The main concept of Tanaka's approach was based on the fact that phase transformation is basically governed by the minimization of the free energy. In this model, Tanaka used the energy equation (first law of thermodynamics) and the Clausius-Duhem inequality (second law of the thermodynamics) as governing equations. Three different internal state variables were used to characterize the material. Two of the internal state variables were used to specify the crystallographic structural change during the plastic deformation, while the third internal state variable describes the extent of phase transition.

Tanaka and Iwasaki later developed a model (Tanaka and Iwasaki, 1985) that focuses more on describing the phenomenon of superelasticity transformation. In this model, the deformation gradient tensor and the entropy density were decomposed to elastic and superelastic parts, neglecting the plastic deformation, which was assumed to have small participation in the irreversible deformation compared to the superelastic

deformation. A single quantity representing a set of scalar internal variables was used to characterize the extent of phase transformation. In 1986, Tanaka modified his model by using an exponential expression for the only internal state variable used in the model, which represents the martensite fraction. Tanaka's model was tested under uniaxial tensile loading condition at different temperature levels, and the model was able to capture the superelastic and shape memory effect behaviors.

Unlike Tanaka's model, in which he used an exponential function to describe the martensite fraction, Liang and Rogers (1990) selected a cosine function to describe the variable. Using the cosine function improved the performance of the model since a martensite fraction value of one or zero would not cause singularity, as it did in Tanaka's model. In 1992 Liang and Rogers expanded their model to account for multi-dimensional behavior of SMAs. Later, Brinson and Lammering (1993) developed a one dimensional finite element model describing the SMA material behavior. Brinson and Lammering used the same constitutive relations used by Tanaka and Liang in their models. Brinson also subdivided the martensitic fraction into two components corresponding to the temperature-induced and stress-induced martensites. In this model the material parameters were assumed to vary linearly with the martensite fraction, this assumption might not be accurate for some particular alloys.

Another approach to create a SMA thermodynamical constitutive model was developed by Boyd and Lagoudas (1994). In this model Boyd and Lagoudas included the effect of phase orientation in studying pseudoelasticity in addition to the phase transformation previously considered by Tanaka and Liang. Boyd and Lagoudas used the same decomposition procedure used by Tanaka and Nagaki.

Kamita and Matsuzaki (1998) used an energy approach from a thermodynamical prospective to describe the phase transformation in SMAs. They introduced the interaction energy as the energy dissipated during the phase transformation. They suggested that the thermodynamic driving force for the phase transformation could be derived form the partial derivative of the interaction energy with respect to the martensitic fraction. Kamita and Matsuzaki were also able to capture the sublooping behavior in their model, which results from incomplete phase transformation cycles.

4.3 Overview of Micromechanical Models

Micromechanical constitutive models are a class of models that are more complex compared with the phenomenological models. In the micromechanical models, the crystallographic data and micromechanics theory is used to estimate the interaction energy which is necessary to calculate the evolution of martensitic transformation (Lim, 1999). In micromechanical models, it is important to relate the macroscopic behavior of the material to its microstructural state. In the special case of thermoelastic martensitic transformation, only two microstructural mechanisms could exist. The first mechanism is the reversible formation of martensite variants from the parent (Austenitic) phase, while the second mechanism is the interfacial motion between the different martensite variants (Patoor et al., 1988). In a three dimensional model, the 24 martensite variants resulting from the Austenite phase have to be considered. In the case of one dimensional model, most of the 24 martensite variants are eliminated and only 2 twin variants are remaining (M- and M+).

Falk (1983) developed one of the early qualitative micromechanical models for SMAs. His model was a one dimensional model that was restricted to single crystals. Falk constructed a Helmholtz free energy function as a function in the strain and temperature. This function describes the behavior of SMAs in its different phases (M-, M+, and A). All of the thermomechanical functions such as entropy and Gibbs free energy could be derived directly from this energy function.

Patoor (1988) and his colleagues studied the behavior of both single crystal and polycrystal SMAs during stress-induced thermoelastic martensitic transformation. Patoor considered only the reversible formation of martensite variants from the austenitc phase, and neglected the motion between different martensitic variables. In this model, Patoor developed an expression for the variation in Gibbs free energy based on the transformation strain rate. At equilibrium this variation in the Gibbs free energy should be zero. Patoor tested the expression he got for a single crystal and it showed a good agreement with the experimental results. Five years later, Sun and Hwang (1993) expressed the direct phase transformation and reorientation of variants using the variation in the free energy, which is divided into energy due to applied stress, temperature and microstructural variables such as transformation or reorientation volume fraction, lattice deformation and interface friction. Rengarajan and his colleagues (1998) continued on the work of Sun and Hwang by developing a finite element model using the same constitutive equations used by Sun and Hwang.

4.4 Cyclic Loading Effect

All of the previously presented constitutive models were tested only under monotonic loading. Since the main focus of this research is to study the behavior of SMAs under seismic loading, it was necessary to give an overview of the past studies that mainly focused on the effect of cyclic loading on the modeling of SMAs.

Most of the constitutive models that were developed to consider the effect of cyclic loading are phenomenological models. This was due to the severe lack of quantitative information on the micromechanics of fatigue in addition to the absence of a solid theoretical foundation on describing the fatigue mechanism in SMAs (Gall et al., 2000). In 1995, Tanaka and his colleagues presented a phenomenological model the takes into account the cyclic behavior of the SMAs. Tanaka's model showed the capability of capturing the hysteretic degradation and the residual strain associated with the cyclic loading. The model was also able to describe the behavior of SMAs in the case of incomplete cycles through hysteretic subloops. A more detailed description of Tanaka's model is presented later in this chapter.

Lagoudas and Bo (1995) studied the cyclic loading effect on SMAs from a thermodynamical perspective. They extended the work that was conducted in 1994 to include an expression for the plastic deformation associated with the cyclic loading. Their model was also able to capture the two way shape memory effect (TWSME) resulting from applying thermal training on the martensite SMA. The TWSME allows the SMA to remember not only its parental austenite shape but also the deformed martensite shape, which could be restored by cooling austenite SMA.

The model that was presented by Lexcellent and Bourbon (1996) showed a good agreement with the experimental results. Lexcellent and Bourbon used the residual martensite volume fraction as an internal state variable and modified the free energy expression accordingly. They only studied the cyclic effect in the pseudoelastic temperature range.

4.5 Sensitivity of Seismic Applications to SMA Models

The previous four sections of this chapter have shown that there are different levels of complexity that could be considered when developing an analytical model to describe the constitutive behavior of SMAs. In order to understand the level of complexity required for SMA models used in seismic applications to achieve a certain level of accuracy, three SMA models are investigated in this chapter. The models include: a simplified model, which represents the experimental-based type of model, a thermomechanical model, which takes into account the stress-strain-temperature relationship in SMAs, and a thermomechanical model that considers also the cyclic loading effects in SMAs. Each of the three models is implemented and tested in a SDOF structure under various loading conditions. The following two subsections will describe the analytical models used in the study.

4.5.1 Simplified Model

A one dimensional experimental-based superelastic phenomenological model was developed to represent the simplest family of SMA constitutive models that could be used in seismic applications. The model is considered an experiment-based model since

the hysteretic properties of the model are predefined and they are independent of the thermomechanical properties of the SMA. The model was developed in a MATLAB framework, since the rest of the study in this chapter is performed using MATLAB. Figure 4.3 shows a schematic of the force-deformation relationship resulting from the simplified model. The figure also shows the parameters required to define the behavior of the model. These parameters include: austenite elastic stiffness (K_A), marteniste elastic stiffness (K_M), phase transformation starting force (F_s), phase transformation finishing force (F_f), the strain hardening ratio during martensitic transformation (S_M), and the unloading force at the end of the reverse transformation (F_u). In this model, the strain at the start and the end of the phase transformation were fixed and were taken equal to 1% and 6%, respectively.

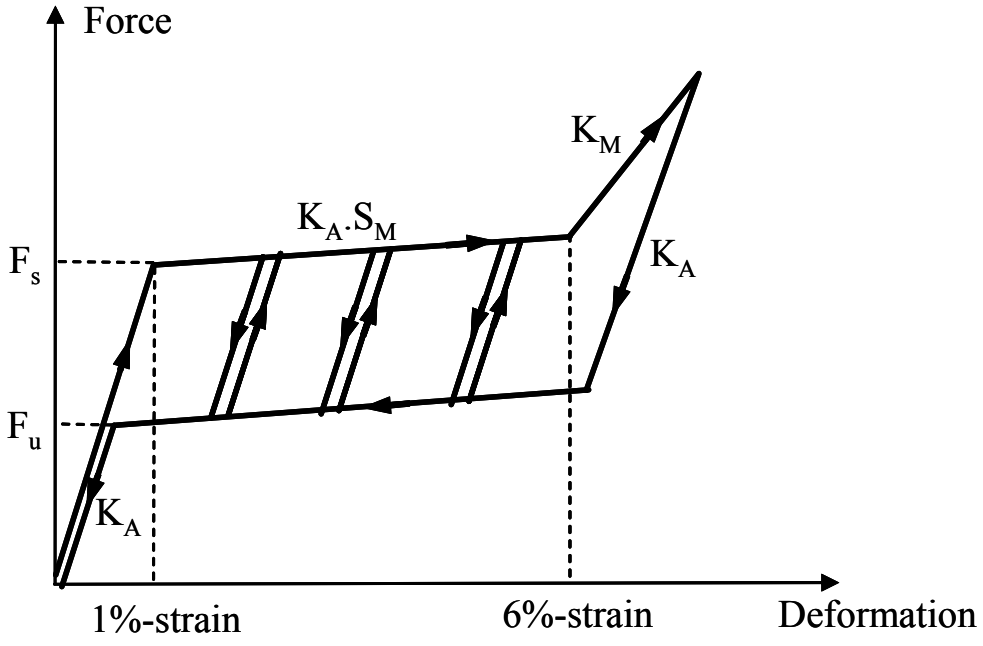

Figure 4.3 Force-deformation relationship of the simplified superelastic SMA model

4.5.2 Thermomechanical Model

A thermomechanical model was developed based on the work of Tanaka and others (1995). This model is characterized by its ability to capture the cyclic loading effects on SMAs in addition to the sublooping behavior resulting from incomplete phase transformation cycles. In this model, Tanaka presents a macroscopic theoretical frame-work to explain the hysteretic behavior of shape memory alloys during thermal and/or mechanical cyclic loadings. Three internal variables were presented in the model. The local stress and strain and the residual martensitic phase accumulated irreversibly due to the cyclic forward/reverse martensitic transformation. From Tanaka's previous work (Tanaka, 1986; Tanaka 1990; Fischer and Tanaka 1992), it was shown that the uniaxial thermomechanical behavior of SMAs could be described by the constitutive relation consisting of the following equation in rate form:

$$\dot{\sigma} = D\dot{\varepsilon} + \Theta\dot{T} + \Omega\dot{\xi} \tag{4.1}$$

where σ, ε, and T are the stress, strain and temperature respectively, D is Young's modulus and $-\Theta / D$ and $-\Omega / D$ are the coefficient of linear expansion and the strain due to transformation, respectively. ξ denotes the volume fraction of the martensite phase. The transformation kinetics in the case of martensitic transformation is described by the following relation:

$$\frac{\dot{\xi}}{1-\xi} = b_M c_M \dot{T} - b_M \dot{\sigma} \geq 0 \tag{4.2}$$

while in the case of reverse transformation the relation is:

$$-\frac{\dot{\xi}}{\xi} = b_A c_A \dot{T} - b_A \dot{\sigma} \geq 0 \tag{4.3}$$

The terms c_M, and c_A are material parameters that can be determined experimentally, while b_M and b_A are material parameters, which will be calculated later. By integrating equations 4.2 and 4.3 we can obtain the following expressions for the transformation kinetics in forward and reverse transformations, respectively:

$$\xi = 1 - \xi_{A0} \exp[b_M c_M (\mu(\xi_{A0}) - T) + b_M \sigma] \tag{4.4}$$

$$\xi = \xi_{M0} \exp[b_A c_A (\alpha(\xi_{M0}) - T) + b_A \sigma] \tag{4.5}$$

where ξ_{A0} and ξ_{M0} are the volume fraction residual austenite and martensite, respectively. Both volume fractions are related to each other with the relation, $\xi_{A0} + \xi_{M0} = 1$. $\mu(\xi_{A0})$ and $\alpha(\xi_{M0})$ are the martensitic and austenitic start transformation temperatures, respectively, and are assumed to be related to the residual austenite and martensite. In the case of Ni-Ti alloys, researchers have found that $\mu(\xi_{A0})$ and $\alpha(\xi_{M0})$ could be taken as the martensite start temperature (M_s) and the austenite start temperature (A_s), respectively. Using equations 4.4 and 4.5, the parameters b_M and b_A can be determined as follows:

$$b_M = \frac{\ln(100\xi_{A0})}{c_M(M_f - \mu(\xi_{A0}))} \tag{4.6}$$

$$b_A = \frac{\ln(100\xi_{M0})}{c_A(A_f - \mu(\xi_{M0}))} \tag{4.7}$$

In order to take into account the effect of residual stress accumulated during cyclic loading, Tanaka introduced three internal variables. Those variables were the residual stress, σ_{ir}, corresponding residual strain, ε_{ir}, and the macroscopic volume fraction of the martensite phase, ξ_{ir}. This martensite is understood not to take part in the subsequent transformations. The stress σ and strain ε now must be understood as local values as follows:

$$\sigma = \Sigma + \sigma_{ir} \tag{4.8}$$

$$\varepsilon = E - \varepsilon_{ir} \tag{4.9}$$

where $\sum$ and E are the global stress and strain respectively. Figure 4.4 shows a schematic drawing that illustrates the relation between local stress σ and global stress $\sum$ with the number of cycles. Assuming all material parameters to be constant, the residual stress could be expressed as:

$$\sigma_{ir} = S[1 - \exp(-\tau / \upsilon)] \tag{4.10}$$

where S is a material parameter, υ is a parameter that governs the speed of the accumulation, and τ is the intrinsic time, which flows only when the transformations take place. In order to exclude the local martensite from subsequent transformations, the

residual martensite phase due to local residual stress for simplicity was given the formula:

$$\dot{\xi}_{ir} = \Psi \dot{\sigma}_{ir} \tag{4.11}$$

where Ψ is a material parameter.

Tanaka and his colleagues tested the model numerically by applying cyclical loading between 0 and 120 Mpa on a specimen made of Cu-based polycrystalline alloy. Figure 4.4 shows the stress-strain hysteresis in the alloy. As it is shown in the figure, the hysteresis loop shifts with the number of cycles and tends gradually to a limit stationary loop.

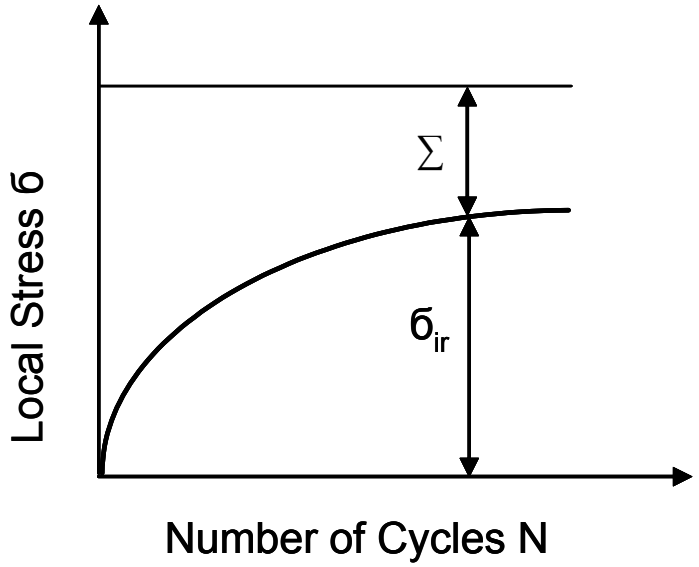

Figure 4.4 Accumulation of residual stress ($б_{ir}$) during the application of cycling loading on the SMA model developed by Tanaka et al. (Tanaka et al., 1995)

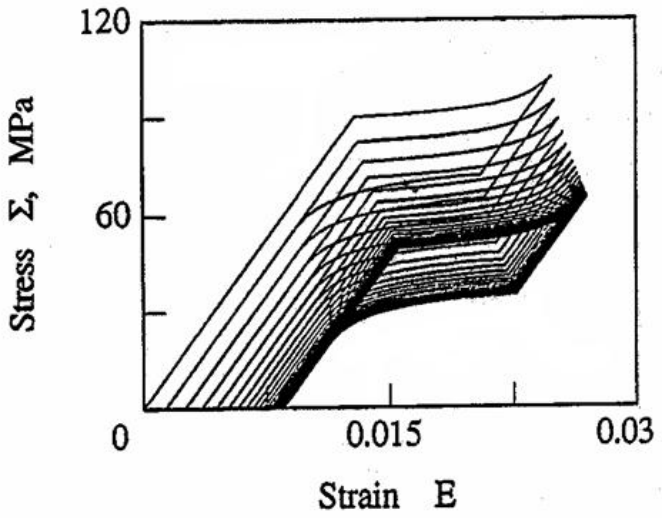

Figure 4.5 Stress-strain hysteresis during cyclic loading for the thermodynamical superelastic SMA model developed by Tanaka et al. (Tanaka et al., 1995)

4.5.3 SDOF Analytical Model

A single degree of freedom (SDOF) stick-mass model is developed using MATLAB for the purpose of comparing the three SMA models under seismic loading. Figure 4.6 shows a schematic of the analytical model used in this study. The model consists of a single mass, m, a restoring force element with an initial stiffness, k, a dashpot that

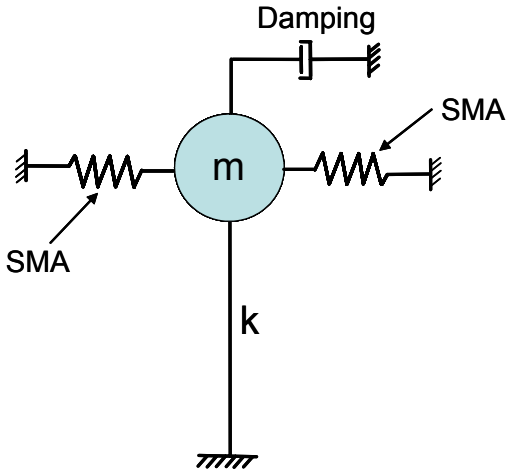

Figure 4.6 Schematic of the SDOF model used in the study.

incorporates the viscous damping, and a two identical tension-only SMA links. The two SMA links are used in this study as an alternative for using a tension-compression link since the mechanical properties of SMAs under compression and tension are not consistent. The SDOF model was governed by the following equation of motion:

$$m\ddot{x} + c\dot{x} + f_r(x,\dot{x}) + f_{sma}(x,\dot{x}) = -m\ddot{x}_g(t) \tag{4.12}$$

where m is the mass of the structure, c is the damping coefficient, x is the displacement, $\dot{x}$ is the velocity, $\ddot{x}$ is the acceleration, $\ddot{x}_g(t)$ is the input ground acceleration, f_r is the restoring force of the structure, and f_{sma} is the restoring force of the SMA links. In order to account for the nonlinearity in the response of the structure f_r and f_{sma} are assumed to be dependent on the structural displacement, x and structural velocity, $\dot{x}$.

The equation of motion was solved numerically using Newmark's method (Chopra,1995). An average acceleration was assumed during each time step (the parameter β was taken equal to ¼). In order to consider the nonlinearity in the structure, the Newton-Raphson method was utilized to perform the iterations on the tangential stiffness of the structure. After each iteration, the residual force is calculated using the following equation:

$$f_{res_i} = -\ddot{x}_{g_i} m - \ddot{x}_i m - \dot{x}_i c - f_{r_i} - f_{sma_i} \tag{4.13}$$

where i is the number of iteration, f_{res_i} is the residual force at the end of the iteration i, $\ddot{x}_{g_i}$ is the ground acceleration at the end of the iteration i, $\ddot{x}_i$ is the structural acceleration

at the end of the iteration i, $\dot{x}_i$ is the structural velocity at the end of the iteration i, f_{r_i} is the structural restoring force at the end of the iteration i, f_{sma_i} is the SMA restoring force at the end of the iteration i, m is the structural mass, and c is the structural damping coefficient. The analysis at a specific time step was considered to be converged if the residual force (f_{res}) was less than a tolerance value that was calculated form the following equation:

$$tol. = 10^{-6} \times \left[\max |\ddot{x}_g(t)| \times m \right] \tag{4.14}$$

Equation 4.14 shows that the tolerance considered in this study depends on the input ground acceleration and mass.

Since the focus of this research is to study reinforced concrete bridges, the Q-hyst model was selected to describe the nonlinear behavior of the structure. The Q-hyst model is an analytical model that was developed to describe the stiffness/strength degradation in the response of reinforced concrete members under cyclic loading. Figure 4.7 shows a schematic of the Q-hyst model force-deformation relationship. As shown in the figure, in the post-yield stage the structure unloads with an unloading stiffness equal to:

$$K_u = K\left(\frac{D_y}{D}\right)^{0.5} \tag{4.15}$$

where K_u is the unloading stiffness, K is the initial stiffness, D_y is the yield displacement, and D is the maximum displacement experienced at either sides. The stiffness of the load-reversal stage is taken equal to the slope of the line joining the unloading branch-

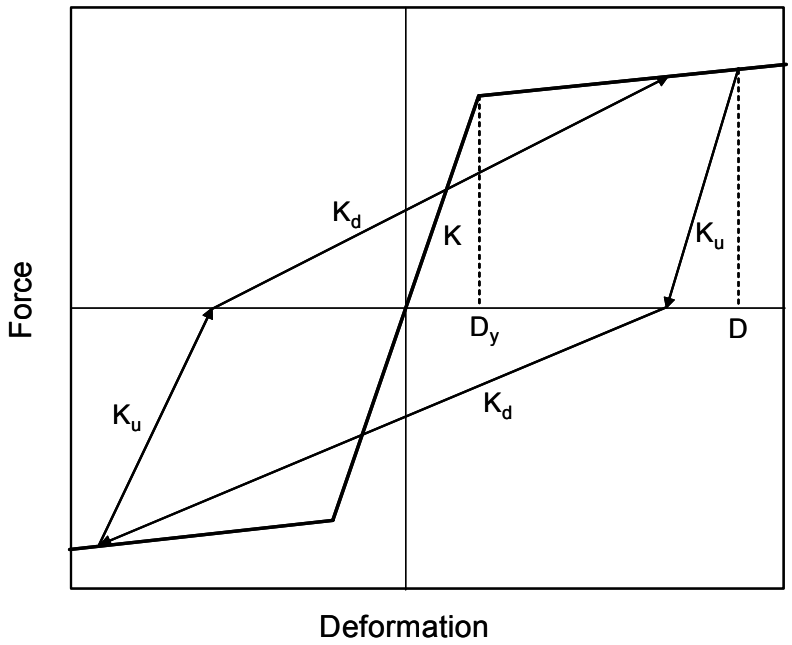

4.7 Q-hyst model used to describe the nonlinear behavior of the SDOF model.

deformation axis intersection point and the point on the curve corresponding to maximum displacement experienced at either sides (Saiidi, 1982).

4.5.4 Ground Motions

One of the main goals of this study was to explore the sensitivity of SMA models to ground motion characteristics. As previously discussed in this chapter, part of the difference between the three SMA models that are considered for this study is due to considering the incomplete loading cycles and the strength degradation/residual deformation resulting from cyclic loading. As a result, the number and intensity of the cycles that the SMA model goes through plays an important role in defining the behavior of the model. The duration of the ground motions was considered to be one of the main parameters controlling the number of cycles in each ground motion and thus affecting the

behavior of SMA models. Thus the effect of long/short duration ground motions is investigated in this study. The number of large-intensity cycles is also included by considering the near-field ground motion records, which in this study are considered to be less than 5 km from the epicenter. This type of ground motion normally contains high frequency components and cycles with relatively large intensity.

For the purpose discussed earlier, three suites (A, B, and C) of ground motion records were selected from past events and used in this study. Each of which consisted of 15 records. The three groups of ground motion records represented records of different parameters. Suites A and B represented far-field records with long and short durations, respectively. The duration of each record was defined as the time interval between the first and last exceedance of the ground acceleration time history to an acceleration threshold of 0.05g. A duration greater than 14 seconds was assumed to define the long and short duration. Table 4.1 shows the locations and characteristics of suites A and B ground motion records along with their durations that were calculated using the 0.05g threshold definition. Suite C consisted of 15 records that are characterized by being measured at stations near the earthquake fault. Suite C ground motion records are presented in Table 4.2. The acceleration response spectrum for each ground motion and the average response spectrum for each group of records were calculated and presented in Figures 4.8, 4.9, and 4.10 for groups A, B, and C, respectively. The average response spectra for the three ground motion groups were compared together in Figure 4.11. It is noticed from the figure, that above the 0.5sec-period the mean spectral acceleration curve for group A fit in between the other two curves.

Table 4.1 Ground motion records of suites A and B

Record	Magnitude	Distance (km)	PGA (g)	Duration (sec.)
Group A (Long duration)				
1989 Loma Prieta, UCSC Lick Observatory	6.9	7.9	0.45	15.1
1978 Tabas, Iran, 9102 Dayhook	7.4	17	0.328	19.6
1995 Kobe, Kobe City	6.9	11.1	0.509	16.5
1992 Cape Mendocino, Rio Dell Overpass	7.1	18.5	0.549	17.5
1994 Northridge, Centinela St.	6.7	30.9	0.465	14.5
1986 Chalfant Valley, Zack Brothers Ranch	6.2	18.7	0.447	16
1992 Landers, Coolwater	7.3	21.2	0.417	18.5
1994 Northridge, Tarzana, Cedar Hill	6.7	17.5	0.99	30.2
1992 Cape Mendocino, Petrolia	7.1	9.5	0.662	20.7
1971 San Fernando, Castaic-Old Ridge Route	6.6	24.9	0.324	15
1992 Cape Mendocino, cape Mendocino	7.1	8.5	1.497	19.2
1989 Loma Prieta, WAHO	6.9	16.9	0.638	20.7
1999 Duzce, Turkey, Bolu	7.1	17.6	0.822	18
1979 Imperial Valley, Cucapah	6.5	23.6	0.309	18
1992 Cape Mendocino, Petrolia	7.1	9.5	0.590	20.2
Group B (Short duration)				
1994 Northridge, Baverly Hills	6.7	20.8	0.617	13
1987 Whittier Narrows, Cedar Hill	6.0	43	0.644	12.7
1986 N. Palm Springs North Palm Springs	6.0	8.2	0.694	8.3
1976 Friuli, 8014 Forgaria Cornino	5.7	13.5	0.260	4.7
1979 Imperial Valley, SAHOP Casa Flores	6.5	11.1	0.506	12.2
1989 Loma Prieta, Gilroy Array #3	6.9	14.4	0.555	10
1989 Loma Prieta, Intern. Airport	6.9	64.4	0.329	13
1983 Coalinga, Pleasant Valley	5.8	17.4	0.602	7.4
1983 Coalinga, Transmitter Hill	5.8	9.2	0.840	7.6
1987 Whittier Narrows, Downey Birchdale	6.0	56.8	0.299	7.5
1986 Chalfant Valley, Bishop LADWP-South St.	6.2	9.2	0.248	10.8
1985 Nahanni, Canada	6.8	6.0	1.096	13.1
1980 Victoria, Mexico	6.4	34.8	0.621	13.3
1986 Chalfant Valley, Benton	6.2	37.2	0.209	10.2
1981 Westmorland, Fire sta.	5.8	13.3	0.368	10.6

Table 4.2 Ground motion records of suite C

Record	Magnitude	Distance (km)	PGA (g)
1980 LiveMore	5.4	3.6	0.258
1984 Morgan Hill, Anderson Dam	6.2	2.6	0.423
1971 San Fernando, Pacoima Dam	6.6	2.8	1.16
1966 Parkfield, Cholame #2	6.1	0.1	0.476
1979 Imperial Valley, EC Meloland Overpass	6.5	0.5	0.314
1984 Morgan Hill, Coyote Lake Dam	6.2	0.1	1.298
1979 Imperial Valley, Bonds Corner	6.5	2.5	0.588
1995 Kobe, KJMA	6.9	0.6	0.821
1979 Coyote Lake, Gilroy #6	5.7	3.1	0.434
1995 Kobe, Takatori	6.9	0.3	0.611
1994 Northridge, LA Dam	6.7	2.6	0.511
1987 Superstitn Hills(B), Parachute Test Site	6.7	0.7	0.377
1979 Imperial Valley,ElCentro, Array#8	6.5	3.8	0.602
1999 Chi-Chi, Taiwan	7.6	0.24	0.419
1992 Erzincan, Turkey	6.9	2.0	0.515

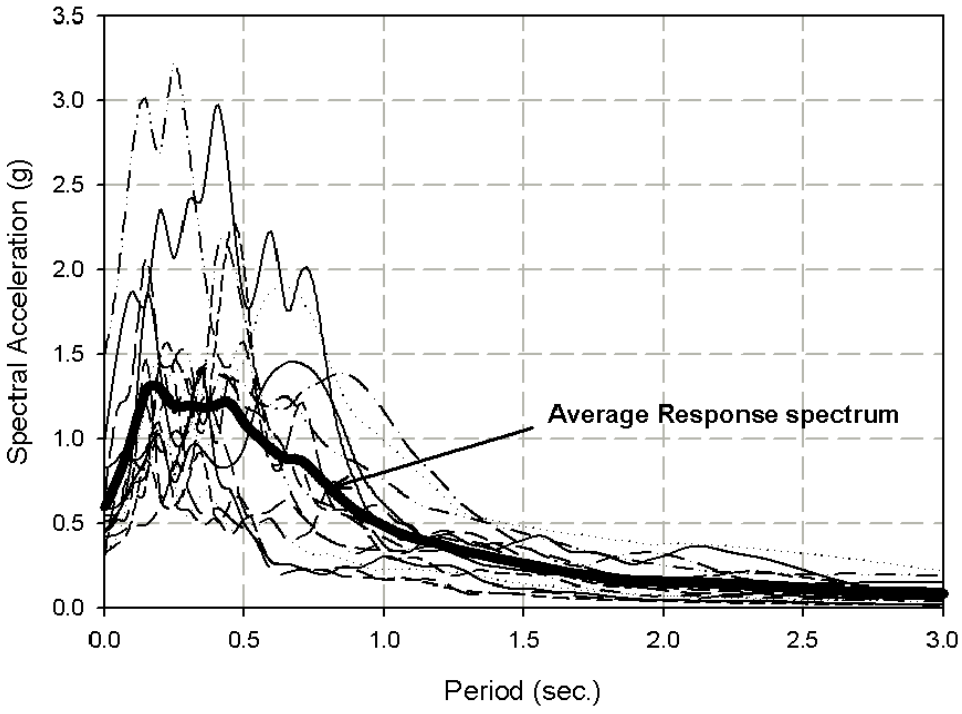

Figure 4.8 Response spectra and average response spectrum (Solid-thick) for suite A

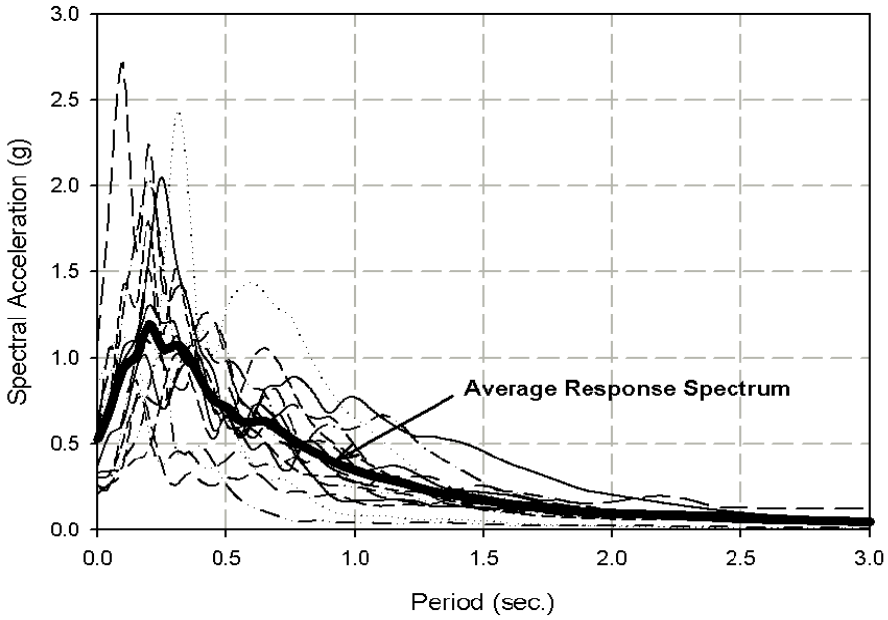

Figure 4.9 Response spectra and average response spectrum (Solid-thick) for suite B

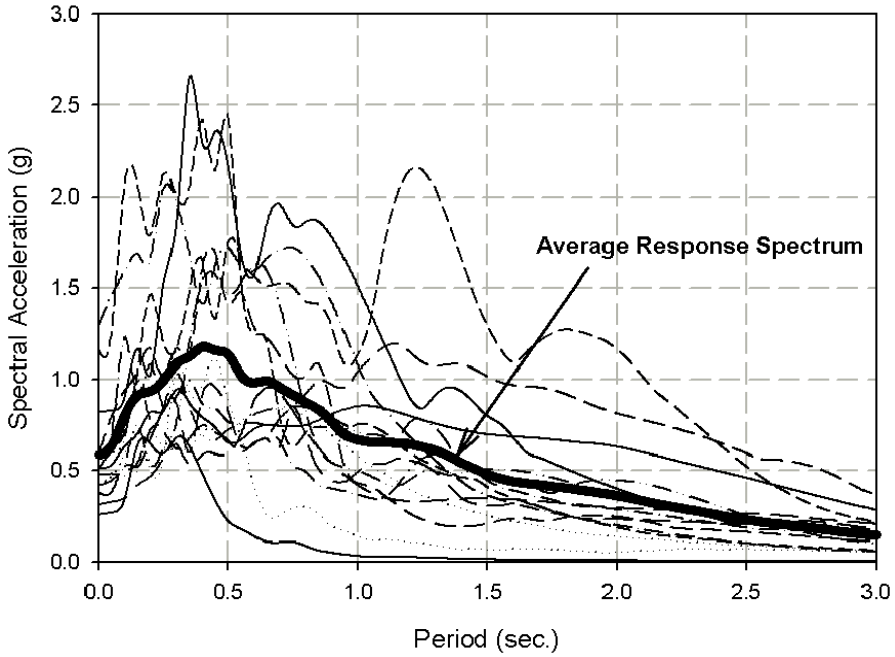

Figure 4.10 Response spectra and average response spectrum (Solid-thick) for suite C

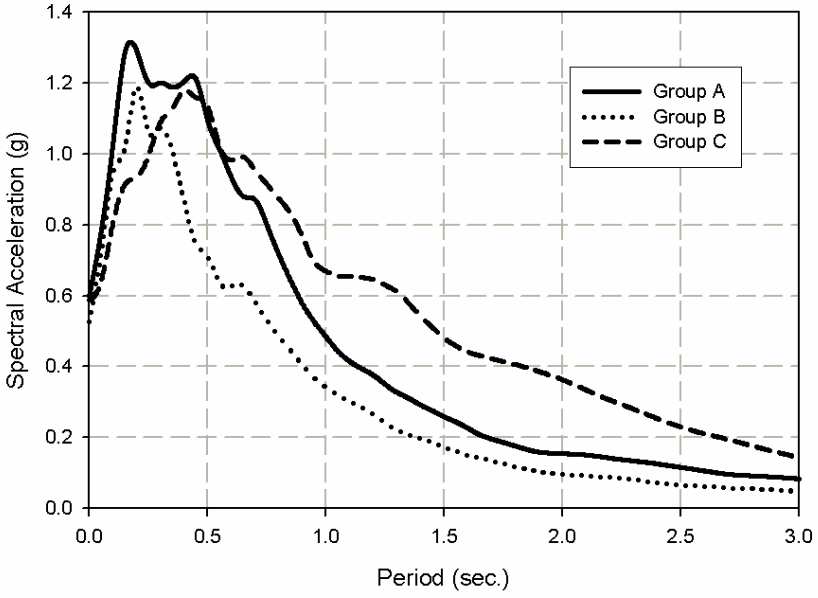

Figure 4.11 Average response spectra for ground motion groups A, B, and C

In order to be consistent regarding the level of scaling of the records, the ground motion records for the three groups were scaled based on the average spectral acceleration curve of group A. This was conducted such that the spectral acceleration value of the ground motion at the natural period of the structure would match the spectral acceleration value of curve A.

4.5.5 Study Parameters

4.5.5.1 SDOF Model Parameters

One of the main focuses of the study was to explore the effect of using SMA models on the structural response at various structural periods. Thus in this study the weight of the structure was assumed to be 1717 KN (3861 kips), while the initial stiffness, k of the structure was assumed to be variable which is calculated from the natural period of the

structure. Four values were considered for the structural natural period 0.25 sec., 0.5 sec., 0.75 sec., and 1.0 sec. In the initial stage of the study the structure was assumed to be linearly elastic. The structural nonlinearity will be included and discussed later in this chapter. The only structural damping considered in this stage was the equivalent viscous damping represented by the dash-pot shown in Figure 4.6. The equivalent viscous damping coefficient was assumed to be 5%.

4.5.5.2 Simplified SMA Model Parameters

Although the structural properties (stiffness) and the ground motion scaling factors were considered as variable in the analysis, the SMA mechanical properties were assumed to be constant during the study. This enabled the researchers to study and compare the performance of the three SMA models at different deformation levels. As mentioned earlier, instead of using a compression-tension SMA link, two tension-only SMA links were connected to both sides of the structure. The two links were assumed to be identical in the mechanical properties. The parameters required to describe the mechanical properties of the simplified SMA model are presented in Table 4.3 (see Figure 4.3 for the notations of the model).

4.5.5.3 Thermomechanical SMA Model Parameters

For the sake of consistency in the comparison between the three SMA models, the parameters of the thermomechanical SMA model was selected such that the constitutive behavior of the three models would match. In other words, the three models were designed to produce the same behavior under monotonic loading. However, under cyclic

Table 4.3 Parameters of the simplified SMA model

Parameter	Description	Value
$\mathbf{K_A}$	Austenite elastic stiffness	1014 KN/mm
$\mathbf{K_M}$	Martensite elastic stiffness	1014 KN/mm
$\mathbf{F_s}$	Phase transformation starting force	7366 KN
$\mathbf{F_f}$	Phase transformation finishing force	8153 KN
$\mathbf{S_M}$	Strain hardening ratio	1.7%
$\mathbf{F_u}$	Unloading force at the end of the phase transformation	3652 KN

loading each model would perform differently. The parameters selected to describe the constitutive behavior of the thermomechancial model is presented in Table 4.4. The detailed description of each parameter was presented earlier in section 4.5.2.

4.5.5.4 Thermomechanical SMA model with cyclic effect parameters

The same parameters that were selected for the thermomechanical model were used also for the thermomechanical model with cyclic effects. However, two more parameters were added to the model to include the effects of cyclic loading. These two parameters are applied in equation 4.10: parameter (S), which defines the maximum residual stress accumulated in the alloy, and parameter (υ), which governs the speed of accumulation during the process of phase transformation. The values of S and υ that were used in the study were 103 KN/m^2 (1.5 kips/in^2) and 0.85. These parameters were selected such that the residual strain and strength degradation would reach 70% of its final value after going through the first complete phase transformation (austenite to martensite) cycle.

Table 4.4 Thermomechanical SMA model parameters

Parameter	Description	Value
D	Austenite Young's modulus	6.894 KN/mm^2
Ω	Phase transformation modulus	-3.447 KN/mm^2
A_s	Austenite start temperature	253 ^{0}K
A_f	Austenite finish temperature	263 ^{0}K
M_s	Martensite start temperature	243 ^{0}K
M_f	Martensite finish temperature	233 ^{0}K
T	Environmental temperature	270 ^{0}K
C_a	Material parameter	0.3
C_m	Material parameter	0.3

The model was also designed to reach a stable condition after six phase transformation cycles. The final reduction in the strength at the end of the sixth cycle was assumed to be approximately 18% of the phase transformation starting force (F_s), this reduction in the strength is associated with about 0.75% residual strain. These values were selected based on previously conducted experimental studies (DesRoches and Delemont, 2002) and (Dolce, 2001).

4.5.6 Analytical Study Results

The SDOF structure was subjected to the three groups of ground motion records. The summary of the analytical results in the case of groups A, B, and C are shown in Figures 4.12a, 4.12b, and 4.12c, respectively. Each of the three figures shows the relationship between the normalized structural lateral displacement and the structural

period. The lateral displacement is normalized using the response of the as-built structure, (i.e. when no SMA links are used). The figures show a comparison between the structural responses using the three SMA models. Each of the points in the figures represents the average of the responses resulting from each group of records. Since the maximum differences observed between the three SMA models were at structural period equal 0.5 sec., the percentage of difference between each of the two thermomechanical models and the simplified model at this specific period is presented on each figure. The number presented above the lines is the difference resulting from using the thermomechanical model with cyclic loading effects, while the number located below the lines is the difference resulting from using the thermomechanical model w/o cyclic effects. The figures show that the response in case of the thermomechanical model is quite close to the response in the case of the simplified model. The average difference between the responses of the two models was between 4% and 5% for each of the three record groups. The maximum difference noticed was 9% in the case of group A. From

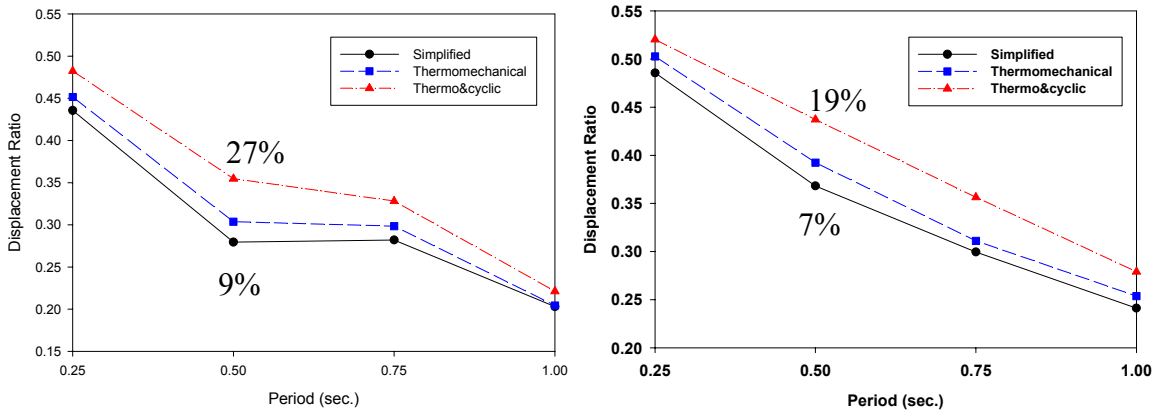

a. Group A b. Group B

Figure 4.12 Summary of the normalized response of the SDOF model using different SMA models when subjected to record groups A, B, and C.

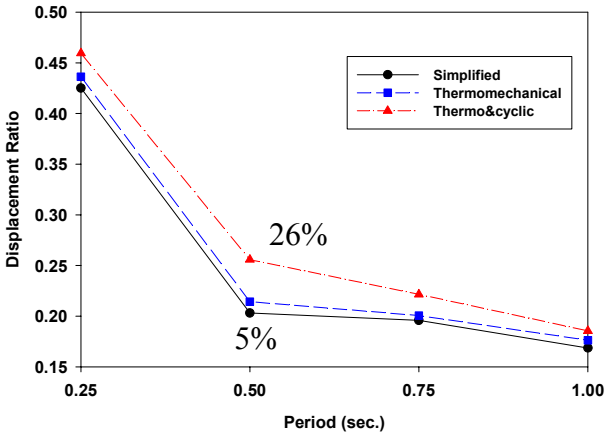

c. Group C

Figure 4.12 (Continued)

From the shown results it is observed that neglecting the effect of sublooping in the simplified model tends to slightly reduce the structural response, especially in the case of structures with high to moderate stiffness. However in the case of flexible structures including the sublooping effects in the SMA models has a minor effect on the behavior of the model. This is probably due to the fact that in the case of flexible structures, the SMA is subjected to higher level of force and thus is forced through more complete phase transformation cycles.

Including the cyclic loading effects (strength degradation and residual strain) in the thermomechanical model with cyclic effects seems to have more effect compared to the sublooping effect. The average difference in the response between the simplified model and the thermomechanical model which includes the cyclic effects was between 14% and 16% for the three ground motion groups. The maximum difference in case of groups A, B and C occurred at the 0.5 sec period and was equal to approximately 27%, 19%, and 26%, respectively. Those results showed that the structural response was more affected

by the cyclic loading effects compared to the sublooping effect. It is also noticed that structures with moderate periods are more sensitive to the cyclic loading effects. This is due to the fact that SMA devices implemented in such structures would experience small to moderate deformations and thus experience relatively small amount of yielding. However when the strength degradation is introduced in the model, the devices experience more nonlinear behavior, which in turn increases the structural response.

Figures 4.12a-4.12c evaluate the effect of ground motion parameters (duration and intensity) on the performance of each of the SMA models. It is observed that the structural response in the case of ground motions with long durations (group A) and large intensities (group C) are more sensitive to the cyclic loading effects compared to the short duration ground motion records (group B). This might be due to the fact that ground motions with short durations would tend to include less number of cycles compared to long durations. The effect of including subloops in the SMA model is clearly effective in the case of short durations as well as long durations. However, the near field ground motions are less sensitive to the behavior of the SMA model during unloading. This behavior was expected due to the fact that near field records usually contains relatively large intensity cycles along with small insignificant cycles. The large ground motion cycles would produce complete cycles in the model and the small cycles are not strong enough to start the phase transformation process.

In order to better understand the behavior of each of the three SMA models, a sample ground motion is selected from each group of records and discussed in more details. The records that were selected to represent the long duration, short duration, and near field

records are: the 1992 Landers at Coolwater record, the 1989 Loma Prieta at Gilroy Array #3 record, and the 1971 San Fernando at Pacoima Dam record, respectively.

4.5.6.1 1992 Landers (Coolwater) Record

Figure 4.13 shows the ground acceleration time history for the 1992 Landers (Coolwater) record. In this study, this ground motion was considered to be of a long duration with an effective duration (first and last exceedance of 0.05g/-0.05g) equal to 18.5sec. Figures 4.14a, 4.14b, and 4.14c show the force-displacement relationship of the simplified, thermomechanical, and thermomechanical with cyclic effects SMA models, respectively under scaled 1992 Landers (Coolwater) record. The response shown in Figure 4.14 is for the SDOF structure with period 0.5 sec, since it was found earlier from Figure 4.13, that the structural response is more sensitive at this period value to the type of SMA model.

The maximum displacements in the case of simplified, thermomechanical, and thermomechanical w/cyclic effect models were 15.5 mm (0.61 in), 17.3 mm (0.68 in), and 38.1 mm (1.5 in). These results show that neglecting the exact sublooping behavior of SMAs in the simplified model reduced the displacement by about 10%, while neglecting both, the sublooping behavior and the cyclic loading effect would result in increasing the displacement by about 59%. This shows that in the case of the 1992 Landers (Coolwater) ground motion, the response of the structure is more sensitive to the cyclic loading effects than the sublooping effect. Figure 14c shows also that the structural flexibility increased significantly when the cyclic loading effects are included.

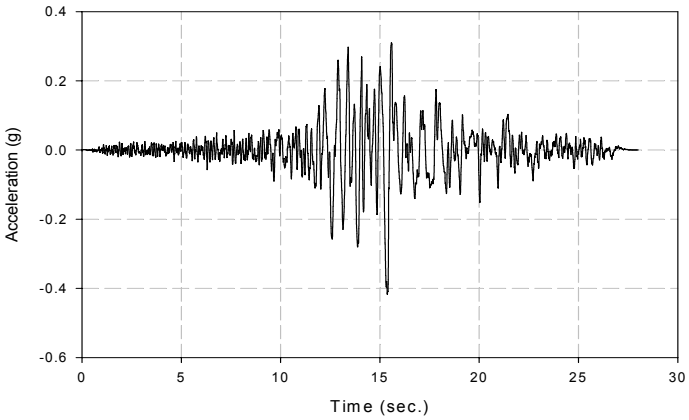

Figure 4.13 Ground acceleration time history for the 1992 Landers (Coolwater) record.

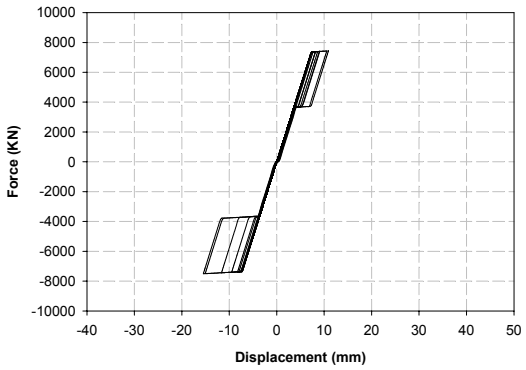

a. Simplified

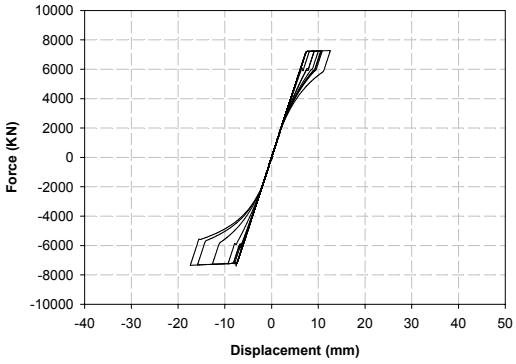

b. Thermomechanical

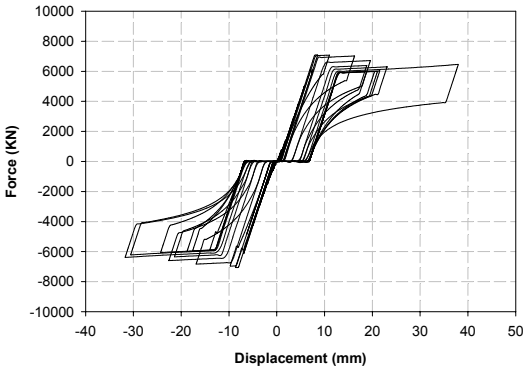

c. Thermomechanical w/cyclic effect

Figure 4.14 Force-deformation relationships for the SMA links using the three SMA models under the scaled 1992 Landers (Coolwater) record.

This behavior was expected due to the accumulation of residual deformation in the SMA links, which leads to introducing a slack in the SMA links that reduces the overall stiffness of the structure.

On the other hand, comparing Figures 4.14a and 4.14b shows that in both cases the SMA link went through the same number of cycles until it reached its maximum deformation. The unloading path was the main difference between the two types of models. In the case of the thermomechanical model shown in Figure 4.15b, the more realistic unloading path of SMAs was considered. This led to a reduction in the level of force during unloading compared to the force level in the case of the simplified model and causes a slight increase in the maximum deformation. Including the cyclic loading effects in the thermomechanical model resulted in a significant difference in the performance of the SMA links. As noticed in Figure 4.15c, a 6.9 mm (0.27 in) residual deformation and a 1326 KN (298 kips) strength reduction was observed. These values correspond to 0.75% residual strain and 18% strength reduction, respectively. With the cyclic effects included, the maximum deformation reached 38.1 mm (1.5 in). It is observed from the figure that the relatively large deformation was due to the fact the structure experienced the ground motion cycle with peak intensity after the cyclic loading effects already took place. The presence of the record's peak cycle towards the second half of the record (see Figure 4.13) helped in increasing the sensitivity of the structural response to the cyclic loading effects.

Although the superelastic SMAs is used in this study as recentering devices, the damping capability of these devices should not be ignored. Looking at the problem from an energy point of view would help in understanding the sensitivity of SMA

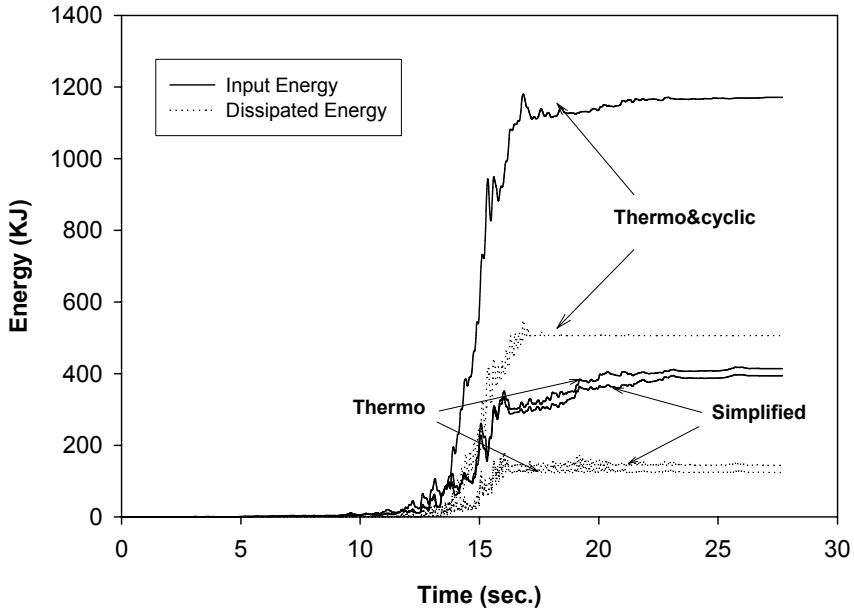

Figure 4.15 Time histories for the input energy and dissipated energy in the case of using different SMA models under the 1992 Landers (Coolwater) record

damping capability to the type of model used to describe the behavior of SMAs. Figure 4.15 shows the time history of the energy input by the earthquake and the energy dissipated by the SMA device in the case of the three SMA models. The energy curves associated with the simplified model and thermomechanical model show that including the sublooping effect had a small effect on the level of input and dissipated energies. The figure shows that in the case of the simplified model the SMA link dissipated about 37% of the total energy, compared to 30% in the case of the thermomechanical model. Following different unloading paths in the case of each model was the main resulted in only 7% difference in the damping capability of the SAM device. Adding the cyclic loading effects to the thermomechanical model increased the level of both input energy and dissipated energy. The increase in the input energy is probably due to the accumulation of residual deformation in the SMA link. The formation of slack in the

SMA links resulted in increasing the velocity of the mass and thus increased the amount of input energy. With the cyclic loading effects included, the SMA link was able to dissipate approximately 43% of the total energy. This shows an improvement in the SMA device's damping capability with inclusion of the cyclic effects. This behavior was expected due to the fact that because of the reduction in strength, the SMA link goes through more cycles with larger intensities. This yields to larger hysteretic area and thus higher damping capability.

4.5.6.2 1989 Loma Prieta (Gilroy Array #3) Record

The 1989 Loma Prieta (Gilroy Array #3) was selected as a sample of the ground motion group (B), which consists primarily of short duration ground motion records. Figure 4.16 shows the ground acceleration time history of the 1989 Loma Prieta (Gilroy Array #3) record. The effective duration of the record was found to be 10sec. The record is considered to be a good example of ground motion records with peak cycles existing at the beginning of the record. This is contrary to what was presented earlier in the case of the 1992 Landers (Coolwater) record.

The force-deformation relationship for the SMA links using the three constitutive SMA models under the 1989 Loma Prieta (Gilroy Array #3) is presented in Figure 4.17. The maximum displacements in the case of the simplified, thermomechanical, and thermomechanical w/cyclic effect models were 23.1 mm (0.91 in), 25.4 mm (1.0 in), and 25.4 mm (1.0 in), respectively. This shows that considering the more accurate behavior during the unloading in SMAs resulted in a difference of about 9%, which is close to the 10% difference noticed earlier in the case of the 1992 Landers (Coolwater) record. This

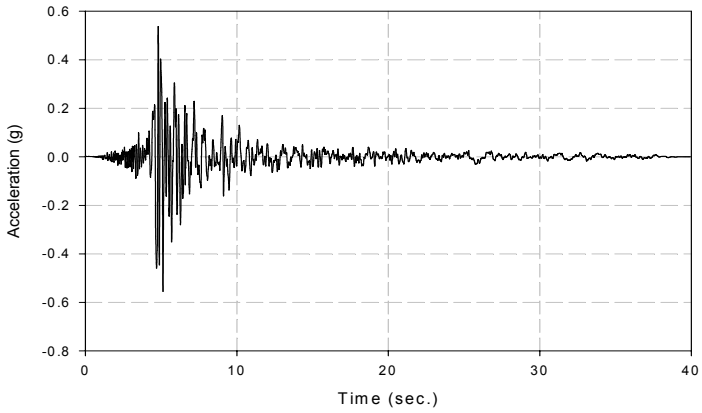

Figure 4.16 Ground acceleration time history for the 1989 Loma Prieta (Gilroy Array #3) record.

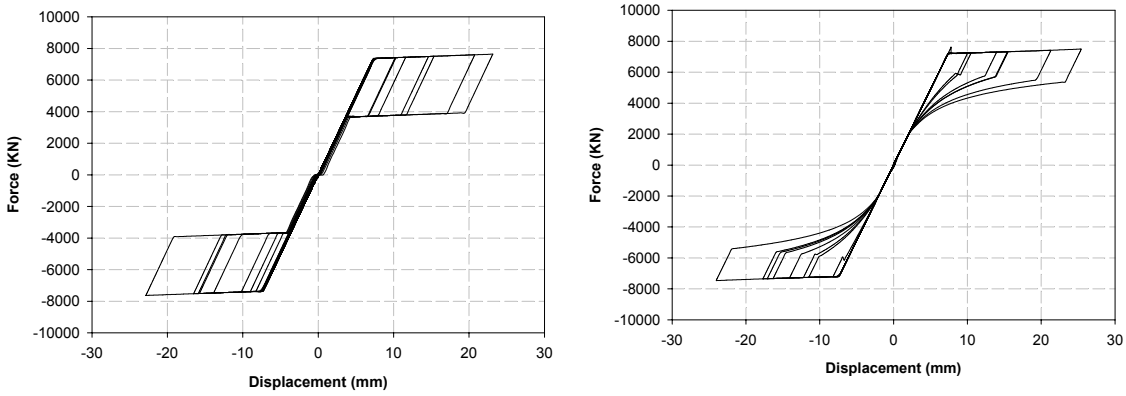

a. Simplified

b. Thermomechanical

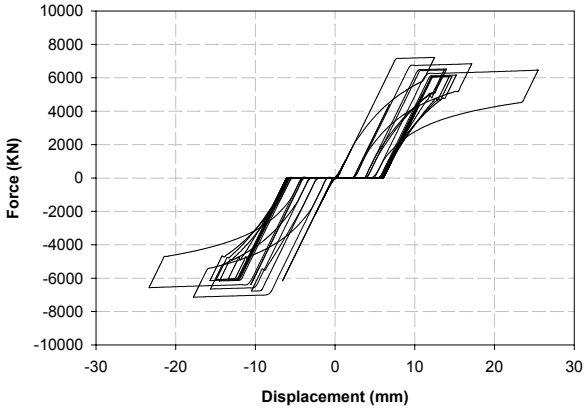

c. Thermomechanical w/cyclic effect

Figure 4.17 Force-deformation relationships for SMA link using various SMA models under the 1989 Loma Prieta (Gilroy Array #3) record.

behavior implies that the approach used to model the sublooping in SMAs is insensitive to the ground motion duration or number of cycles. It is noticed from Figures 4.17a and 4.17b that the SMA themoemchanical model experienced a larger displacement during the peak cycle. This is probably due to the modeling effects, which continue accumulating with the number of cycles.

Considering the effects of cyclic loading in the SMA constitutive model changed the behavior of the link, and forced it to experience a larger number of cycles; however the maximum deformation was not affected. This behavior is understood through reviewing the time history of the record in Figure 4.16 and noticing the relatively small cycles that exist during the early time of the record followed by a peak cycle at a time of about 5 sec. The small cycles were not enough to develop a significant amount of residual martensite link experienced the same number of cycles in the case of using the simplified model and the thermomechanical model that considers the actual behavior of SMAs during unloading. The maximum displacement reached during the cycles following the peak cycle was almost equal in the case of the two SMA models. However, in the SMA and thus were not enough to allow the accumulated residual deformation and degraded strength to reach its maximum value. When the peak cycle struck early in the record, the strength degradation and residual deformation accumulation was not totally complete, and thus the structure did not reach its maximum flexibility that was expected as a result of the cyclic loading effects. This shows that the structural response is less sensitive to the type of SMA model when subjected to short durations, which usually contain less number of cycles.

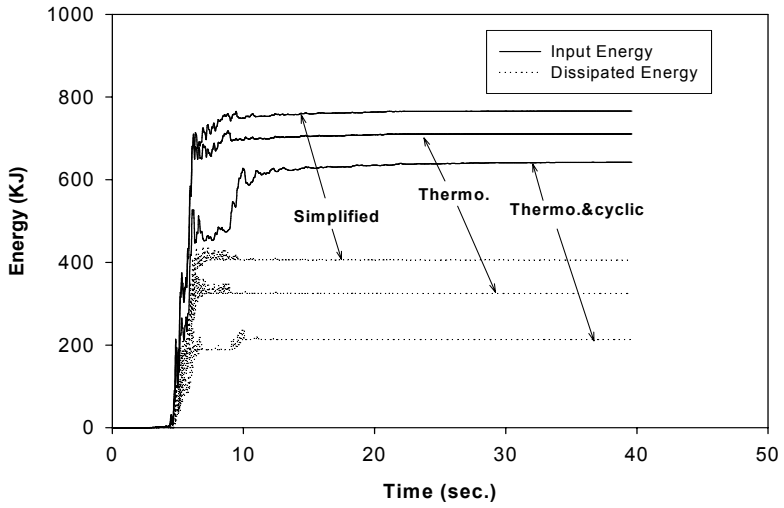

Figure 4.18 Time histories of the earthquake input energy and the SMA link dissipated energy using different SMA models under the scaled 1989 Loma Prieta (Gilroy Array #3).

Figure 4.18 presents the earthquake input energy and the SMA link dissipated energy time histories when using different SMA constitutive model. Comparing the input energy level at the en of the record to the dissipated energy level for the simplified and thermomechanical models it is noticed that in the case of the simplified model, the SMA link dissipated about 53% of the total input energy, while in the case of the thermomechanical model it dissipated about 46%. This difference is due to the change in the hysteretic shape developed by each of the two models. Although the use of the cyclic effects in the SMA model increased the damping capability in the case of the 1992 Landers (Coolwater) record as previously seen in Figure 4.15, it seems to have a different effect in the case of the 1989 Loma Prieta (Gilroy Array #3) record. The reason behind this behavior is that there were few number of major cycles in the record and the fact that the peak cycle was early in the record resulted in small deformations in the SMA link as was discussed earlier in this section. The small deformations accompanied by the

reduction in the hysteretic area due to the cyclic loading effect resulted in a reduction in the damping capability of the SMA link.

4.5.6.3 1971 San Fernando (Pacoima Dam) Record

The third and last type of ground motion record studied in this analysis a near field record. This type of ground motions is characterized by relatively large content of high frequency and large intensity cycles. As an example of such type of ground motions is the Pacoima Dam station record from the 1971 San Fernando earthquake. The station was approximately 2.8 kms from the earthquake's epicenter. Figure 4.19 shows the ground acceleration time history for that record. As shown in the figure, the record is characterized by a number of cycles with an intensity that exceeded 0.5g. The peak ground acceleration (PGA) for this record was 1.16g.

The force-deformation relationships of the SMA link using the three types of SMA constitutive models under the 1971 San Fernando (Pacoima Dam) record are presented in Figure 4.20. The maximum displacements in the case of using the simplified model, thermomechanical model, and thermomechanical model w/cyclic effect was 9.9 mm (0.39 in), 11.7 mm (0.46 in), and 27.4 mm (1.08 in), respectively. Approximately 15% difference was observed in the maximum displacement when the accurate behavior of SMAs during unloading was neglected. This difference is considered to be minor and in the same range as the differences experienced in the case of far field records. When the cyclic effects of SMAs were considered, the maximum response of the structure was

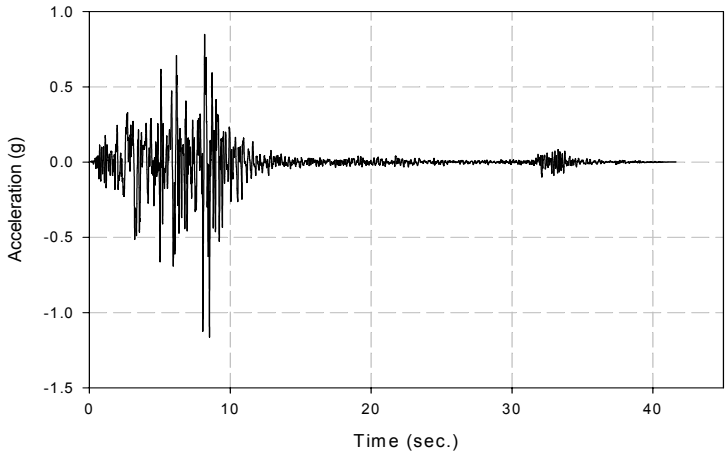

Figure 4.19 Ground acceleration time history for the 1971 San Fernando (Pacoima Dam) record.

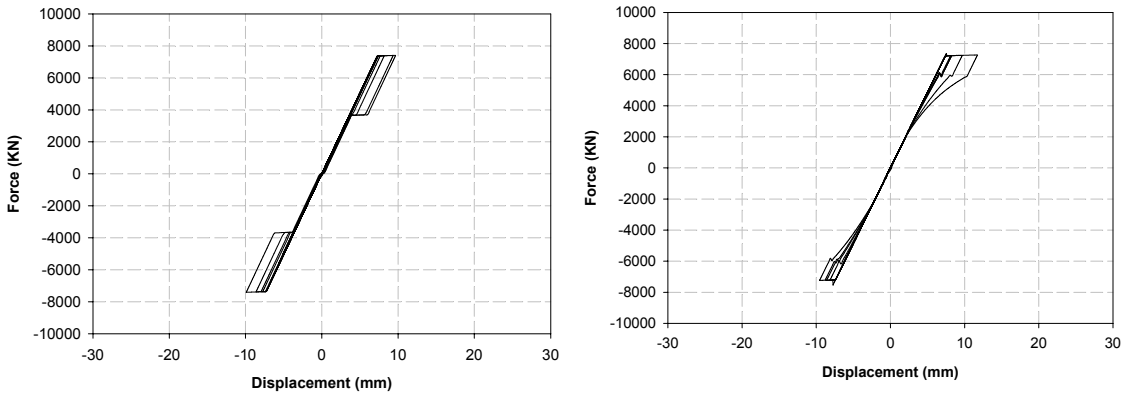

a. Simplified

b. Thermomechanical

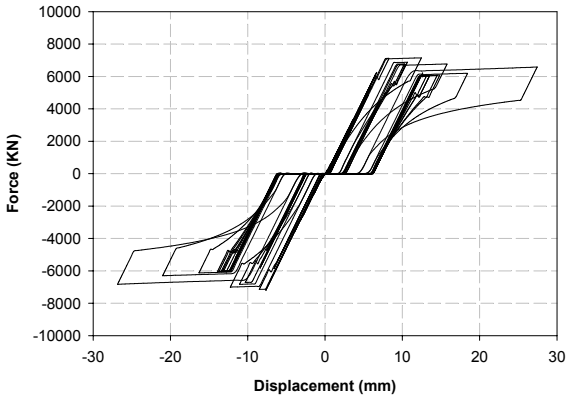

c. Thermomechanical w/cyclic effect

Figure 4.20 Force-deformation relationships of the SMA link using different SMA models under the scaled 1971 San Fernando (Pacoima Dam) record.

reduced by approximately 64% compared to the simplified model response. This difference was due to the existence of relatively large number of cycles with large intensity in the record. At the first few seconds of the record there was a number of large-intensity cycles, which weakened the structure through the cyclic effects of SMA link and thus once the peak cycle hit it produced large displacement.

Comparing Figures 4.20a and 4.20b shows an agreement between the simplified model and thermomechanical model in the number of cycles that the SMA link went through during the record. However, much more number of cycles was experienced when the effect of cyclic loading was incorporated in the thermomechanical SMA model. Figure 4.20c illustrate that the SDOF was able to resist most of the early cycles in the record with experiencing relatively small deformation. This was due to the early occurrence of these cycles in the record. Thus the degradation in the properties of the SMA link was not in effect yet. However, once the peak cycle occurred it caused relatively large displacement in the structure. This was due to the large intensity of the peak cycle and the degraded strength of the SMA link.

A comparison between the three constitutive SMA models from energy perspective is presented in Figure 4.21. The figure shows the time histories of the earthquake input energy and the energy dissipated by the SMA link using the three constitutive SMA models. As shown in the figure, the behavior of the simplified model and the thermomechanical model was close form an energy point of view. In both cases the SMA link dissipated about 17% of the total input energy. The relatively small energy dissipated by the SMA link in the case of the simplified and thermomechanical model

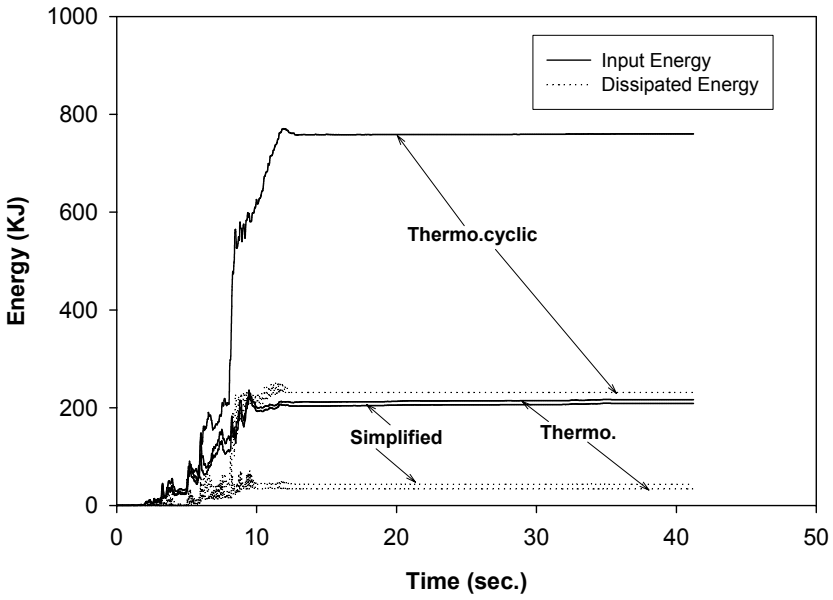

Figure 4.21 Time histories of the earthquake input energy and the SMA dissipated energy using different SMA models under the scaled 1971 San Fernando (Pacoima Dam) record.

was due to the small excitation experienced by the SMA link during the entire record. This behavior is noticed from Figures 4.20a and 4.20b, where the force-deformation curves in the case of both models enclosed a relatively small hysteretic area.

Figure 4.21 illustrates that the incorporation of cyclic loading effects in the SMA model had a significant effect on the energy response of the SMA link. The level of input energy increased significantly compared to the simplified and thermomechanical model cases. This results from the increase in the level of deformation experienced by the structure in the case of the thermomechanical model w/cyclic effects. When the cyclic effects were considered in the analysis, the SMA link was able to dissipate approximately 30% of the total input energy. The increase in the level of energy dissipated by the SMA link was due to the large hysteretic area produced by large-intensity cycles in the record,

which struck the structure after the degradation of the SMA properties took place due to cyclic loading effects.

4.5.7 Structural Nonlinearity Effect

In the study that was presented in the previous section, the SDOF structure was assumed to behave elastically. The effect of structural nonlinearity on the sensitivity of the structural response to the ground motion parameters is discussed in this section. A SDOF model with a ductility ratio equal 4.0 was considered in this study. In this context the ductility ratio is defined as the ratio of the maximum structural response to the structural response at yield. The parameters used in this study for the SDOF model and the SMA models matched the parameters used for the elastic SDOF study.

Figures 4.22a, 4.22b, and 4.22c show the study results in the case of subjecting the SDOF model to ground motion groups A, B, and C, respectively. The response shown on the vertical axis of each figure is the maximum displacement of the SDOF normalized to the maximum displacement in the case of the as-built structure. Each of the points represents the average response of the 15 records used to represent each ground motion group. The percentage of difference in the structural response resulting from using the three SMA models at period equal 0.5 sec. is also presented in each figure. As noticed from the figure, a relatively minor effect in the range of 4%-6% was observed when the sublooping behavior was considered by using the thermomechanical model instead of the simplified model. The maximum differences in any of the three ground motion group cases did not exceed 8%. The small influence on the structural response associated with

considering the sublooping behavior of SMAs during unloading was also noticed in the case of the elastic structure.

Considering the effects of cyclic loading in the SMA thermomechanical constitutive model had more impact on the structural response compared to the case where only the sublooping behavior was considered. The average response differences between the simplified model and the thermomechanical model w/cyclic effects in the case of ground motion groups A, B, and C were 16%, 8%, and 18%, respectively. A maximum difference of 23%, 15%, and 39% was also observed in the case of using ground motion groups A, B, and C, respectively. Those results showed good agreement with the results that was presented earlier for the elastic case. The structural response seems to be more sensitive to the cyclic loading effects, especially in the case of ground motion records with long duration and/or large intensity. The differences in the responses of the three SMA models decrease at high level of structural flexibility. This is due to the large displacements of the structure, which force the SMA model to exceed the elastic range, where the phase transformation takes place and act in the martensitic elastic range. In the martensitic elastic range there are minor differences between the three SMA models resulting in minor differences in the structural response.

In summary, the simplified model showed good agreement with the more complex thermomechanical model. Considering incomplete phase transformation cycles in the SMA model resulted in a difference in the maximum response that was below 9% in average. However, the cyclic loading effect seems to be having more impact on the structural response that could reach 39% in average, especially in the case of ground motion records with long duration and/or large intensities.

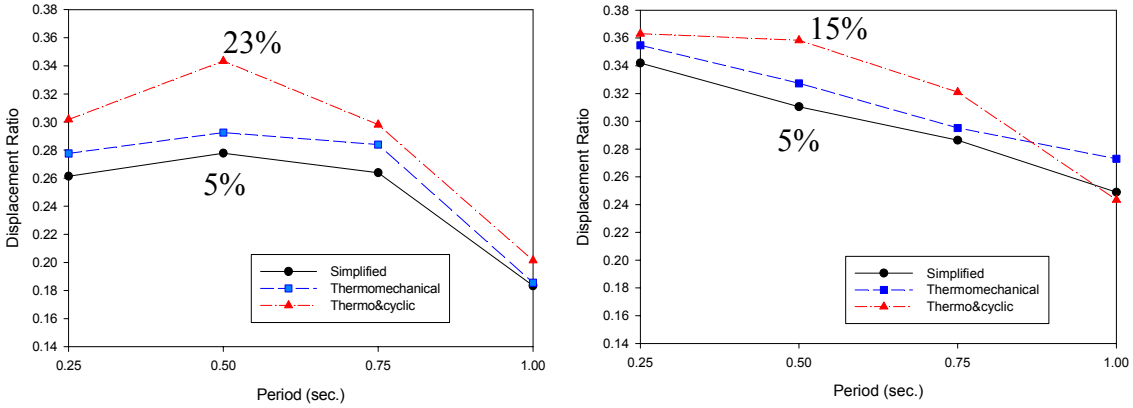

a. Group A

b. Group

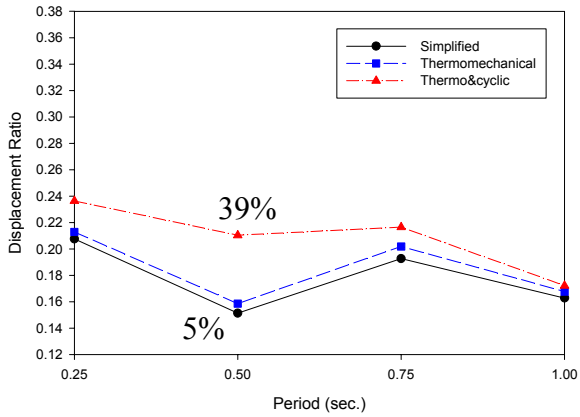

c. Group C

Figure 4.22 Summary of the nonlinear SDOF normalized response using different SMA models and subjected to record groups A, B, and C.

CHAPTER 5

SENSITIVITY OF HINGE OPENING TO THE MECHANICAL PROPERTIES OF SHAPE MEMORY ALLOYS

5.1 Introduction

Shape memory alloys are known for having several mechanical properties that are highly dependant on the composition of the alloy, the processing techniques, and the ambient temperature. A detailed discussion of the mechanical properties of SMAs and the factors affecting these properties was presented earlier in section 3.3. In order to fully evaluate the efficacy of SMA restrainers in limiting the hinge opening response in multiple-frame bridges, two parametric studies are presented in this chapter. The first study investigates the effect of using SMA restrainers with various hysteretic properties on the structural behavior of the retrofitted bridge. The second study focuses on examining the effect of the ambient temperature variation on the performance of SMA restrainers. Each parametric study is presented in a separate section of this chapter.

5.2 Simplified Bridge Model

The simplified 2-DOF analytical bridge model that was developed by DesRoches and Fenves (1997) was utilized in the analysis of this chapter. The 2-DOF model represents two adjacent frames in a MF bridge. The model assumes that the two frames are isolated from the rest of the bridge and thus the effect of the abutments was excluded from the model. A hinge gap equal to 12.7 mm (0.5 in.) was assumed between the two frames. Figure 5.1 shows two adjacent frames in a MF bridge and a schematic for the model that was used in the analysis. As shown in the figure, each frame was modeled as

a stick-mass element. A dashpot was introduced in the model to represent the equivalent viscous damping in the structure. The frictional resistance at the hinge bearing was also included in the model. The SMA restrainers were implemented in the model by using a tension-only link element with a slack (*S*). The dynamic response of the model was governed by the following equation:

$$M\ddot{x}(t) + C\dot{x}(t) + F_r(x(t)) + F_{fr}(x(t)) + F_{SMA}(x(t)) = -M.1.\ddot{x}_g(t) \tag{5.1}$$

where M is the mass matrix, C is the damping coefficients matrix, F_r is the vector of the frames restoring force, F_{fr} is the vector of restoring force due to friction at the hinge bearing, F_{SMA} is the vector of restoring force resulting from SMA restrainers. The x, $\dot{x}$, and $\ddot{x}$ are the frames displacement, velocity, and acceleration vectors. On the right hand side of the equation, the vector 1 is the influence vector and the vector $\ddot{x}_g$ is the ground motion acceleration input.

An important factor that has a significant influence on the hinge opening response is the impact between the two frames. The 2-DOF model considered in this study accounts for pounding between the two frames by applying the principle of momentum conservation. The coefficient of restitution (Goldsmith, 1960) was used to relate the velocities of the two frames prior and after impact. Since this coefficient was proven to be of a minor effect on the relative displacement between the two frames (DesRoches and Fenves, 1997), it was assumed to have a constant value of 0.8 in the entire study.

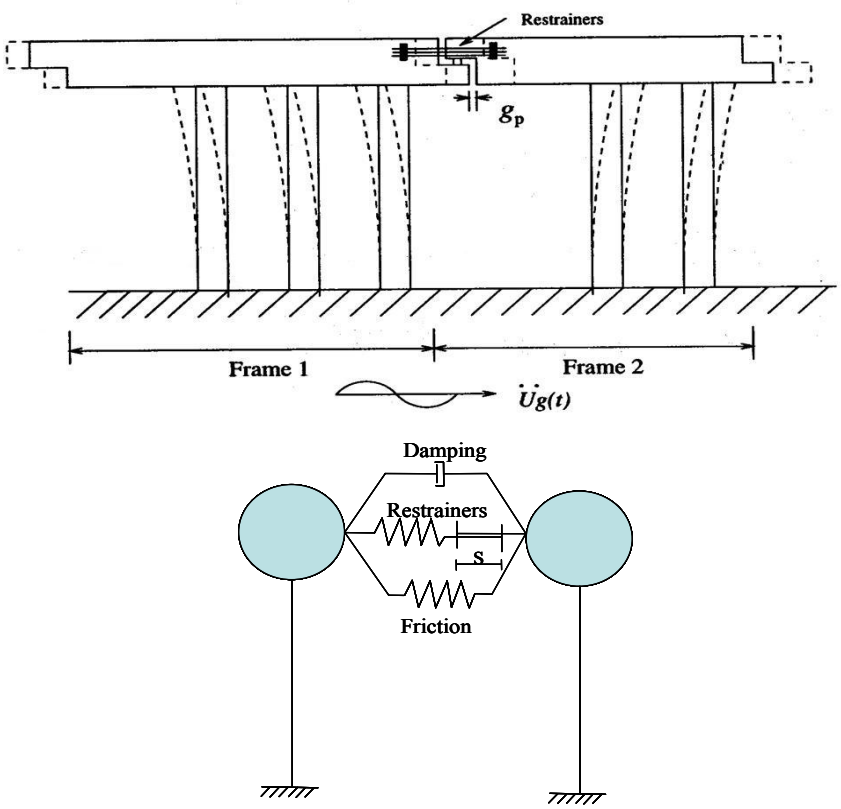

Figure 5.1 Two adjacent frames in a multi-frame bridge and a schematic of the 2-DOF analytical model used in the analysis.

The nonlinearity of the two frames is considered in the model by utilizing the Q-Hyst model that was described earlier in chapter 4. In addition to the restoring force resulting from the structural stiffness of the frames, equation 1 shows that the friction at the hinge bearings was also considered in the model. A Coulomb friction model was used to describe the frictional behavior between bridge's superstructure and the elastomeric bearing pads. The frictional resistance used in the analysis was assumed to be constant and equal to 667 KN (150 kips), which is a typical value for multiple-frame bridges.

In this model, Newmark's method (Chopra, 1995) was utilized to perform the numerical integration of equation 1. The Newton-Raphson iterative scheme was used to

account for the nonlinearity of the frames. The analysis was performed using a time step equal to 0.002sec.

5.3 Ground Motion Records

A suite of 20 ground motion records were used to perform the two sensitivity studies in this chapter. The ground motion records were selected from historical earthquakes that occurred within the United States as well as several other countries. Table 5.1 presents a description of the 20 ground motion records used in the study. As shown in the table, the 20 records were selected in a manner that they would cover a wide range of earthquake ground motion characteristics. The moment magnitudes of the events used in the analysis varied from 5.8 M_w to 7.1 M_w. The ground motions were recorded at a distance that ranged from 6.0 km to 64.4 km. This distance represents the perpendicular distance from the recording station to the fault rupture. The peak ground acceleration of the selected records varied between 0.25g and 1.5g. An important ground motion characteristic that describes the frequency contents of the record is the predominate period of the record T_g. The predominate period is defined as the period corresponding to the maximum input of kinetic energy received by a 5% damped linear elastic SDOF system (Miranda and Bertero, 1994). Knowing that the kinetic energy is primarily controlled by two variables, the mass and the velocity of the structure, and that the structure's mass is constant, the maximum kinetic energy is mainly controlled by the velocity. Thus the predominate period was calculated as the period corresponding to the maximum pseudo-velocity.

Table 5.1 Ground motion records used in the analyses

Record	Magnitude (M_w)	Distance (km)	PGA (g)	T_g (sec)
1994 Northridge, Beverly Hills	6.7	20.8	0.62	0.26
1971 San Fernando, Castaic-Old Ridge Route	6.6	24.9	0.32	0.34
1989 Loma Prieta, UCSC Lick Observatory	6.9	17.9	0.45	0.36
1980 Mamoth Lakes, Long Valley Dam	6.3	15.5	0.43	0.45
1989 Loma Prieta, Gilroy Array #3	6.9	14.4	0.56	0.47
1995 Kobe, Kobe City	6.9	11.1	0.51	0.48
1992 Cape Mendocino, Rio Dell Overpass	7.1	18.5	0.55	0.48
1994 Northridge, Centinela St.	6.7	30.9	0.47	0.53
1989 Loma Prieta, Intern. Airport	6.9	64.4	0.33	0.67
1983 Coalinga, Transmitter Hill	5.8	9.20	0.84	0.72
1987 Whittier Narrows, Downey Birchdale	6.0	56.8	0.30	0.73
1994 Northridge, Tarzana, Cedar Hill	6.7	17.5	0.99	0.74
1992 Cape Mendocino, Petrolia	7.1	9.50	0.66	0.76
1986 Chalfant Valley, Bishop LADWP-South St.	6.2	9.20	0.25	0.78
1985 Nahanni, Canada	6.8	6.00	1.10	0.83
1999 Duzce, Turkey, Duzce	7.1	8.20	0.54	0.83
1992 Cape Mendocino, cape Mendocino	7.1	8.50	1.50	0.89
1989 Loma Prieta, WAHO	6.9	16.9	0.64	0.98
1999 Duzce, Turkey, Bolu	7.1	17.6	0.82	0.99
1979 Imperial Valley, Cucapah	6.5	23.6	0.31	1.10

5.4 Effect of Shape Memory Alloys Hysteretic Properties

A major task that would face a bridge engineer while designing restrainer cables/rods made of SMAs is to decide on the optimum shape of the SMA hysteresis that would result in the best performance of the restrainers in limiting the bridge's hinge opening and hence reducing the risk of superstructure unseating during earthquakes. This requires a better understanding of the sensitivity of structural response of the bridges which are retrofitted using SMA restrainers to the SMA hysteretic shapes and properties. For that purpose a sensitivity study using the simplified MF bridge model is presented in this section. The 2-DOF simplified bridge model that was discussed in section 5.2 is used in

this study. A tension-only link element was implemented in the bridge model to represent the SMA restrainers. The simplified SMA constitutive model that was presented and discussed in section 4.5.1 was implemented in the bridge model to describe the constitutive behavior of SMA restrainers. The restrainers were assumed to have a slack, *S*, equal to 12.7 mm (0.5 in.).

5.4.1 Bridge Parameters

Based on the results of research conducted by other researchers (DesRoches and Fenves, 1997), it was found that the hinge opening problem in bridges is primarily affected by the period ratio ρ (i.e. ratio between the periods of the two frames) and the ductility ratio μ (i.e. ratio between maximum and yield displacements) of the bridge frames. Hence these two parameters were the only bridge parameters considered in the sensitivity study. The ratio of the two frame masses was taken as 1.0 with the mass of each frame corresponding to a frame weigh of approximately 22240 KN (5000 kips). In this study the stiffness of the restrainers was considered to be a function of the overall bridge stiffness. The overall bridge stiffness is represented by the modified stiffness of the frames, K_m, which is calculated from the following equation:

$$K_m = \frac{1}{\mu} \cdot \left[\frac{k_1 \cdot k_2}{k_1 + k_2} \right] \tag{5.2}$$

where k_1 and k_2 are the initial stiffness of the two bridge frames. The effect of inelasticity of the frames was considered in equation 2 by introducing the ductility ratio μ of the frames in the denominator. This was done in order to replace the initial stiffness of

the frames by their effective stiffness assuming that the frames act in an elastic perfectly plastic behavior. Based on preliminary analyses, the ratio between the initial stiffness of the SMA restrainers and the frames modified stiffness, K_m was taken as 4.0. The phase transformation starting stress for the SMA restrainers was calculated based on 36-in length restrainers with the phase transformation starting at a strain equal to 1% and assuming that the SMA is totally martensite at a strain equal to 6%.

5.4.2 Design of the Sensitivity Analysis

In order to limit the number of simulations required for the sensitivity study a preliminary study was conducted in order to determine the parameters that should be considered for the analysis. The main goal of this preliminary study was to investigate whether the interactions of the bridge parameters and the hysteretic shape of the SMA restrainers have an effect on the hinge opening. As mentioned earlier the frames period ratio ρ and the ductility ratio μ were the only two bridge parameters considered in the study.

In order to study the interaction between these two bridge parameters and the SMA restrainers hysteretic shape, the multifactor experimental design technique (Hayter, 2002) was used. In this technique an analysis of variance table is constructed to decide whether there is an interaction between a number of factors (variables) and a specific response variable. The designer of the experiment assigns a certain number of levels (values) to each of the factors considered in the analysis. Each level contains a certain number of observations, which are basically values for the response variable when the factor is assigned this specific level. The mean of these observations is calculated and compared

to other means from other levels to investigate whether considering different levels for a factor of interest is affecting the response variable. A very powerful tool that is often used to compare these means is the analysis of variance method. In order to construct an analysis of variance table, the sum of squares for each of the factors as well as different interactions and errors are calculated. Using the calculated sum of squares the F-statistic for each of the factors and its interactions are calculated. The last step in constructing the analysis of variance table is to check whether the calculated F-statistics could be considered as observations from an F-distribution. This is easily attained by calculating the probability that an observation equal to or larger than the F-statistic could be obtained from an F-distribution. This probability is known as the P-value. The P-values are tested at the end of the analysis to check the influence of different factors and their interactions on the response variable. Since P-values are basically probability values they only take values between 0.0 and 1.0. P-values closer to the value 1.0 indicate small and minor effects for the interactions between the studied factors.

Five factors were considered for the preliminary study in which two of them were bridge parameters and the rest were parameters that describe the hysteretic shape of the SMA. Parameters α, β, and γ were assumed to be three independent parameters which fully define the hysteretic shape of the SMA. Figure 5.2 shows a schematic for the force-displacement relationship for the SMA restrainers with the three parameters shown on the figure. As shown in the figure, parameter β represents the hysteresis height ratio, which was defined as the ratio between the force at the end of the reverse transformation and the force at the start of phase transformation. The α and γ parameters represent the strain hardening ratios during phase transformation and post phase transformation, respectively.

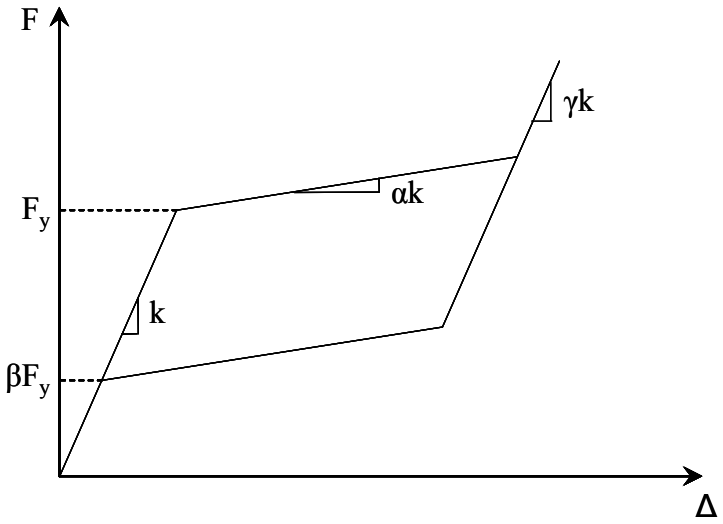

Figure 5.2 SMA hysteretic shape parameters considered in the Sensitivity analysis

Through the rest of this chapter the parameter α will be referred to as the initial strain hardening ratio, while the parameter γ will be referred to as the secondary strain hardening ratio.

Two levels were considered for each of the five factors. The two levels represent two values for the studied factor that are well separated. Table 5.2 shows the five factors considered in the preliminary study with their corresponding two levels. The 0.4 and 0.7 values for the frames period ratio factor were selected such that they would represent different levels of relative response between the two frames. The value of ductility ratio μ equal 1.0 represents the case when the frames are elastic, while the second level of ductility ratio where μ is equal to 4.0 represents the inelastic case. Parameters α, β, and γ were assigned level values that would reproduce practical hysteretic shapes for the SMAs used in the study.

Table 5.2 Factors and levels considered for the design of the sensitivity analysis

Levels	ρ (T_2/T_1)	μ	α	β	γ
1	0.4	1.0	0.0	0.1	0.3
2	0.7	4.0	0.2	0.9	0.9

Five ground motion records were considered to be the replicates at each level. The five records considered in the preliminary study were: the 1994 Northridge, Beverly Hills record, the 1980 Mamoth Lakes, Long Valley Dam record, the 1999 Duzce, Turkey at Bolu record, the 1992 Cape Mendocino record, and the 1989 Loma Prieta, WAHO record. The records were scaled such that their spectral acceleration at the fundamental period of the structure (1.0 sec.) would be equal to 0.85g. The scaled response spectra of the five records are shown in Figure 5.3.

The analysis of variance table was constructed using JMP, a statistical software developed by SAS Company (www.jmp.com). The software conducted a full factorial

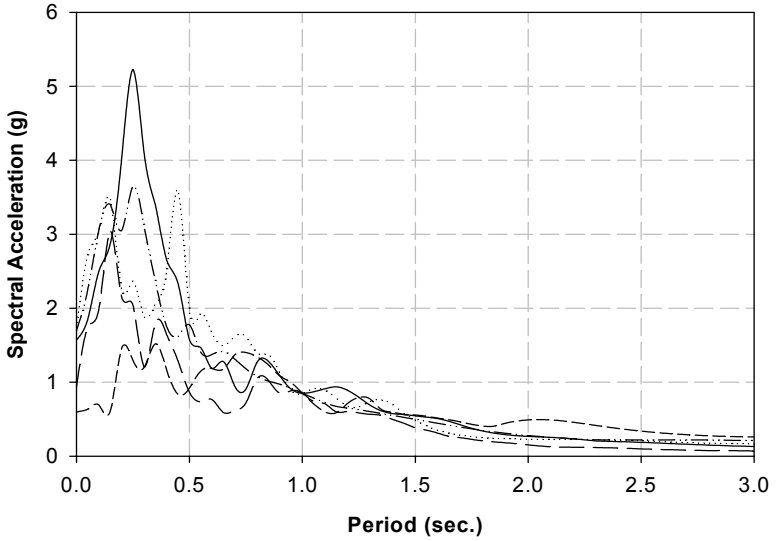

Figure 5.3 Response spectra of the five records used in the design of the sensitivity analysis after scaling them to 0.85g at a period equal to 1.0 second.

design where all the possible combinations between the five factors were considered. In this case 32 combinations were considered for each ground motion. Figures 5.4 and 5.5 show the maximum hinge displacement ratio (MHDR) and the maximum drift ratio (MDR) results of the preliminary study, respectively. The MHDR response is defined as the maximum hinge opening of the retrofitted bridge after being normalized by the hinge opening of the as-built bridge, while the MDR response is defined as the maximum drift of the retrofitted bridge's stiffer frame after being normalized by the maximum frame drift of the as-built bridge. The stiffer frame drift response was chosen since it tends to increase with the use of restrainers while the drifts of the flexible frames tend to decrease with the use of restrainers.

The vertical axis of the plot represents the three hysteretic parameters and their possible combinations with the two bridge parameters. The horizontal axis represents the

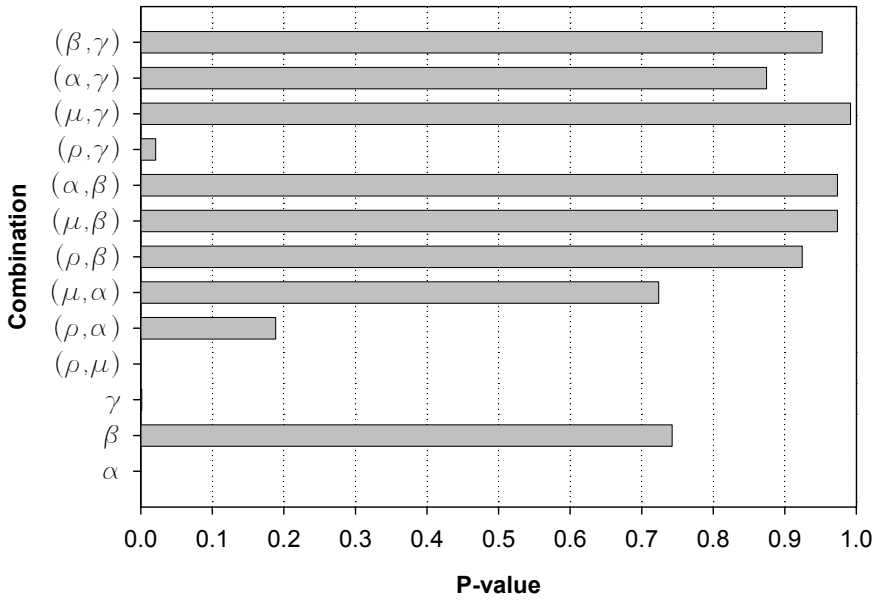

Figure 5.4 P-values associated with the MHDR response using different factor combinations.

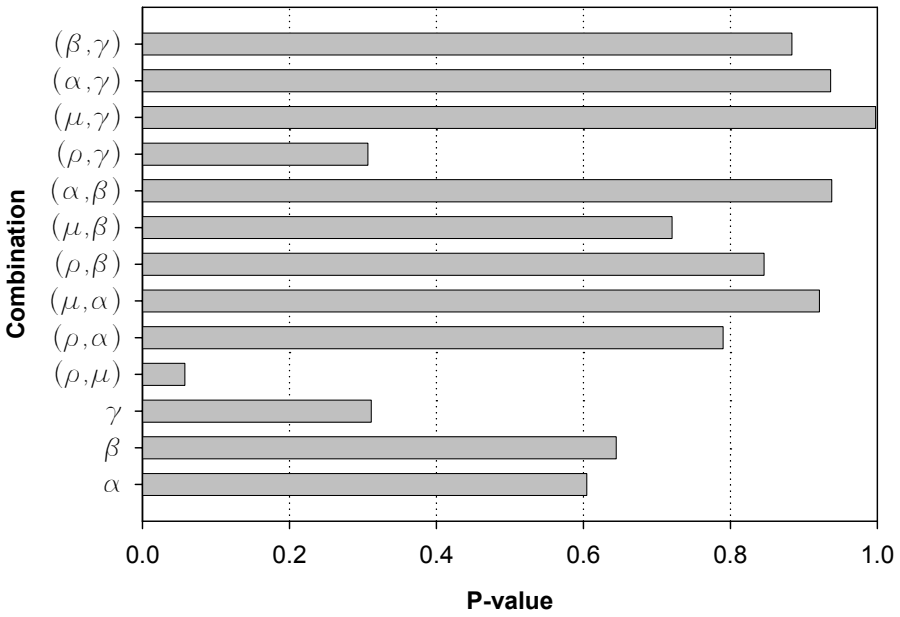

Figure 5.5 P-values associated with the MDR response using different factor combinations.

P-values, which typically lies between 0.0 an 1.0. The figures show that all of the combinations involving the β factor resulted in P-values that are larger than 0.9. This behavior was backed by the fact that the P-value associated with the β factor was approximately 0.74 and 0.64 in the case of the MHDR and MDR response, respectively. These P-values were considered as relatively high values. These results indicate that the hysteretic height represented by the parameter β has a minor influence on the MHDR and MDR responses of the bridge.

In order to support the conclusion that was observed from Figures. 5.4 and 5.5, the force-displacement relationships in the case of the 1989 Loma Prieta at WAHO ground motion record is shown in Figure 5.6. The frames period ratio ρ and ductility demand ratio μ were equal to 0.7 and 1.0, respectively. The α and γ hysteretic parameters were assumed to be constant and equal to 0.0 and 0.9, respectively. Two extreme values were

assumed for the factor β. The two β values considered in Figures 5.6a and 5.6b are 0.1 and 0.9, respectively. Although the two figures show the exact behavior during loading, the unloading behavior is significantly different in each case. This leads to variation in the hysteretic energy dissipated in each case. Despite the difference in the hysteretic area enclosed in each case, the figures show that the maximum displacement, which represents the maximum hinge opening was not affected. In both cases the maximum hinge opening was approximately equal to 3.3in, which corresponds to about 7.8%-strain. This shows that the hinge opening problem in bridges is primarily a recentering problem rather than energy dissipation. Based on this conclusion, the effect of the β parameter will be neglected in the remainder of this chapter.

On the other hand Figure 5.4 shows that the P-values associated with the hysteretic parameters α and γ are almost zero. This proves the sensitivity of the MHDR response to damping problem, thus the damping capacity of the SMA devices has a small effect on

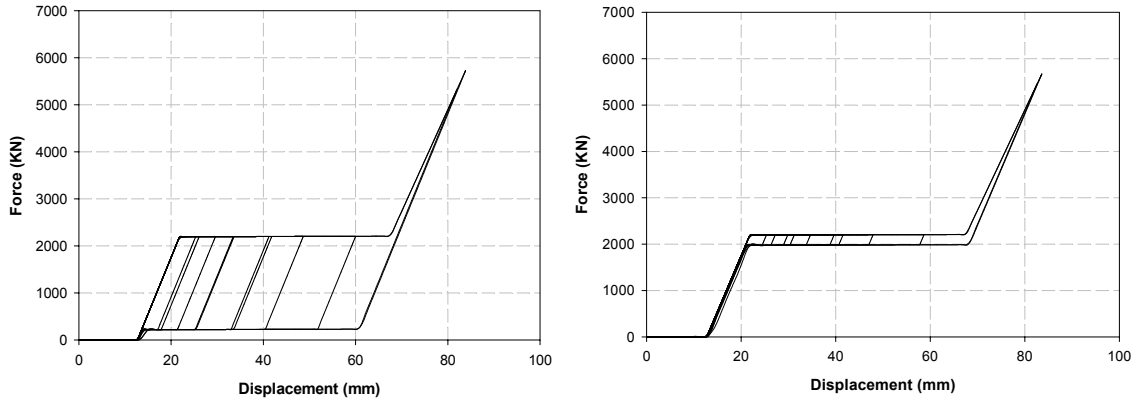

a. β=0.1 b. β=0.9

Figure 5.6 Force-displacement responses using various SMA hysteretic height under the 1989 Loma Prieta at WAHO ground motion record.

both parameters. Figure 5.5 shows that MDR response are less sensitive to these parameters compared to the MHDR response. In order to investigate the necessity of including the interaction between the bridge parameters and the SMA hysteretic parameters, the P-values corresponding to various factor combinations were tested. Figure 5.4 shows that the two P-values that are relatively small are the P-values corresponding to the interaction between the frame period ratio ρ and each of the hysteretic parameters α and γ. Figure 5.5 shows that the P-values associated with the frame ductility ratio μ were relatively large. This indicates that the interaction between the frame ductility ratio and the hysteretic shape of the SMA restrainers has a minor effect on the hinge opening response and the frame drift response. The figure also shows that the interaction between the two hysteretic parameters α and γ has a small effect on the MHDR and MDR responses. Based on these conclusions the (ρ,α) and the (α,γ) interactions are the only interactions considered for the sensitivity study.

5.4.3 Sensitivity Analyses

A sensitivity analysis was conducted to study the effect of variability in the SMA restrainers hysteretic shape on the bridge response. Based on the results presented in the previous subsection, the bridge frames ductility ratio μ were assumed to be constant in this study and equal to 1.0, which represents the elastic case. Two sensitivity analyses were conducted to study the effect of variability in the SMA hysteretic shape on the performance of these restrainers as bridge retrofit devices. The first sensitivity analysis focused on studying the effect of variability in the SMA initial strain hardening ratio α, while the second study focused on the SMA secondary strain hardening ratio γ. The

hysteretic height of the SMA restrainers was assumed to be constant throughout the study and thus the parameter β was assumed to be equal to 0.4. The ratio between the initial stiffness of the SMA restrainers and the frames modified stiffness k_m was assumed to be 4. The 20 ground motion records, which were presented in Table 5.1 were used in the study. The records were scaled such that the record's spectral acceleration value at the fundamental period of the structure would be equal to 0.8g. The fundamental period of the structure was assumed to be constant and was equal to 1.0sec.

5.4.4 Results of the Sensitivity Analyses

5.4.4.1 Effect of Initial Strain Hardening Ratio (α)

In order to study the effect of variability in the initial strain hardening ratio α on the MHDR and MDR responses the secondary strain hardening ratio γ was assumed to be constant and equal to 0.7. In order to give the reader an idea of the shape of the SMA force-displacement relationship at different values of parameter α, Figure 5.7 is presented

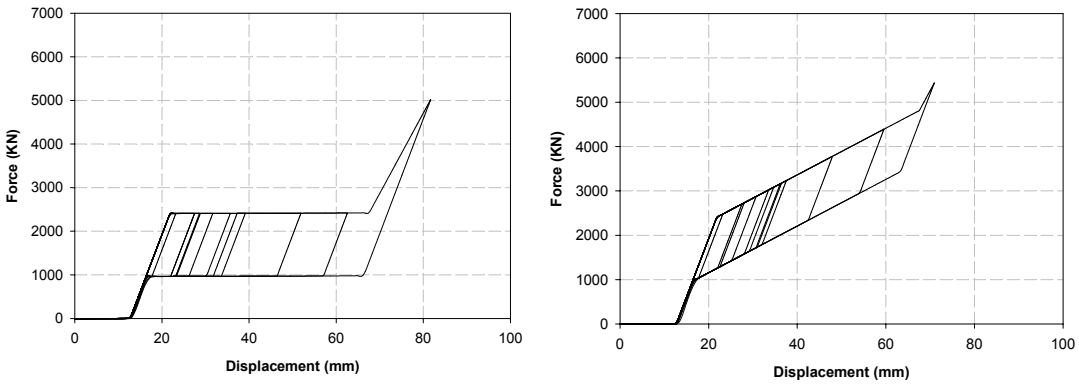

a. α=0.0 b. α=0.2

Figure 5.7 Force-displacement relationship of SMA restrainers under the 1989 Loma Prieta at WAHO record using different values of α.

below. Figures 5.7a and 5.7b represent the force-displacement relationship of the SMA restrainers at α values equal to 0 and 0.2, respectively under the 1989 Loma Prieta at WAHO record. The maximum force reached by the restrainers in the case of α equal to 0 and 0.2 was 1129 kips and 1222 kips, respectively, which indicates an increase of approximately 8%. The force increase was associated with a decrease in the hinge opening of approximately 15%.

Table 5.3 shows the average and the error bars of the MHDR and the MDR of the 20 ground motion records in the case of using different frames period ratios, ρ. The horizontal axis of each of the plots represents the value of the strain hardening ratio during phase transformation α. The second column of the table which presents the MHDR results indicates that there is consistency in the trend in each of the MHDR plots. This was observed based on the fact that for most of the case except for case of ρ=0.8, the values of the standard deviation at all α values were nearly the same. Although the standard deviation values in the case of ρ=0.8 tend to decrease with increasing α, this only affected the curvature of the line. However the trend of the curved line remained the same.

The third column of Table 5.3 shows that for the MDR response, the standard deviation values were almost the same for different values of α, which illustrates the consistency of the behavior trend. Based on the results presented in Table 5.3 it was clear that the mean values of the MHDR and MDR responses could be representative of the overall behavior.

In order to better understand the effect of interaction between the initial strain hardening ratio α and the frames period ratio ρ on the MHDR and MDR responses,

Table 5.3 Sensitivity of the mean MHDR and MDR responses to the α parameter.

ρ (T_2/T_1)	*MHDR*	*MDR*
0.3	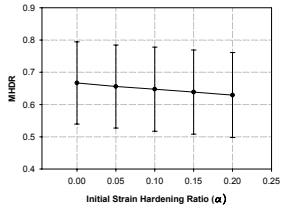	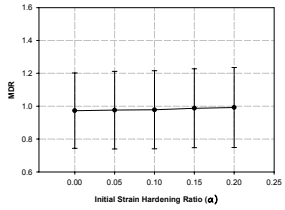
0.4	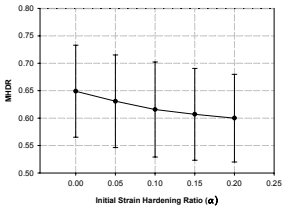	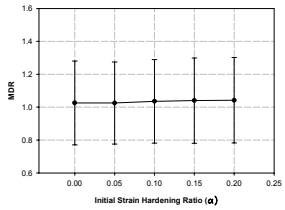
0.5	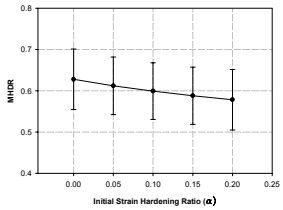	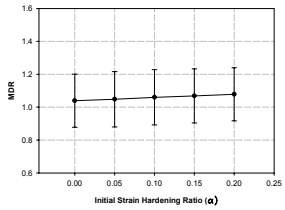
0.6	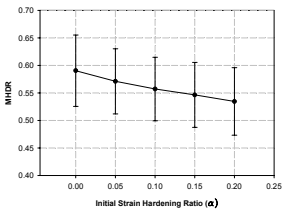	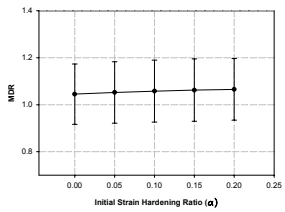
0.7	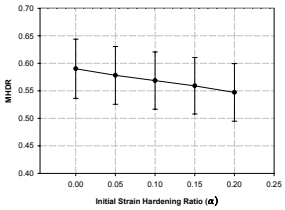	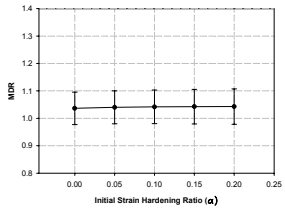
0.8	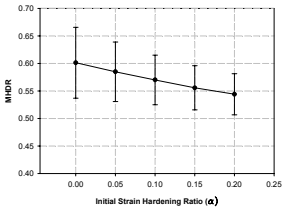	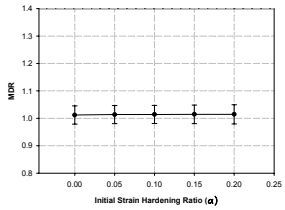
0.9	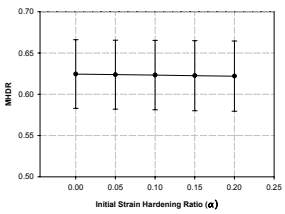	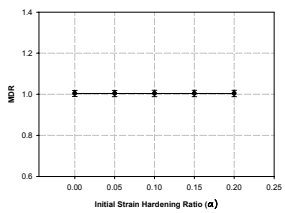

Figures 5.8 and 5.9 are presented below. The 3-D plots presented in the Figures. 5.8 and 5.9 are considered to be a summary of the results presented earlier in Table 5.3. The vertical axis in each of the 3-D plots represents the studied response, while the two horizontal axes represent the two parameters, α and ρ. Each of the 3-D plots presents the mean response of the suite of records that was used in the analyses.

Figure 5.8 shows that the SMA restrainers are most effective in limiting the maximum hinge opening when the period ratio of the two adjacent frames is moderate, (i.e. approximately 0.6). The efficiency of the restrainers tends to decrease at lower or higher period ratios. The figure shows that increasing the initial strain hardening ratio α resulted in reducing the maximum hinge opening by approximately 5%-10% depending on the period ratio of the two frames. However, at extremely high period ratio where ρ was equal to 0.9, the parameter α seemed to have a negligible effect on the response of the hinge opening. This is due to the fact that at high period ratios the frames tend to move in phase rather that out of phase resulting in a relatively small hinge opening. This would cause the SMA restrainers to remain elastic and thus the parameter α would be insignificant.

Figure 5.9 shows a trend that is mostly opposite to the trend that was observed earlier in Figure. 5.8 where the maximum frame drifts increases whenever the maximum hinge opening is reduced. This was expected since limiting the relative displacement between the two frames requires introducing additional force to join the two frames. This force is introduced through using the restrainers. Whenever the restrainer force is increased and in order to maintain equilibrium at the hinge, a large force has to be transferred to the bridge frames increasing the frame drifts. Figure 5.9 shows that the MDR response is

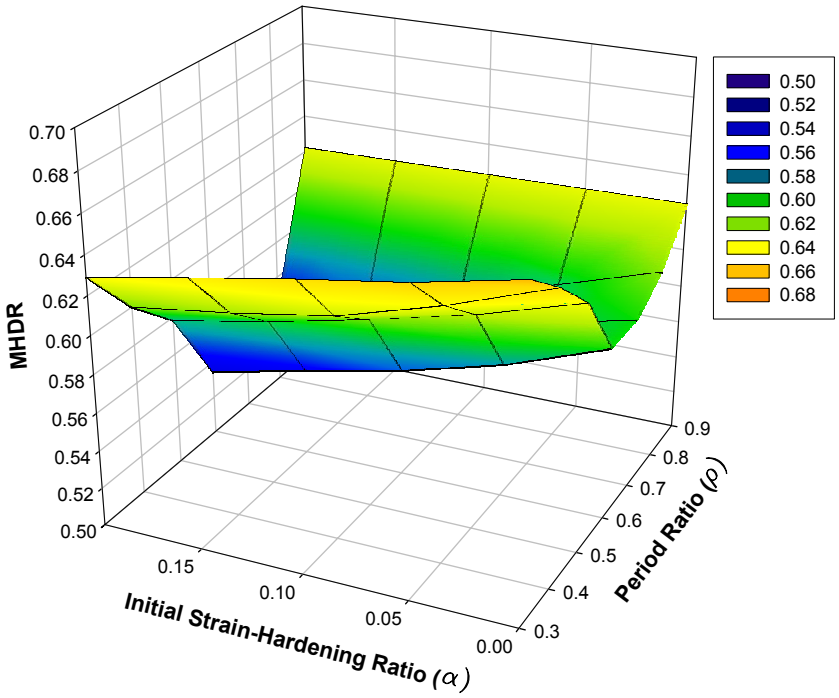

Figure 5.8 Mean MHDR response at various α and ρ values.

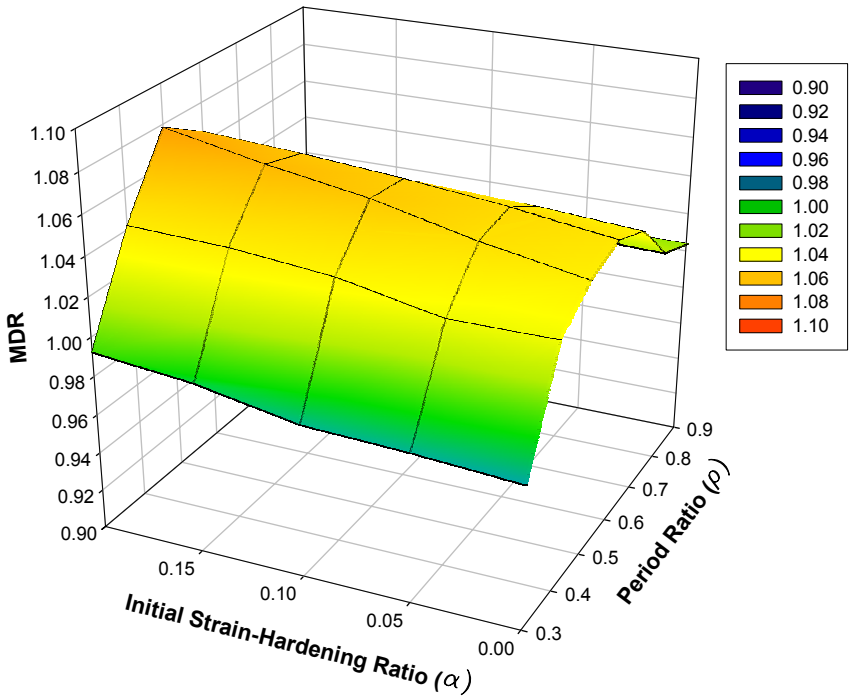

Figure 5.9 Mean MDR response at various α and ρ values.

more affected by the period ratio of the frames rather than the SMA initial strain hardening ratio. The figure shows a slight increase of approximately 1%-4% in the maximum drifts with increasing the parameter α. However at large period ratios the frame drifts are almost unaffected by the parameter α.

Based on Figures 5.8 and 5.9 it could be observed that the initial strain ratio has a higher effect on the hinge opening value compared to the frame drifts. Thus, an increase in the initial strain ratio of the SMA restrainers would reduce the hinge opening with approximately no associated increase in the ductility demands of the bridge frames.

5.4.4.2 Effect of Secondary Strain Hardening Ratio (γ)

In this section the results of the analysis that was conducted to investigate the effect of variability in the SMA secondary strain hardening ratio γ on the MHDR and MDR response. The same scaled suite of ground motion records that were used in the previous section were used in this study. The α and β parameters of the SMA restrainers were assumed to be constant and was taken equal to 0.05 and 0.4, respectively. In order to understand the effect of changing the γ parameter on the shape of the force-displacement relationship of the SMA restrainers, Figure 5.10 is presented below. The Figure shows the force-displacement relationship of SMA restrainers at γ equal to 0.3 and 0.9. The 1989 Loma Prieta at WAHO record was used. The figure shows that although an increase of approximately 28% in the restrainers maximum force was observed at higher value of γ, a minor reduction of approximately 2% was observed in the associated maximum hinge opening. This is due to the large slope of the secondary strain hardening branch, which represents the martensitic elastic behavior. At large values of γ a large

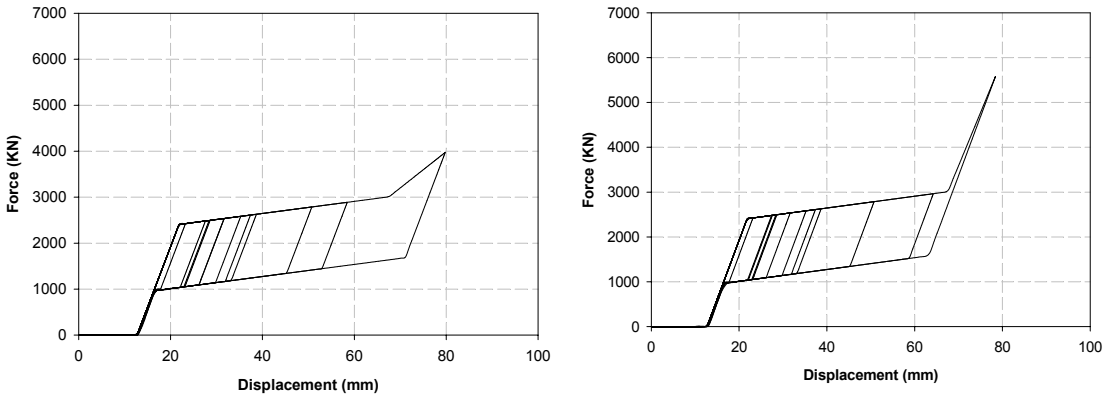

a. γ=0.3 b. γ=0.9

Figure 5.10 Force-displacement relationship of SMA restrainers under the 1989 Loma Prieta at WAHO record using different values of γ.

increase in the force level would result in a small relative displacement between the two frames.

The mean MHDR and MDR response values as well as the standard deviations resulting from running the suite of ground motions using different period ratio values are presented in Table 5.4. The table presents the variation in the MHDR and MDR responses with the γ parameter. As shown in the second column, the standard deviation values of the MHDR which correspond to different γ values in each plot were close. This indicates that the trends represented by the MHDR mean values could represent the entire set of results.

On the other hand, the results presented in the third column of Table 5.4 indicate that in the cases of ρ=0.3 and ρ=0.4, the standard deviation values vary depending on the γ values. The maximum difference in the standard deviation in the case of ρ equal to 0.3 was approximately 41%, while in the case of ρ equal to 0.4 the maximum difference was

Table 5.4 Sensitivity of the mean MHDR and MDR responses to the γ parameter.

ρ (T_2/T_1)	*MHDR*	*MDR*
0.3	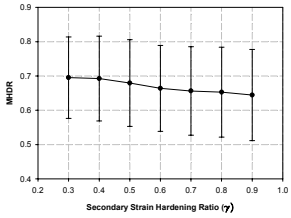	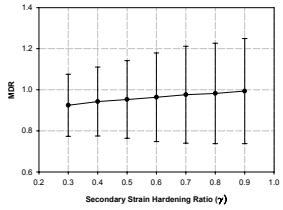
0.4	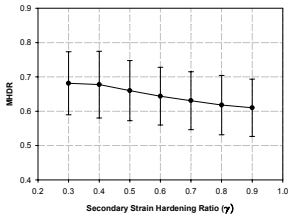	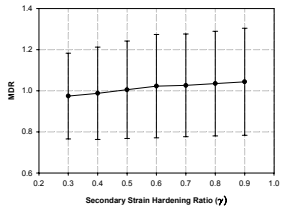
0.5	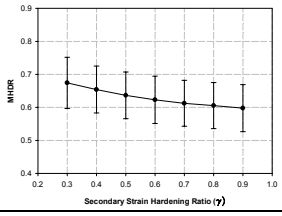	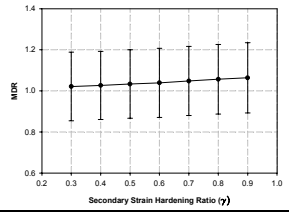
0.6	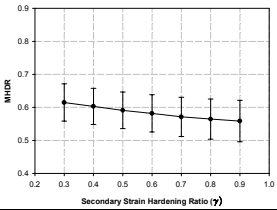	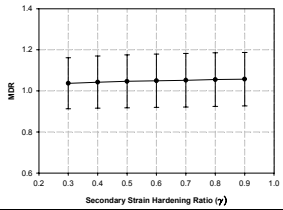
0.7	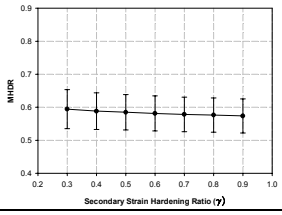	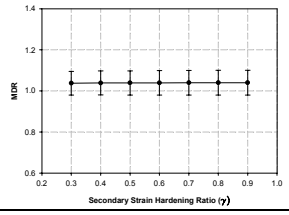
0.8	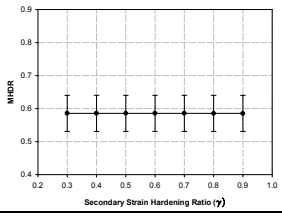	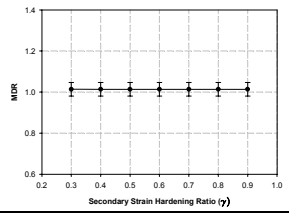
0.9	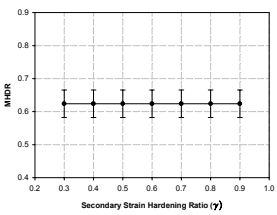	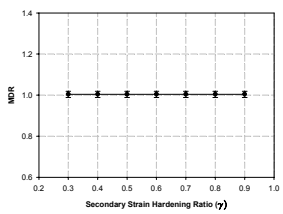

20%. This indicates that the trend of the MDR response in the case of small period ratios depends on the ground motion characteristics. However for larger period ratios the standard deviation values were almost constant at different values of γ.

In order to study the interaction between the two studied parameters ρ and γ, the results that were presented in Table 5.4 are represented in a 3-D format in Figures 5.11 and 5.12, respectively. Figures 5.11 and 5.12 present the mean values of the MHDR and MDR responses, respectively. The MHDR results shown in Figure 5.11 are all less than unity. This indicates that the SMA restrainers were effective in reducing the hinge opening compared to the as-built case through the entire analysis. However, as observed earlier in the previous section, the restrainers showed more efficacy when the period ratio of the two adjacent frames was moderate. For most of the period ratio values the figure shows a reduction in the hinge opening response when SMA restrainers with larger secondary strain hardening ratio were used. The amount of reduction in the hinge opening varied depending on the ρ values. However, a maximum reduction of approximately 11% was observed at ρ equal to 0.5. At large values of ρ the γ parameter seems to have no effect on the MHDR results. This was expected due to the relatively small hinge opening values experienced by the bridge due to the highly in-phase motion of the two frames. At such small hinge opening the SMA restrainers do not experience a phase transformation. Even when the phase transformation was initiated in some cases, there is a large probability that it would not be completed, i.e. the martensite would not reach its elastic range.

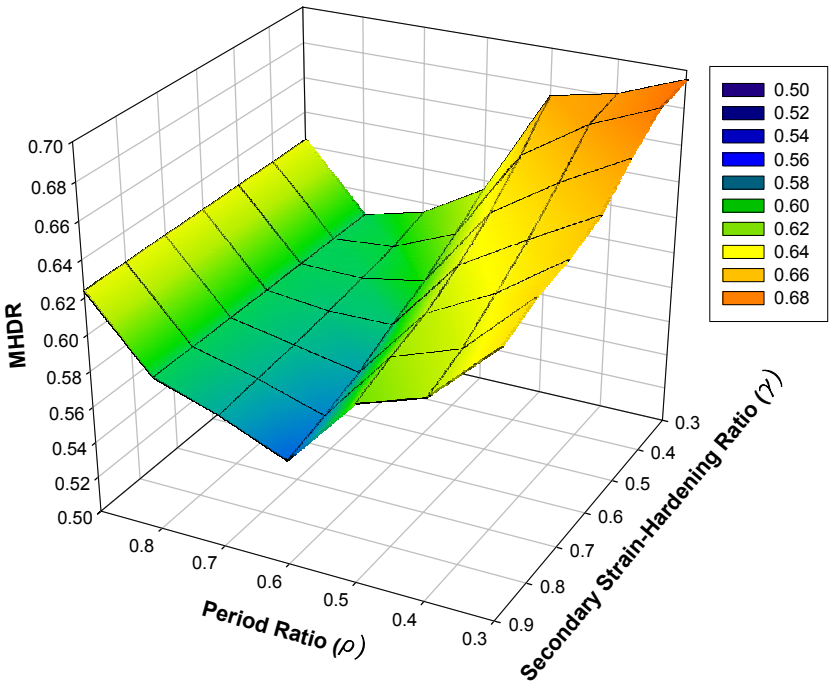

Figure 5.11 Mean MHDR response at various γ and ρ values

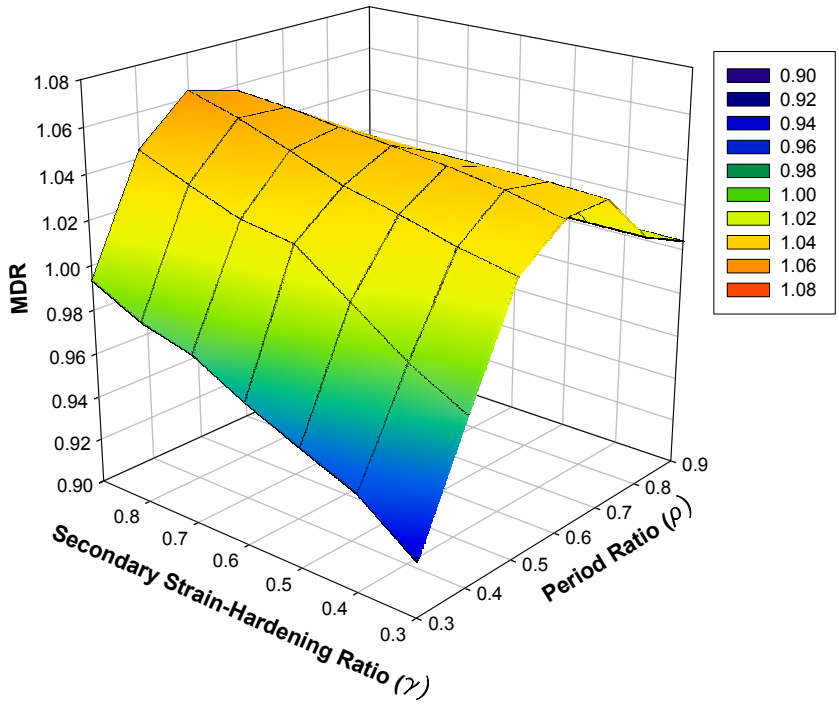

Figure 5.12 Mean MDR response at various γ and ρ values

On the other hand the MDR results in Figure 5.12 varied between 0.92 and 1.04, which means that retrofitting the bridge with the SMA restrainers might cause increase in the ductility demand of the frames in some cases. From the figure it is noticed that such behavior is mostly expected at moderate period ratios. Although it was observed earlier from Table 5.4 that the trend of the MDR response behavior at small period ratios is highly dependent on the characteristics of the ground motions, the mean values at these ρ values were used in developing Figure 5.12. A general trend was observed in the figure whenever the γ parameter increases, the MDR response increases as well. The average in crease in the MDR response was approximately 4%. However, at large period ratios the drift values seem to be unaffected by the SMA secondary strain hardening ratio. This is due to the incomplete phase transformation that the SMA restrainers go through.

In summary, the results presented in this section have shown that the SMA's hysteretic height has a minor effect on the hinge opening and frame drifts. Both, the initial and secondary strain hardening ratios have similar effect on the hinge opening that was in the range of 5%-10% in average, while their effect on the frame drifts seemed to be in the range of 1%-4% in average. The results the hysteretic properties of SMAs have more impact on the hinge opening response in the case of bridges with moderate period ratios.

5.5 Effect of Ambient Temperature

One of the most important characteristics of SMAs is its sensitivity to temperature. The phase transformation in SMAs from the austenitic phase to the martensitic phase and vise versa depends on the transformation temperatures A_s, A_f, M_s, and M_f, which were

previously defined in chapter 3. The hysteretic characteristics of the material are defined based on the environmental ambient temperature. Figure 5.13 shows a schematic drawing illustrating different hysteretic behavior for the same material when tested under different temperatures. As shown in Figure 5.13a, when the temperature, T_1, is below M_f a shape memory effect behavior is expected since the material consists of martensite in the stress-free condition. Once the temperature is raised above M_f but still below A_f at temperature T_2, both austenite and martensite are developed in the material. This mix will lead to a hysteretic behavior similar to that is shown in Figure 5.13b. The amount of residual strain mainly depends on the temperature, which determines the percentage of austenite in the alloy. Again by raising the temperature above A_f, a fully austenitic material is developed leading to a superelastic behavior as illustrated in Figures 5.13c and

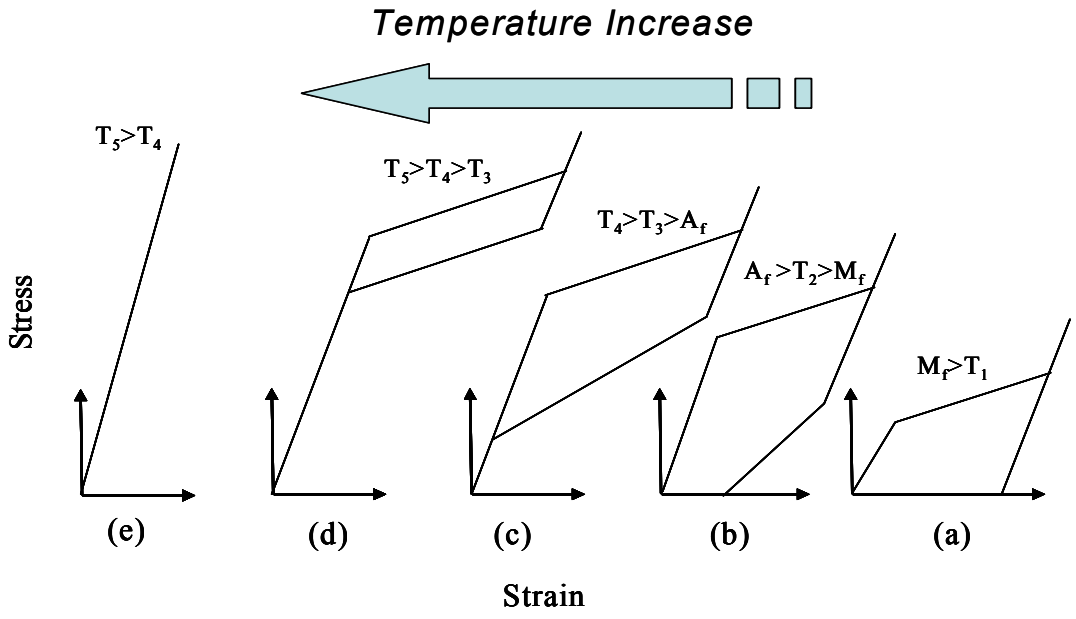

Figure 5.13 Effect of temperature on the hysteretic behavior of SMAs

5.13d. Both hysteresis shown the figures are showing superelastic behavior at different temperatures T_3 and T_4, where $T_4 > T_3$. As shown in the figure, a higher temperature will lead to a higher transformation stress with a smaller enclosed area. Once the temperature is raised above the Curie point T_5, no hysteretic loop is observed and the material acts as a linear elastic material (see Figure 5.13e) (Neizgodka and Sprekels, 1988).

SMAs restrainers that are going to be used in bridges will eventually be exposed to the environment and hence it will be vulnerable to significant changes in the ambient temperature. This section presents a sensitivity study that focus on the effect of variability in ambient temperature on the performance of SMA restrainers in bridges.

5.5.1 Design of the Sensitivity Analysis

The 2-DOF bridge model that was used in the sensitivity analysis that was presented in section 5.4 was utilized in this study as well. The bridge parameters were given the same values used in section 5.4. However, in order to obtain a more accurate constitutive behavior for SMAs under various ambient temperatures, the SMA thermomechanical model w/o cyclic effects that was presented earlier in section 4.5.2 was used to model the SMA bridge restrainers. This model provided more flexibility in choosing the levels of temperature that could be used in the analysis, since it is capable of capturing both the martensitic and austenitic behaviors.

In order to perform an efficient sensitivity study with the least number of runs required for the analysis, statistical tools were utilized to conduct a design for the sensitivity analysis. Based on the assumptions presented earlier in section 5.4, the only two bridge parameters considered in the study were the frame period ratio ρ and the

frame ductility ratio μ. On the other hand, the SMA thermomechanical model was given a constant set of parameters, which are presented in Table 5.5. The length of the restrainers was assumed to be 914 mm (36 in.). The cross sectional area of the restrainers was assumed to be 1936 cm^2 (300 $in.^2$) in the case of elastic bridge frames. However, in the case of ductile frames, the restrainer cross sectional area was divided by the frames ductility ratio μ in order to account for the reduction in the frames effective stiffness. The parameters of the SMA model and the restrainers were selected such that the SMA restrainers would experience a complete phase transformation cycle especially at small temperature values.

Table 5.5 Set of parameters used for the thermomechancial SMA model

Parameter	Description	Value
D	Austenite Young's modulus	6.894 KN/mm^2
Ω	Phase transformation modulus	-0.24 K/mm^2
$\mathbf{A_s}$	Austenite start temperature	253 ^0K
$\mathbf{A_f}$	Austenite finish temperature	263 ^0K
$\mathbf{M_s}$	Martensite start temperature	243 ^0K
$\mathbf{M_f}$	Martensite finish temperature	233 ^0K
$\mathbf{C_a}$	Material parameter	0.25
$\mathbf{C_m}$	Material parameter	0.25

Table 5.6 Parameter values used for designing the sensitivity analysis

Levels	PR	μ	Temperature(^{0}K)
1	0.4	1.0	265
2	0.7	4.0	315

The design of experiment technique that was discussed and used earlier in section 5.4 was used in this study was well. Two levels were considered for each of the three parameters (ρ, μ, and Temperature). Table 5.6 shows the values of the parameters considered in the preliminary study. The first temperature value considered was 265 ^{0}K (17 ^{0}F), which is just above A_f, while the second temperature value considered was 315 ^{0}K (107 ^{0}F), which is considered to be a realistically high temperature that may occur in some regions during summer. Five ground motion records were used as replicates for the statistical study. These ground motions are: the 1994 Northridge, Beverly Hills record, the 1980 Mamoth Lakes, Long Valley Dam record, the 1999 Duzce, Turkey at Bolu record, the 1992 Cape Mendocino record, and the 1989 Loma Prieta, WAHO record. The records were scaled such that the spectral acceleration at the structures fundamental period would be equal to 0.7g.

Using the JMP statistical software the variance tables for the MHDR and MDR responses were generated. The summary of results of the MHDR and MDR variance tables are presented in Figures 5.14 and 5.15, respectively. As observed in the figures, the P-values corresponding to the interaction between the three parameters were approximately 0.85 and 0.94 in the case of MHDR and MDR responses, respectively. Those probability values are considered to be high enough indicating that the interaction between the three parameters has a minimal effect on the hinge opening and frame drift responses. Thus, the effect of interaction between the three parameters will be ignored throughout this analysis. On the other hand, the interaction between the temperature and each of the two bridge parameters will be studied independently.

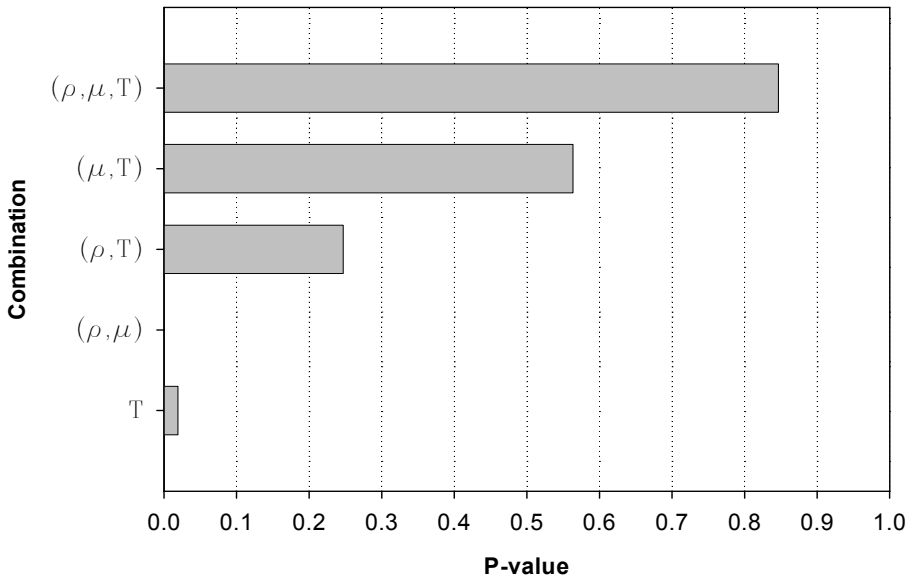

Figure 5.14 P-values associated with the MHDR response using different factor combinations.

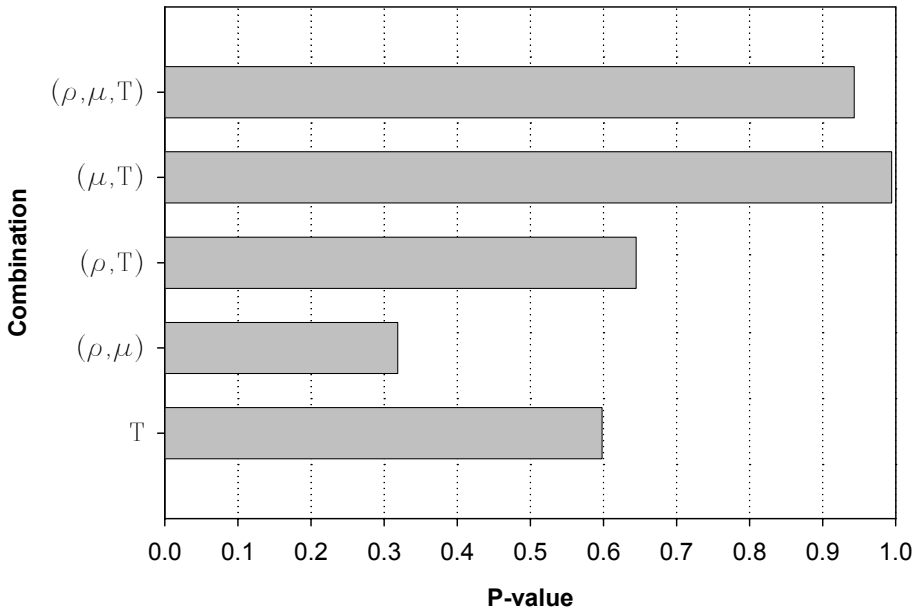

Figure 5.15 P-values associated with the MDR response using different factor combinations

5.5.2 Sensitivity Analyses

Two sensitivity analyses were conducted to investigate the effect of variability in the ambient temperature on the performance of the SMA restrainers in MF bridges. In the first analysis all the bridge parameters were assumed to constant except the frames ductility ratio μ, while in the second analysis the frames period ratio ρ was the only bridge parameter that was assumed to variable. The simplified 2-DOF bridge model that was discussed earlier was subjected to the suite of ground motion records that were presented in Table 5.1 after scaling them to 1.0g spectral acceleration value at the 1.0sec-period, which was the structure's fundamental period.

5.5.3 Results of the Sensitivity Analyses

5.5.3.1 Ductility Ratio Analysis

In this study the period ratio of the frames was assumed to be constant. A ρ value equal to 0.6 was selected for the study, which is considered as a practical value for the frames period ratio. In order to provide the reader with a better understanding of how the thermomechanical SMA model that was used in the study takes the effect of ambient temperature into account, Figure 5.16 is presented below. The figure represents the force-displacement relationship for the SMA restrainers that were used in the study at different temperatures. In the case shown in the figure, the ductility ratio of the frames was taken as 3.0 and the frame period ratio was equal to 0.6. The scaled 1994 Northridge at Beverly Hills record was used in plotting the figure. The temperature varied from 255 ^{0}K (-0.7 ^{0}F), which is slightly higher than the A_s temperature to 315 ^{0}K (107 ^{0}F), which is 52 ^{0}K above the A_f temperature. As shown in the figure, at the 255 ^{0}K-temperature, the

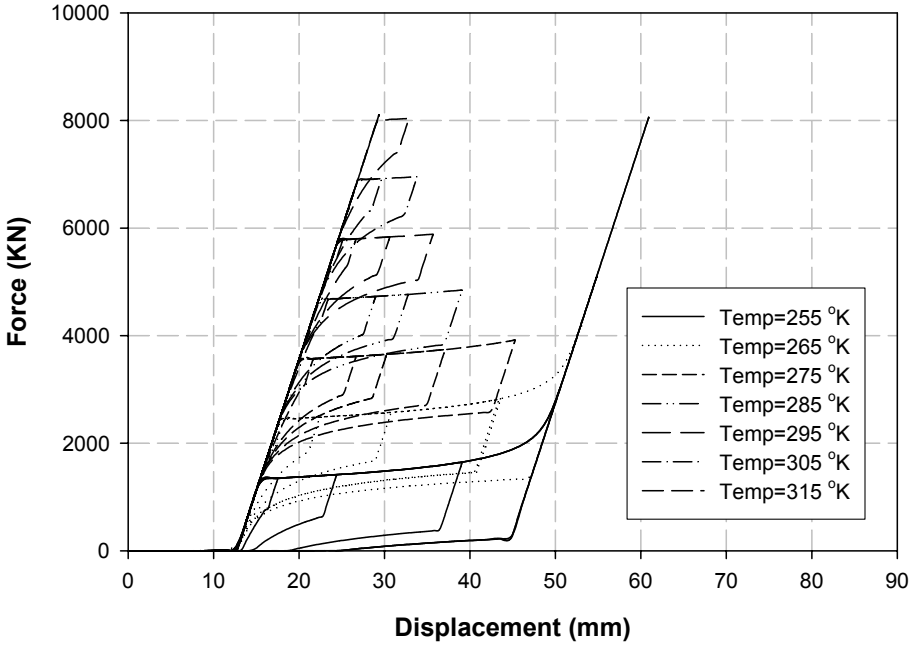

Figure 5.16 Force-displacement relationship of SMA restrainers at different temperatures using the 1994 Northridge at Beverly Hills scaled record.

force-displacement curve tends to unload plastically (i.e. there was residual displacement associated with the unloading of the restrainers). The amount of residual displacement depends mainly on the maximum displacement that the restrainers experienced. Since the 255 ^{0}K-temeprature lies between the A_s and A_f temperatures, the alloy is partially austenite and partially martensite. However for the rest of the presented temperature, the alloys were totally austenite since the corresponding temperatures were higher than A_f. Increasing the temperature elevates the SMA hysteresis and thus the maximum displacement decreases at higher ambient temperatures.

Table 5.7 Sensitivity of the average MHDR and MDR responses to the ambient temperature at various ductility ratio values.

μ	***MHDR***	***MDR***
1.0	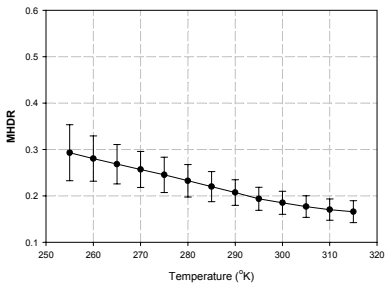	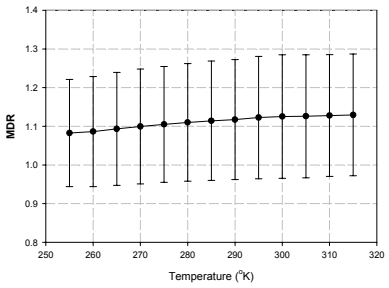
3.0	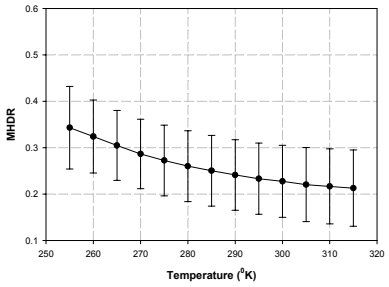	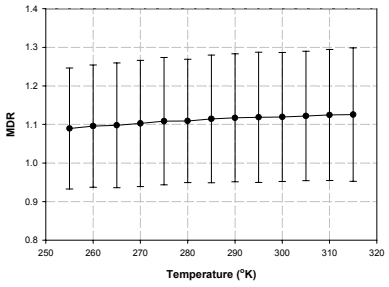
5.0	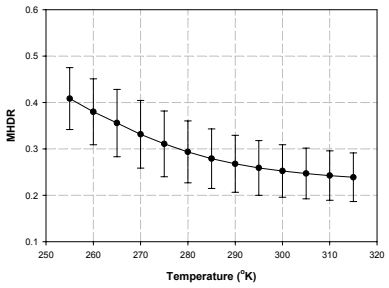	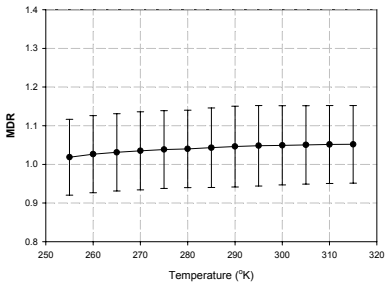
7.0	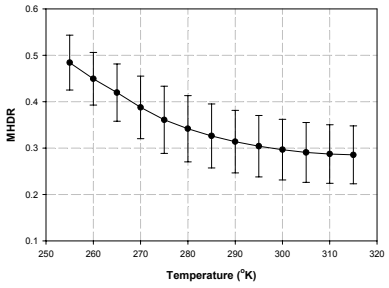	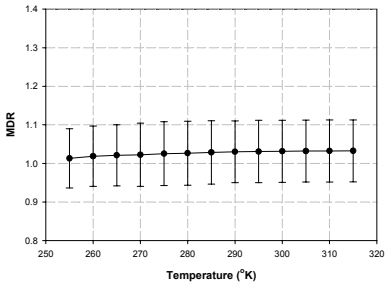

Table 5.7 presents the results of the sensitivity analysis that was conducted to study the effect of temperature on the MHDR and MDR responses at various ductility ratios μ. Each of the four figures presents the mean values resulting from the 20 ground motion records as well as the corresponding standard deviations. The second column shows that for μ values that were equal to 3, 5, and 7 the standard deviation values of the MHDR response were relatively close. However, for the case where μ was equal to 1, the standard deviation values decreased with increasing temperature. The maximum observed difference in the standard deviation values of the MHDR was approximately 61%. Although this difference is considered to be relatively high, it should have a minimal effect on the trend of the results since the error bars seems to almost have the same trend as the mean response.

On the other hand, the MDR mean and standard deviation results presented in the third column of Table 5.7 show closeness of the standard deiviations in each of the figures. This indicates that the trend of the MDR mean values could be considered as representative for the trend of the entire results.

Figures 5.17 and 5.18 show a 3-D representation of the summary of results presented in Table 5.7. The two figures show the mean values of the MHDR and MDR responses, respectively. As shown in Figure. 5.17, the SMA restrainers seem to be performing better at higher temperatures. A reduction in the hinge opening is observed when the SMAs are performing at higher ambient temperature. The amount of reduction in the MHDR response varied depending on the demand ductility ratio of the bridge frames. The figure shows that for bridges with extremely large ductility (μ=7.0), the plastic behavior of the SMA restrainers at temperatures less that A_f, which was taken as 263 ^{0}K

(14 ^{0}F) affects the effectiveness of the restrainers significantly. In the case of μ equal to 7.0, an increase in the temperature from 255 ^{0}K (-0.7 ^{0}F), which was slightly higher than the A_s to 265 ^{0}K (17 ^{0}F), which was slightly higher than A_f caused the MHDR to reduce by approximately 13%. If the temperature kept increasing above 265K untill it reaches 315K, the MHDR would experience a reduction of approximately 32%. This shows that ductile MF bridges are more sensitive to the residual displacement associated with decreasing the temperature below A_f. The effect of decreasing the temperature below A_f tends to decrease at smaller ductility levels.

On the other hand Figure 5.18 shows that increasing the temperature tends to increase the MDR response for all frame ductility levels. An approximately 1%-4%

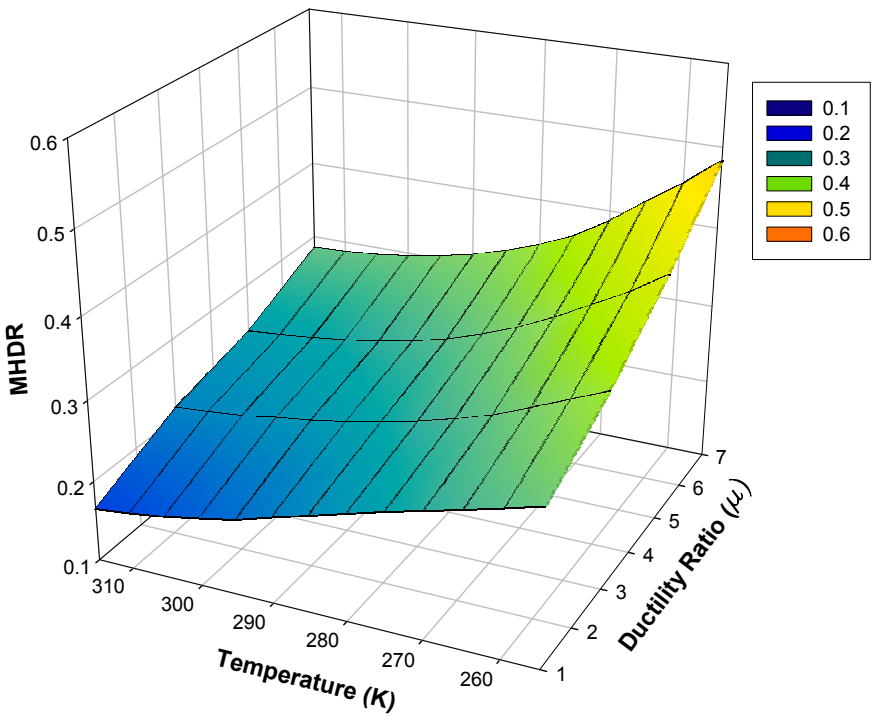

Figure 5.17 Mean MHDR responses at various temperature and ductility ratio values.

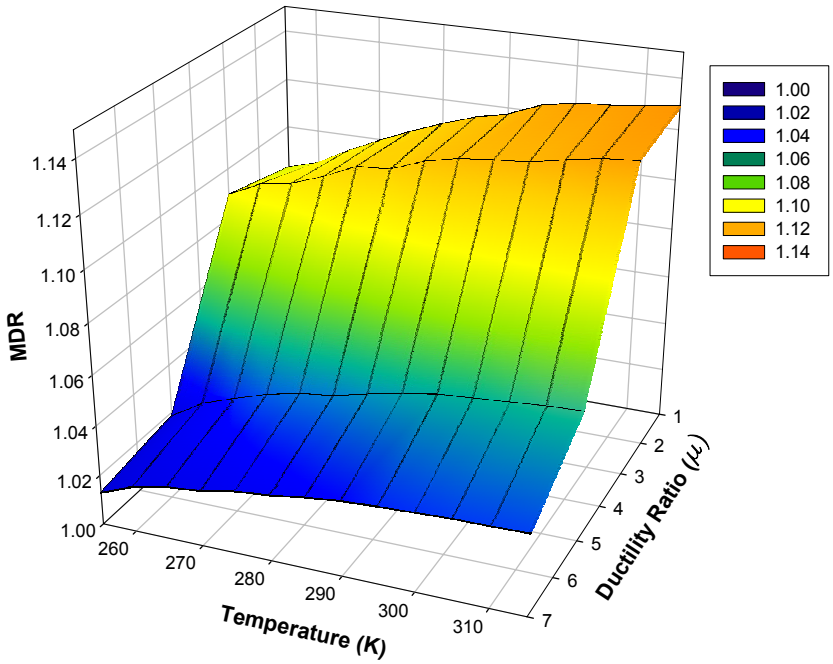

Figure 5.18 Mean MDR responses at various temperature and ductility ratio values.

maximum difference was observed in the MDR responses at all ductility levels. However this difference tends to increase in the case of frames with less ductility demand ratio. The figure indicates that the frame drifts are more sensitive to the ductility ratio of the bridge frames rather than the increase in the ambient temperature. It is also important to notice that this behavior might be due to the fact that the standard deviation values shown in Table 5.7, which corresponds to the MDR responses, were relatively high. This indicates that the effect of ambient temperature on the frame drifts highly depends on the characteristics of the ground motion record.

5.5.3.2 Period Ratio Analysis

The main focus of this study was to investigate the effect of ambient temperature on the performance of SMA restrainers that are used in bridges with various frames period ratios. Through this analysis, the frames ductility ratio was assumed to be constant. The frames were assumed to behave elastically (i.e. the ductility demand ratio was taken as 1.0). The bridge parameters and ground motion records that were used in this study were similar to that were used in the previous study.

Table 5.8 shows the MHDR and MDR mean responses and their associated standard deviation values. In most of the cases shown in the figures, the mean response seems to represent the response of the entire analysis.

The results of the MHDR and MDR mean responses are presented in a 3-D format in Figures 5.19 and 5.20, respectively. Figure 5.19 shows that the SMA restrainers were more effective in limiting the hinge opening in the case of moderate period ratios. Although increasing the ambient temperature reduced the MHDR response in all period ratio values, the effect of increasing the temperature was more noticeable at moderate period ratios where the maximum reduction in the MHDR was approximately 24%, 37%, and 45% at period ratios 0.6, 0.7, and 0.8, respectively. It is noticed from the figure that at period ratios 0.8 and 0.9, the majority of the reduction in the MHDR response occurred when the temperature was raised above A_f, i.e. when the SMA restrainers were totally austenite. This indicates that at higher period ratios the hinge opening is more sensitive to the amount of residual displacement. Thus reducing the temperature where the SMA restrainers were designed for would highly affect the bridges with relatively high period ratios.

Table 5.8 Sensitivity of the average MHDR and MDR responses to the ambient temperature at various period ratio values.

ρ (T_2/T_1)	*MHDR*	*MDR*
0.4	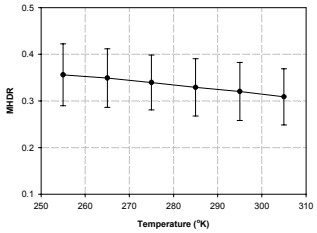	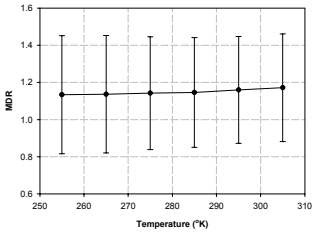
0.5	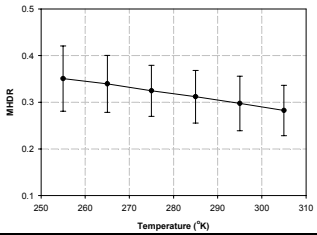	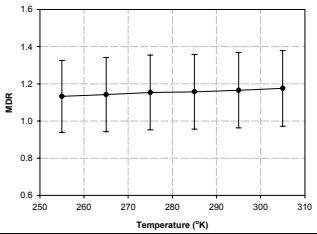
0.6	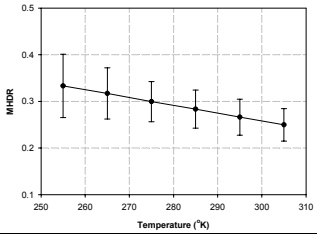	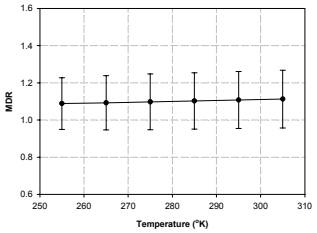
0.7	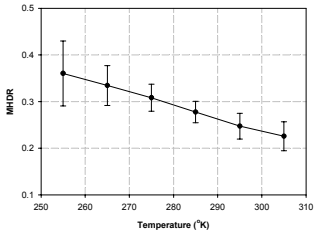	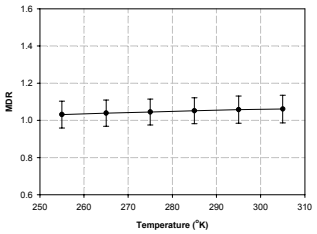
0.8	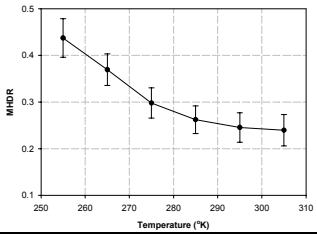	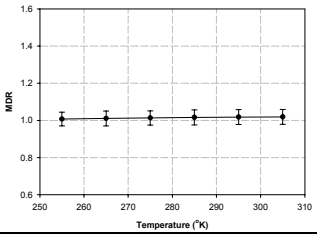
0.9	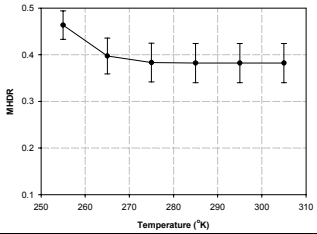	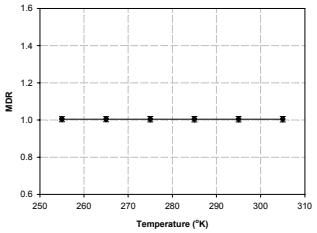

Figure 5.20 shows that in all of the studied case the SMA restrainers resulted in higher maximum drifts compared to the as-built case. However the maximum drifts increased with reducing the period ratio of the bridge frames. The effect of temperature on the frame drifts seems to be minimal especially at larger period ratios.

In summary, the results of this section show that SMA restrainers are more effective in limiting hinge opening at higher ambient temperatures. The hinge opening is more sensitive the variation in the ambient temperature in the case of bridges with large ductility and/or moderate-to-high period ratios. The results also showed that 1/3-1/2 of the changes in the hinge opening occur in the vicinity of the austenite finish temperature. The effect of variability in the ambient temperature on the frame drifts of the bridge was limited to a range of 1%-4% regardless of the bridge properties.

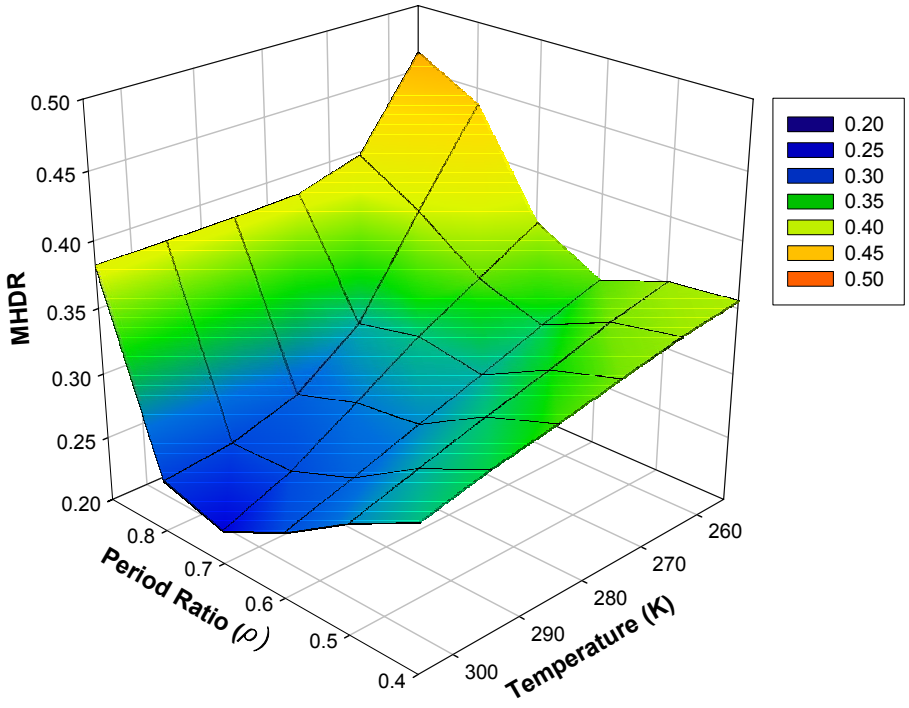

Figure 5.19 Mean MHDR responses at various temperature and period ratio values.

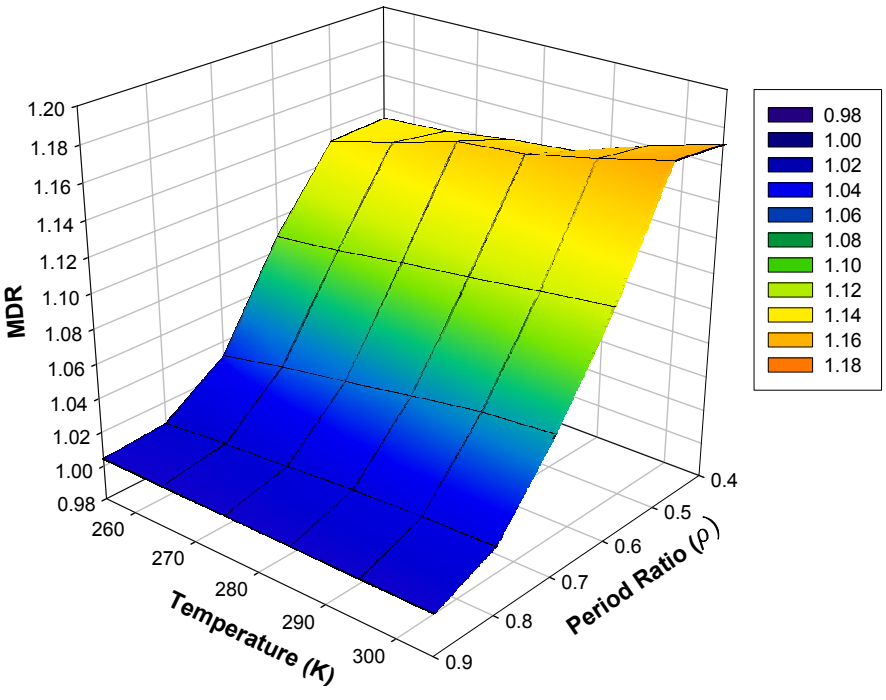

Figure 5.20 Mean MDR responses at various temperature and period ratio values.

CHAPTER 6

COMPARISON BETWEEN SHAPE MEMORY ALLOY RESTRAINERS AND OTHER RETROFIT DEVICES

6.1 Introduction

One of the major tasks of this study is to compare the performance of the proposed superelastic SMA restrainers in MF bridges with the performance of other bridge retrofit devices. The comparison includes traditional steel restrainers, which are widely used in bridges, metallic dampers, and the viscoelastic solid dampers. The main focus in this chapter is to investigate the efficacy of each device in limiting the hinge opening in MF bridges. The effect that each device has on the lateral drifts of the bridge frames is used as an indication on the change in the frames ductility demands triggered by the device. The study takes into account the variability in the bridge structural properties as well as the level of ground shaking. In order for the comparison to be realistic the design of each retrofit device is sought to be totally based on the bridge characteristics. The following sections present the analytical model that was utilized in the analysis, the models of the retrofit devices, the ground motion records, and the study results.

6.2 As-built Model

The analytical bridge model that was considered in this study consisted of two adjacent frames with a gap in between as shown in Figure 6.1a. The as-built model was developed using the earthquake finite element program OpenSees. The OpenSees framework uses object-oriented techniques, which helps in cutting down the computational time that would be required to conduct this study. In addition, OpenSees

includes extensively large library of finite elements and materials, which are directly related to seismic applications (http://opensees.berkeley.edu/).

Each frame was modeled as stick-mass with the mass of the frame lumped at one node. The two frames were assumed to have identical masses which were corresponding to approximately 20906 KN (4700 kips). The restoring force of the frames was modeled using the uniaxial bilinear hysteretic material provided by OpenSees. This type of material provides pinching in the force and deformation during reloading as well as considering damage due to ductility and energy dissipation. The unloading stiffness could be adjusted with the appropriate degradation based on the ductility of the analyzed member. Through this analysis, for the sake of simplicity the pinching effect was taken into consideration while the ductility and energy dissipation effects were ignored. The ductility demands of the frames were defined using an iterative scheme, where the yield strengths of the frames were modified iteratively. A 5% strain hardening ratio was assumed for the bridge frames once they start yielding. The initial stiffness of the flexible frame was assumed to be constant through the analysis. In order to provide a realistic natural period of 1.0sec for the flexible frame, its initial stiffness was taken equal to 84.1 KN/mm (480.5 kips/in). Figure 6.1b shows the force-deformation relationship for the flexible frame under the 1989 Loma Prieta at the UCSC Lick Observatory record. The targeted ductility ratio of the frame was 4.0. As shown in the figure including the pinching effect resulted in a reduction in the initial stiffness prior to reloading.

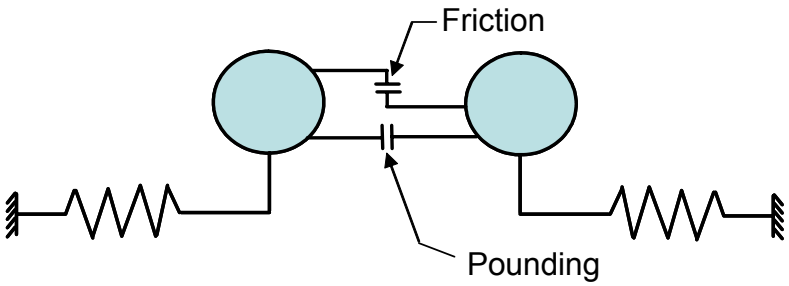

a. Bridge model

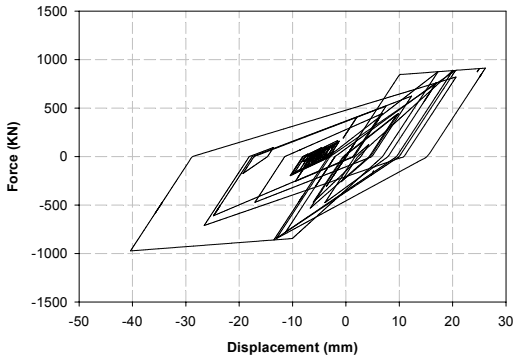

b. Flexible frame

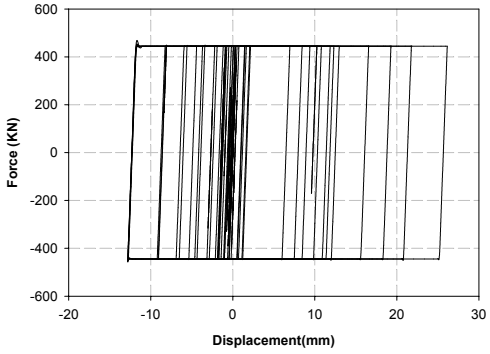

c. Bearing friction

Figure 6.1 Schematic of the analytical bridge model and the force-deformation relationship of the flexible frame and the friction at bearing under the 1989 Loma Prieta at the UCSC Link Observatory record.

The friction at the elastomeric bearings was accounted for using an elastoplastic element with relatively large stiffness and 445 KN (100 kips) yield strength, which is a typical value in a MF frames. This element would produce a Coulomb type of friction between the two frames. Figures 6.1c shows the force-deformation relationship of the friction element under the 1989 Loma Prieta at the UCSC Lick Observatory record. On the other hand, the pounding between the two frames were modeled using a relatively rigid compression-only link with a gap. The gap separating the two frames was taken as

12.7 mm (0.5 in) through the rest of the study.

6.3 Retrofit Devices

Three retrofit devices were selected for the comparison with study with the SMA device. These three devices are steel cable restrainers, metallic dampers, and viscoelastic dampers. The force-deformation relationships of the four devices considered in this study are presented Figure 6.2. The following subsections describe the models developed in OpenSees to study the considered devices

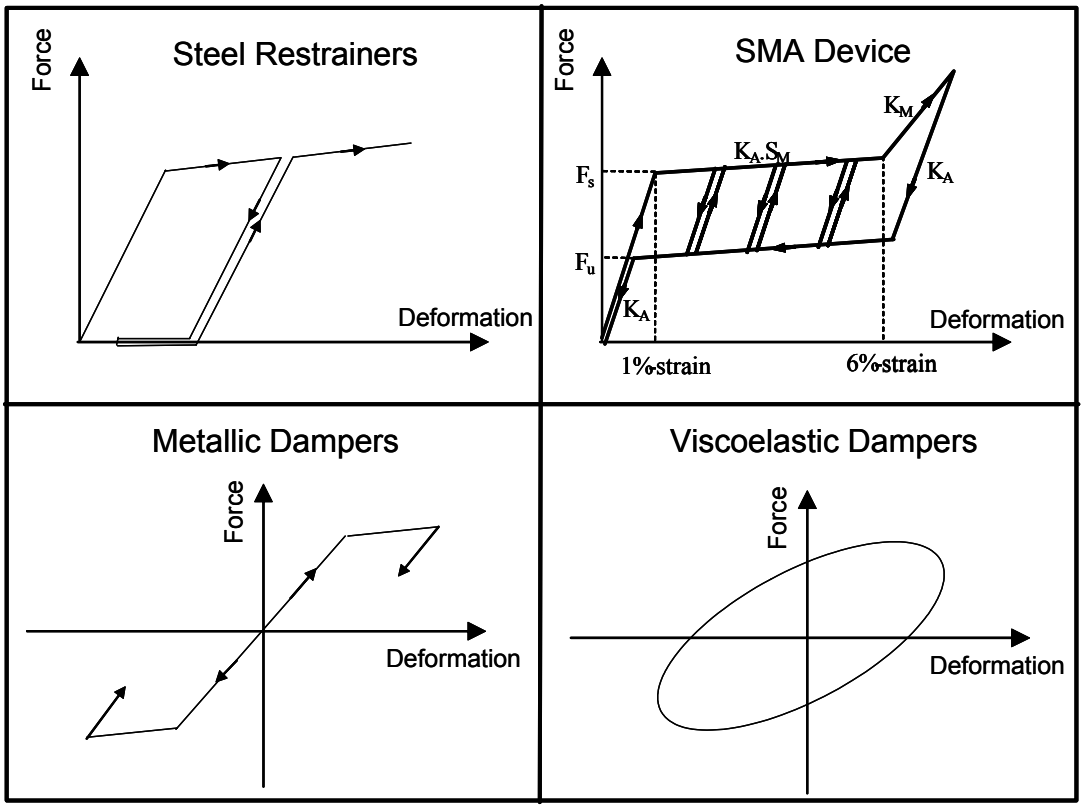

Figure 6.2 Force-deformation relationship of the four types of devices considered in the study.

6.3.1 Steel Restrainer Cables

The most currently used unseating prevention device in bridges is the steel restrainer cables. The configuration and performance of this device in past earthquakes have been discussed earlier in Chapter 2. The steel restrainers were modeled as tension-only elements with an initial slack to account for the thermal expansion of the bridge. Since the steel restrainers engage only under tensile loading, and due to its plastic behavior, the yielding of the restrainers produces a permanent deformation in the restrainers after unloading. This tends to delay the engagement of the device in the proceeding cycles. In order to model such behavior in OpenSees two materials had to be combined in series. Since the Steel01 material implemented in OpenSees provides tension/compression bilinear type of behavior, a tension-only elastic material with an initial gap was added in series. The initial modulus of the steel restrainers was calculated based on the following equation:

$$E_r = \frac{E_s . E_e}{E_s + E_e} \tag{6.1}$$

where E_r is the initial modulus of the restrainers, E_s is the initial modulus of the Steel01 uniaxial material, and E_e is the initial modulus of the elastic material with gap. The strain hardening of the steel restrainers beyond yielding was assumed to be relatively small and thus was neglected. Figure 6.2 shows a schematic of the force-deformation behavior of the modeled steel restrainer cables. Since this study involves the metallic and viscoelastic dampers, which do not require slack in order to engage, the steel restrainer cables were assumed to have a zero slack throughout this study.

6.3.2 Shape Memory Alloy Devices

An important advantage of using OpenSees in this study was the fact that it is an open source program. The open-source feature provides the capability of adding new material behaviors to the OpenSees library and using them with various types of elements. Due to the lack of material behaviors in OpenSees that would be able to capture the superelastic behavior of the SMAs, a new SMA material was implemented in the OpenSees library under the name SMA01. The SMA01 material was modeled as a uniaxial material with an initial slack, which follows the same simplified constitutive behavior that was described earlier in section 4.5.1. The SMA01 material uses the same parameters that were presented earlier in Figure. 4.3 and are represented for convenience in Figure 6.2. In order to be compatible with the steel restrainer cables, the SMA restrainers were modeled with a zero slack.

Two SMA devices were considered in this study. The first device was a tension-only device, which is consistent with the steel restrainer cables. The second device was a tension/compression device, which acts symmetrically under reversible loading. The second SMA device was considered for the sake of consistency with the metallic and viscoelastic dampers, which are basically devices that act in both tension and compression.

6.3.3 Metallic Dampers

The third type of retrofit device that was considered in this study is the metallic damper. These devices are displacement-controlled devices, which exhibit a bilinear

behavior, thus it was modeled in OpenSees using the uniaxial material Steel01. The mechanical behavior of the Steel01 material is shown in Figure 6.2.

6.3.4 Viscoelastic Dampers

The last type of retrofit devices that was considered in the comparison was the viscoelastic dampers. A discussion on the mechanical behavior of these devices was presented earlier in chapter 2. Researchers had developed various types of models to describe the constitutive behavior of the viscoelastic dampers. The Kelvin/Voigt model is one of the most simple and accurate models that have been used to represent the behavior of the viscoelastic dampers. The model basically consists of a dashpot and a spring elements connected in parallel such that they would have identical strain and additive stress. This model was implemented in OpenSees through the combination of an elastic material and a viscous material in parallel. The viscous material was assumed to be linear (i.e. the stress varies linearly with the strain rate). Figure 6.2 shows the mechanical behavior of the viscoelastic dampers.

6.4 Ground Motion Records

A suite of 25 historical ground motion records were used in this study. Table 6.1 presents a list of these records and their characteristics. The ground motion records covered a broad range of values for the earthquake magnitude, epicentral distance, peak ground acceleration (PGA) and predominate period (T_g). Figure 6.3 shows the response spectra for the 25 records that were used in the study.

Table 6.1 Ground motion records used in the analysis

Record	Magnitude (M_w)	Distance (km)	PGA (g)	T_g (sec)
1994 Northridge, Beverly Hills	6.7	20.8	0.62	0.26
1987 Whittier Narrows, Cedar Hill	6.0	43.0	0.64	0.31
1986 N. Palm Springs, North Palm Springs	6.0	8.20	0.69	0.34
1971 San Fernando, Castaic-Old Ridge Route	6.6	24.9	0.32	0.34
1989 Loma Prieta, UCSC Lick Observatory	6.9	17.9	0.45	0.36
1980 Mamoth Lakes, Long Valley Dam	6.3	15.5	0.43	0.45
1989 Loma Prieta, Gilroy Array #3	6.9	14.4	0.56	0.47
1995 Kobe, Kobe City	6.9	11.1	0.51	0.48
1992 Cape Mendocino, Rio Dell Overpass	7.1	18.5	0.55	0.48
1994 Northridge, Centinela St.	6.7	30.9	0.47	0.53
1986 Chalfant valley, Zack Brothers Ranch	6.2	18.7	0.45	0.57
1989 Loma Prieta, Intern. Airport	6.9	64.4	0.33	0.67
1983 Coalinga, Pleasant Valley	5.8	17.4	0.60	0.69
1992 Landers, Coolwater	7.3	21.2	0.42	0.71
1983 Coalinga, Transmitter Hill	5.8	9.20	0.84	0.72
1987 Whittier Narrows, Downey Birchdale	6.0	56.8	0.30	0.73
1994 Northridge, Tarzana, Cedar Hill	6.7	17.5	0.99	0.74
1992 Cape Mendocino, Petrolia	7.1	9.50	0.66	0.76
1986 Chalfant Valley, Bishop LADWP-South St.	6.2	9.20	0.25	0.78
1985 Nahanni, Canada	6.8	6.00	1.10	0.83
1999 Duzce, Turkey, Duzce	7.1	8.20	0.54	0.83
1992 Cape Mendocino, cape Mendocino	7.1	8.50	1.50	0.89
1989 Loma Prieta, WAHO	6.9	16.9	0.64	0.98
1999 Duzce, Turkey, Bolu	7.1	17.6	0.82	0.99
1979 Imperial Valley, Cucapah	6.5	23.6	0.31	1.10

6.5 Parametric Study

6.5.1 Study Parameters

In order to cover various bridge properties, which are critical to the hinge opening problem in bridges, the comparison study between different retrofit devices was conducted in the form of a parametric study with the bridge parameters being the main parameters in the study. The bridge parameters which were considered in the study were the period ratio (ρ) of the two adjacent frames, and the ductility demand ratio (μ). The period ratio values considered for the study varied between 0.3, which represents the

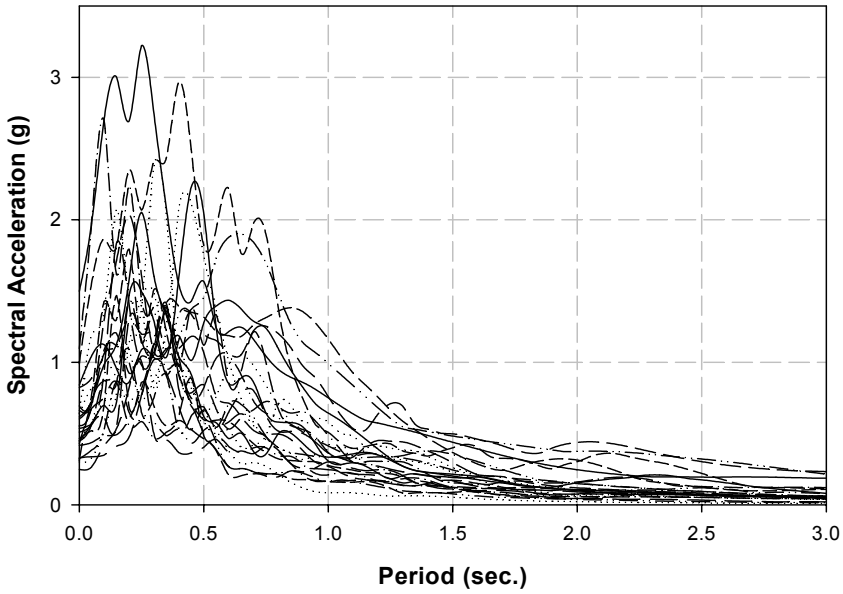

Figure 6.3 Response spectra of suite of 25 ground motion records that were used in the analysis.

extremely out of phase case and 0.9, which represents the nearly in-phase case. The analysis was conducted assuming that the bridge frames behave elastically as well as inelastically. For the inelastic case, ductility demand ratios equal to 2 and 4 were considered. The mechanical properties of the retrofit devices were based on the bridge parameters. The design procedures that were used to design the retrofit devices will be discussed later in the following section.

In order to investigate the effect that the ground motion intensity has on the performance of the devices, a parametric study was conducted at different levels of ground shaking. The suite of ground motion records were scaled such that the spectral acceleration at 1.0 sec., which is the natural period of the as-built structure would be the same in all ground motion cases. The records were scaled to different levels of target spectral acceleration at the fundamental period of the structure. The target spectral

acceleration was related to the median spectral acceleration value of the 25 records at 1.0 sec. by a spectral factor SF. The SF is defined as the ratio between the target spectral acceleration and the median spectral acceleration of the 25 records at the structural natural period. Two values were considered for the SF parameter. Those values were 1.0 and 1.5. The SF value equal to 1.0 was thought to represent the case were the bridge is subjected to a ground motion intensity close to the intensity which the retrofit devices were designed to withstand. On the other side, the 1.5 SF value represents the case where the bridge retrofit device are forced to behave at higher demand larger shaking levels than the ones for which they were designed.

6.5.2 Design of Retrofit Devices

In order for the study to be realistic, all retrofit devices were designed based on the properties of the bridge frames as well as the ground motion records that were used in the analysis. The philosophy of the design method was to ensure that the effective stiffness of each device is the same.

The steel restrainer cables were chosen to be the device that would control the design of the rest of the devices. The reason behind selecting the steel restrainers was the fact that it is the most commonly used device for protection against bridge unseating. Although a number of studies had been conducted in the past to come up with a design methodology for steel restrainer cables in bridges, the Caltrans design criteria states that "A satisfactory method for designing the size and number of restrainers required at expansion joints is not currently available" (Caltrans, 1999). However the design method that was proposed by DesRoches and Fenves (2000) showed an acceptable agreement

with the time history analysis in predicting the restrainer stiffness required to limit the hinge opening to a certain value. This design method has the advantage of considering the out-of-phase behavior of the adjacent frames as well the inelastic behavior. Thus the DesRoches and Fenves design method was used in designing the steel restrainers that were used in this study.

6.5.2.1 DesRoches and Fenves Design Method

The main design parameters that are used in this method are the frames stiffnesses, masses, and ductility demand ratio. Since in this study the masses of the two frames were held constant as well as the stiffness of the flexible frame, the only two design parameters were the stiffness of the stiffer frame and the ductility demand ratio of the two frames. The steel restrainers were designed using the following steps:

1) Calculate the maximum allowable hinge opening (D_r): The restrainer cables were designed to remain elastic and thus the hinge opening was limited to the yield displacement of the restrainers. Based on a 10-ft restrainers length and a 1.75% yield strain the allowable hinge opening (D_r) was found to be 2.1in.

2) Calculate the initial hinge opening: The hinge opening with no restrainers is first calculated based on the maximum displacements of the two frames D_1 and D_2. The maximum displacements are obtained from the design response spectrum using the following equation:

$$D_i = \left(\frac{T_{eff_i}}{2\pi}\right)^2 S_a(T_{eff_i}, \zeta_{eff_i}) \tag{6.2}$$

where the natural period of the frame i is $T_{eff_i} = 2\pi\sqrt{\frac{m_i}{k_{eff_i}}}$. The m_i, k_{eff_i} and ζ_{eff_i} are the mass, effective stiffness, and effective damping ratio of frame *i*. As indicated by equation 6.2, both the stiffness and damping ratio of the frames have to be modified to account for the inelasticity in the frames. Assuming that the frames follow an elastic perfectly plastic behavior their effective stiffnesses are $k_{eff_i} = k_i / \mu$. Where k_i is the initial stiffness of the frame i, and μ is the ductility ratio. On the other hand the damping ratio is modified to account for the frames ductility using the Takeda hysteresis relationship (MacRae et al., 1993):

$$\zeta_{eff} = \zeta + \frac{1 - \frac{0.95}{\sqrt{\mu}} - 0.05\sqrt{\mu}}{\pi} \tag{6.3}$$

where ζ is the elastic damping ratio. For this analysis ζ was assumed to be 0.05. For the μ values 1, 2, and 4 that were considered for the study, the corresponding values for ζ_{eff} were 0.05, 0.13, and 0.19, respectively.

After determining the T_{eff} and ζ_{eff} values for the two frames, the spectral acceleration value S_a is determined based on the appropriate design response spectrum. In order to relate the designed restrainers with the ground motion records that is used in the study, the design response spectrum was defined as a factor of the median response spectrum of the suite of records. After a number of trials it was found that the restrainers design method developed by DesRoches and Fenves results in restrainers with relatively large.

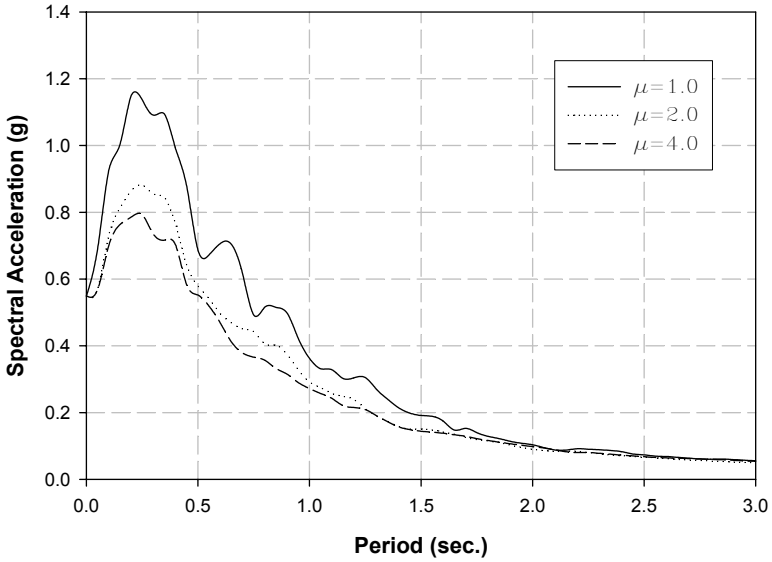

Figure 6.4 Design response spectrum curves for the three ductility levels that were used in the analysis.

stiffness. Thus in order to make the restrainers more flexible the design response spectrum was taken as 75% of the median response spectrum for the suite of ground motion. A design response spectrum curve was generated for each of the three ductility levels. Figure 6.4 shows the three design spectrum curves, which were used in the analysis

After D_1 and D_2 have been determined from equation 6.2, the hinge opening with no restrainers is calculated using the complete quadratic combination (CQC) rule as follows:

$$D_{h_0} = \sqrt{D_1^2 + D_2^2 - 2\rho_{12} D_1 D_2} \tag{6.4}$$

where D_{h_0} is the initial hinge opening and ρ_{12} is the cross-correlation coefficient, which is calculated as follows:

$$\rho_{12} = \frac{8\sqrt{\zeta_{\text{eff}_1}\zeta_{eff_2}}(\zeta_{eff_1} + \beta\,\zeta_{eff_2})\beta^{3/2}}{(1-\beta^2)^2 + 4\zeta_1\zeta_2\beta(1+\beta^2) + 4(\zeta_1^{\,2} + \zeta_2^{\,2})\beta^2} \tag{6.5}$$

where $\beta = \mathrm{T}_{\mathrm{eff}_2} / \mathrm{T}_{\mathrm{eff}_1}$.

If the calculated $D_{h_0} > D_r$ the remainder of the steps of the design procedure are used to determine required restrainers stiffness, while if $D_{h_0} < D_r$, the minimum restrainer stiffness is used based on the following equation:

$$k_{r_{\min}} = 0.5 k_{eff_{\text{mod}}} \tag{6.6}$$

where $k_{eff_{\text{mod}}}$ is the modified effective stiffness of the two frames and is calculated as follows:

$$k_{eff_{\text{mod}}} = \frac{k_{eff_1} k_{eff_2}}{k_{eff_1} + k_{eff_2}} \tag{6.7}$$

3) Calculate the required stiffness: The required stiffness for the restrainers is determined from the following equation:

$$k_r = \frac{k_{eff_{\text{mod}}}(D_{h_0} - D_r)}{D_{h_0}} \tag{6.8}$$

4) Calculate the hinge opening with restrainers: Assuming that the restrainer behavior is linearized, modal analysis is conducted for the two frames after installing the designed restrainers. The mass and stiffness matrices that were used in the analysis are:

$$M = \begin{bmatrix} m_1 & 0 \\ 0 & m_2 \end{bmatrix} \tag{6.9}$$

$$K = \begin{bmatrix} k_{eff_1} + k_r & -k_r \\ -k_r & k_{eff_2} + k_r \end{bmatrix} \tag{6.10}$$

The modal hinge opening for mode i is determined from the following equation:

$$D_{h_i} = P_i S_{a_i}(T_{eff_i}, \zeta_{eff_i}) \tag{6.11}$$

where the modal participation factor P_i is calculated as follows:

$$P_i = \frac{\varphi_i^T M 1}{\varphi_i^T K \varphi_i}(a^T \varphi_i) \tag{6.12}$$

where φ_i is the mode shape determined from the modal analysis, 1 is a unit vector, and $a = \begin{bmatrix} -1 \\ 1 \end{bmatrix}$. The maximum hinge opening is then determined from combining the modal responses of the two modes using the CQC combination rule as follows:

$$D_h = \sqrt{D_{h_1}{}^2 + D_{h_2}{}^2 - 2\rho_{12} D_{h_1} D_{h_2}} \tag{6.13}$$

If $D_h < D_r$ then the design is complete. If not then the stiffness of the restrainers is modified based on the next step.

5) Calculate the incremental restrainer stiffness: The stiffness of the restrainers is modified using the following equation:

$$k_{r_{j+1}} = k_{r_j} + (k_{eff_{\text{mod}}} + k_{r_j}) \frac{(D_{h_j} - D_r)}{D_{h_j}} \tag{6.14}$$

Steps 4 and 5 are repeated until the resulting hinge opening D_h is less than or equal to the allowable hinge opening D_r.

Table 6.2 shows the stiffness of the steel restrainers, which were designed using DesRoches and Fenves restrainer design method. The table presents the restrainers stiffness values at the period ratio and ductility ratio values that were considered in the study.

6.5.2.2 Design of Shape Memory Alloy Devices:

As was mentioned earlier the main philosophy that was followed in designing the retrofit devices that were involved in this study is to ensure that the effective stiffness added to the structure by each device is the same. In the case of the SMA devices, the

Table 6.2 Stiffness values for the designed steel restrainers.

$(\rho=T_2/T_1)$	*Restrainer Stiffness k_r (kips/in)*		
	$\mu=1.0$	$\mu=2.0$	$\mu=4.0$
0.3	406	563	405
0.4	488	385	304
0.5	479	300	201
0.6	400	240	152
0.7	330	174	108
0.8	216	115	37
0.9	147	66	33

device is capable of reaching approximately 6%-8% strain with no residual strain after unloading. At this level of strain, the SMA would likely have experienced most of the phase transformation from austenite to martensite, however the strain hardening due to the martensite elastic behavior would not have initiated yet and thus a controlled level of force is associated with the SMA hysteresis. Due to the low residual strain and force associated with the end point of phase transformation, this point was selected as a controller for the target displacement and stiffness, which the SMA device is designed accordingly.

Figure 6.5 shows a schematic of the hysteretic behavior considered for the superelastic SMA device compared to the steel restrainers behavior. Notice from the figure, the phase transformation end point for the SMA was assumed to be at the 6%-strain. The effective stiffness of the SMA device at that point was assumed to be equal to the designed steel restrainer initial stiffness. The strain at the phase transformation initial point was assumed to be 1%, which is typical for most SMAs. The SMA hysteretic height as well as the strain hardening ratios during and after phase transformation was assumed to be constant through out the study. The unloading SMA force was taken as

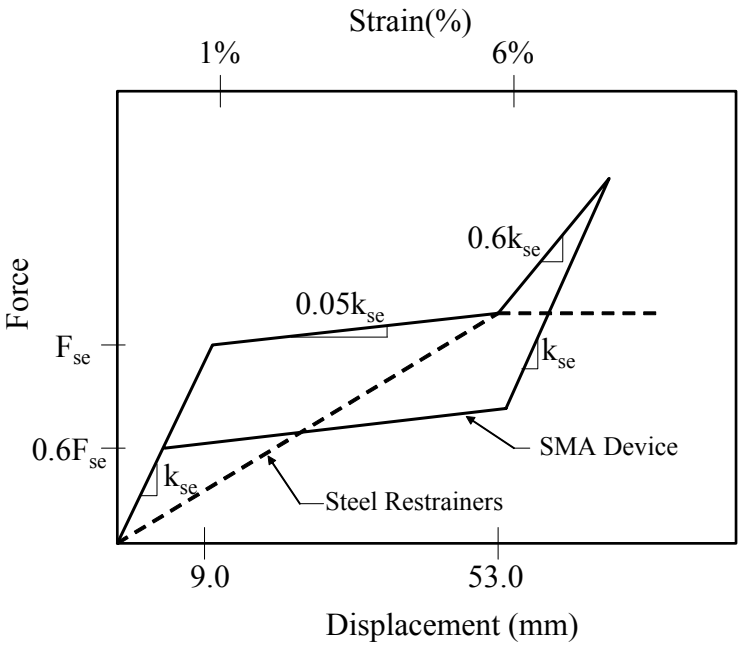

Figure 6.5 Schematic showing the SMA device hysteretic behavior compared to the steel restrainers behavior.

60% of the force at the beginning of phase transformation. During phase transformation the SMA device was assumed to experience 5% strain hardening. After the completion of the phase transformation the martensitic elastic modulus was assumed to be 60% of the austenetic elastic modulus. Both devices were assumed to engage at zero strain (i.e. the slack was not accounted for in the study). For the case when the tension/compression feature of the SMA device is considered, the tension and compression mechanical properties of the SMA were assumed to be identical.

6.5.2.3 Design of Metallic Dampers:

Since the metallic dampers are characterized by a bilinear constitutive behavior, their loading backbone curve is similar to that of the SMAs during phase transformation. However both devices behave differently during unloading. Based on this similarity, the

metallic dampers were designed such that they would exhibit the same loading curve as the SMAs prior to reaching the completion of the phase transformation. Beyond the phase transformation range, both devices behave differently. Figure 6.6 shows a comparison between the constitutive behavior of the metallic dampers, and the SMA devices.

6.5.2.4 Design of Viscoelastic Dampers:

Since the viscoelastic dampers were modeled in OpenSees as a combination in parallel of elastic and viscous materials, the properties of each of the two materials had to be designed separately. The elastic component of the model is responsible of providing the device with its effective stiffness, while the viscous component provides the hysteretic behavior. Thus the modulus of the elastic material was assigned a value equal

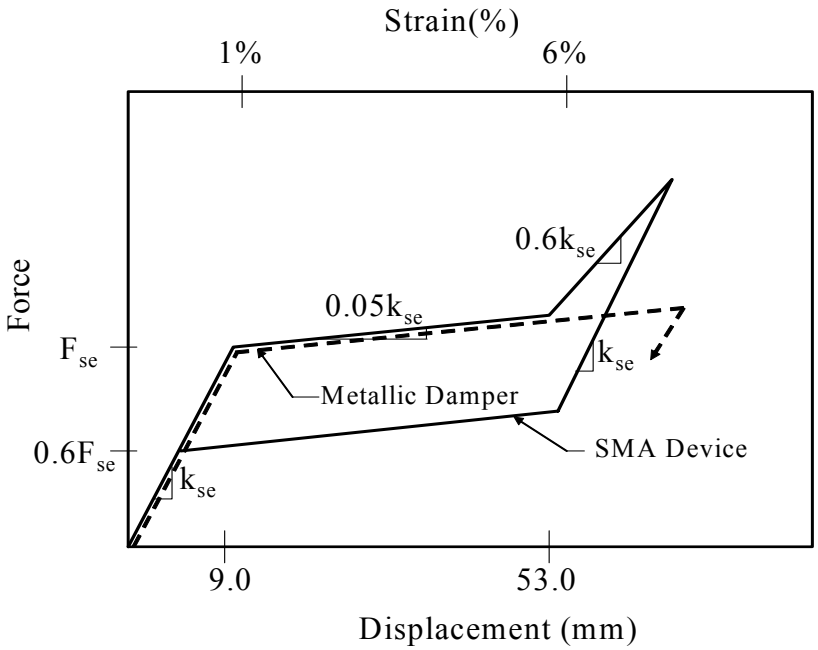

Figure 6.6 Comparison of the constitutive behavior of SMA devices and metallic dampers.

to the initial stiffness of the steel restrainers. Equation 2.2 that was presented earlier in Chapter 2 and represented below for convenience demonstrated the relationship between the damping coefficient C_d of the viscous material and the elastic component k_d.

$$C_d = \frac{k_d \eta}{\omega} \tag{2.2}$$

Experimental studies have shown that the loss factor η is not sensitive to the frequency of the excitation and it is typically around 1.3. On the other hand, for this study the cyclic frequency of the excitation was assumed to be equal to the average cyclic frequencies of the 25 records used in the study, which was approximately 1.82 Hz. After substituting in equation 2.2 for the values of η and ω we get:

$$C_d = k_d / 8.8 \tag{6.15}$$

Equation 6.15 shows that the viscous material damping coefficient is directly related to the elastic material stiffness, which was assumed to be equal to the stiffness of the steel restrainers. Figure 6.7 shows the relationship between the mechanical behavior of the viscoelastic dampers and the designed steel restrainers.

6.6 Analysis Results

6.6.1 As-built Results

The hinge opening results of the as-built bridge model are presented in Figure 6.8.

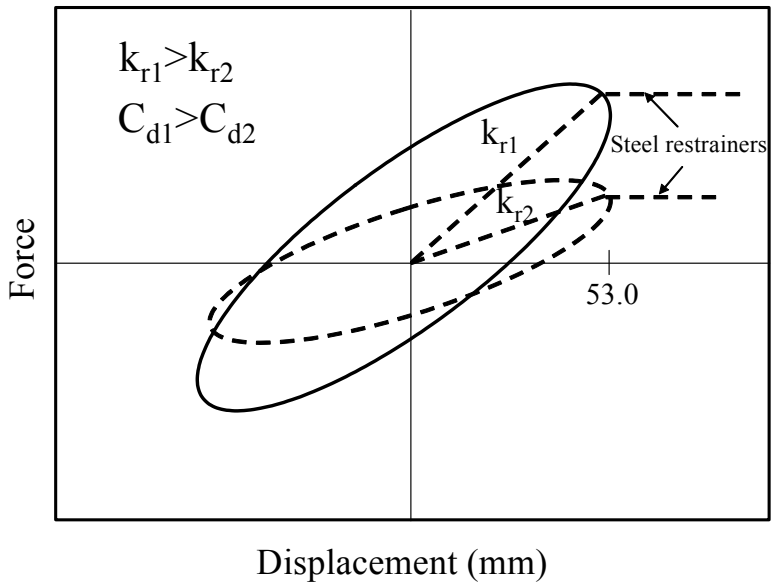

Figure 6.7 Comparison of the constitutive behavior of viscoelastic dampers and steel restrainers.

The results presented in parts a and b of the figure are for the scaling factors SF equal to 1.0 and 1.5, respectively. The figure presents the median results of the maximum hinge openings resulting from running the suite of records at various frame period ratios and ductility ratios. The figure shows that the maximum hinge opening typically decreases with increasing frame period ratios and ductility ratios. This behavior is expected due to the in-phase type of behavior associated with high period ratios and ductility ratios. The ground motion scaling factor did not seem to have a major effect on the trend of the data. However an increase in the maximum hinge opening was observed at the larger ground motion intensity. For a moderate value of ρ equal to 0.6, the median maximum hinge opening increased by approximately 42%, 64%, and 154% in the case of ductility ratios equal to 1.0, 2.0, and 4.0, respectively. This shows that for MF bridges with moderate

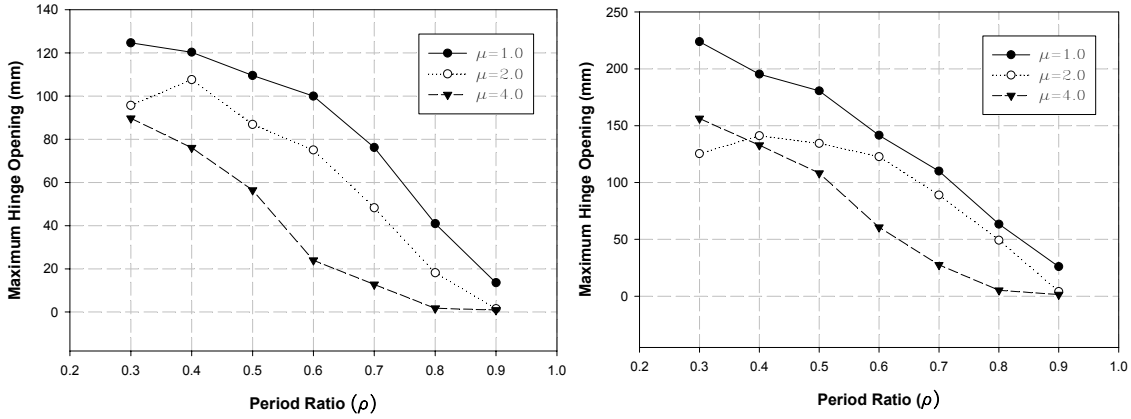

a. SF=1.0 b. SF=1.5

Figure 6.8 Median response of the as-built model maximum hinge opening under different intensity levels of ground shaking

period ratios, the ground motion intensity has more impact on the hinge opening value at higher levels of frame ductility.

6.6.2 Shape Memory Alloy Devices Results

The median responses of the maximum strain experienced by the tension-only and tension/compression SMA devices due to the applied suite of ground motion records are presented in Figures 6.9a and 6.9b, respectively. Each of parts a and b in the figure shows the response at the two ground motion scaling factors that were considered in the study. The figures show that the maximum strain in the SMA devices decreases with the increase in the frames period ratio and ductility ratio. All the four cases shown in Figure 6.9 showed a maximum strain value of approximately zero in the case of period ratio equal to 4 and ductility ratio equal to 0.9. This is due to the highly in-phase type of motion associated with such high period ratio and ductility ratio values.

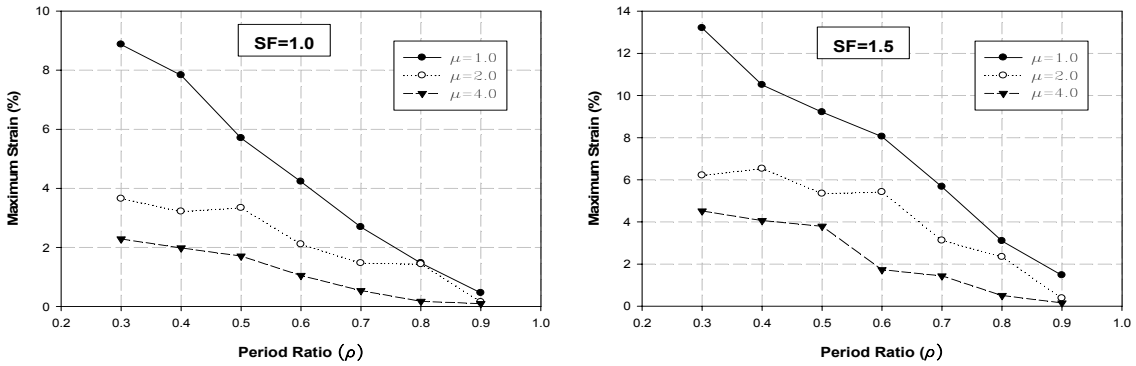

a. Tension-only SMA device

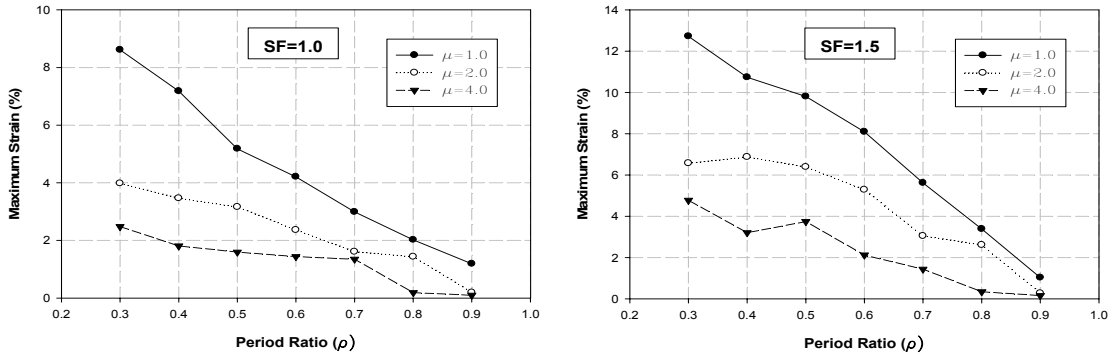

b. Tension/Compression SMA device

Figure 6.9 Median responses of the SMA devices maximum strain values

The effectiveness of the SMA devices in limiting the hinge opening at various levels of frame ductility and period ratio is illustrated through Figure 6.10. The figure shows the mean MHDR response at various period ratios, ductility ratios, and ground motion scaling factors for the tension-only and tension/compression SMA device. The figure shows that the effectiveness of SMA devices in limiting the hinge opening in MF bridges highly depends on the frames period ratio and ductility ratio. The MHDR response seems to follow different trend in the case of the elastic bridge compared to the inelastic bridge cases. All of the four sub-figures presented illustrate that in the case of the elastic

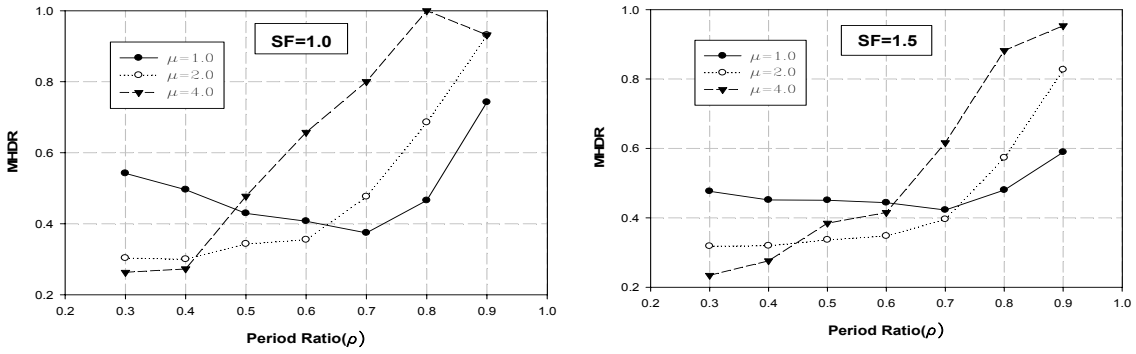

a. Tension-only SMA device

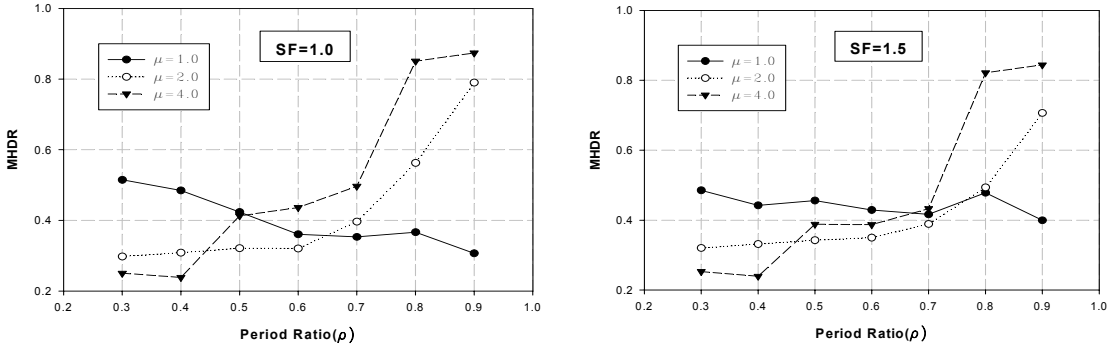

b. Tension/Compression SMA device

Figure 6.10 Mean maximum hinge displacement ratio response of the SMA devices

bridge the SMA devices tend to be less effective at smaller period ratios compared to the inelastic cases. In the case of moderate period ratios the effectiveness of the SMA devices seem to be unaffected by the bridge ductility. However at high period ratios the SMA devices seem to be of more effect in the elastic bridge case. This was expected due to the relatively large hinge opening in the elastic as-built bridge associated with small period ratios. The figures also illustrate that the SMA devices show more consistent in their effectiveness at lower bridge ductility levels. For example, in the case of tension-only SMA devices subjected to SF equal to 1.5, the differences between the mean MHDR values at period ratios 0.3 and 0.9 were 19%, 61%, and 76% in the case of ductility ratios

1, 2 and 4, respectively. This shows that the effectiveness of SMA devices is highly affected by the period ratio of the bridge frames which are more ductile. On the other hand, increasing the ground motion scaling factor did not have a significant effect on the trend of the MHDR behavior.

The effect that the SMA devices have on the ductility demand of the bridge frames is illustrated through Figures 6.11 and 6.12. The figures present the mean MDR response of the flexible frame and stiff frame, respectively at various frame period ratios, ductility ratios, and ground motion scaling factors. The figures show similar behaviors at the two ground motion scaling factors that were considered in the study. Figure 6.11 shows that using SMA devices tends to reduce the maximum drifts of the flexible frame. The reduction in the maximum drift of the flexible frame increases at smaller period ratios. This was expected since at large period ratios the two frames are in-phase which results in a small hinge opening and thus small restoring force associated with the SMA devices. The MDR is not highly sensitive to the ductility of the frames. This is illustrated through the close behaviors which the elastic case and inelastic case with μ equal 2 are experiencing. However larger drifts were noticed when the ductility ratio of the frame was increased to 4.

Figure 6.17 shows that for MF bridges with moderate to high period ratio values the ductility of the bridge frames has minor effect of the stiff frame drift response. For the moderate to high period ratio bridge, the SMA devices have small effect on the stiff frame drifts. However at smaller period ratios the SMA devices seem to reduce the maximum drifts in the case of the elastic bridge while increasing it in the inelastic bridge case. This behavior is due to the sensitivity of the ductile frames to the restoring force of

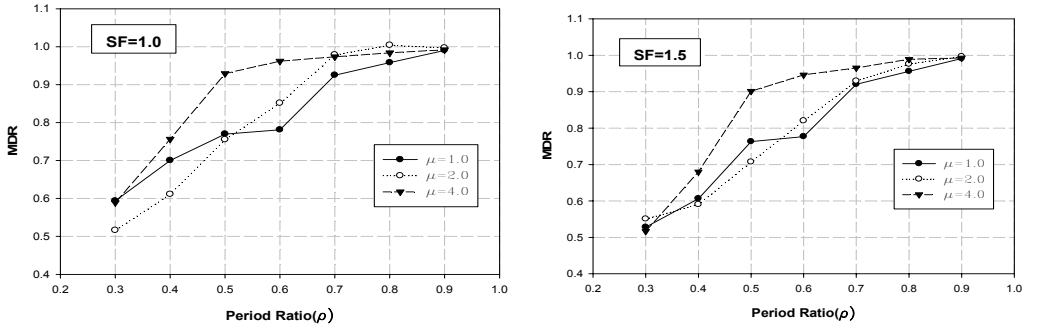

a. Tension-only SMA device

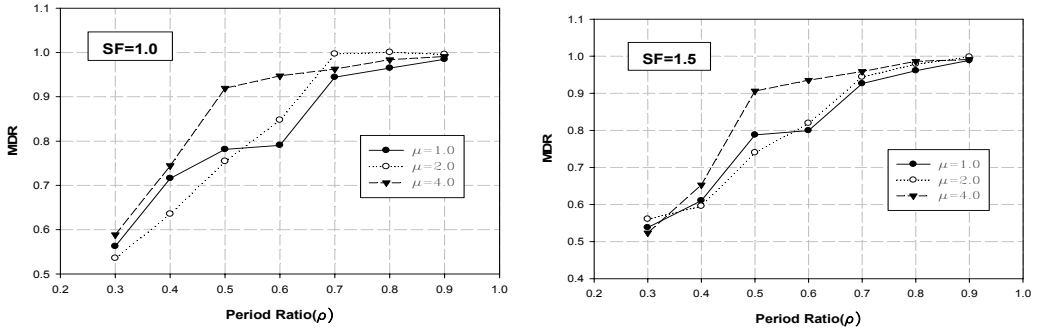

b. Tension/Compression SMA device

Figure 6.11 Mean maximum drift ratio for the flexible frame using the SMA devices

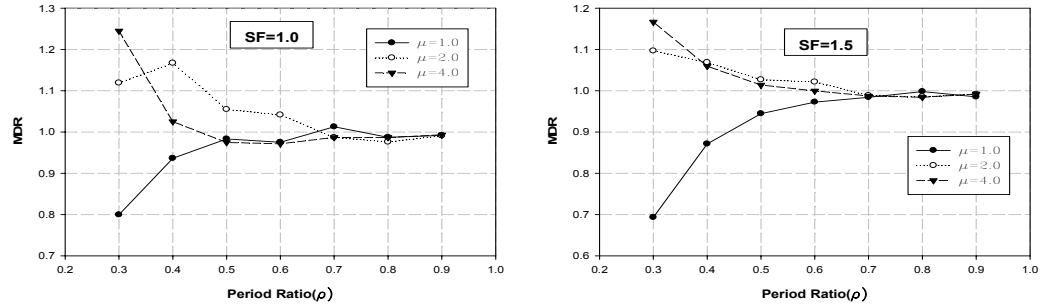

a. Tension-only SMA device

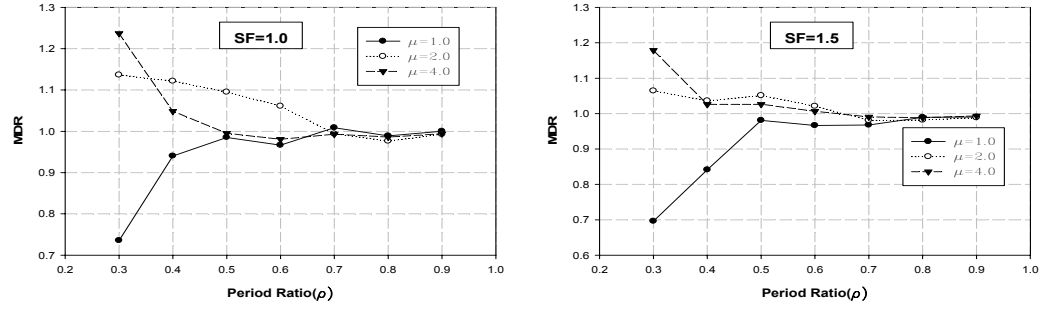

b. Tension/Compression SMA device

Figure 6.12 Mean maximum drift ratio for the stiff frame using the SMA devices

the SMA devices. The case where the ductility ratio of the frames was taken as 2 showed higher maximum drifts compared to the case with ductility ratio equal to 4 at small period ratios. This is most likely due to the relatively large SMA force in the low ductile case compared to the case of high ductility.

6.6.3 Comparison of Retrofit Devices Results

Figure 6.13 presents a comparison of the MHDR mean responses in the case of using steel restrainers, tension-only SMA devices, tension/compression SMA devices, metallic dampers and viscoelastic dampers as retrofit devices in a MF bridge with various frame period and ductility ratios and under two levels of ground motion scaling. The response shown is the mean of the MHDR values resulting from the 25 records that was presented earlier in this chapter.

The figure illustrates that all of the studied devices were able to limit the hinge opening. In all cases, the steel restrainers were less effective compared with the other devices. This was due to the tension-only behavior of the steel restrainers which when combined with the yielding behavior of the steel results in an increase in the accumulation of residual displacement and reduction in the effectiveness of the device. The figures show that in all cases the tension-only SMA device performed as effective as the other devices. However the effectiveness of the SMA device tends to decrease at higher period ratios. This is most likely due to the fact that all of the other devices behave elastically at the large period ratios and thus the small contribution of the elastic compression behavior of each of the tension/compression devices is of more significant. The average reduction in MHDR resulting from using the tension-only SMA devices

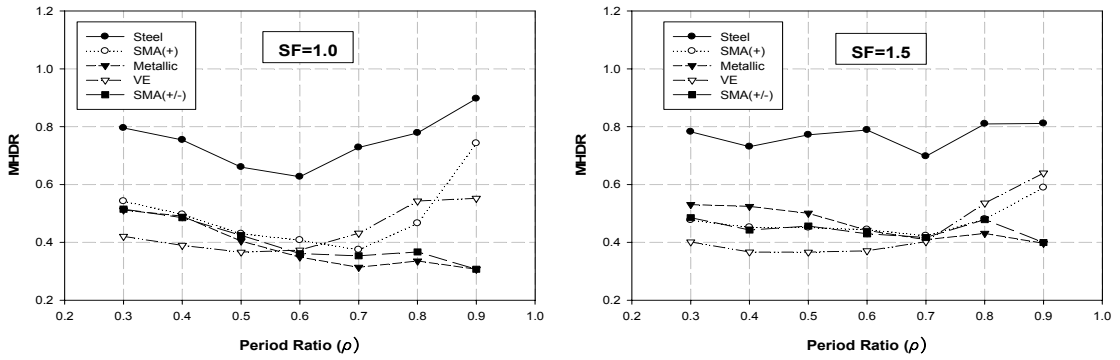

a. μ=1.0

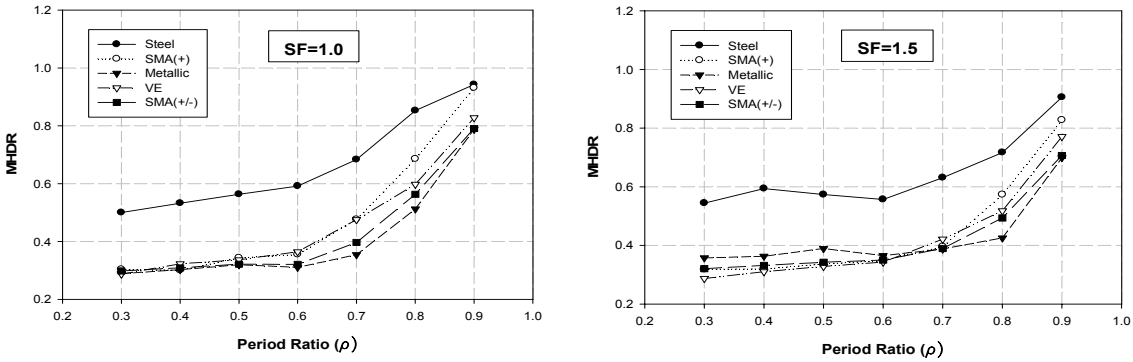

b. μ=2.0

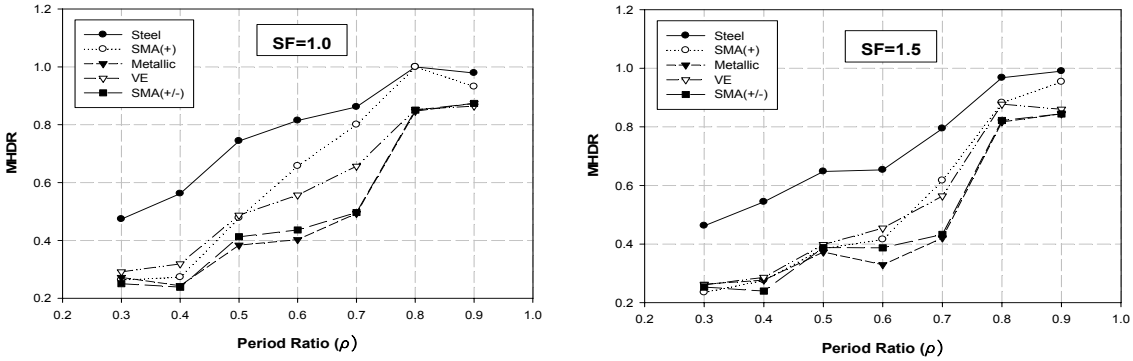

c. μ=4.0

Figure 6.13 Mean values of the maximum hinge displacement ratio responses in the case of using various retrofit devices

compared to the steel restrainers were 39%, 33%, and 30% in the case of ductility ratio 1, 2, and 4, respectively.

The figures show that the three tension/compression devices behave in an almost similar pattern in most of the studied cases. However the tension/compression SMA devices and the metallic dampers tend to be more similar in their behavior compared to the viscoelastic dampers. This is due to the identical initial stiffness that both devices have. In addition to the fact that both devices are displacement controlled while the viscoelastic damper behavior highly depends on the displacement rate. In the elastic bridge case, the tension/compression SMA device and the metallic damper reduce the hinge opening similarly except at higher period ratios where the metallic dampers show slight advantage compared to the SMA device. When the ground motion scaling factor is increased to 1.5, the SMA device performed better than the metallic damper in low-to-moderate period ratios. The same type of behavior was observed in the case of ductility ratio equal 2.0. However when the ductility ratio was increased to 4.0 the two devices acted almost identical in most of the period ratio cases regardless of the ground motion intensity. The more effective behavior of the SMA devices at low ductility levels and/or high ground motion intensities is related to the martensitic strain hardening of the SMA devices. When the ductility of the bridge increases or in the case of high period ratios the out of phase behavior of the two frames tends to decrease and thus the SMA devices do not experience martensitic strain hardening.

Comparing the viscoelastic dampers to the tension/compression SMA devices illustrates that the viscoelastic dampers are most effective in the elastic bridge case, especially in the case of low to moderate period ratios. For inelastic bridge response, the

viscoelastic dampers performed similarly to SMA devices or with less efficiency depending on the ductility and period ratio of the frames. At period ratio of 0.7 and SF equal to 1.5, the differences between the mean MHDR values of the tension/compression SMA devices and the viscoelastic dampers were approximately 4%, 7%, and 23% at μ equal to 1, 2, and 4, respectively. This shows that at higher period ratios and/or higher bridge ductility the viscoelastic dampers seem to lose a significant portion of its effectiveness compared to the SMA devices. This is due to the dependency of the viscoelastic dampers on velocity of hinge rate. At smaller period ratios and while the structure is elastic the rate of the hinge opening is higher than other cases due to the out-of-phase motion and the pounding effect between the two frames. In order to relate the conclusions which were observed from Figure 6.13 to the constitutive behavior of each of the studied devices, the force-displacement relationship of the five devices is presented in Figure 6.14. In this figure, the 1992 Cape Mendocino at Rio Dell Overpass record was used at scaling factor 1.5, the frames ductility ratio was equal to 2.0 and their period ratio was equal to 0.5.

The MDR mean response of the flexible frame and the stiff frame is presented in Figures 6.15 and 6.16, respectively. The figure presents a comparison between the MDR mean responses for the cases of the five retrofit devices at various frame period ratios and ductility ratios. Figure 6.15 illustrates that using any of the five devices reduces the drifts of the more flexible frame to a certain extent compared to the as-built bridge case. However the reduction in the maximum drifts decreases at higher period ratios since at such period ratios smaller effective stiffness was assumed for the retrofit devices. At all

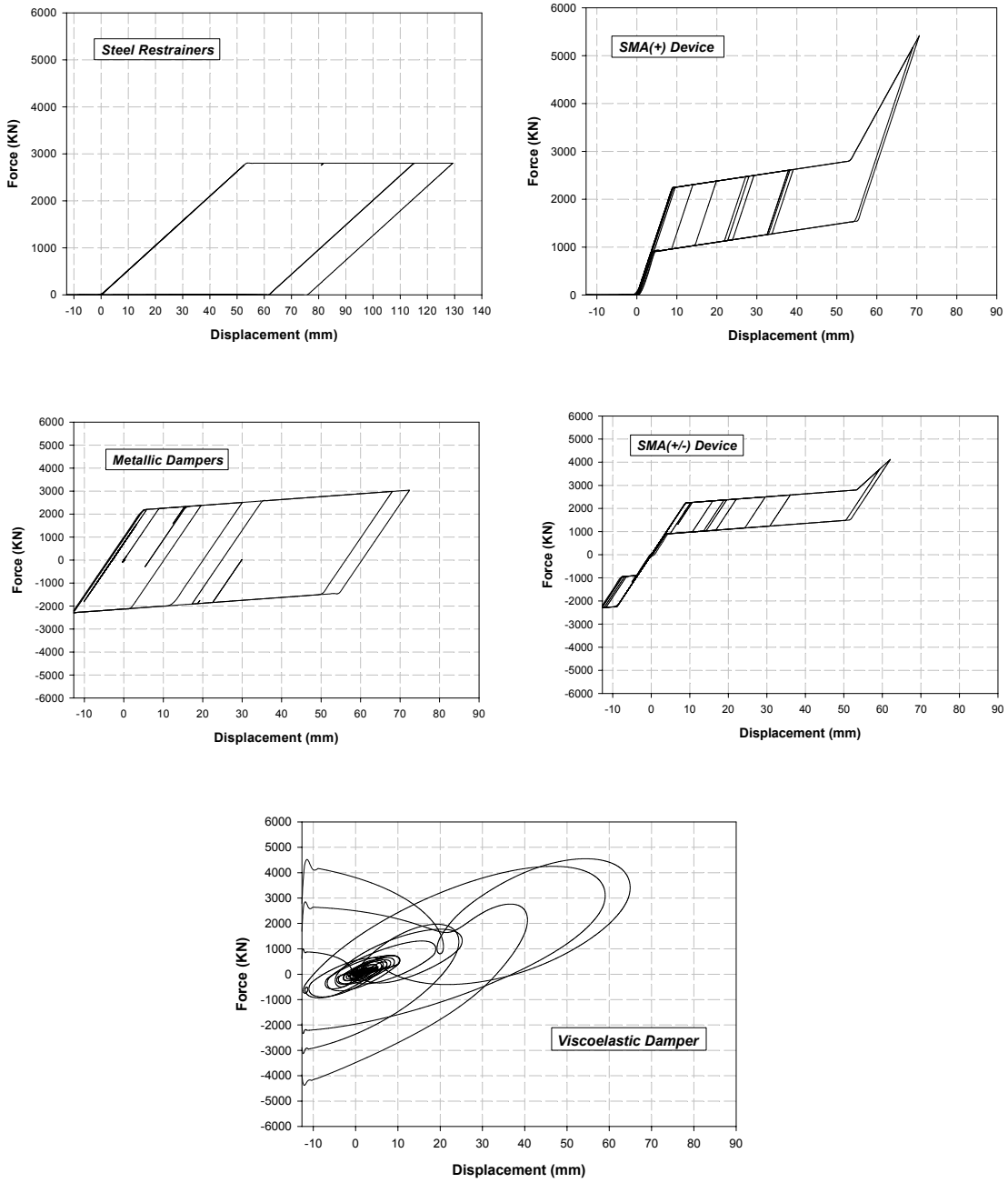

Figure 6.14 Force-displacement relationships for the five retrofit devices used in the study under the 1992 Cape Mendocino at Rio Dell Overpass record.

ductility levels the steel restrainers seemed to be less effective in reducing the drifts of the flexible frame. In the case of the inelastic bridge and regardless of the ductility ratio values, all retrofit devices except the steel restrainers seemed to have approximately the same effect on the drifts of the flexible frames. In the elastic case only the there were minor differences observed in the effectiveness of each device. For low to moderate period ratios the viscoelastic dampers was performing slightly better in reducing the MDR response.

The MDR mean response of the stiff frame that is shown in Figure 6.16 illustrates that using any of the five devices in an inelastic bridge increases the maximum drifts of the stiff frame compared to the as-built case, especially in the case of smaller period ratios. This behavior was expected due the out-of-phase motion between the two frames and the large effective stiffness of the retrofit devices. In both cases where the ductility ratio was equal to 2.0 and 4.0, the five devices had a similar effect on the drifts of the stiff frame. This shows that once the bridge enters the inelastic stage the difference between the five devices have a similar effect on the bridge's ductility demand. On the other hand if the bridge remained elastic all of the retrofit devices except the steel restrainers reduced the maximum drift of the stiff frame. In the elastic case the viscoelastic dampers and the metallic dampers had more effect in reducing the maximum drifts compared to the SMA devices or the steel restrainers. This is most likely due to their relatively large hysteretic damping effect.

An important factor that defines the efficacy of each of the retrofit devices is the post-earthquake permanent deformations that could occur to the bridge's components. Since the focus of this study is on limiting the hinge openings in the MF bridges, the

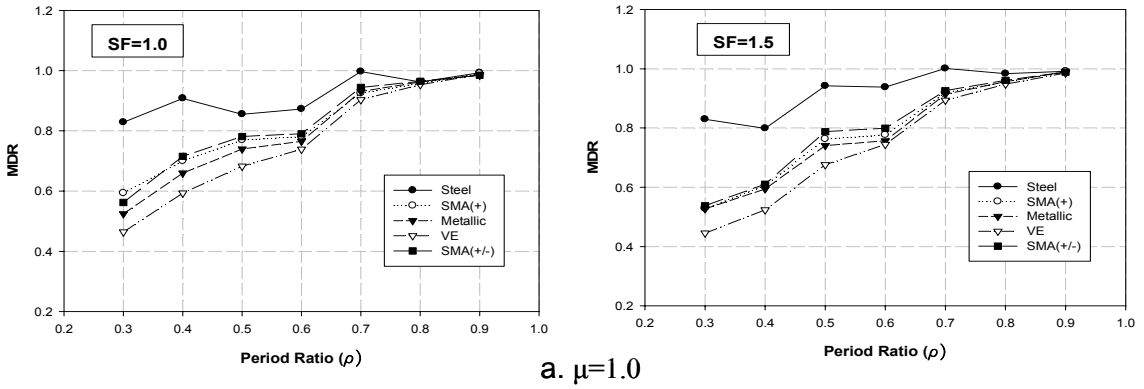

a. μ=1.0

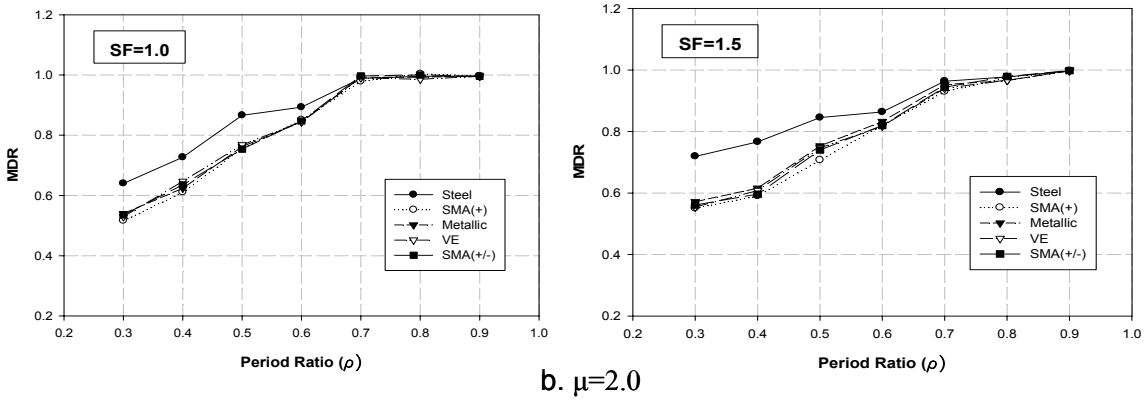

b. μ=2.0

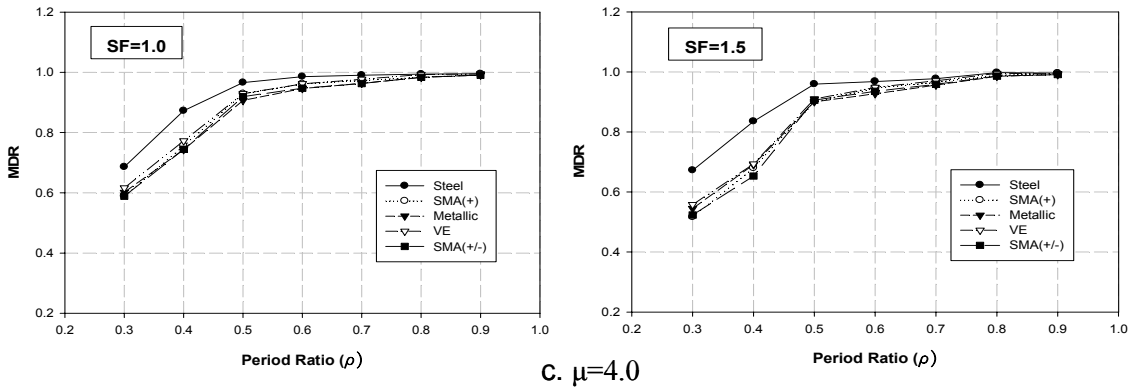

c. μ=4.0

Figure 6.15 Mean values of the maximum drift ratio responses for the flexible frame in the case of using various retrofit devices.

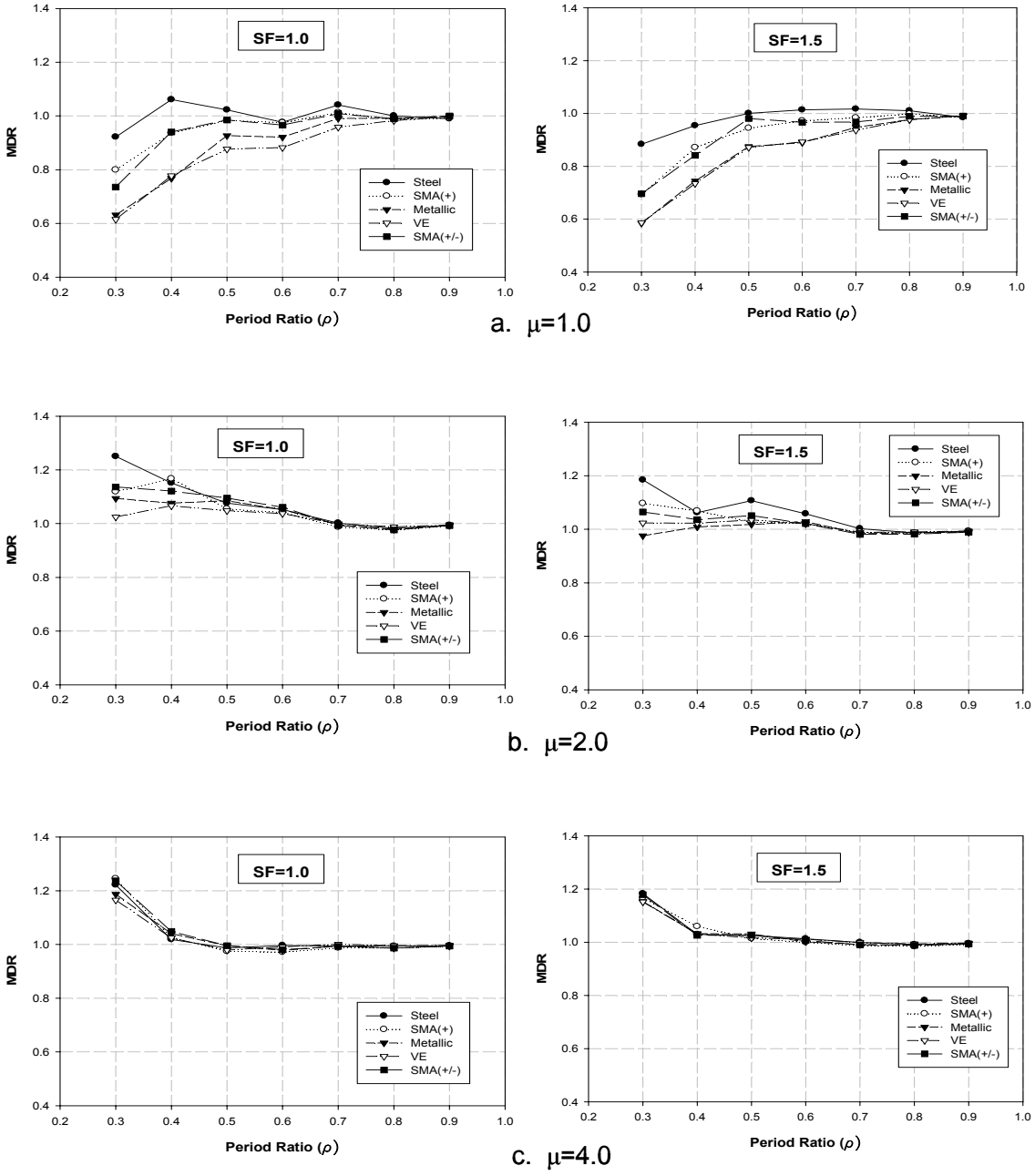

Figure 6.16 Mean values of the maximum drift ratio responses for the stiff frame in the case of using various retrofit devices.

post-earthquake hinge opening which will be referred to as the residual hinge opening was studied. The amount of residual hinge opening will control the functionality of the bridge after the occurrence of an earthquake.

Figure 6.17 shows a comparison between the mean values of the residual hinge opening in the case of using various retrofit devices as well as in the case of the as-built bridge. The residual hinge opening response was monitored at various frames period ratios, ductility ratios, and ground motion scaling factors. Since the occurrence of a residual hinge opening would require the yielding of the bridge frames, the case where the bridge was assumed to remain elastic was not considered in this study. As shown in the figure, the residual hinge openings tend to decrease with the increase of the frames period ratio until it reaches almost zero at a period ratio equal to 0.9. At such high period ratios the two frames act essentially in-phase. Although yielding of the frames could occur a residual hinge opening is most likely unexpected. The figure also illustrates that a large residual hinge opening that could reach approximately 38 mm (1.5 in) at small period ratios is possible in the as-built bridge that is subjected to a moderate ground motion intensity, which is represented by the SF equal to 1.0 case. At higher intensities this residual hinge opening could increase by approximately 67%. The steel restrainers resulted in the least reduction in the residual hinge openings. This was expected due to the fact that the steel restrainers go through accumulation of residual displacement once the restrainers yield. The tension/compression behavior of the metallic dampers increased its efficiency in limiting the residual hinge opening compared to the steel restrainers. However at SF equal to 1.0 the average residual hinge opening mean values at the smaller period ratios were approximately 6.4 mm (0.25 in) and 5.8 mm (0.23 in) at

ductility ratio values 2.0 and 4.0, respectively. While for SF equal to 1.5 those values were 10.7 mm (0.42 in) and 9.9 mm (0.39 in). The figure also illustrates that using the tension/compression SMA devices and the viscoelastic dampers prevented the occurrence of residual hinge opening. This is due to the recentering nature which is inherited in both devices.

In summary, the parametric study showed that the steel restrainers are the least effective devices in limiting the hinge opening in bridges. The tension-only SMA device is as effective as other devices at smaller period ratios. However, at moderate-to-high period ratios, the tension/compression devices are more effective. On average the SMA tension-only device improved the reduction in the hinge opening by approximately 34% compared to steel restrainers. On the other hand, the tension/compression SMA devices showed better efficiency than the metallic dampers in reducing the hinge opening in the case of bridges with low-to-moderate period and/or ductility ratios which are subjected to relatively strong ground motions. The tension/compression SMA devices were also more effective than the viscolelastic dampers when used in bridges with low-to-moderate period ratios, especially in bridges with large ductility.

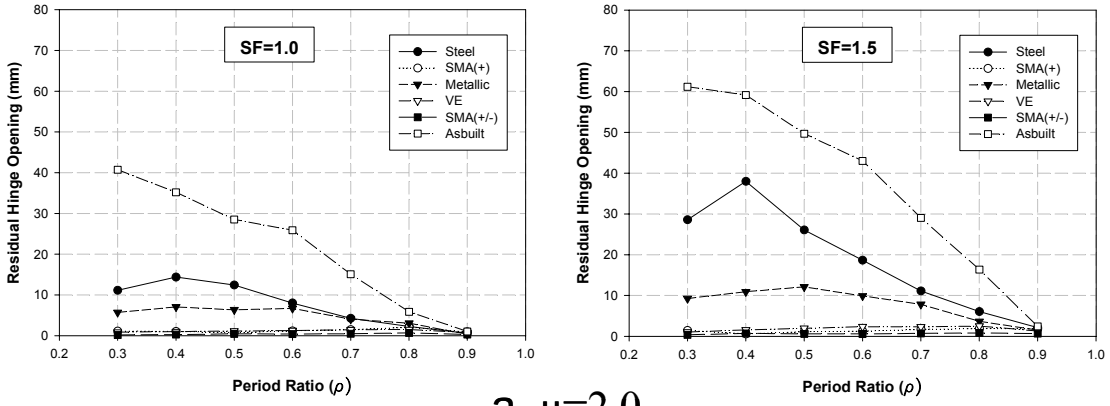

a. μ=2.0

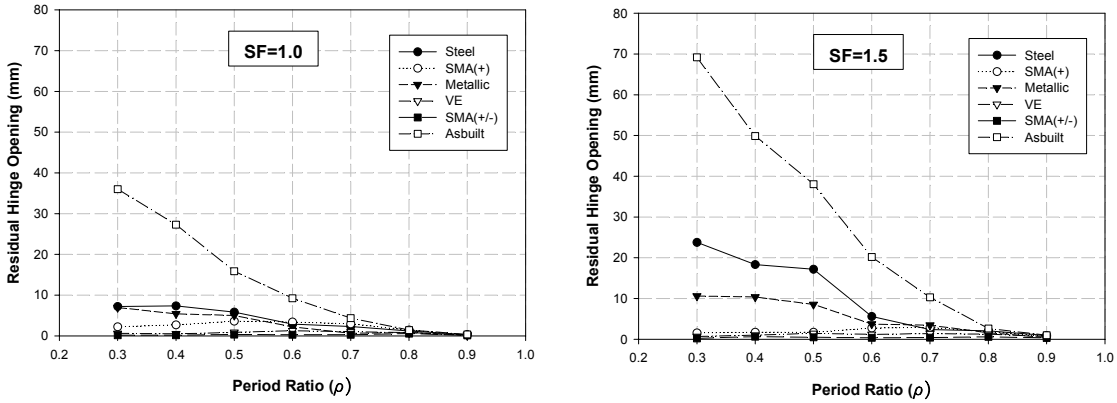

b. μ=4.0

Figure 6.17 Mean values of the residual hinge opening responses in the case of using various retrofit devices

CHAPTER 7

CASE STUDIES USING MULTIPLE DEGREE OF FREEDOM BRIDGE MODEL

7.1 Introduction

This chapter presents three case studies involving the use of superelastic SMA devices in multiple frame bridges. The intension behind conducting these case studies is to validate the results of the sensitivity analyses that were conducted and presented earlier in Chapters 5 and 6 using a simplified 2-DOF model. The chapter starts with a description of the properties of the multiple frame bridge that was used as a prototype. Next, a description of the analytical model that was developed for the prototype bridge using OpenSees is presented. This is followed by a description of the ground motion records that were used in the analysis and the description and results of the three case studies. The first and second case studies focus on investigating the effect of variability in the SMA's hysteretic properties and the ambient temperature, respectively on the efficacy of the SMA devices that are used in the seismic retrofit of MF bridges. The third study compares the capabilities of SMA devices as well as other devices in limiting the hinge openings in MF bridges during earthquakes.

7.2 Prototype Bridge

In order to capture accurately the behavior of MF bridges which are constructed in an area of high seismicity, the College Avenue Undercrossing Bridge located in the Alameda County in the city of Oakland, California was used as a prototype in this study. This structure was designed in 1966 and constructed in 1970. The main reason behind

selecting this bridge for the study was the relatively large number of frames (six) which would provide an opportunity to investigate situations with various period ratio values. In order to get an idea of the bridge general layout and design, the detailed drawing plans of the bridge provided by The California Department of Transportation (Caltrans), are located in Appendix A of this dissertation.

As shown in the general plan drawing of the bridge, the structure mainly consists of two one-way bridges. The right bridge allows the movement towards the city of Concord, while the left bridge allows movement towards the city of Oakland. The two bridges were constructed as two separate structures. The model that was used in the analyses of this chapter was developed based on the details of the right bridge. As noticed in the bridge plan drawing, the right bridge consists of six frames separated by five intermediate hinges. The total length of the bridge was 412 m (1351.5 ft), while the width of the bridge's cross section was 21 m (69 ft). The bridge deck consisted of reinforced concrete box girders with 1.4 m (4.5 ft)-height. The deck was supported by 18 reinforced concrete two-rectangular column bents. Due to the layout of the bridge, three of the 18 bents were constructed with a skewed angle between the bent axis and the longitudinal bridge axis, while the rest of the bents were normal to the bridge axis. The number of bents supporting each frame varied between 2 and 4 depending on the layout of the bridge. The end spans of the bridge were supported using an integral diaphragm abutment on one end of the bridge while the other end was supported by a seat abutment with a backwall.

In 1981 and 1992 the bridge was retrofitted under the Caltrnas Phase I and Phase II retrofit plans, respectively. In the first phase, Caltrans installed additional steel

restrainers in some of the bridge's intermediate hinges, while in the second phase some of the bent columns were provided with steel casing. In order to study the performance of various retrofit devices in as-built bridges the columns steel jacket was not included in the bridge model.

7.3 Multiple Degree of Freedom Model

Since the hinge opening problem is mainly due to the movement of the bridge in the longitudinal direction and since the College Avenue Undercrossing Bridge is mainly a straight bridge with only 1/6 of its bent constructed with skewness, a 2-D model was sought to be adequate enough to capture the bridge behavior in the longitudinal direction. A 2-D MDOF model was developed for the right College Avenue Undercrossing Bridge using OpenSees. As mentioned earlier the main reason behind selecting this bridge for the study was the large number of frames that would provide a wide range of frames period ratios. Preliminary analyses of the bridge have shown that the period ratios of the adjacent frames varied from 0.82 to 1.0. These values were considered to be too close to one, and would result in an in-phase motion. In order to provide a wider range of period ratio values the height of some of the columns were modified. Figure 7.1 presents the bridge's cross section and the general layout of the bridge after modifying its columns height. The only modifications occurred were in the columns of frames number 1, 3, and 4, where the columns height of Frame 1 was reduced by 10% and the columns height of Frame 2 was increased by 25%, and the columns height of Frame 4 was reduced by 30%

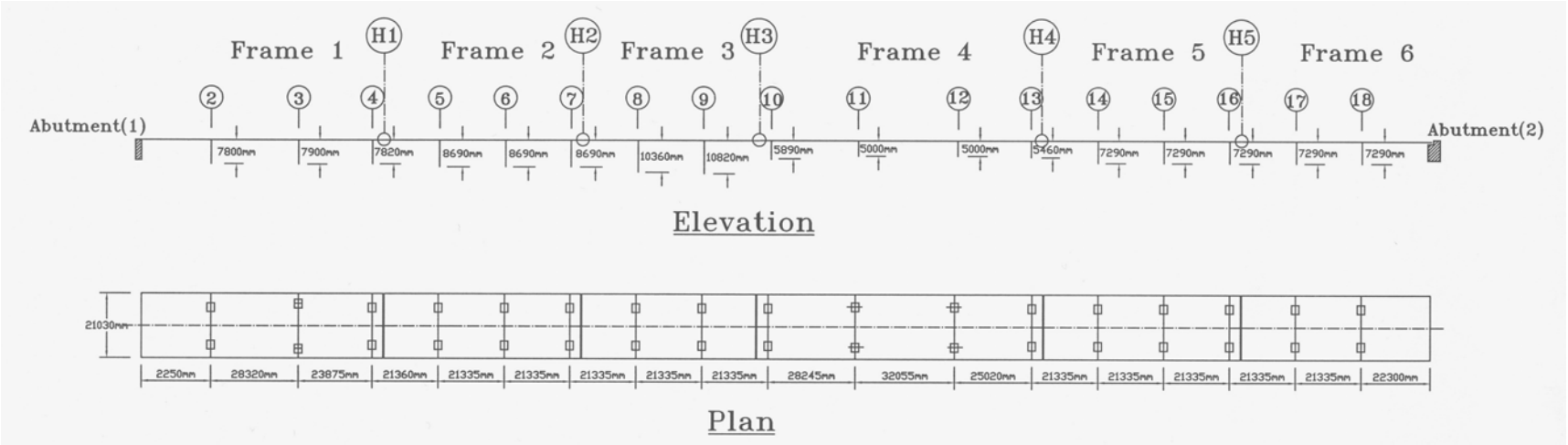

Figure 7.1 General Layout and cross section of the right College Avenue Undercrossing Bridge after modifying the column heights of Frames 1, 3, and 4

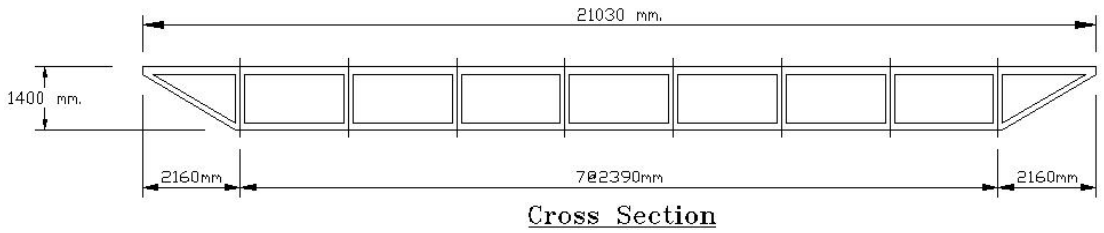

Figure 7.1 (Continued)

A description of the models that were developed for the bridge components is provided in the following subsections.

7.3.1 Deck Model

The bridge deck was modeled using 101 nodes joined together with 95 of the OpenSees elastic beam/column element. Due to the relatively high stiffness of the deck it was assumed to behave elastically. The mass of the deck was lumped at the nodes. The reinforced concrete was assumed to be of normal weight, and thus its density was assumed to be 24347 N/m^3 (155 lb/ft^3). The weight of the bridge wearing and barriers was assumed to be 18971 N/m (1.3 kips/ft). The weight of the bent caps and end diaphragms was also included in the model.

7.3.2 Column Model

As mentioned earlier, the bridge superstructure is supported by several bents which were distributed along each of the 6 frames. The number of bents varied from one frame to another. Three bents were used to support Frames 1, 2, and 5; two bents were used to support Frames 3 and 6; and 4 bents were used to support Frame 4. Each bent consisted of 2 rectangular columns. The dimensions of the columns were 2140 mm (7 ft) height

and 1070 mm (3.5 ft) width. The columns were reinforced with 32 no. 11 bars, except the columns of the skewed bents. The columns of the skewed bent were reinforced using 32 no. 18 bars. However since the bridge was assumed to be straight, the 32 no. 11 bars were used in the modeling of the entire bridge columns. On the other hand, no. 4@305 mm (12 in) stirrups were used along the height of the column.

The columns were modeled in OpenSees using the nonlinear beam/column elements with two integration points assumed at the ends of each element. Each column was divided into 7 elements. The top and bottom elements represented the bent cap and the foundation footing, respectively. They were modeled as rigid elements with the intermediate column elements assumed to behave nonlinearly.

The nonlinear behavior of the columns was modeled by utilizing the option provided by OpenSees to define the characteristics of the cross section at each integration point. The cross section of the columns was modeled using fiber elements. Figure 7.2 presents the cross section of the bridge column and the discretization that was used in defining the section of the column in OpenSees using the fiber elements. Under longitudinal movements, the columns were expected to experience bending about its weak axis. Hence it was more appropriate to divide the section into fibers along the shorter side of the column's section. As shown in the figure, the fiber section consisted of 10 rectangular fibers representing the core area of the section, 24 rectangular fibers representing the cover area of the section and 32 fibers representing the steel rebars. The constitutive behavior of the concrete fiber elements was modeled using the uniaxial Concrete01 material, while the steel rebar fibers were modeled using the Steel01 material. Based on the bridge plans the compressive strength for the unconfined concrete

was taken as 34.4 MPa (5 ksi) and the columns were reinforced using grade 40 steel rebars.

In order to calibrate the model developed in OpenSees for the column section, the moment-curvature relationship of the column section developed in OpenSees was compared with the moment-curvature relation resulting from USC-RC software which was developed at the University of Southern California to predict the behavior of reinforced concrete cross sections. The USC-RC utilizes the Mander model (Mander, 1988) to predict the behavior of the unconfined and confined concrete. Thus USC-RC was used to calculate the material parameters required to define the Concrete01 OpenSees material. Applying the Mander formulas resulted in a confined compressive strength equal to 35.6 MPa (5.18 ksi). Confining the concrete resulted in an increase in

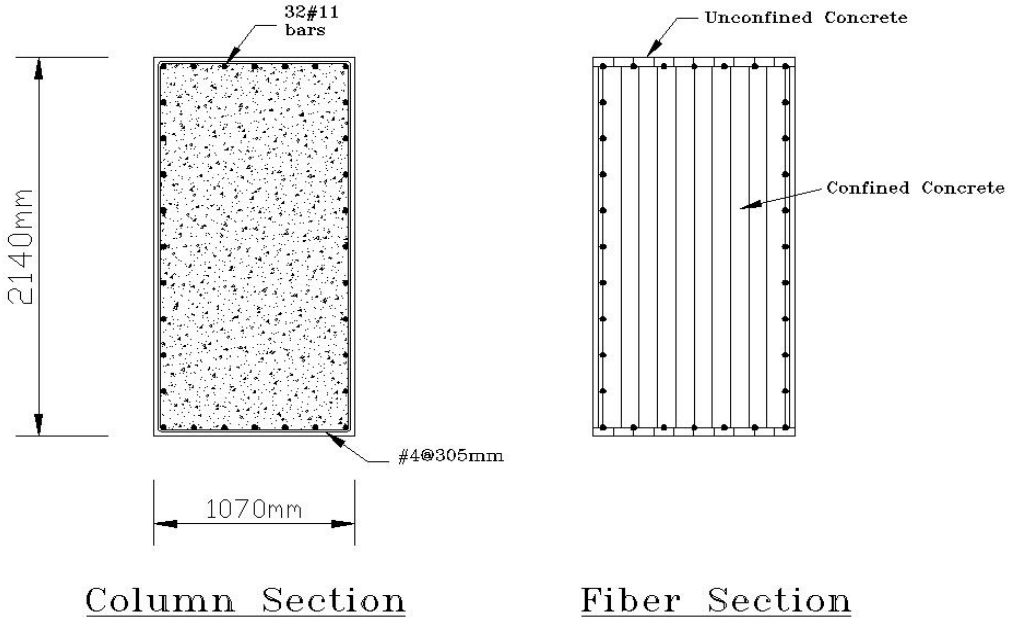

Figure 7.2 Cross section of the bridge column and the discritized fiber section that was used to develop the column's model in OpenSees

the maximum concrete strain from 0.39% to 0.58%. On the other hand the strain hardening ratio of the Steel01 material that was used to model the reinforcement bars was assumed to be 2.5%.

Figure 7.3 presents the moment-curvature relationships resulting from OpenSees and USC-RC. The USC-RC software was used to predict the moment-curvature of the section under monotonic loading and dynamic loading. Under monotonic loading the grade 40 reinforcement bars experience a typical horizontal yielding plateau, while under dynamic loading the steel bars experience a bilinear behavior. Figure 7.3 presents the USC-RC in both cases. As shown in the figure OpenSees was able to predict the yield moment of the cross section accurately. Beyond the point of yielding the behavior of the cross section modeled in OpenSees was close to that resulting from USC-RC using the steel bilinear (dynamic) behavior. The yielding plateau resulted in a reduction in the moment values especially at the zone where the steel bars experience a horizontal

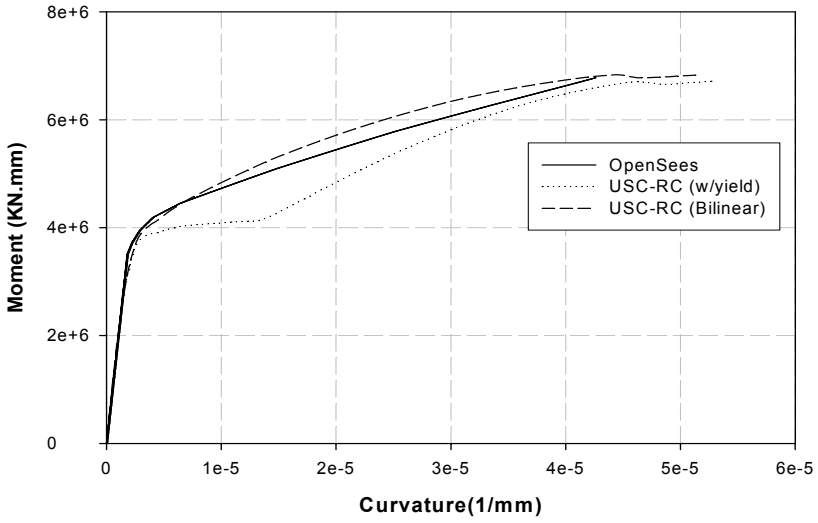

Figure 7.3 Moment-curvature relationships of the column cross section resulting from OpenSees and USC-RC

yielding plateau. The figure indicates that the column model that was developed in OpenSees using fiber elements was accurate enough to be used in the study.

7.3.3 Abutments Model

The two end spans were supported by two different types of abutments. Abutment 1 (see Figure 7.1) was a diaphragm (integral) abutment while the Abutment 2 was a seat abutment. The following subsections describe the analytical models developed for each abutment type.

7.3.3.1 Seat Abutment

Figure 7.4 shows a schematic of the seat abutment that was used to support Frame 6 of the right College Avenue Undercrossing Bridge. As shown in the figure, the abutment consisted of a backwall where the bridge deck sits and a wing wall at one side of the abutment. The abutment was supported using 65 piles distributed over the abutment foundation. The back side of the abutment was supporting a backfill soil that reached the top of the abutment. This backfill soil provided a passive lateral resistance for the abutment which had to be considered in the abutment model. This passive resistance is activated when the abutment moves toward the soil. On the other side of the abutment there was no such backfill and thus the active resistance of the abutment (i.e. when the abutment moves away from the soil) was assumed to be totally provided by the piles. Due to the large height of the backfill soil, the pile resistance in the passive direction was assumed be inactive in the case of small abutment-tip movement. Hence the resistance of the piles was neglected in the passive direction.

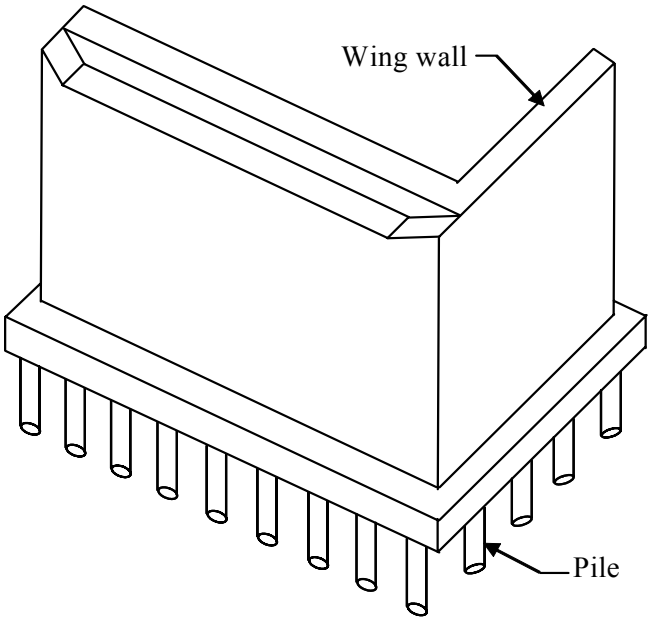

Figure 7.4 Schematic of the seat abutment used to support the right College Avenue Undercrossing Bridge.

Based on the previous discussion, the lateral resistance of the seat abutment was modeled in OpenSees using a tension-compression hysteretic element with different properties in the tension and compression. The compression behavior of the hysteretic element represents the passive resistance of the abutment while the tension behavior represents the active resistance. Based on the 1999 Caltrans Seismic Design Criteria the initial passive stiffness was recommended to be between 11.5 and 28.7 KN/mm/1.0 m (20 and 50 kips/in/1.0 ft) of the abutment width. To be more conservative, the initial passive stiffness was taken as 11.5 KN/mm/m (20 kips/in/ft). Although Caltrans described the behavior of the abutments as elastic perfectly plastic with an ultimate strength of 372 KN/m^2 (7.7 $kips/ft^2$), the experimental test results conducted by Maroney et al. in 1994 showed a nonlinear behavior for the abutments. Martin and Yan (1995) conducted an analytical study using various backfill soil types. The results of their study showed that

in the case of a cohesionless backfill the ultimate strength of the abutments is reached at an abutment tip-displacement of approximately 6% of the abutment height. Based on those research results, the force-deformation considered for the passive resistance of the seat abutment was as shown in Fig. 7.5. The abutment was assumed to start yielding at tip-displacement of approximately 0.6% of the abutment height (h). The abutment was assumed to follow a linear path from the initial point of yielding to the ultimate yielding force. The ultimate passive resistance force was calculated based on the height (h) and width (w) of the abutment.

When the abutment is pulled away from the soil, the resistance of the abutment is provided primarily by the lateral resistance of the supporting piles. According to the 1999 Caltrans Seismic Design Criteria, the lateral stiffness of each pile could be assumed as 7.0 KN/mm (40 kips/in). Accordingly, the active effective stiffness of the abutment could be calculated as 7.0 KN/mm/pile (40 kips/in/pile) multiplied by the number of piles. The piles were assumed to reach their ultimate capacity at a lateral displacement

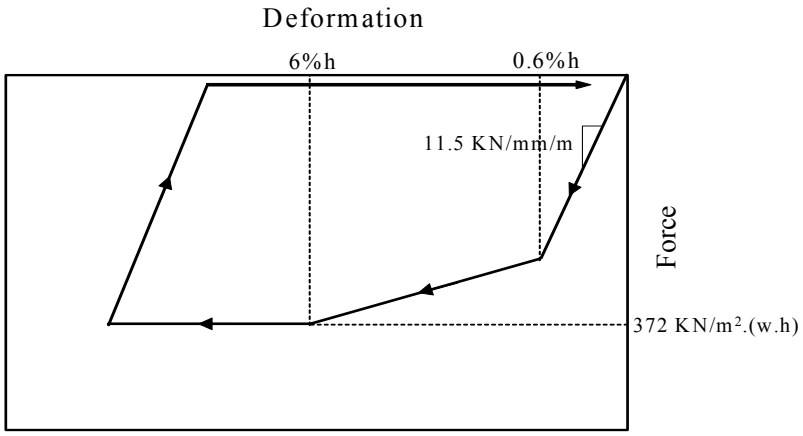

Figure 7.5 Force-deformation of the passive resistance of the seat abutment

equal to 25.4 mm (1.0 in). However due to the resistance provided by the soil surrounding the piles, the abutment was expected to start showing signs of yielding when the surrounding soil yields. The point where the first yielding starts to occur was assumed to be around 30% of the ultimate yielding deformation (25.4 mm [1.0 in.]). Based on this information, the active initial stiffness of the abutment could be calculated. Figure 7.6 shows the active force-deformation relationship of the abutment.

Based on the properties presented in Figures 7.5 and 7.6 the final force-deformation relationship assumed for the hysteretic material simulating the 6.1m x 21.7m (20`x 68`) seat abutment behavior is presented in Figure 7.7. As shown in the figure, the element behaves in a tension-only compression-only type of behavior. Both active and passive resistances were modeled to behave plastically.

7.3.3.2 Diaphragm Abutment

The abutment supporting the end span of Frame 1 was of the diaphragm (integral)

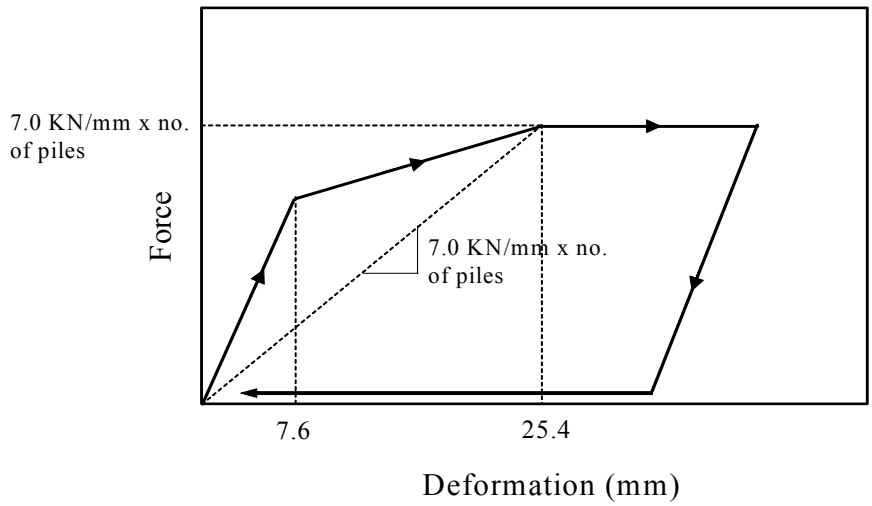

Figure 7.6 Force-deformation of the active resistance of the seat abutment

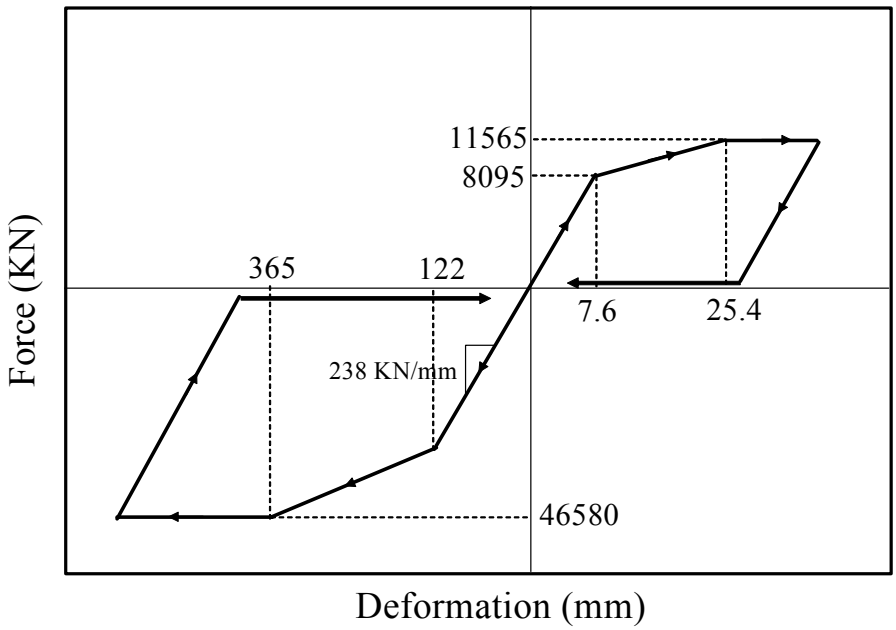

Figure 7.7 Force-deformation relationship used for representing the active and passive resistance of the seat abutment

abutment type, meaning the deck and the diaphragm are poured monolithically, which provides an integral interaction between the abutment and the bridge deck. In this case the abutment is contributing to the overall stiffness of the bridge with its lateral stiffness only. The rotation stiffness of the abutment plays an important role as well. Thus the abutment was modeled using a hysteretic material spring representing the lateral stiffness of the abutment and a rotational linear spring representing the rotational stiffness of the abutment. The abutment lateral stiffness was calculated based on the assumption discussed earlier in section 7.3.3.1. Figure 7.8 shows the force-deformation relationship used to represent the lateral stiffness of the 2.9m x 21.7m (9.5`x 68`) diaphragm abutment. The active resistance was calculated based on 11 piles.

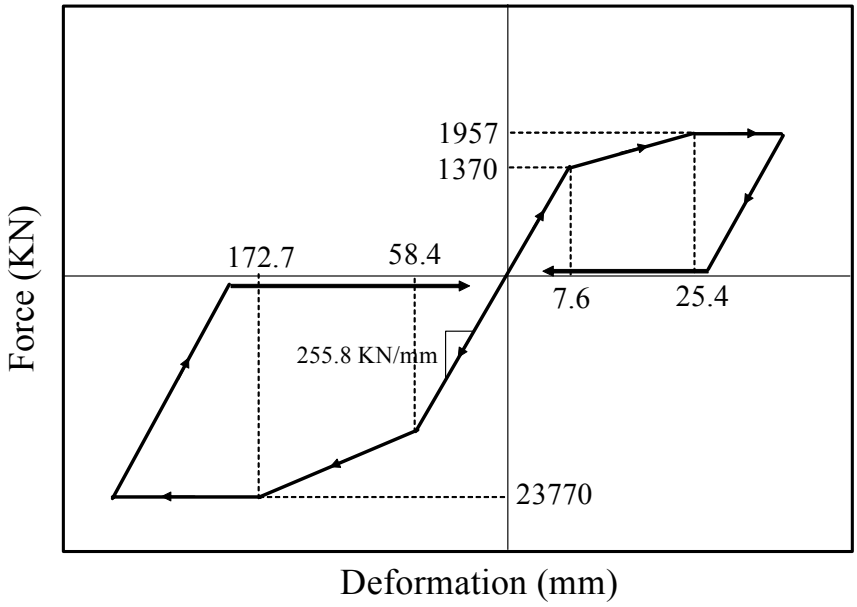

Figure 7.8 Force-deformation relationship used for representing the active and passive resistance of the diaphragm abutment

The rotational stiffness of the diaphragm was assumed to be provided by the piles only. The effect of the backfill soil was neglected. This assumption thought to be valid in this specific case since the abutment height was relatively small (2.9 m [9.5 ft]). Fang in 1991 provided an algebraic equation that could be used to calculate the rotational stiffness of a pile as a function of its diameter:

$$k_r = 0.15 d^3 E_s (E_p / E_s)^{0.77} \tag{7.1}$$

where k_r is the rotational stiffness of the pile, d is the pile diameter, E_s is the Young's modulus of the soil, and E_p is the Young's modulus of the pile. However in order to be able to apply this formula, the length of the piles has to exceed the active length (l_c), which is calculated as follows:

$$l_c = 2d(E_p / E_s)^{0.22} \quad (7.2)$$

Assuming that the soil surrounding the piles are sand with modulus equal to 34.4 MPa (5 ksi), and that the piles are 305 mm (12 in)-diameter piles which are made of concrete with a modulus that is equal to approximately 21924 MPa (3190 ksi), the active length would be approximately 2.5 m (8.3 ft). The lengths of the piles used in the construction of the bridge varied between 10.7 m (35 ft) and 13.7 m (45 ft). Thus, equation 7.1 could be used to calculate the rotation stiffness of the piles. Substituting equation 7.1 results in a rotational stiffness that is equal to 2.12×10^8 KN.mm/rad (187000 kips.in/rad) for each pile. Since the piles supporting the abutment were lined up in a straight line, the total rotational stiffness of the abutment could be calculated by multiplying the stiffness of one pile with the total number of piles. For the 11 piles used to support the diaphragm abutment, the total rotational stiffness was found to be 2.327×10^8 KN.mm/rad (2060000 kips.in/rad).

7.3.4 Foundation Model

The bridge columns were supported using pile foundations. The pile foundation was thought to be providing a lateral and a rotational stiffness at the base of the column. Hence the effect of the foundation was taken into account in the model by using a linear lateral and rotational springs connected to the column base. Due to the similarity between the effect of piles on the column base and their effect in providing the active resistance for the abutments, the initial stiffness of the piles was calculated in a fashion similar to the one that was demonstrated in Figure 7.6. Based on the 7.0 KN/mm (40

kips/in) effective stiffness provided by each pile, the initial lateral stiffness was found to be 16.3 KN/mm/pile (93.2 kips/in/pile). The total lateral stiffness of the foundation is calculated as follows:

$$k_{l,total} = k_l \cdot N \tag{7.3}$$

where $k_{l,total}$ is the total lateral stiffness provided by the foundation, k_l is the lateral stiffness of each pile including the surrounding soil, and N is the number of piles supporting the footing.

The rotational stiffness of each pile was calculated using equation 7.1. In order to calculate the total rotational stiffness of the foundation, the following equation was used:

$$k_{r,total} = k_r \cdot N + k_v \cdot S_n^{\,2} \tag{7.4}$$

where $k_{r,total}$ is the total rotational stiffness of the footing, k_r is the rotational stiffness of each pile calculated from equation 7.1, N is the number of piles supporting the footing, k_v is the vertical stiffness of the pile, and S_n is the perpendicular distance from the center of the pile to the centroidal axis of the pile group about which the rotation is expected. Based on the study presented by Martin and Yan (1995), assuming an ultimate compression capacity of the pile of 800 KN (180 kips) and friction capacity and bearing capacity of approximately 533.8 KN (120 kips) and 266.9 KN (60 kips), respectively produces a total vertical stiffness (k_v) of approximately 175 KN/mm/pile (1000

kips/in/pile). Substituting in equation 7.4 would result in the rotational stiffness at the base of each column.

7.3.5 Bearing Model

Elastomeric bearings were provided at each intermediate hinge and at the hinge of the seat abutment to transfer the force from one frame to another and from the superstructure to the substructure. The lateral resistance provided by the elastomeric pads is first due to the shear resistance of the pads. Once the lateral displacement exceeds the ultimate shear strain of the pads, the concrete starts sliding. Based on the 1999 Caltrans Seismic Design Criteria the dynamic coefficient of friction between concrete and elastomeric pads is approximately 0.4 and the ultimate shear strain experienced by the pads is $\pm$150%. However to be conservative, the elastomeric pads were assumed to fail at a $\pm$100% shear strain. The pads used were 254mm x 50mm x 305mm (10in x 2in x 12in), hence the pads were assumed to behave linearly until it displaces laterally by 50.8 mm (2 in) then the concrete starts to slide developing a plastic type of behavior. The reaction at the hinges was assumed to be approximately 1210 KN (270 kips). This would result in an ultimate lateral resistance of approximately 476 KN (107 kips). Thus, the elastomeric pads were modeled in OpenSees using an elasto-plastic Steel01 material with an initial modulus of 9.4 KN/mm (53.5 kips/in). Figure 7.9 shows the force-deformation used to model the elastomeric bearings.

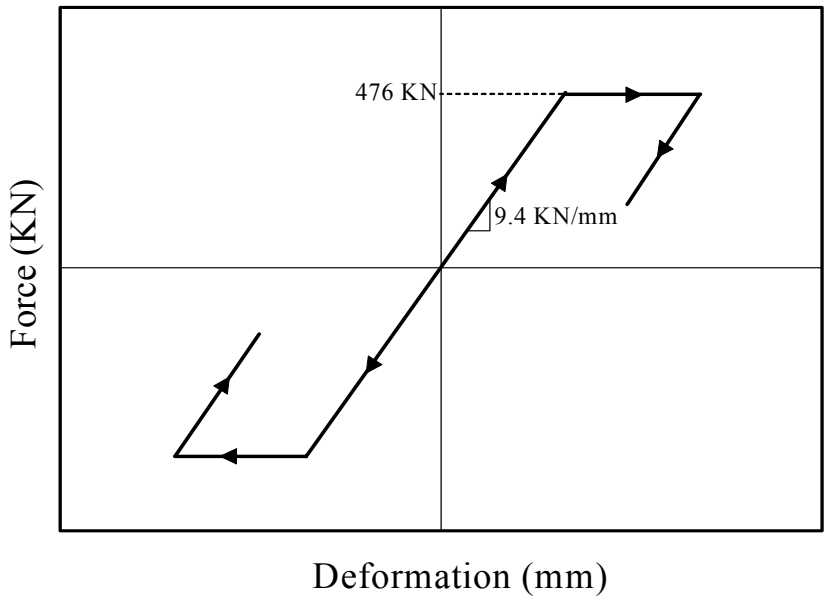

Figure 7.9 Force-deformation used to describe the behavior of the elastomeric pads

7.3.6 Pounding Model

The bridge frames were separated by a 25.4 mm (1.0 in.)-gap to allow for thermal expansion. Frame 6 was seated on the seat abutment with a 6.0in-clearance between the end diaphragm of the frame and the abutment backwall. This gap was assumed to be large enough so that it might prevent the passive resistance of the abutment from contributing in the overall behavior of the bridge. Thus the gap used in this study at the abutment hinge was equal to 76 mm (3.0 in). The intermediate hinge gaps and the abutment gap were accounted for by using a linear compression-only element with an initial gap between the two adjacent structural components. When the two structural components are in contact the gap is closed and the linear element starts engaging. The linear element was assumed to be rigid enough to account for the pounding effect between the adjacent components.

7.4 Modal Analysis

The modal analysis of the as-built bridge was performed using OpenSees. The mode shapes, periods, and effective modal mass ratio of the first 6 modes are shown in Figure 7.10. As shown in the figure, each one of the six modes represented the lateral vibration of one of the frames. The independent behavior of the frames was due to the fact that the only linkage between the adjacent frames was the elastomeric bearings which had a relatively small stiffness compared to the stiffness of the frames. The most flexible frame was Frame 3 which had a natural period of 0.61 sec. Frame 4 which was right next to Frame 3 had a natural period of 0.3 sec. The relatively small period ratio (0.49) between the two frames would probably result in an out of phase type of motion between the two frames. On the other side Frame 2 with its 0.38sec. produces a period ratio of approximately 0.63 with Frame 3. This moderate period ratio value is most probably expected in typical bridges. The period ratios between Frames 4 and 5 and between Frames 5 and 6 were 0.86 and 0.89, respectively. These values represent a moderate-to-high type of period ratios which is highly recommended by Caltrans. The highest period ratio between two adjacent frames in the bridge was between Frames 1 and 2. Their period ratio was approximately 0.95. With such high period ratio value an in phase type of motion is highly expected.

The figure also presents the effective modal mass ratios for each mode. As shown in the figure, the effective modal mass ratios of the first 6 modes dominated the entire response of the structure with a total of approximately 98.6% of the total mass of the bridge. The effective modal mass was distributed almost evenly between the first six modes. However the largest modal contributions were from Modes 3 and 6 with

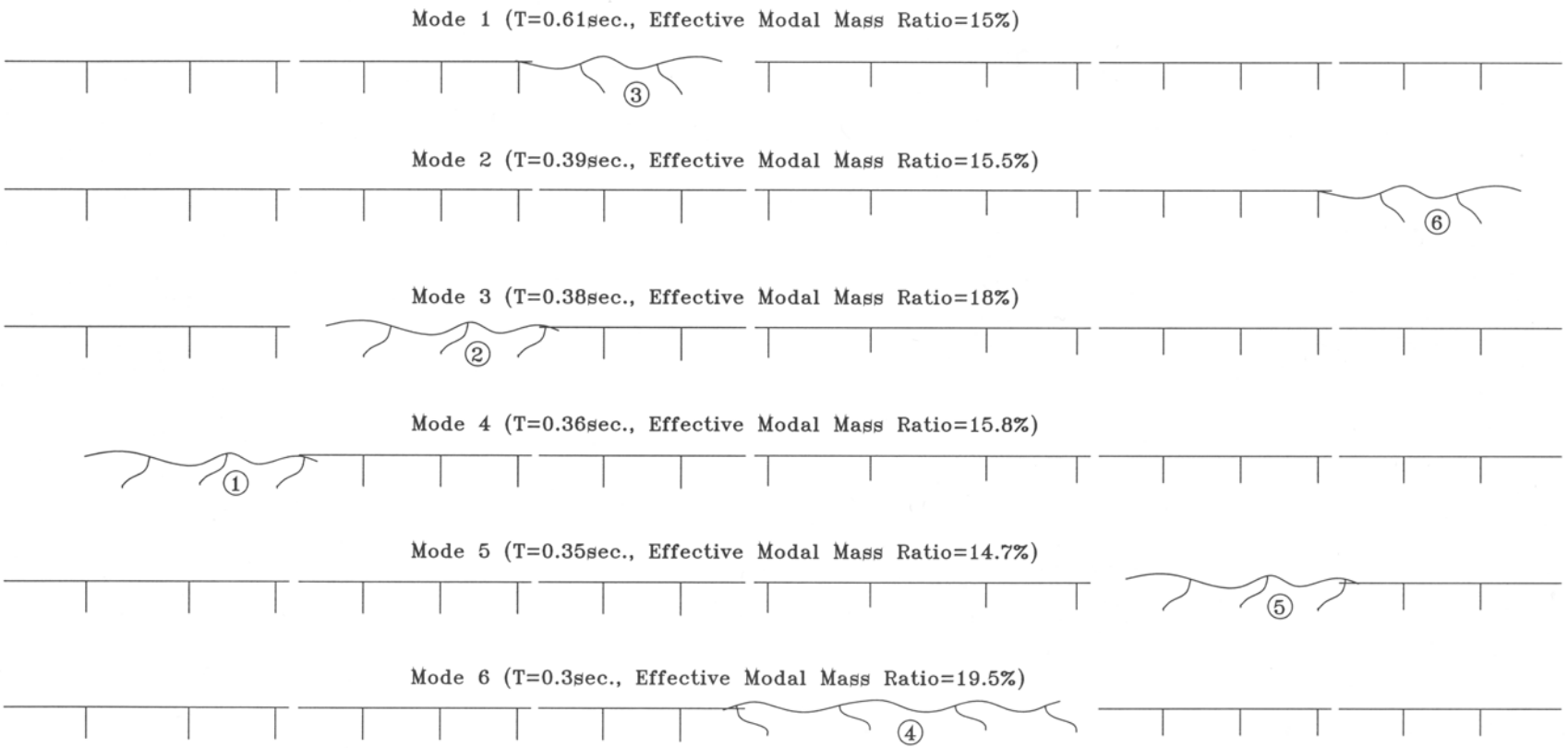

Figure 7.10 First six mode shapes, period, and effective modal mass ratios of the modeled multiple frame bridge that was used in the study

effective modal mass ratios of 18% and 19.5%, respectively. This is probably due to their relatively large mass compared to other frames.

7.5 Retrofitted Bridge

As mentioned previously, the College Avenue Undercrossing went through retrofit procedures during the two retrofit phases conducted by Caltrans after the 1971 San Fernando earthquake. The plans (see Appendix A) provided by Caltrans for the College Avenue Undercrossing indicated that during the first phase, hinges 1 and 2 were provided with 6 and 4 restrainer units, respectively, while hinges 3, 4, and 5 were provided with 2 restrainer units. During the second retrofit phase, 2 restrainer units were added at hinges 3, 4 and 5 making a total number of 4 units at each of hinges 2 through 5.

In order to be consistent in the bridge model, four restrainer units were assumed at each intermediate hinge including Hinge 1. Each of the units consisted of 5-3.7 m (12 ft) long cables with a cross section area for each cable equal to 142 mm^2 (0.22 in^2). Based on a yield stress equal to 1210 MPa (176 ksi) and a modulus of elasticity equal to 69,000 MPa (1000 kips/in), the stiffness of the restrainers at each hinge was approximately 107 KN/mm (611.2 kips/in), and the yield strength of the restrainers was approximately 6886 KN (1548 kips). The restrainers would experience yielding at a deformation equal to approximately 64 mm (2.53 in), which corresponds to a strain equal to 1.75%.

7.6 Design of Retrofit Devices

The retrofit devices that was used in the three case studies presented in this chapter were all designed using the same methodology that was described earlier in section 6.5.2.

The methodology is built on designing the devices such that they would possess an effective stiffness equal to the initial stiffness of the steel restrainers used in the bridge. The retrofit devices were modeled using the same techniques described earlier in section 6.3. Applying this design method resulted in the mechanical properties presented in the following subsections for each of the devices studied in this chapter:

7.6.1 SMA Devices

Figure 7.11 presents a schematic showing the mechanical properties used for the SMA devices based on an effective stiffness at 6%-strain equal to the stiffness of the steel restrainers. As shown in the figure, the transformation strain hardening and the martensitic strain hardenings were assumed to be 5% and 65%, respectively. This resulted in an initial stiffness equal to approximately 515 KN/mm (2943 kips/in) and a transformation stress equal to 5498 KN (1236 kips) for the SMA devices. The devices were assumed to unload at a force that is equal to half of the transformation force.

7.6.2 Metallic Dampers

Metallic dampers were designed such that they would possess an initial stiffness and yield strength equal to the initial stiffness and transformation force of the SMA devices, respectively.

7.6.3 Viscoelastic Solid Dampers

The elastic component of the viscoelastic dampers were designed with a modulus equal to the stiffness of the steel restrainers (107 KN/mm). The damping coefficient of

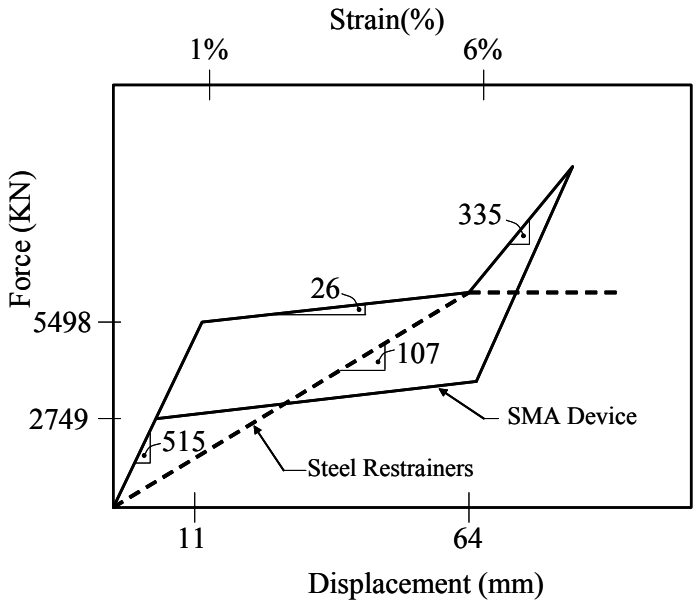

Figure 7.11 Mechanical properties of the SMA devices and steel restrainers used in the case studies.

the damper's viscous component was calculated using equation 2.2. The equation is presented below for convenience.

$$c_d = k_d \eta / \omega \tag{2.2}$$

In this study the k_d was taken equal to 107 KN/mm (611.2 kips/in), η was equal to 1.3, and ω was equal to 12.57 rad/sec., which corresponds to a cyclic frequency equal to 2 Hz. The cyclic frequency was selected in the range of the predominate frequencies of the records which were used in the study.

Table 7.1 Ground motion records used in the three case studies.

Record	Magnitude (M_w)	Distance (km)	PGA (g)	T_g (sec)
1995 Kobe, Kobe	6.9	11.1	0.51	0.48
1994 Northridge, Centinela St.	6.7	30.9	0.47	0.53
1992 Landers, Coolwater	7.3	21.2	0.42	0.71
1994 Northridge, Tarzana, Cedar Hill	6.7	17.5	0.99	0.74
1985 Nahanni, Canada	6.8	6.0	1.10	0.83
1999 Duzce, Turkey, Duzce	7.1	8.20	0.54	0.83
1989 Loma Prieta, WAHO	6.9	16.9	0.64	0.98

7.7 Ground Motion Records

A suite of seven ground motion records was used in the three case studies presented in this chapter. The names and properties of the 7 records are presented in Table 7.1. As shown in the table, the records have epicenter distance that varied from 6.0 to 30.9 kms, peak ground acceleration (PGA) varied between 0.42g and 1.1g, and predominate period (T_g) varying between 0.48 sec. and 0.98 sec. The 7 ground motion records were scaled to specific spectral acceleration value at the fundamental period of the bridge. This spectral acceleration value varied from one case study to another based on the nature of the study.

7.8 Case Study 1: Comparison of Retrofit Devices

7.8.1 Description

This study focuses on comparing tension-only and tension/compression SMA devices with other bridge retrofit devices. Five devices were considered in this study. Those devices were the same devices that were presented and utilized in the parametric study presented in Chapter 6. The studied devices were: traditional steel restrainers, metallic dampers, viscoelastic solid dampers, tension-only and tension/compression

superelastic shape memory alloy devices. The design and properties of the used devices were presented in sections 7.5 and 7.6. Each of the five devices was installed at the five intermediate hinges of the bridge model. The main focus of the study was to compare the performance of the five devices in limiting the openings at the bridge hinges during earthquakes. The study also focused on comparing the ductility demand level added by each device by examining the frame drifts and the amount of force transferred through the device to the bridge components.

7.8.2 Results

The retrofitted bridge was subjected to the seven ground motion records presented earlier in Table 7.1 after scaling their spectral acceleration at the fundamental period of the bridge to 2.5g. Such relatively large spectral acceleration value was used to insure that some of the hinges would experience excessive displacements, which would be expected in the case of strong earthquakes. Table 7.2 presents the maximum hinge openings experienced by each of the five hinges under the 7 ground motion records when using the 5 retrofit devices as well as in the case of the as-built bridge. The table also presents the percent reduction occurring in the hinge opening values due to the use of the 5 devices compared to the as-built hinge opening values. The table shows that the largest hinge openings occurred at Hinge 3 which possesses the smallest period ratio (0.49). In a typical bridge such hinge would be vulnerable to unseating and hence would require more attention.

Table 7.2 Maximum hinge opening results at various hinges using different retrofit devices.

Earthquake	Retrofit Device	Hinge 1		Hinge 2		Hinge 3		Hinge 4		Hinge 5		Average
		MHD(mm)	Red.(%)	MHD(mm)	Red.(%)	MHD(mm)	Red.(%)	MHD(mm)	Red.(%)	MHD(mm)	Red.(%)	Red.(%)
Kobe	As-built	47	0	92	0	138.94	0	61	0	56	0	0
	SMA(+/-)	31	34	43	53	61.29	56	18	70	23	59	54
	Metallic	36	22	13	86	51.81	63	9	86	8	85	68
	VE	11	77	14	85	49.86	64	18	71	19	66	73
	Steel	39	16	42	54	72.79	48	31	49	31	45	42
	SMA(+)	17	64	32	65	61.90	55	20	67	22	60	62
Northridge (Centinela St.)	As-built	82	0	65	0	217.94	0	65	0	65	0	0
	SMA(+/-)	28	66	44	32	121.33	44	58	11	18	72	45
	Metallic	14	83	44	32	165.30	24	17	74	16	76	58
	VE	13	84	43	33	101.16	54	26	60	16	75	61
	Steel	42	49	66	-2	166.45	24	44	32	41	37	28
	SMA(+)	23	72	67	-4	114.96	47	49	25	20	69	42
Landers	As-built	66	0	128	0	159.80	0	40	0	46	0	0
	SMA(+/-)	41	39	36	72	102.33	36	32	20	14	70	47
	Metallic	13	81	59	54	140.73	12	4	90	6	86	65
	VE	37	44	40	68	86.24	46	17	59	13	71	58
	Steel	67	-1	57	56	169.06	-6	35	12	31	32	18
	SMA(+)	35	47	47	63	104.82	34	23	43	20	56	49
Northridge (Tarzana)	As-built	66	0	84	0	127.95	0	48	0	87	0	0
	SMA(+/-)	44	32	36	57	57.73	55	23	51	13	85	56
	Metallic	43	34	7	91	42.94	66	11	78	9	90	72
	VE	24	64	15	82	48.22	62	16	67	14	84	72
	Steel	48	26	40	52	65.95	48	32	32	32	64	45
	SMA(+)	50	24	33	61	49.33	61	23	51	22	75	54
Nahanni	As-built	152	0	121	0	195.16	0	59	0	83	0	0
	SMA(+/-)	92	39	67	45	101.45	48	22	62	28	67	52
	Metallic	77	49	31	75	117.50	40	14	75	18	78	63
	VE	36	76	27	78	86.40	56	18	69	19	77	71
	Steel	98	35	45	62	166.93	14	39	34	59	28	35
	SMA(+)	80	48	44	64	105.76	46	26	55	27	67	56
Duzce	As-built	59	0	74	0	162.40	0	26	0	43	0	0
	SMA(+/-)	20	66	27	64	86.91	46	16	38	13	71	57
	Metallic	9	85	17	76	87.16	46	14	44	8	81	67
	VE	12	79	23	68	76.12	53	8	67	11	75	69
	Steel	22	64	31	57	124.93	23	20	24	29	33	40
	SMA(+)	14	76	18	75	81.09	50	19	25	21	53	56
Loma Prieta	As-built	59	0	53	0	208.45	0	79	0	55	0	0
	SMA(+/-)	46	22	42	21	105.46	49	33	58	30	46	40
	Metallic	32	46	28	47	123.40	41	26	67	17	69	54
	VE	15	74	24	54	94.53	55	29	64	14	74	64
	Steel	48	19	34	37	157.08	25	46	41	38	31	31
	SMA(+)	35	41	36	32	105.79	49	22	72	21	62	51

In order to visualize the effect of each device in limiting the displacement at Hinge 3, a graphical comparison of the hinge displacements in the case of the five devices as well as the as-built case is presented in Figure 7.12. The figure also presents the amount of residual hinge openings associated with each case. In order to relate the effectiveness of each device with its mechanical properties, the force-displacement relationships of the five devices used at Hinge 3 under the scaled 1999 Duzce, Turkey record are presented in Figure 7.13.

Figure 7.12 illustrates that all of the five devices were effective in limiting the maximum hinge openings to a certain extent in most of the cases. However, the steel restrainers were the least effective device. Since steel restrainers are tension-only devices

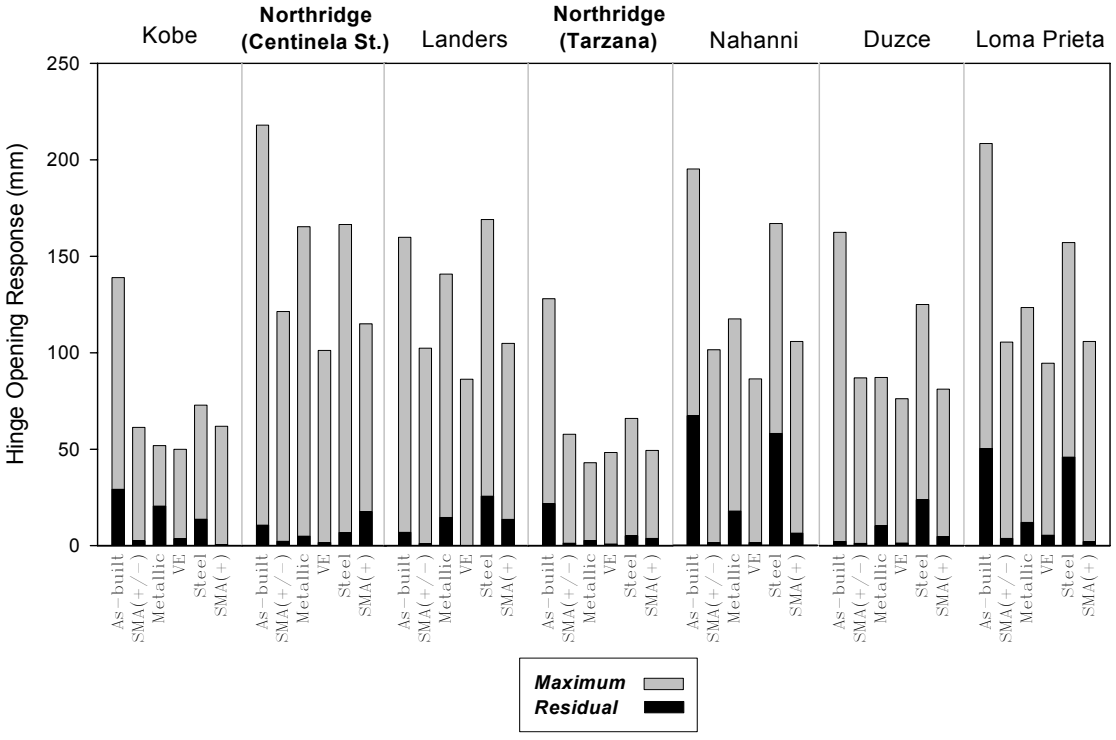

Figure 7.12 Maximum and residual hinge opening responses at Hinge 3 using various retrofit devices.

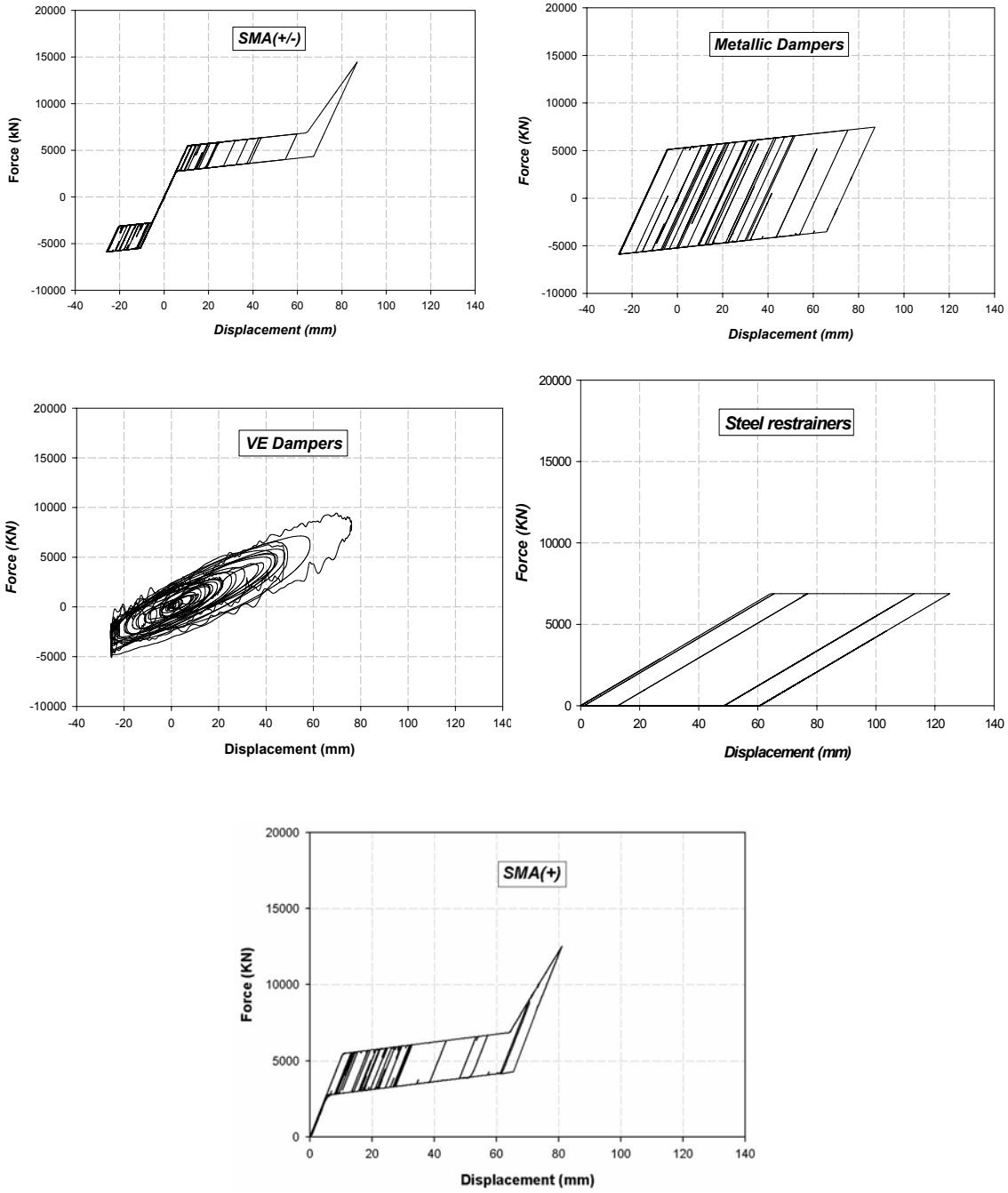

Figure 7.13 Force-displacement relationships of the five devices used at Hinge 3 under the scaled 1999 Duzce, Turkey ground motion record.

it was more appropriate to compare it with the tension-only SMA device. In all of the 7 cases, the tension-only SMA device was more effective in limiting the maximum hinge openings compared to the steel restrainers. The average reduction in the maximum hinge opening caused by the steel restrainers was approximately 25%, while the average reduction caused by using the tension-only SMA device was approximately 49%. In the case of the Landers record, the steel restrainers increased the hinge opening compared to the as-built case. This illustrates the limited effectiveness of the currently used steel restrainers.

Another point of interest is the permanent damage occurring to the bridge, which highly affects its functionality post earthquakes. The amount of residual hinge openings associated with the steel restrainers was extremely large in some cases such as in the case of the Nahanni and the Loma Prieta records where the residual hinge openings reached approximately 58 mm (2.3 in), and 46 mm (1.8 in), respectively. On the other hand, the residual hinge openings in the case of the tension-only SMA device did not exceed 18 mm (0.7 in). The difference in the performance of the two devices was expected due to the recentering capability associated with the SMA devices.

Comparing the SMA devices with the metallic dampers and the VE dampers illustrated that in 5 out of the 7 cases, the SMA devices were able to limit the maximum hinge openings more effectively compared to the metallic dampers. Those cases were the ones where the as-built maximum hinge openings were the largest (i.e. larger than 150 mm [6.0 in]). The metallic dampers showed slightly more effectiveness than the SMA devices in limiting the maximum hinge openings in the cases where the maximum hinge opening of the as-built bridge was low-to-moderate (i.e. less than 140 mm [5.5 in]). The

effectiveness of the metallic dampers in those cases was expected due to the larger damping capability associated with the metallic dampers. However, this effectiveness did not prevent the occurrence of relatively large residual hinge openings, where in some cases it reached approximately 20 mm (0.8 in). This is due to the lack or recentering capability in the metallic dampers. The fact that the SMA devices showed superiority performance compared to the metallic dampers in the case of excessive hinge openings arises from the fact that SMA devices strain hardens at large displacements. This martensitic strain hardening behavior combined with the superelasticity behavior makes the SMA devices more effective as unseating prevention devices compared to the metallic dampers.

Figure 7.12 also shows that the VE dampers perform slightly better than the SMA devices. The average reduction in the maximum hinge opening caused by using VE dampers was approximately equal to 56%, while in the cases of the tension-only and tension/compression SMA devices, the average reduction in the maximum hinge opening was approximately 49% and 48%, respectively. This slight increase in the effectiveness from the VE dampers side is expected due to the fact that those devices are able to revert back to their original shape once the load is removed. This behavior provides the VE dampers with recentering capability which resulted in a relatively small residual hinge openings associated with the VE dampers. In addition to the recentering capability, the VE dampers are capable of dissipating more hysteretic energy compared to the SMA devices.

Although VE dampers were slightly more effective than SMA devices in limiting the maximum hinge openings, examining and comparing the forces transmitted to the bridge

frames through the two types of devices showed that the forces transmitted through the VE dampers in some cases were extremely large compared to the cases of SMA devices. An example of such behavior is the case of the scaled 1994 Northridge (Centinela St.) record. Figure 7.14 presents the force-displacement relationships of the tension/compression SMA devices and the VE dampers that were used at Hinge 1. Although the maximum deformation experienced by both devices was not large, the VE dampers induced an extremely large force at the point when the two frames pounded together. This force reached approximately 15,000 KN (3,372 kips), which was approximately 2.5 times the value of the force induced by the tension/compression SMA devices. Such behavior illustrates that using a velocity-dependant device at the bridges intermediate hinges might cause unnecessary extremely large forces to be transmitted to the bridge components and hence cause damage to the bridge. The displacement-dependent SMA devices are characterized by a flat plateau at small-to-moderate deformations which controls the level of force transmitted to the structural elements.

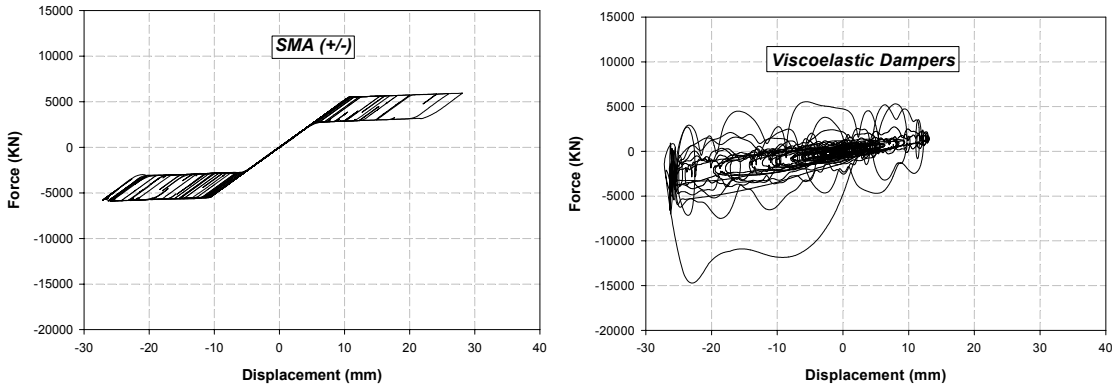

Figure 7.14 Force-displacement relationship of the tension/cmpression SMA devices and the viscoelastic dampers used at Hinge 1 under the scaled 1994 Northridge (Centinela St.) record.

The effect of using different retrofit devices on the lateral drifts of the frames was also examined in this study. Table 7.3 presents the results of the maximum drifts experienced by the bridge frames in the case of using different retrofit devices as well as in the case of the as-built bridge. The table also presents the normalized values of the maximum drifts using the as-built results. The right column of the table shows that the average changes in the maximum drifts was affected by less than 6% compared to the as-built case. The results show inconsistent relationship between the maximum frame drifts and the type of retrofit device used. This behavior was noticed earlier in the parametric study presented earlier in Chapter 6 (see Figures 6.15 and 6.16).

Table 7.3 Maximum drifts of the six bridge frames using different retrofit devices.

Earthquake	Retrofit Device	Frame 1		Frame 2		Frame 3		Frame 4		Frame 5		Frame 6		Average
		MD(mm)	Norm.	MD(mm)	Norm.	MD(mm)	Norm.	MD(mm)	Norm.	MD(mm)	Norm.	MD(mm)	Norm.	Norm.
Kobe	As-built	155	1.00	183	1.00	192	1.00	125	1.00	125	1.00	120	1.00	1.00
	SMA(+/-)	176	1.14	161	0.88	149	0.78	120	0.96	126	1.01	139	1.16	0.99
	Metallic	184	1.19	165	0.90	145	0.76	118	0.94	129	1.04	141	1.17	1.00
	VE	170	1.10	162	0.88	153	0.80	118	0.94	134	1.07	146	1.21	1.00
	Steel	164	1.06	157	0.86	165	0.86	125	1.00	118	0.95	123	1.02	0.96
	SMA(+)	181	1.17	165	0.90	151	0.79	120	0.96	121	0.97	139	1.16	0.99
Northridge (Centinela St.)	As-built	281	1.00	295	1.00	329	1.00	174	1.00	151	1.00	173	1.00	1.00
	SMA(+/-)	289	1.03	276	0.94	259	0.79	187	1.07	183	1.21	189	1.09	1.02
	Metallic	318	1.13	289	0.98	257	0.78	186	1.07	178	1.18	196	1.14	1.05
	VE	292	1.04	286	0.97	243	0.74	191	1.10	172	1.14	189	1.09	1.01
	Steel	285	1.01	285	0.97	309	0.94	180	1.04	171	1.13	176	1.02	1.02
	SMA(+)	304	1.08	288	0.98	243	0.74	186	1.07	183	1.22	204	1.18	1.04
Landers	As-built	238	1.00	258	1.00	242	1.00	183	1.00	154	1.00	108	1.00	1.00
	SMA(+/-)	296	1.24	274	1.06	238	0.98	181	0.99	137	0.89	96	0.89	1.01
	Metallic	309	1.30	278	1.07	235	0.97	178	0.97	137	0.89	96	0.89	1.02
	VE	286	1.20	274	1.06	232	0.96	182	1.00	142	0.92	96	0.89	1.01
	Steel	265	1.11	264	1.02	218	0.90	184	1.00	149	0.97	96	0.89	0.98
	SMA(+)	294	1.23	265	1.02	227	0.94	183	1.00	140	0.91	98	0.91	1.00
Northridge (Tarzana)	As-built	144	1.00	148	1.00	177	1.00	130	1.00	146	1.00	170	1.00	1.00
	SMA(+/-)	180	1.24	177	1.20	168	0.95	136	1.05	129	0.89	144	0.84	1.03
	Metallic	189	1.31	168	1.14	164	0.93	136	1.05	140	0.96	165	0.97	1.06
	VE	176	1.22	178	1.20	161	0.91	125	0.96	142	0.97	160	0.94	1.04
	Steel	167	1.16	184	1.25	163	0.92	129	1.00	140	0.96	172	1.01	1.05
	SMA(+)	185	1.28	185	1.25	155	0.88	128	0.98	136	0.93	158	0.93	1.04
Nahanni	As-built	260	1.00	304	1.00	324	1.00	158	1.00	181	1.00	210	1.00	1.00
	SMA(+/-)	251	0.96	252	0.83	272	0.84	209	1.32	211	1.16	219	1.04	1.03
	Metallic	251	0.96	253	0.83	275	0.85	177	1.12	201	1.11	225	1.07	0.99
	VE	247	0.95	249	0.82	277	0.86	194	1.23	204	1.12	221	1.05	1.00
	Steel	248	0.95	284	0.94	278	0.86	168	1.06	190	1.05	213	1.01	0.98
	SMA(+)	263	1.01	248	0.82	269	0.83	209	1.32	212	1.17	239	1.13	1.05
Duzce	As-built	239	1.00	268	1.00	305	1.00	149	1.00	176	1.00	197	1.00	1.00
	SMA(+/-)	217	0.91	246	0.92	272	0.89	189	1.27	200	1.14	209	1.06	1.03
	Metallic	207	0.87	239	0.89	267	0.87	185	1.25	211	1.20	232	1.18	1.04
	VE	217	0.91	244	0.91	261	0.85	183	1.23	204	1.16	226	1.15	1.03
	Steel	231	0.97	258	0.96	282	0.93	171	1.15	198	1.13	213	1.08	1.04
	SMA(+)	215	0.90	239	0.89	267	0.87	186	1.25	208	1.19	227	1.15	1.04
Loma Prieta	As-built	291	1.00	324	1.00	353	1.00	182	1.00	213	1.00	244	1.00	1.00
	SMA(+/-)	272	0.93	294	0.91	277	0.78	197	1.08	221	1.04	238	0.97	0.95
	Metallic	293	1.00	284	0.88	307	0.87	201	1.10	226	1.06	251	1.03	0.99
	VE	285	0.98	290	0.90	279	0.79	192	1.05	218	1.03	248	1.01	0.96
	Steel	294	1.01	307	0.95	327	0.93	189	1.04	203	0.95	237	0.97	0.97
	SMA(+)	300	1.03	297	0.92	295	0.83	203	1.11	224	1.05	245	1.00	0.99

7.9 Case Study 2: Ambient Temperature Effect

7.9.1 Description

This study focuses on the effects that ambient temperature has on the effectiveness of SMA restrainers in limiting hinge openings in multiple frame bridges. In this study SMA restrainers were designed and modeled for a certain ambient temperature. The restrainers were then subjected to a plus or minus change in the ambient temperature. The hinge openings as well as the frame drifts were examined in each case.

An important step in the design of superelastic SMA restrainers is making a decision on the transformation temperatures of the alloy. Since the study focuses only on the superelastic behavior of the SMAs, the most significant transformation temperature is the austenite finish temperature (A_f). In order to ensure that the SMA restrainers would remain elastic, the A_f has to be relatively low compared to the ambient temperature expected during the life of the bridge. Considering the case of the College Avenue Undercrossing, and based on the average annual temperatures expected in Alameda County, California, an average annual temperature of approximately 289^0 K (60^0 F) is expected. Hence in this study, the A_f was assumed to be 255^0 K (0^0 F). The SMA restrainers were designed at the average temperature (289^0 K) such that they would posses mechanical properties identical to the properties discussed and presented earlier in section 7.6.1. However, those properties were expected to be sensitive to ambient temperature and hence they would change with changes in the ambient temperature.

Research has shown that the phase transformation stress varies linearly with the ambient temperature for temperatures above A_f (Gao and Huang, 2002). Based on the results provided by Gao and Huang it was noticed that an increase in the transformation

stress equal to approximately 4.8 MPa (0.7 ksi) is reasonable for SMAs which experience an increase equal to 0.55^0 K (1.0^0 F) in their temperature. Hence the following equation was developed to govern the relationship between the transformation force in the SMAs and the ambient temperature:

$$F_y = F_y^{A_f} + 0.7 \times Area\ of\ restrainers \times (T - A_f) \tag{7.5}$$

where F_y is the SMA transformation force in kips, $F_y^{A_f}$ is the transformation force at temperature equal to A_f in kips, T is the ambient temperature in Fahrenheit. In this equation A_f is expressed in Fahrenheit. In order to determine the area of the restrainers, the transformation force at temperature A_f was assumed to be half the transformation force at the average annual temperature (i.e. $F_y^{A_f}$ was assumed to be 618 kips). By substitution in Equation 7.5 the corresponding area of the restrainers was found to be approximately 9484 mm^2 (14.7 in^2).

Three levels of temperature were considered in the study. The first level represents the average annual temperature where the SMA restrainers were designed for. The other two levels were assumed to represent an increase and a decrease equal to 22^0 K (40^0 F) in the average temperature. Thus the three ambient temperature values considered in the study were 266^0 K (20^0 F), 289^0 K (60^0 F), and 310^0 K (100^0 F).

7.9.2 Results

After implementing the designed SMA restrainers in the bridge model, the bridge was subjected to the 7 ground motion records presented in Table 7.1 after scaling their

spectral acceleration at the natural period of the structure to 2.0g. The results of the maximum hinge displacements (MHDs) as well as the differences between the MHDs in each of the cases with respect to the case were the restrainers were designed for (60^0 F) are presented in Table 7.2. The differences shown in negative indicate a decrease in the MHD, while the positive values indicate an increase. As shown in the tables the effect of changes in the ambient temperature differs from one hinge to the other and is highly dependant on the ground motion characteristics. However, most of the cases showed that increasing the ambient temperature would result in a reduction in the MHD. This is also illustrated through the average differences occurring at the 5 hinges for each ground motion record. In 4 out of the 7 records, a reduction in the MHD is observed with increasing the temperature. These reductions varied between 2% and 17%. On the other hand, a decrease in the ambient temperature would result most likely in an increase in the MHD. The average differences in the case of all of the 7 records indicated such behavior, with an increase that varied between 3% and 52%.

Comparing the results of hinges with relatively large period ratios such as hinges 2 and 3 with other hinges shows that the percentage of differences in the MHDs associated with the changes in the ambient temperatures are more dramatic in the case of the hinges with moderate-to-high period ratios. This observation was also illustrated by the parametric study presented in chapter 5 (see Figure 5.29). In order to better understand such behavior, the maximum openings at hinges 3 and 4 are presented in Figure 7.15 for the three temperature levels considered in the study. Hinge 3 with frame period ratio equal to 0.49 represents intermediate hinges with relatively low period ratios, while Hinge 4 with frame period ratio equal to 0.85 represents intermediate hinges with

Table 7.4 Maximum hinge displacement results at various levels of temperature under various ground motion records.

Earthquake	Temp. (^{0}F)	Hinge 1		Hinge 2		Hinge 3		Hinge 4		Hinge 5		Average
		MHD(mm)	diff. (%)	MHD(mm)	diff. (%)	MHD(mm)	diff. (%)	MHD(mm)	diff. (%)	MHD(mm)	diff. (%)	diff.(%)
Kobe	20	18	3	17	-2	53	27	24	33	19	-8	11
	60	17	0	18	0	42	0	18	0	20	0	0
	100	15	-13	16	-11	33	-21	15	-16	16	-24	-17
Northridge (Centinela St.)	20	17	-5	62	-5	95	6	27	17	19	2	3
	60	17	0	66	0	89	0	23	0	19	0	0
	100	19	8	57	-14	90	1	25	8	16	-11	-2
Landers	20	31	109	49	12	88	-1	16	28	28	113	52
	60	15	0	44	0	89	0	12	0	13	0	0
	100	20	34	35	-20	90	1	12	-5	14	5	3
Northridge (Tarzana)	20	19	24	17	-30	59	10	32	41	18	2	9
	60	16	0	25	0	54	0	23	0	18	0	0
	100	20	25	37	49	40	-26	19	-18	17	-5	5
Nahanni	20	11	-10	20	-17	85	4	23	42	21	19	7
	60	12	0	24	0	82	0	17	0	18	0	0
	100	14	11	18	-22	64	-22	14	-17	17	-2	-10
Duzce	20	8	-29	13	4	77	37	15	24	11	-9	5
	60	12	0	12	0	57	0	12	0	12	0	0
	100	12	4	14	13	46	-19	15	30	12	3	6
Loma Prieta	20	47	49	36	67	83	10	28	50	23	21	39
	60	32	0	21	0	76	0	19	0	19	0	0
	100	30	-6	23	9	60	-21	15	-20	15	-21	-12

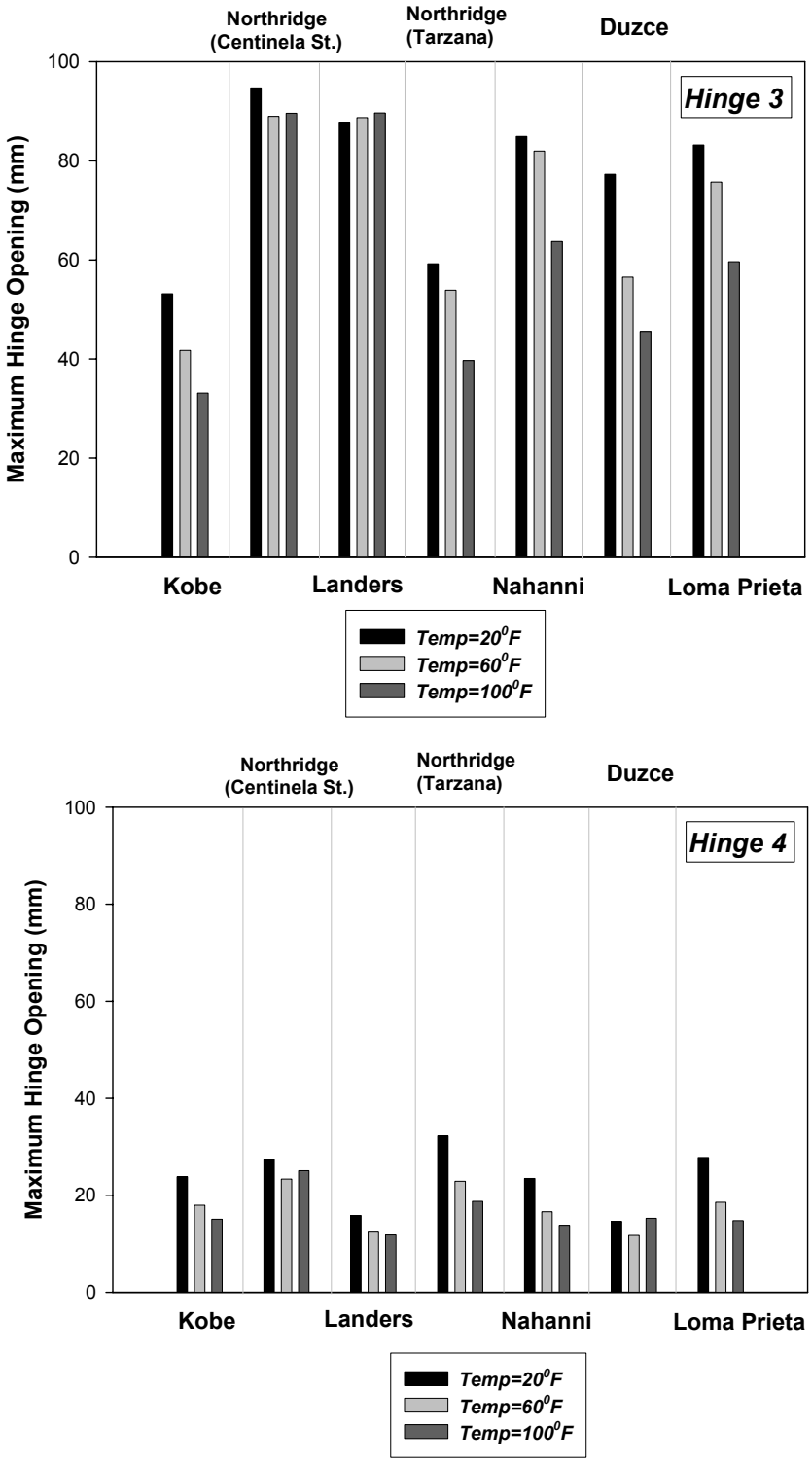

Figure 7.15 Maximum hinge opening at hinges 3 and 4 at various ambient temperatures when the College Avenue Undercrossing was subjected to the 7 earthquake records.

moderate-to-high period ratios.

Figure 7.15 shows larger hinge opening associated with Hinge 3 compared to that associated with Hinge 4. This was expected due to the out of phase type of motion expected between Frames 3 and 4. The figure shows that increasing the temperature from 289^0 K (60^0 F) to 310^0 K (100^0 F) reduced the maximum hinge opening in most of the cases. The average reduction noticed at hinges 3 and 4 were 15% and 9%, respectively. The figure also illustrates that a reduction in the ambient temperature from its average value at 289^0 K (60^0 F) to a temperature equal to 266^0 K (20^0 F) would increase the hinge opening in the majority of the cases. The average increases in the hinge opening observed at hinges 3 and 4 were 13% and 34%. These results indicate that for hinges with moderate-to-high period ratios, a reduction in the ambient temperature is more severe to the hinge opening compared to an increase in the temperature. The effect of variability in the ambient temperature would be better understood by reviewing the mechanical behavior of the SMA restrainers at various temperature levels. Hence, the force-displacement relationship of the SMA restrainer installed at hinges 3 and 4 are presented in Figure 7.16. The results presented in Figure 7.16 resulted from subjecting the bridge to the scaled WAHO record from the 1989 Loma Prieta earthquake.

As shown in Figure 7.16, increasing the ambient temperature resulted in increasing the SMAs transformation force. In the case of hinges with moderate-to-high period ratios (Hinge 4), the expected hinge openings are typically limited to a level below the martensitic level, hence, the maximum level of force reached by the restrainers increase with increasing the temperature. On the other hand, for hinges with relatively low period rations, such as Hinge 3, large deformations are expected and thus the SMAs are

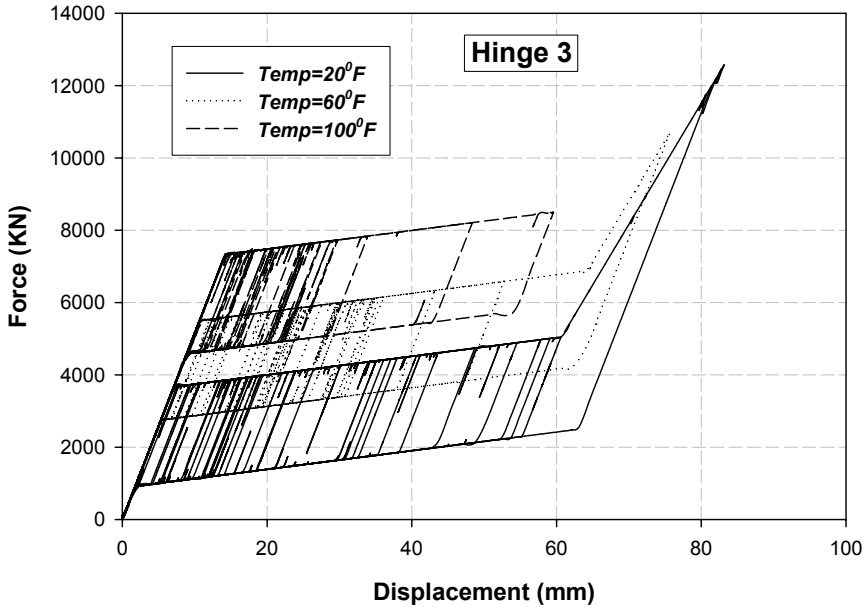

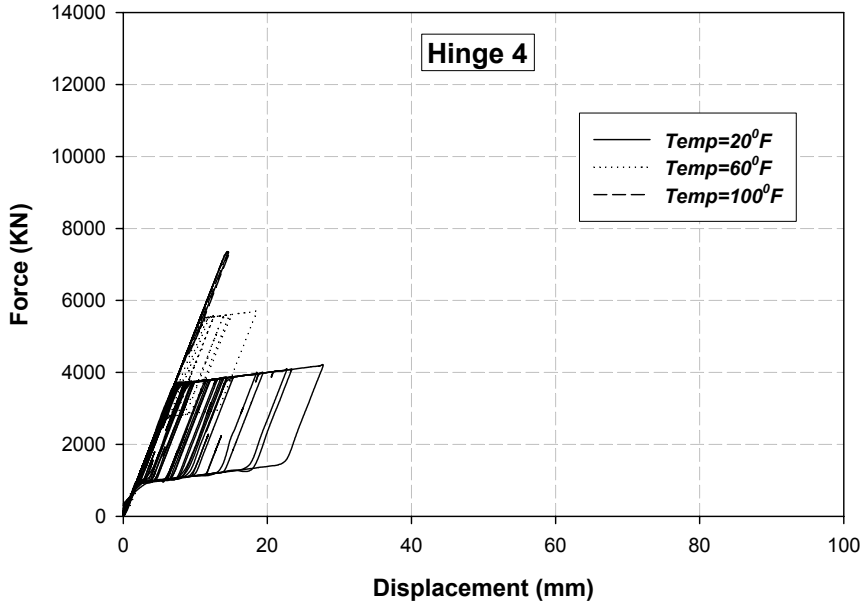

Figure 7.16 Force-displacement relationship of the SMA restrainers used at hinges 3 and 4 under at various temperature levels under the scaled 1989 Loma Prieta, WAHO record.

expected to experience martensitic strain hardening. This would make it more difficult to predict the maximum level of force reached by the SMAs. This probably resulted in the behavior observed in Figure 7.15 where in few cases, changing the ambient temperature seemed to have a minor effect on the MHD. Such behavior was observed in the Landers earthquake record.

In order to investigate the effect of changes in the ambient temperature on the ductility demand of the bridge frames, the maximum drifts (MDs) experienced by the 6 frames of the bridge as well as the differences in the MDs associated with increasing or decreasing the ambient temperature are presented in Table 7.5. As shown in the table, the effect of ambient temperature on the frame drifts was not consistent and in most of the cases minor changes was observed in the MDs when changing the ambient temperature. The right column of the table showing the average differences experienced by the 6 frames illustrates that in 5 of the 7 cases the drifts were reduced with reducing the temperature and increased when increasing the temperature. The percent of reduction in the MDs varied between 0.8% and 2%, while the percent of increase in the MDs varied between 0.9% and 3.4%. These values are typical with the values observed earlier in the parametric study presented in Chapter 5 (see Figure 5.20), which indicates that the temperature variation has minor effects on the frame drifts.

7.10 Case Study 3: Hysteretic Properties Effect

7.10.1 Description

This case study focuses on investigating the effect of using SMAs with different hysteretic shapes on its effectiveness as bridge restraining devices. SMA restrainers of

Table 7.5 Maximum frame drifts results at various levels of temperature under various ground motion records.

Earthquake	Temp. (^{0}F)	Frame 1		Frame 2		Frame 3		Frame 4		Frame 5		Frame 6		Average
		MD(mm)	diff. (%)	MD(mm)	diff. (%)	MD(mm)	diff. (%)	MD(mm)	diff. (%)	MD(mm)	diff. (%)	MD(mm)	diff. (%)	diff.(%)
Kobe	20	146	0.4	139	-0.5	128	1.8	107	2.6	102	-10.9	125	-3.8	-1.7
	60	146	0.0	140	0.0	126	0.0	104	0.0	114	0.0	130	0.0	0.0
	100	149	2.6	142	1.4	126	0.1	105	0.8	109	-5.1	119	-8.3	-1.4
Northridge (Centinela St.)	20	237	-1.6	234	-0.7	199	-2.8	154	1.6	125	-5.4	151	-2.9	-2.0
	60	240	0.0	235	0.0	204	0.0	151	0.0	132	0.0	156	0.0	0.0
	100	244	1.4	242	2.7	208	1.9	156	3.0	136	3.2	158	1.8	2.3
Landers	20	233	-2.4	219	-2.4	197	-2.0	154	0.9	127	2.8	93	-5.9	-1.5
	60	239	0.0	224	0.0	201	0.0	153	0.0	123	0.0	99	0.0	0.0
	100	243	1.8	227	1.2	201	-0.3	151	-1.0	124	0.8	102	3.0	0.9
Northridge (Tarzana)	20	157	-2.3	156	-3.9	141	7.0	103	-6.2	111	-0.9	131	1.7	-0.8
	60	160	0.0	162	0.0	131	0.0	109	0.0	112	0.0	129	0.0	0.0
	100	164	2.6	160	-1.1	134	1.9	113	3.4	118	5.1	125	-3.6	1.4
Nahanni	20	191	-0.1	181	-0.3	197	-0.5	125	-1.5	146	-1.5	170	-0.8	-0.8
	60	191	0.0	181	0.0	198	0.0	127	0.0	148	0.0	171	0.0	0.0
	100	195	2.2	181	0.0	198	-0.4	140	10.0	158	6.6	175	2.1	3.4
Duzce	20	150	0.4	182	1.9	208	8.4	137	-1.1	160	-4.4	186	-4.5	0.1
	60	150	0.0	178	0.0	192	0.0	139	0.0	168	0.0	195	0.0	0.0
	100	146	-2.6	170	-4.4	185	-3.5	151	8.6	178	6.4	202	3.6	1.3
Loma Prieta	20	235	-3.7	218	-0.4	202	6.2	151	-1.1	161	1.1	190	5.7	1.3
	60	244	0.0	219	0.0	190	0.0	153	0.0	159	0.0	180	0.0	0.0
	100	241	-1.1	217	-0.9	189	-0.7	154	0.6	160	0.5	180	0.4	-0.2

different shapes were installed in the intermediate hinges of the modeled bridge. Two shapes were considered for the SMA hysteresis. Figure 7.17 shows a schematic of the stress-strain relationship of the two shapes considered for the SMA hysteresis. A shown in the figure, shape A represents the family of SMAs that is characterized by a flat plateau and a steep martensitic strain hardening, while shape B represents SMAs with relatively steep plateau and a moderate martensitic strain hardening.

The implemented SMA01 uniaxial material that was discussed in section 6.3.2 was used in modeling the SMA restrainers. The initial stiffness and the transformation force of the two SMA restrainers were assumed to be identical and equal to 515 KN/mm (2943 kips/in) and 5498 KN (1236 kips), respectively. The strain hardening during phase transformation was assumed to be 2% and 12% for Shapes A and B, respectively, while the martensitic strain hardening was taken as 80% and 40% in the cases of Shape A and Shape B, respectively. Both shapes were assumed to have identical hysteretic height, where the unloading stress was assumed to be half of the transformation stress.

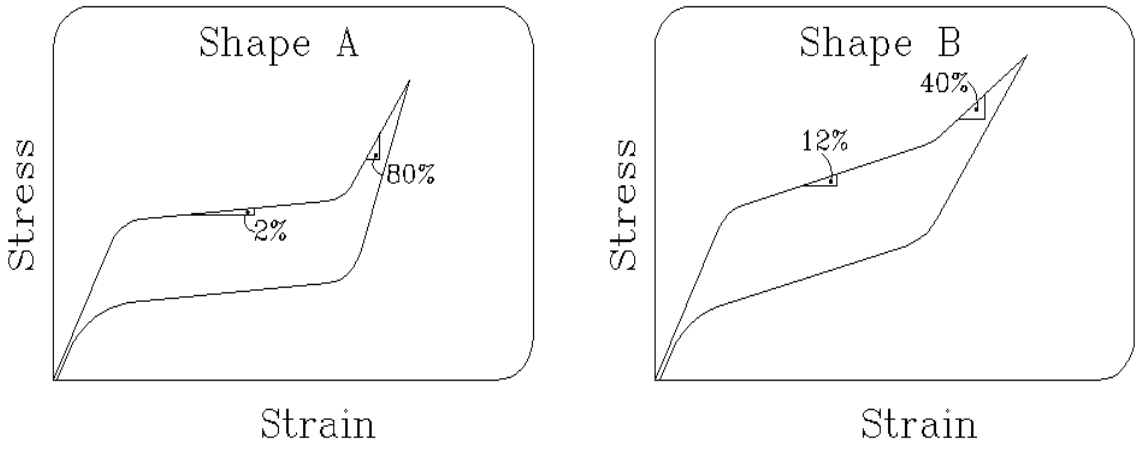

Figure 7.17 Schematic of the two SMA hysteretic shapes considered in the case study.

7.10.2 Results

The bridge model was subjected to the 7 ground motions that were presented in section 7.7 after scaling their spectral acceleration at the fundamental period of the structure (0.61 sec.) to 2.0g. The preliminary examination of the results showed that the hinge openings at hinges 1, 2, 4, and 5 were quite small and hence, in most of the cases, the SMA restrainers did not experience martensitic strain hardening which would allow a comparison between the two studied hysteretic shapes. Thus, the results of Hinge 3 are the only results presented in this section.

Figure 7.18 presents a comparison between the maximum hinge opening results for hinge number 3 using SMAs with Shapes A and B under the 7 records. As noticed from the figure, in 4 out of the 7 cases, the SMA restrainers were stretched beyond the elastic range 64 mm (2.53 in) and thus experienced martensitic strain hardening, while in the rest

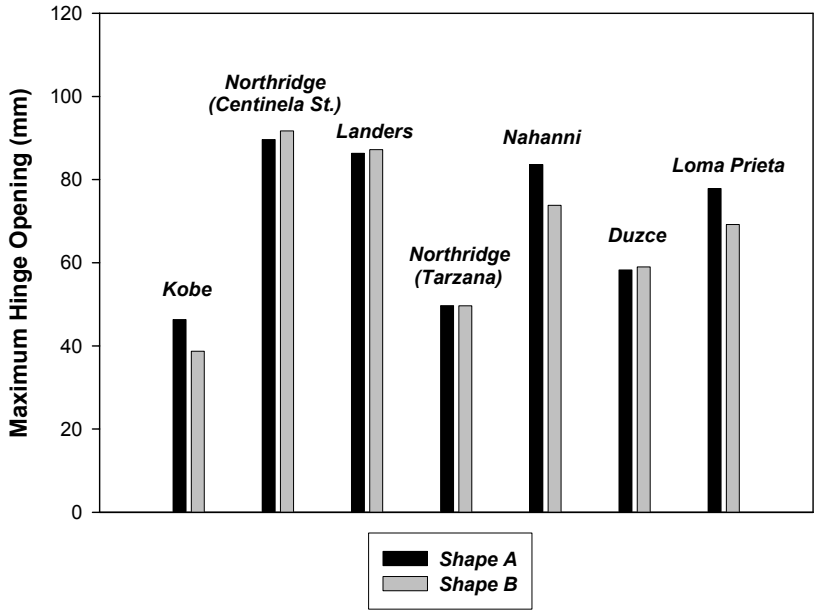

Figure 7.18 Maximum hinge opening results at Hinge 3 using SMA restrainers with different hysteretic shapes.

of the cases the SMAs experienced only strain hardening due to phase transformation. The figure also show that 4 out of the 7 cases showed minor effect due to the changes considered in the hysteretic shape. All of the three cases that were affected by changing the SMAs hysteretic behavior illustrated that SMAs with steep plateau (Shape B) would result in less hinge openings compared to that with flat plateau (Shape A). The differences in the maximum hinge openings in the case of Kobe, Nahanni, and Loma Prieta records were approximately 16%, 12%, and 11%, respectively. The large martensitic strain hardening associated with Shape A (80%) seems to have a minor effect compared to the 12%-phase transformation strain hardening associated with Shape B.

In order to understand better the results presented in Figure 7.18, the force-displacement relationship of the SMA restrainers at Hinge 3 under the Loma Prieta record is presented in Figure 7.19. The figure shows less displacement associated with

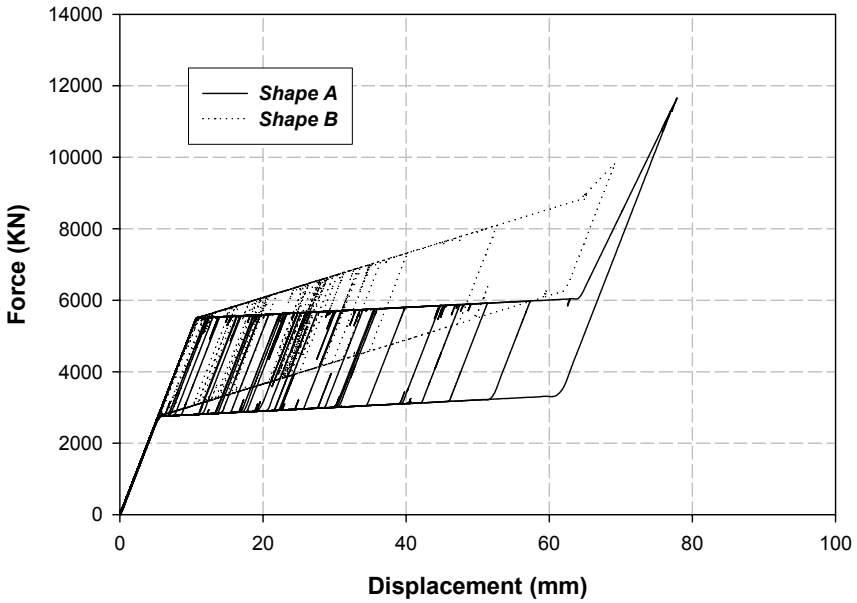

Figure 7.19 Force-displacement relationships of the two types of SMA restrainers used at Hinge 3 under the scaled 1989 Loma Prieta, WAHO record.

the steep hysteresis, despite of the large martensitic strain hardening associated with the hysteresis with flat plateau. This is probably due to the fact that during most of the record, the SMAs are experiencing low-to-moderate deformations, which are highly affected by the slope of the plateau rather than the strain hardening beyond the elastic range. The martensitic strain hardening would expect to have more effect in the case of extremely large deformations.

Considering the effect of SMAs hysteretic properties on the frames ductility was examined through monitoring the drifts of the frames. Figure 7.20 presents the maximum drifts experienced by the two frames at both sides of Hinge 3 (i.e. Frames 3 and 4). As noticed form the figure, the hysteretic shape of the SMAs had an insignificant effect on the frame drifts. The differences between the drifts resulting from using Shapes A and B were all less than 6%. This supports the result observed earlier in the parametric study presented earlier in Chapter 5.

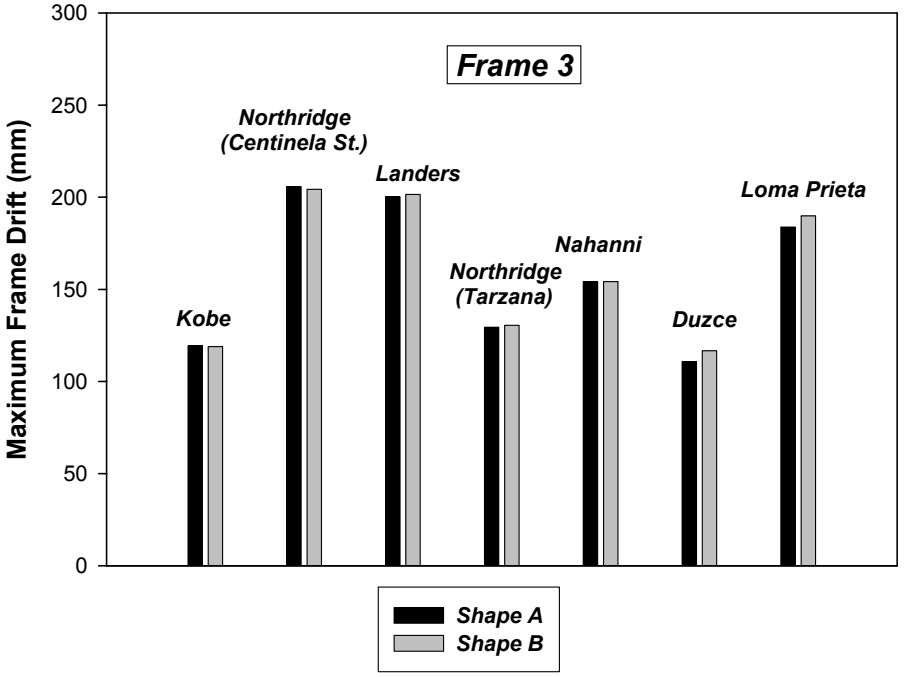

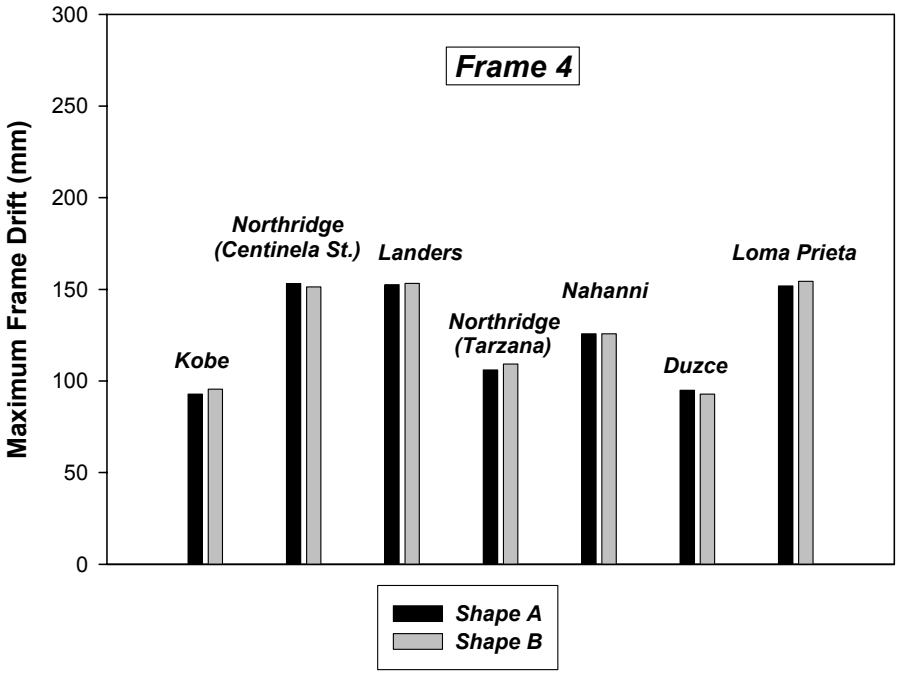

Figure 7.20 Maximum drifts of frames 3 and 4 when using SMA restrainers with different hysteretic shapes.

CHAPTER 8

CONCLUSIONS AND RECOMMENDATIONS

8.1 Summary and Conclusions

This dissertation presents an analytical study that is focused on exploring the feasibility of using superelastic shape memory alloys as seismic retrofit devices for multiple frame bridges. Part of the study is directed towards evaluating the mechanical behavior of SMAs under seismic loading using SMA constitutive models with various levels of complexity. The effect of variability of the SMAs hysteretic and mechanical properties was also addressed in this dissertation. The last part of this work was directed towards comparing the efficiency of SMA retrofit devices with other devices, namely metallic dampers, and viscoelastic dampers.

A study was conducted using three SMA constitutive models with various levels of complexity. The models varied in their ability to capture the hysteretic shape of the superelastic SMAs. Two of the models were able to capture the effect of incomplete phase transformation cycles (sublooping). One of these models was capable of capturing the strength degradation and residual deformation associated with cyclic loading.

Overall, the results showed an agreement in the results of the simplified SMA models and the more complex SMA models. Considering the sublooping effects in the SMA models affected the maximum structural response by less than 9% in average. The structural response showed more sensitivity to the cyclic loading effects, where the maximum difference observed was approximately 39% on average. The structural

response seemed to be less sensitive to the cyclic loading effects in the case of ground motion records with short durations.

A study was presented that focused on evaluating the effect of SMA hysteretic height and shape on the effectiveness of SMA devices in reducing the intermediate hinge opening in multiple frame bridges subjected to earthquakes. The study was conducted using a simplified 2 DOF bridge model. The results of the study showed that the hinge opening and frame drift are not sensitive to the SMAs hysteretic height. This result illustrated that hinge opening is more sensitive to recentering problem rather than damping or force. It was also observed that the slope of the SMAs hysteresis (during and after phase transformation) have a slight effect in the range of 5% to 10% on the hinge opening and in the range of 1% to 4% on the frame drifts depending on the period ratio of the frames. A bridge with moderate period ratio would be more affected by the changes in the SMAs hysteretic shape.

The behavior of SMAs is known to be strongly dependent on temperature. The effect of variability in the ambient temperature on the efficiency of SMA restrainers in limiting intermediate hinge opening in multiple frame bridges was investigated. The results of the study showed that SMA devices are more effective in limiting the hinge opening at higher ambient temperatures. The effect of temperature changes on the hinge opening was more pronounced at temperatures near the austenite finish temperature. Approximately 1/3-1/2 of the changes in the hinge opening occur in the vicinity of A_f. It was also noticed that the hinge opening in bridges with large ductility and/or moderate-to-high period ratio are more sensitive to temperature changes. A change in the hinge

opening of approximately 45% was observed in the case of 0.8 period ratio. The results also showed that the frame drifts were not affected by the change in ambient temperature.

A parametric study was conducted to compare the effectiveness of SMA tension-only and tension/compression restrainer with other devices that are used to limit hinge opening. The other devices included in the study were the conventional steel restrainers, metallic dampers, and viscoelastic solid dampers. The parametric study showed that the steel restrainers are the least effective device in limiting the hinge opening in bridges. The tension-only SMA devices were more effective in limiting the hinge opening by approximately 34% compared to the steel restrainers. The results also showed that the tension-only SMA device is as effective as other devices at smaller period ratios. In comparing the tension/compression SMA device with other devices it was found that the tension/compression SMA devices were more effective than the metallic dampers in the cases where unseating is more likely to occur such as the case of bridges with low-to-moderate period ratios and bridges which are subjected to ground motions with large intensities. On the other hand, the tension/compression SMA devices were more effective than the viscoelastic dampers in the case of bridges with large ductility.

In addition to evaluating the maximum hinge displacement, the residual hinge opening was studied. The results showed that steel restrainers and metallic dampers were not able to prevent residual hinge opening, especially when subjected to strong ground motions. However, the tension/compression SMA devices and the viscoelastic devices were able to eliminate residual hinge openings in all cases.

Finally, three case studies were conducted to evaluate the conclusions that were found in the parametric studies that were mentioned earlier. In those case studies, a

multiple degree of freedom model was developed for the College Avenue Undercrossing Bridge in Alameda County, California. The bridge model was subjected to 7 ground motion records with different characteristics.

The study revealed that the steel restrainer were able to reduce the maximum hinge opening by 25% in average, while the SMA devices were able to reduce it by 50%. In 5 out of the 7 records that were considered in the study, the tension/compression SMA devices resulted in less hinge opening compared to the metallic dampers. The metallic dampers also performed poorly in eliminating the residual hinge openings. In most of the 7 ground motion records, the SMA devices and the viscoelastic devices have similar effectiveness in limiting hinge displacement. The difference between the hinge openings in both cases was in the range of 5% to 7%. However, the results showed that the viscoelastic dampers induced an unnecessary large force at the intermediate hinges that could reach 2 to 3 times the forces induced by the SMA devices. This behavior was especially observed in the case of hinges separating relatively stiff frames. This shows that a displacement-dependent device would be more appropriate for controlling the hinge opening response rather than a velocity-dependent device.

Evaluating the effect of changes in the ambient temperatures on the hinge opening showed that in most of the cases, increasing the ambient temperature reduces the hinge opening and vise versa. The results also showed that bridges with moderate-to-high period ratios are more sensitive to the changes in the ambient temperature. A 40 ^{0}F reduction in the temperature resulted in an average increase of approximately 34% at hinges with moderate-to-high period ratios compared to 13% only in the case of hinges with lower period ratios.

Evaluating the effect of SMAs hysteretic properties on the hinge opening showed that in 3 out of the 7 cases the maximum hinge opening was affected by the SMAs hysteretic shape. The change in the hinge opening in those cases was in the range of 10% to 15%. A hysteresis with steeper plateau would reduce the hinge opening more than a hysteresis with a flat plateau. It was also noticed that the slope of the loading plateau during phase transformation has more effect on the hinge opening compared to the slope after phase transformation.

8.2 Recommendations for Future Research

The parametric studies presented in Chapter 4 focused on the response of a single-degree-of-freedom structure connected to SMA links with different constitutive models used for the SMA links. A future study should be conducted to investigate the effect of SMA modeling on the behavior of multiple frame bridges. This future study should account for the bridge characteristics as well as other SMA characteristics that were not included in this study such as the strain rate effect.

In most of this study, the methodology that was used to design the SMA devices was built on a target strain equal to the elastic strain of the SMA used (about 6%). A better understanding on how to design SMA devices in multiple frame bridges based on the bridge characteristics and ground motion properties is still required.

Since the phase transformation temperature of SMA highly control the mechanical behavior of the alloy, a study is still required to determine the optimum transformation temperatures that are suitable for every type of environment.

This study focused only on exploring the feasibility of using superelastic SMAs in multiple frame bridges. A future study is required to investigate the feasibility of using a hybrid device which is formed of austenitic and martensitic SMAs. In order to get full benefit from such device, it should be studied under a reversal type of loading.

APPENDIX A

DESIGN PLANS FOR THE COLLEGE AVENUE UNDERCROSSING

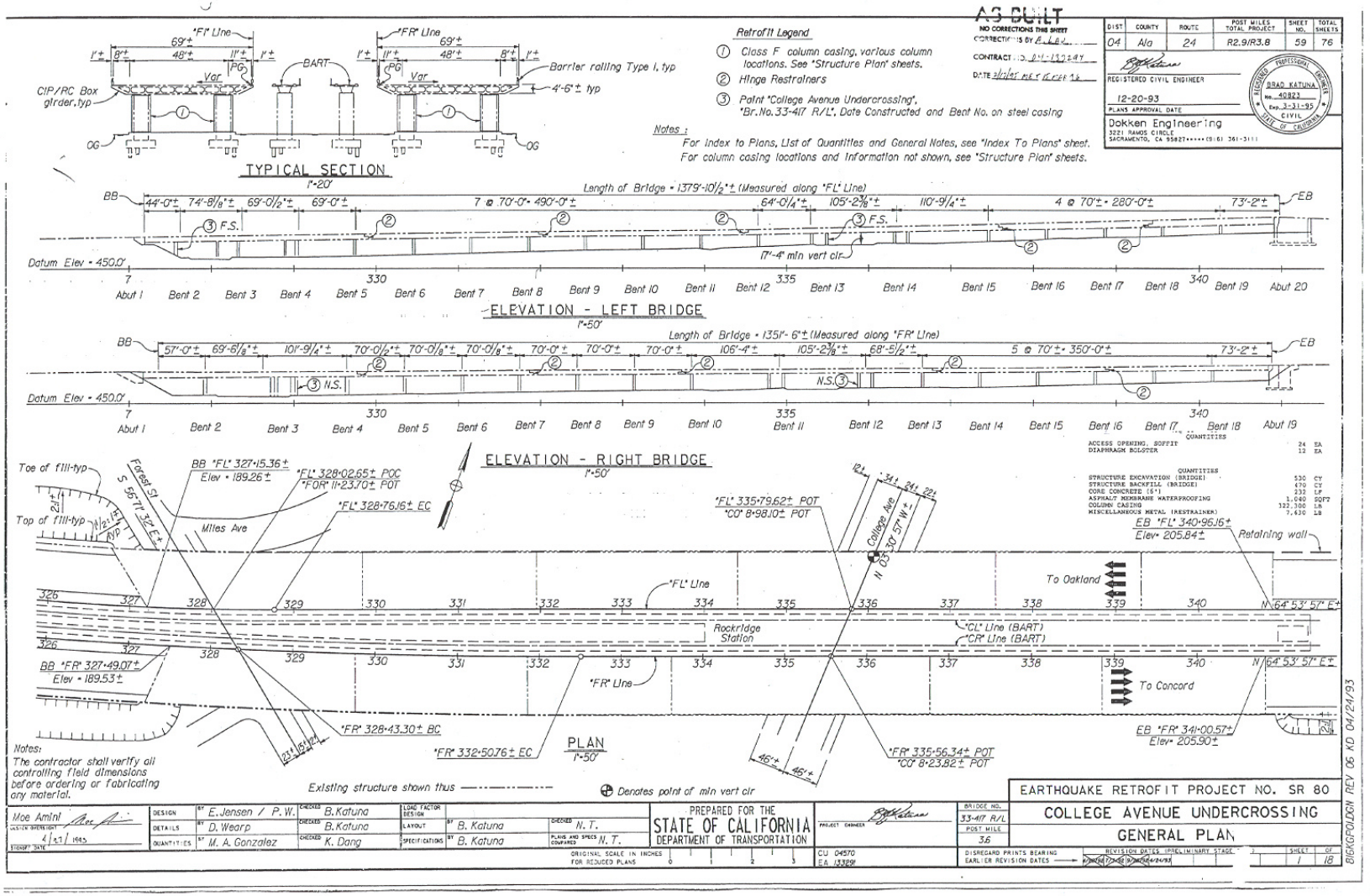

Figure A.1 General plan of the bridge

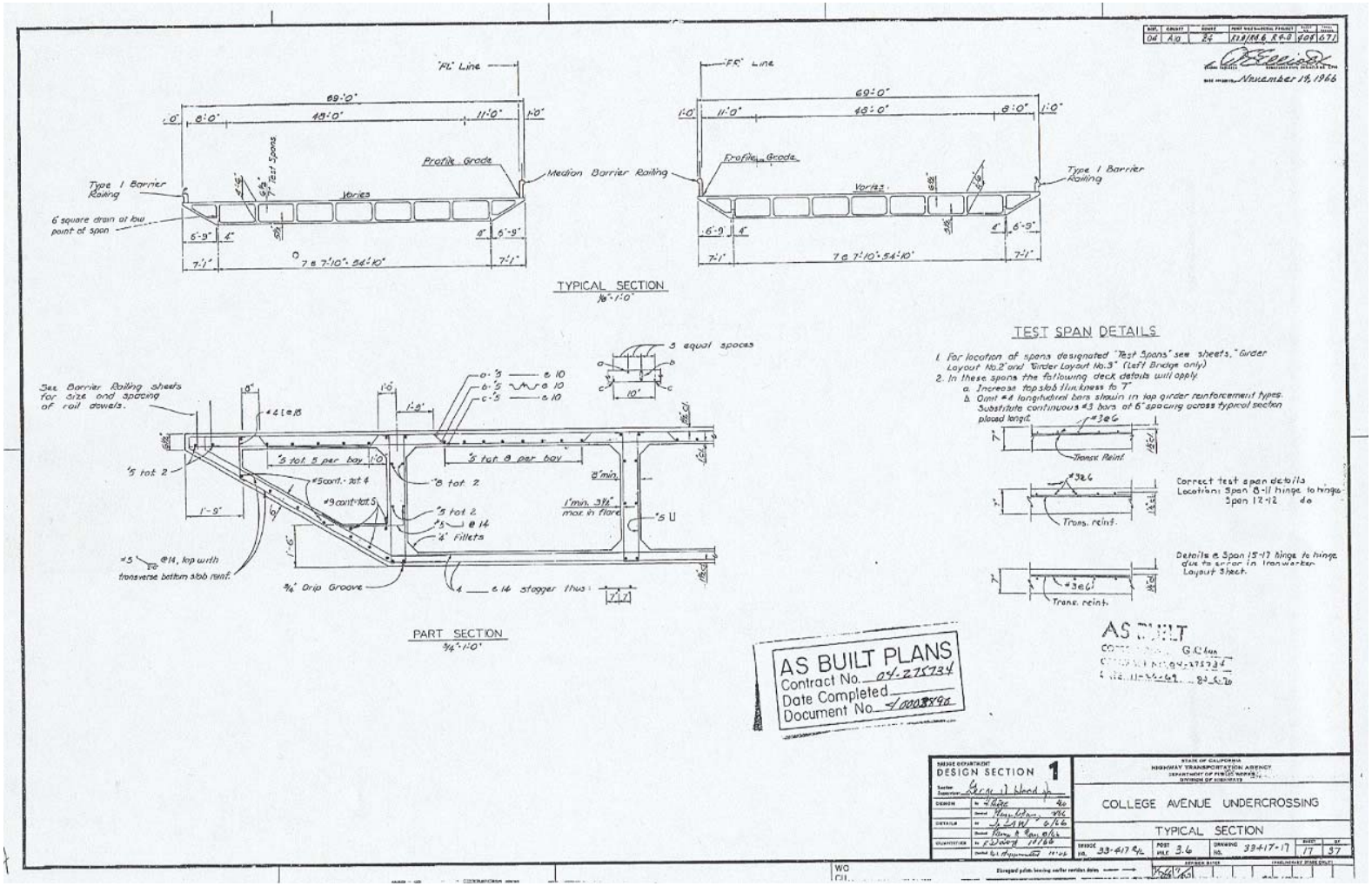

Figure A.2 Typical cross section of the bridge.

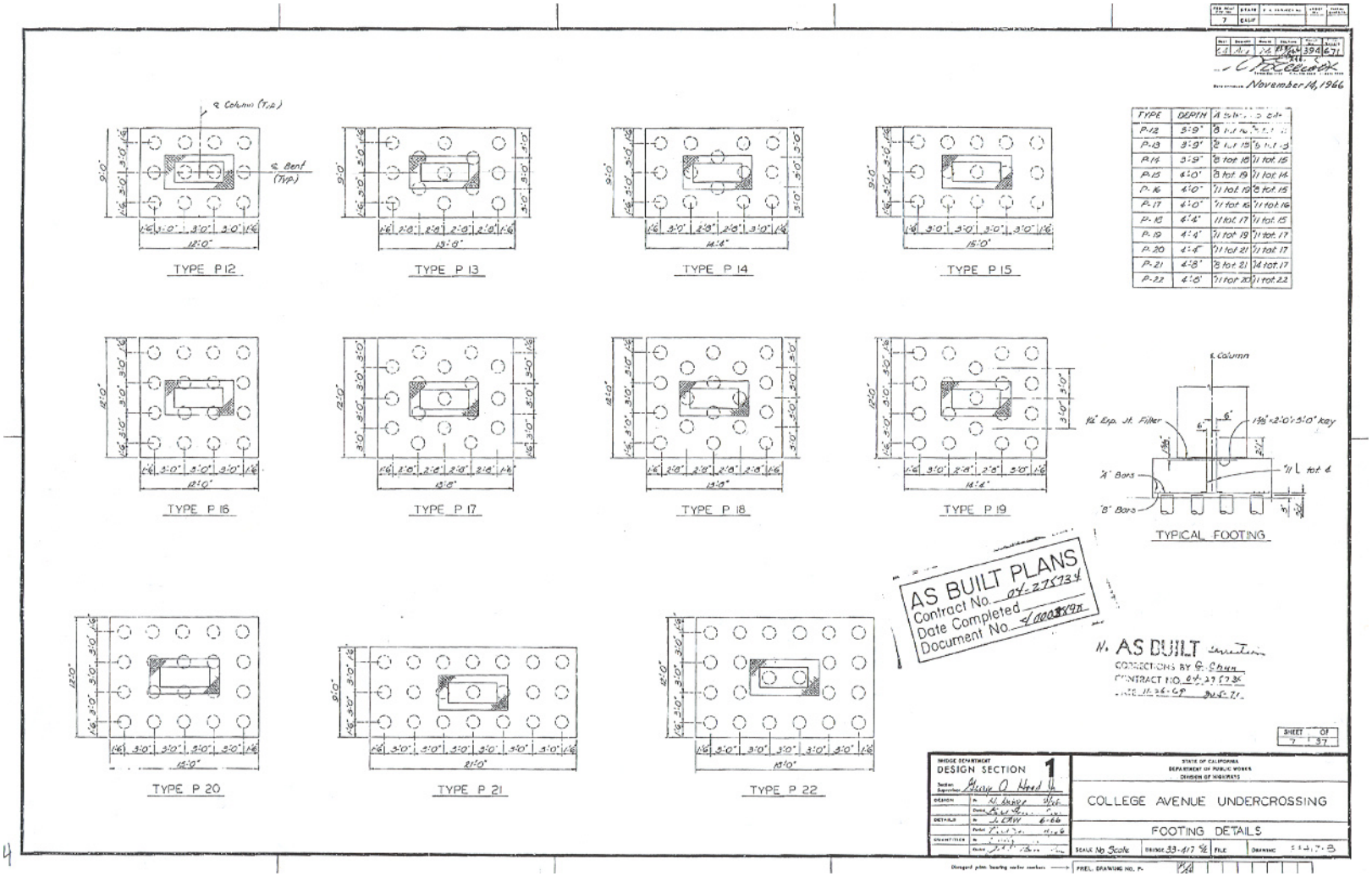

Figure A.3 Detailing of the bridge footings.

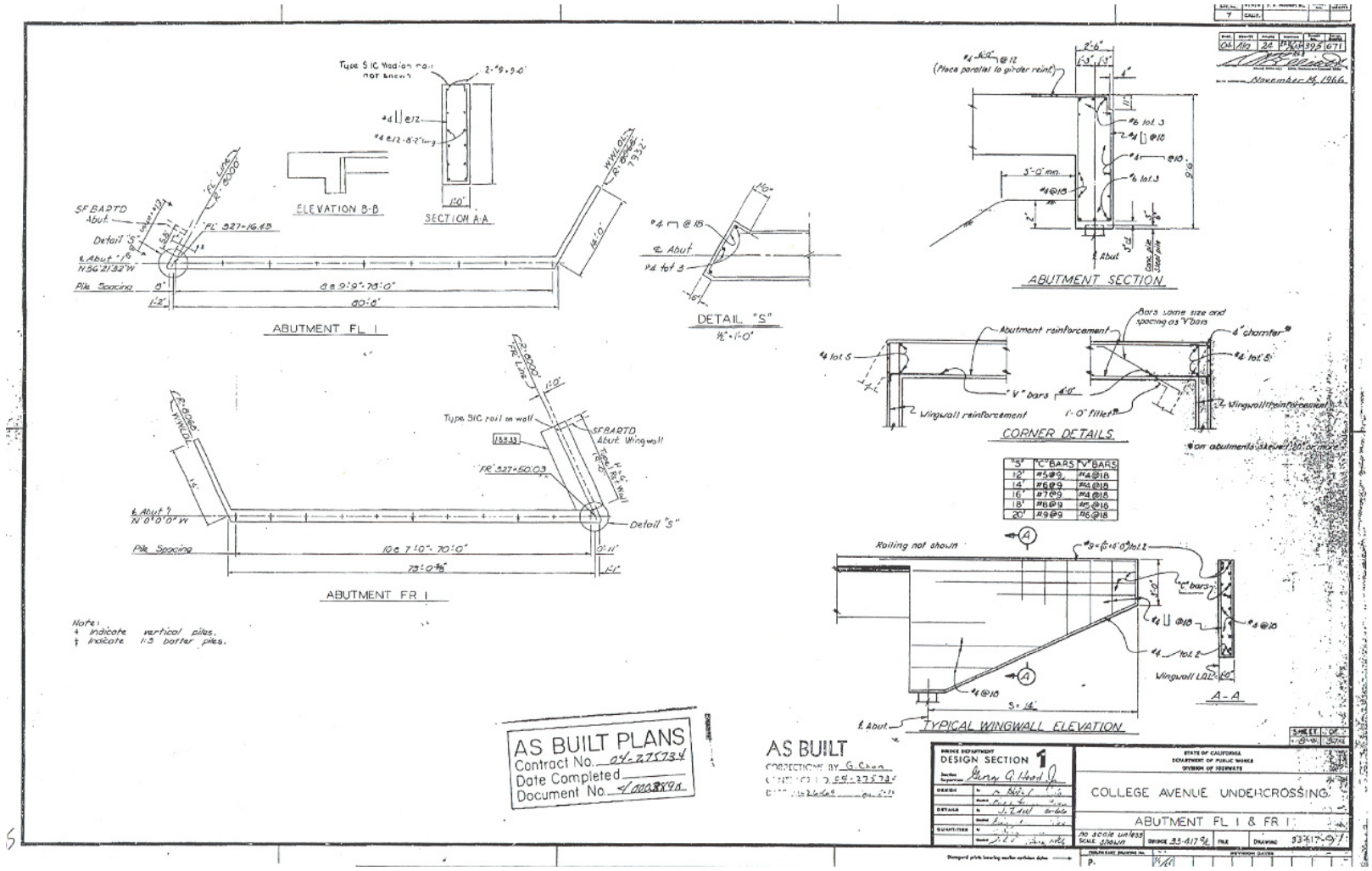

Figure A.4 Detailing of the integral abutment.

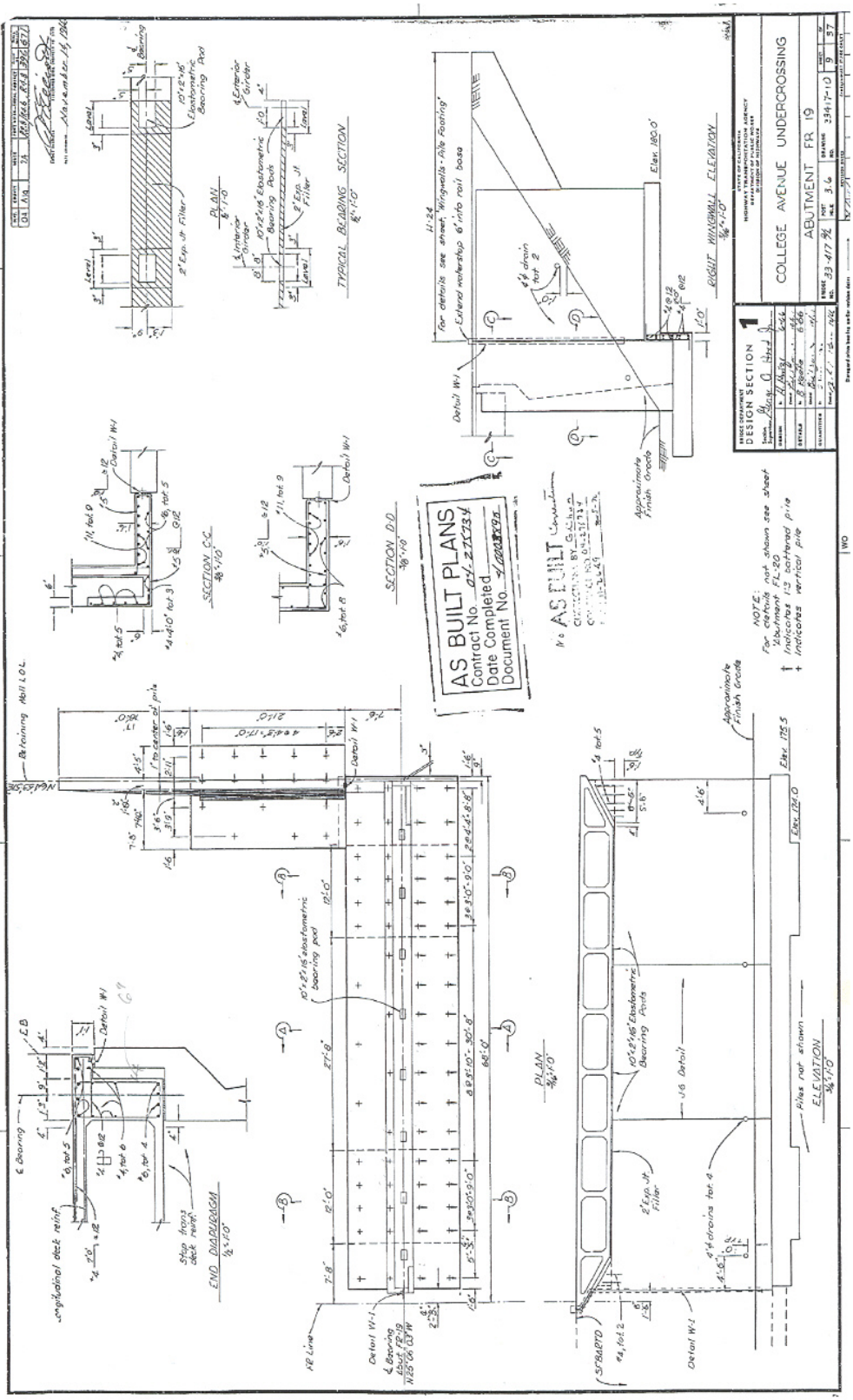

Figure A.5 Detailing of the seat abutment.

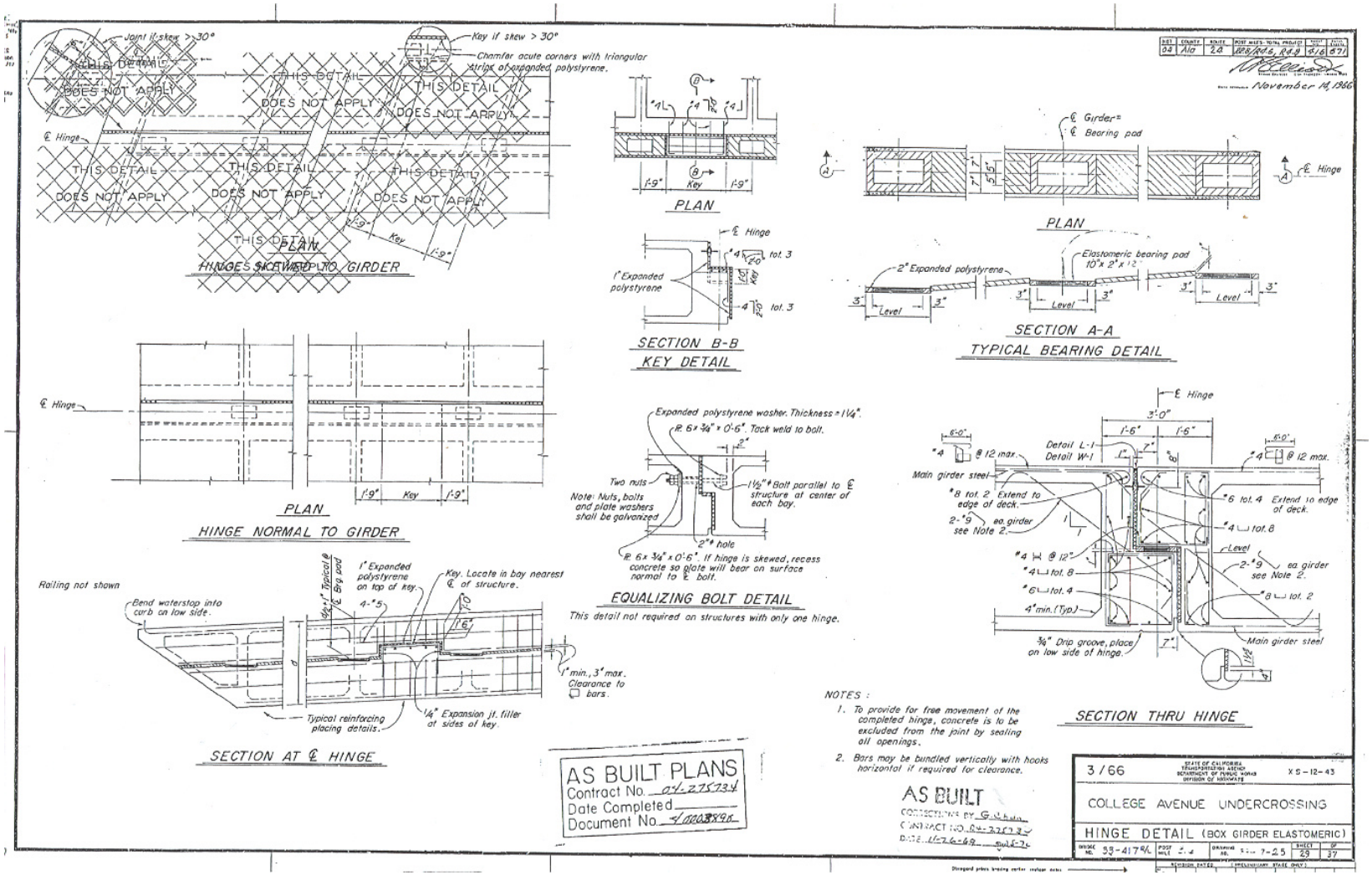

Figure A.6 Detailing of the bridge intermediate hinges.

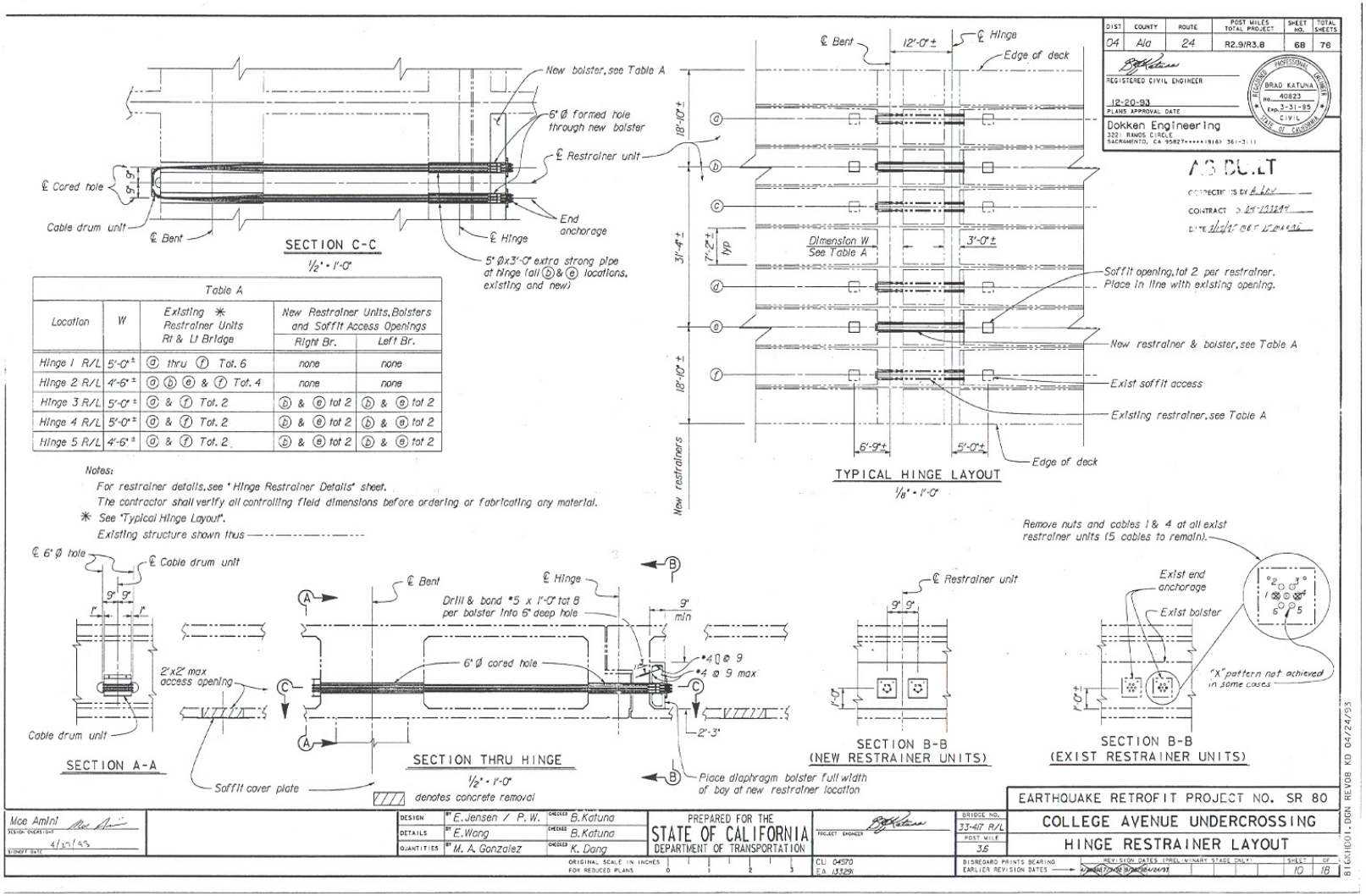

Figure A.7 Detailing of the restrainers used at the intermediate hinge of the bridge.

REFERENCES

Birman V., (1997) "Review of mechanics of shape memory alloy structures", *Applied Mechanics Review*, Vol. 50. No. 11, part 1, pp. 629-645.

Bo Z. and Lagoudas D.C., (1995) "A thermodynamic constitutive model for cyclic loading of shape memory alloy materials with application to two way training", *SPIE*, Vol. 2441, pp. 118-130.

Boyd J.G. and Lagoudas D.C., (1994) "A thermodynamical constitutive model for the shape memory effect due to transformation and reorientation", *SPIE*, Vol. 2189, pp. 276-288.

Brinson L.C. and Lammering R., (1993) "Finite element analysis of the behavior of shape memory alloys and their applications", *International Journal of Solids and Structures*, Vol. 30, No. 23, pp. 3261-3280.

Caltrans (1999) "Seismic design Criteria", *California Department of Transportation*, Version 1.1, July.

Chen G., Mu H., and Both E.R., (2001) "Metallic dampers for seismic design and retrofit of bridges", Report No. RDT 01-005*, Missouri Department of Transportation*.

Chopra A.K., (1995) "Dynamics of Structures. Theory and Applications to Earthquake Engineering", by *Prentice Hall, Inc.*

Cooper J.D., Friedland I.M., Buckle I.G., Nimis R.B. and Bob N.M. (1994) "The Northridge earthquake: Progress made, lessons learned in seismic-resistant Bridge design", *Public Roads* Vol. 58, No. 1, pp. 26-36.

Delemont M.A., (2002) "Seismic retrofit of bridges using shape memory alloys", M.Sc. Thesis, *School of Civil and Environmental Engineering, Georgia Institute of Technology,* Atlanta, GA, U.S.A.

DesRoches R. and Delemont M., (2002) "Seismic retrofit of simply supported bridges using shape memory alloys", *Engineering Structures*, Vol. 24, pp. 325-332.

DesRoches R. and Fenves G.L., (1997) "New design and analysis procedures for intermediate hinges in multiple-frame bridges", *California Department of Transportation*, Report No. UCB/EERC-97/12, December.

DesRoches R. and Fenves G.L., (2000) "Design for seismic cable hinge restrainers for bridges", Journal of Structural Engineering, April, pp. 500-509.

Dolce M., Cardone D., (2001) “Mechanical behavior of shape memory alloys for seismic applications, 2. Austenite NiTi wires subjected to tension”, *International Journal of Mechanical Sciences*, Vol. 43, pp. 2657-2677.

Dolce M., Cardone D., and Marnetto R., (2000) “Implementation and testing of passive control devices based on shape memory alloys”, *Earthquake Engineering and Structural Dynamics*, Vol. 29, pp. 945-968.

EERI Turkey CD-ROM (2003) “Kocaeli, Turkey Reconnaissance Report and Separate Full Color Images”

EERI Taiwan CD-ROM (2003) “Chi-Chi Taiwan, Earthquake of September 21, 1999 Reconnaissance Report and Additional Images”

EQllS and K. Steinbrugge, http://nisee.berkeley.edu/eqiis.html

Falk F., (1983) “One-dimensional model of shape memory alloys”, *Arch. Mech*., Vol. 35, No. 1, pp. 63-84.

Fang H., (1991) “Foundation engineering handbook”, *Kluwer Academic Pub*.

Feng M.Q., (1994) “Use of Dampers as Hinge Restrainers for Seismic Protection of Bridges”, *Proceedings of the NEHRP Conference and Workshop on Research on the Norhtridge, California Earthquake of January 17*.

Feng M.Q., Kim J., Shinozuka M., and Purasinghe R., (2000) “Viscoelastic dampers at expansion joints for seismic protection of bridges*”, Journal of Bridge Engineering,* American Society of Civil Engineers, February, pp. 67-74.

Fischer F.D., Tanaka K., (1992) “A micromechanical model for the kinetics of martensitic transformation”, *Int. Journal of Solids and Structures*, Vol. 29.

Friend C. and Morgan N., "Fatigue/Cyclic Stability of Shape-Memory Alloys", *SMST 99: Proceedings of the First European Conference on Shape Memory and Superelasticity*, 1999, pp. 115-128.

Gall K. and Sehitoglu H., (1999) "The role of texture in tension-compression asymmetry in polycrystalline NiTi", *International Journal of Plasticity*, Vol. 15, pp. 69-92.

Gall K., Sehitoglu H., and Chumlakov Y., (2000) “NiTi experiments versus modeling: Where do we stand?”, *SPIE*, Vol. 3992, pp. 536-547.

Gao X.Y. and Huang W.M., (2002) “Transformation start stress in non-textured shape memory alloys”, Smart Material and Structures, Vol. 11, pp. 256-268.

Goldsmith W., (1960) “Impact: the theory and physical behavior of colliding solids”, *Edward Arnold*, London, England

Graesser E.J. and Cozzarelli F.A., (1991) “Shape-memory alloys as new materials for aseimic isolation”, *Journal of Engineering Mechanics*, Vol. 117, No. 11, pp. 2590-2608.

Hanson R.D, and Soong T.T., (2001) “Seismic design with supplemental energy dissipation devices”, Earthquake Engineering Research Institute, MNO-9.
Hayter A., (2002) "Probability and Statistics for Engineers and Scientists," 2nd edition, Duxbury, ISBN 0-534-38669-5

Hsu Y.T. and Fu C.C., (2004) “Seismic effect on highway bridges in Chi Chi earthquake”, *Journal of Performance of Constructed Facilities*, ASCE, February.

James C.D., (2002) “The 1923 Tokyo Earthquake and Fire”, *University of California, Berkeley,* http://nisee.berkeley.edu/kanto/tokyo1923.pdf

Kamita T. and Matsuzaki Y., (1998) “One-dimensional pseaudoelastic theory of shape memory alloys”, *Smart Materials and Structures*, Vol. 7, pp. 489-495.

Kawashima K. and Unjoh S., (1994) “Seismic response control of bridges by variable dampers”, *Journal of Structural Engineering*, Vol. 120, No. 9, September, pp. 2583-2601.
Otsuka K. and Wayman C.M., (1998) “Shape Memory Materials”, *Cambridge University Press*.

Lexcellent C. and Bourbon G., (1996) “Thermodynamical model of cyclic behavior of Ti-Ni and Cu-Zn-Al shape memory alloys under isothermal undulated tensile tests”, *Mechanics of Materials*, Vol. 24, pp. 59-73.

Liang C. and Rogers C.A., (1990) “One-dimensional thermomechanical constitutive relations for shape memory materials”, *Journal of Intelligent Material Systems and Structures*, Vol. 1, no. 2, pp. 207-234.

Liang C. and Rogers C.A., (1992) “The multi-dimensional constitutive relations of shape memory alloys”, *Journal of Engineering Mathematics*, Vol. 26, No. 3, pp. 429-443.

Lim T.J. (1999) “Behavior of a Ni-Ti Shape Memory Alloy Under Cyclic Proportional and Nonproportional Loading”, Ph.D. Thesis, *School of Mechanical Engineering, Georgia Institute of Technology,* Atlanta, GA, U.S.A.

MacRae G., Priestley N.M.J., and Tao J., (1993) “P-Delta designs in seismic regions”, Report No. UCSD/SSRP-93/05, Structural System Research Project, University of California, San Diego, La Jolla, May.

Mander P.P. (1988) “Theoretical stress-strain model for confined concrete”, Journal of Structural Engineering, ASCE, Vol. 114, No. 8, pp. 1804-1849.

Maroney B., Kutter B., Romstad K., Cahi Y.H., and Vanderbilt E. (1994) "Interpretation of large scale bridge abutment test results", Proceedings of 3rd Annual Seismic Research Workshop, California Department of Transportation, CA, June, 27-29.

Martin G.R. and Yan L., (1995) "Modeling passive earth pressure for bridge abutments", Geotechnical Special Publication 55, Earthquake-Induced movements and seismic remediation of existing foundations and abutments, ASCE Annual National Convention, San Diego, October.

Miranda E., Bertero V.V., (1994) "Evaluation of strength reduction factors for earthquake-resistant design", *Earthquake Spectra*, Vol. 10, No. 2, pp. 357-379.

Niezgódka M. and Sprekels J., (1988) "Existence of solutions for a mathematical model of structural phase transitions in shape memory alloys", *Mathematical Methods in Applied Sciences*, Vol. 10, pp. 197-223.

Patoor E., Eberhardt A., and Berveiller M., (1988) "Thermomechanical behavior of shape memory alloys", *Arch. Mech*., Vol. 40, No. 5-6, pp. 775-794.

Piedboeuf M.C., Gauvin R., and Thomas M., (1998) "Damping behavior of shape memory alloys: strain amplitude, frequency and temperature effects", *Journal of Sound and Vibration*, Vol. 214, No. 5, pp. 885-901.

Rengarajan G., Kumar R.K., and Reddy J.N., (1998) "Numerical modeling of stress induced martensitic phase transformations in shape memory alloys", *International Journal of Solids and Structures*, Vol. 35, No. 14, pp. 1489-1513.

Roberts J.E., (1994) "Practical lessons from the Loma Prieta Earthquake", Report from a symposium sponsored by the Geotechnical Board and the Board on National Disasters of the National Research Council, *National Academy Press, Washington D.C.*

Saiidi, M. (1982) "Hysteresis models for reinforced concrete", *Journal of the Structural Division*, ASCE, Vol. 108, No. 5, pp. 1077–1087.

Saiidi M. and Maragakis E., (1995) "Effectiveness of hinge restrainers as seismic retrofit measure", *Fourth International Bridge Engineering Conference*, August.

Schiff A.J. (1995) "Northridge Earthquake, Lifeline Performance and Post-Earthquake Response", *American Society of Civil Engineers,* August.

Schiff A.J., (1998) "Hyogoken-Nanbu (Kobe) Earthquake of January 17, 1995, Lifeline Performance", *American Society of Civil Engineers,* August.

Serneels A., (1999) "Shape Memory Alloy Characterisation and Optimisation", *SMST-99: Proceedings of the First European Conference on Shape Memory and Superelasticity*, 1999, pp. 6-23.

Shaw J.A., (2002) “A Thermomechanical Model for a 1-D Shape Memory Alloy Wire with Propagating Instabilities”, *International Journal of Solids and Structures*, Vol. 39, pp. 1275-1305.

Soong T.T. and Dargush G.F., (1997) “Passive energy dissipation systems in structural engineering”, *John Wiley & Sons Ltd*.

Sun Q.P. and Hwang K.C., (1993) “Michromechanics modeling for the constitutive behavior of polycrystalline shape memory alloys-I. Derivation of general relations”, *Journal of Mechanics and Physics of Solids*, Vol. 41, No. 1, pp. 1-17.

Tanaka K., (1986) “A thermomechanical sketch of shape memory effect: One-dimensional tensile behavior”, *Res Mechanica*, Vol. 18, pp. 251-263.

Tanaka K., (1990) “A phenomenological description on thermomechanical behavior of shape memory alloys”, J. Pressure Vessel Technology, Vol. 112.

Tanaka K. and Iwasaki R., (1985) “A phenomenological theory of transformation superelasticity”, *Engineering fracture mechanics*, Vol. 21, No. 4, pp. 709-720.

Tanaka K., and Nagaki S., (1982) “A thermomechanical description of materials with internal variables in the process of phase transitions”, *Ingenieur-Archiv*, Vol. 51, pp. 287-299

Tanaka K., Nishimura F., Hayashi T., Tobushi H., and Lexcellent C., (1995) “Phenomenological Analysis on Subloops and Cyclic Behavior in Shape Memory Alloys Under Mechanical and/or Thermal Loads”, *Mechanics of Materials*, Vol. 19, pp. 281-292.

Tobushi H., Shimeno Y., Hachisuka T., and Tanaka K., (1998) "Influence of strain rate on superelastic properties of TiNi shape memory alloys", *Mechanics of Materials*, 30, pp. 141-150.

Wu K., Yang F., Pu Z., and Shi J., (1996) “The effect of strain rate on detwinning and superelastic behavior of NiTi shape memory alloys”, *Journal of Intelligent Material Systems and Structures*, Vol. 7, pp. 138-144.

Yashinsky M., (1998) “Performance of bridge seismic retrofits during Northridge earthquake”, *Journal of Bridge Engineering*, Vol. 3, No. 1, February.

VITA

Bassem Andrawes obtained his Bachelor degree in 1996 from the department of civil engineering at Ain Shams University, Cairo, Egypt. He worked as instructor for three years at Ain Shams University. During that time he was working as a part-time bridge engineer at Sabri Samaan consulting firm in Cairo, Egypt. Mr. Andrawes started his graduate studies in 1999 at Iowa State University. He obtained his Master degree in civil engineering in 2001. The title of his Master's thesis was "Lateral Impact Response for Prestressed Concrete Girder Bridges with Intermediate Diaphragms". He started pursuing his Ph.D. in Georgia Tech in August 2001.